Reconstructing the Late-Quaternary evolution of the central Israeli coastal zone

Thesis · February 2017

1 author:

Gilad Shtienberg
University of California, San Diego

Reconstructing the Late-Quaternary evolution of the central Israeli coastal zone

Gilad Shtienberg

A THESIS SUBMITED FOR THE DEGREE

"DOCTOR OF PHILOSOPHY"

University of Haifa

Faculty of Humanities

Department of Marine Civilizations

February 2017

Reconstructing the Late-Quaternary evolution of the central Israeli coastal zone

By: Gilad Shtienberg

Supervised by: Dr. Dorit Sivan

Dr. Justin K. Dix

A THESIS SUBMITED FOR THE DEGREE

“DOCTOR IN PHILOSOPHY”

University of Haifa

Faculty of Humanities

Department of Marine Civilizations

February 2017

Approved by__ Dorit Sivan. Date___22.2.2017___

(Supervisor)

Approved by________ __________Date___22.2.2017___

(Supervisor)

Approved by__________________________Date______________

(Chairperson of PhD committee)

I would like to dedicated my PhD thesis to

Acknowledgments

Contribution letter

I Gilad Shtienberg, declare that the thesis entitled

“Reconstructing the Late Quaternary Israeli coastal evolution and implicating anthropogenic impact” and the work presented in the thesis are both my own, and have been generated by me as the result of my own original research. I confirm that:

- This work was done wholly or mainly while in candidature for research degree at this University;
- where I have consulted the published work of others, this is always clearly attributed;
- where I have quoted from the work of others, the source is always given. With the exception of such quotations, this thesis is entirely my own work;
- I have acknowledged all main sources of help;
- Parts of this work have been published as:

Shtienberg, G., Dix, J., Waldmann, N., Makovsky, Y., Golan, A., Sivan, D. 2016. Late-Pleistocene evolution of the continental shelf of central Israel, a case study from Hadera. *Geomorphology* 261, 200-211.

S**htienberg, G**., Dix, J., Roskin, J., Waldmann, N., Bookman, R., Taha, N., Sivan, D. 2017. New perspectives on coastal landscape reconstruction since the last interglacial cycle - a test case from central Israel. *Palaeogeography, Palaeoclimatology, Palaeoecology (Palaeo3*) 468 503-519.

Shtienberg, G., Dix, J., Shahack-Gross, R.., Yasur-Landaua, A., Roskin, J., Bookman, R., Waldmann, N., Shalev, S., Sivan, D., Anthropogenic overprints on natural coastal aeolian sediments, a case study from the periphery of ancient Caesarea, Israel. *Anthropocene* 19, 22-34.

- Other papers that I have contributed to during my doctoral studies, but are not detailed within this thesis, include:

Roskin, J., Sivan, D., **Shtienberg, G**., Roskin, E., Porat, N., Bookman, R., 2015. Natural and human controls of the Holocene evolution of the beach, aeolian sand and dunes of Caesarea (Israel). *Aeolian Research* 19, 65-85.

Sivan, D., Sisma-Ventura, G., Greenbaum, N., Bialik, O.M., Williams, F.H., Tamisiea, M.E., Rohling, E.J., Frumkin, A., Avnaim-Katav, S., **Shtienberg, G**., Stein, M. 2016. Eastern Mediterranean sea levels through the last interglacial from a coastal-marine sequence in northern Israel. *Quaternary Science Reviews* 145, 204-225.

Sisma-Ventura, G., Bialik, M.O., **Shtienberg, G**., Greenbaum, N., Frumkin, A., Sivan, D. 2017. Millennial-submillennial last interglacial sea level high stands, deduced from erosional notches exposed at the galilee coast, Israel. *Palaeogeography, Palaeoclimatology, Palaeoecology (Palaeo3*) 470, 1-10.

- Work related to this thesis has been presented at the following conferences:

Shtienberg, G., Dix, J., Waldmann, N., Makovsky, Y., Golan, A., Sivan, D. 2015. The last Glacial-Interglacial cycle sequence portrait through high resolution seismic data from the central coast of Israel. Israel's Geomorphological Research Group, The University of Tel-Aviv (In Hebrew).

Shtienberg, G., Dix, J., Waldmann, N., Makovsky, Y., Golan, A., Sivan, D. 2015. Tales of a submerged landscape: the last Glacial-Interglacial cycle sequence using high resolution seismic data from the central coast of Israel. The Geological Survey of Israel, Kinar (In English).

Shtienberg, G., Dix, J., Roskin, J., Bialik, O., Golan, A., Sivan D. 2016. Late-Pleistocene evolution of the East Mediterranean shallow continental shelf of north-central Israel. EGU. Vienna, Austria (In English).

Shtienberg, G., Dix, J., Roskin, J., Sivan D., 2016. Coastal and Shallow shelf modelling, a base for strategic decisions and future research. Mopp-Medflood. Bremen, Germany (In English).

- I have also provided contributions to the following work presented at conferences:

Roskin, J., Sivan, D., Bookman, R., **Shtienberg, G**. 2015. The Holocene evolution of the beach and inland aeolian sand of the north-central Mediterranean coast of Israel. Batsheva de Rothschild Seminar: Environmental Science and Policy - Challenges in the South Eastern Mediterranean (In Hebrew).

Roskin, J., Roskin, J., Sivan, D. Bookman, R., **Shtienberg, G**. 2015. The Holocene evolution of the beach and inland aeolian sand of the north-central Mediterranean coast of Israel. EGU, Vienna, Austria (In English).

- Work related to this thesis that will be presented:

Shtienberg, G., Dix, J., Roskin, J., Waldmann, N., Shahack-Gross, R., Yasur-Landau, A., Sivan, D., Anthropogenic soil unit – human fingerprints on natural processes, a test case from the area around Caesarea, Israel. Honor Frost Foundation *(HFF) conference*. Nicosia, Cypress (To be presented in English in October 2017).

- I have also provided contributions to the following work that will be presented:

Sivan, D., **Shtienberg, G**., The Israeli coastal wetlands – a unique environment for studying Holocene human settlement patterns for future archaeological prospections in the coastal zone. New Technologies, Hazards and Geo-Archaeology conference. Athens, Greece (To be presented in English in November 2017).

Table of content

Reconstructing the Late-Quaternary evolution of the central Israeli coastal zone

Gilad Shtienberg

Abstract

The coastal zone, which comprises both current terrestrial and marine environments, frequently contains sedimentary sequences that provide detailed records of changing depositional environments. During the Late Quaternary, relative sea level (RSL) fluctuations have had a major influence on aggradation and erosion patterns, and hence the distribution of sediments across the coastal environments. Additional natural regional (e.g. climate) to local scale (e.g. fluvial processes and topography), and latterly anthropogenic influences affected the preserved coastal stratigraphic architecture. This study investigates the influence of these controls on the morphogenesis of the central Israeli coastal zone during the Late Quaternary through a 4-D reconstruction. A multi-disciplinary approach was applied by compiling existing elevation raster grids, bathymetric charts, borehole data-sets, archaeological and historical records and sub-bottom profiles. Additionally, new geophysical and coring operations were conducted on the shallow shelf - terrestrial parts of the study area analysed through petro-sedimentological methods, radiometric dating techniques, and microarchaeology. Based on seismic stratigraphic analysis, seven seismic units were identified and characterised for the shallow shelf subsurface, and have been correlated with the borehole's petro-sedimentological results to produce the chronostratigraphy for the area. This model reveals that Nilotic-sourced littoral sand, intermittently transported inland by wind, was either lithified into aeolianite or pedogenized into palaeosol from about 110 ka to 8 ka. Dark silty clay wetland units were deposited from the Last

Glacial Maximum until the present between the aeolian coastal ridges adjacent to streams that cut the Israeli coastal plain and flow westward. These units are covered by beach and aeolian quartz sand dated from 6.6 to 0.1 ka. Diachronous thicknesses and lithological dissimilarities were identified between the lowland sections and the coastal aeolianite ridges. Streams were found to be a dominant influence on the stratigraphical composition and related facies architecture, affecting aeolian pedogenesis as well as alluvial processes. Climate, mainly influenced by precipitation and dust input, induced pedogenic processes; while sea-level drop during the Last Glacial Maximum reduced sediment deposition in the shallow offshore. This in turn affected aeolian transport, reducing sediment accumulation on the palaeo-coastal plain. In the periphery of the ancient settlement of Caesarea several Early Islamic period grey artefact-bearing facies, interbedded between loose late Holocene aeolian sand, were identified. These pedo-sediments possess components of fertilization, and are suggested to have been aeolian sand that was enriched for agriculture. The palaeoenvironmental model presented in the current study serves as an example for understanding the evolution of similar low-latitude siliciclastic-rich low-gradient shelf-coastal areas during the last glacial-interglacial cycle, demonstrating the influence of local to global forcing factors on these environments. Furthermore, the 4-D reconstruction provides evidence of human impact on the coastal environment during historical times.

List of tables

List of figures

Appendices

1. Introduction

1.1. Global to local scale forcing factors influencing coastal evolution

During the Quaternary, relative sea level (RSL) fluctuations had a major influence on the sedimentary archives of the coastal zone, which encompasses both current terrestrial and adjacent shallow marine environments. The effect of sea-level on accommodation space is one of the major influences on aggradation and erosion, and hence on the distribution of sediments across these environments (Rodriguez et al., 2010; Zhou et al., 2014; Rowe and Bristow, 2015a; Sander et al., 2015). Additional interconnected factors, operating at all scales, also play important roles in depositional-erosional phases and pedogenic processes that shape the litho-stratigraphic architecture of the coastal area. These include: sea condition and prevailing wind direction (Enzel et al., 2010; Ben-Israel et al., 2015; Lindhorst and Betzlet, 2016), precipitation, sediment and dust input (Larrasoaña et al., 2008; Maher, 2011 and ref. therein), vegetation cover (Muhs and Betties, 2003; Maher, 2011); processes governed by relief factor (Dan et al., 1968); hydrological conditions (Pelle et al., 2013); bioturbation (Yaalon, 1997); and, over the last 4000 years, anthropogenic influence (Woods, 1995; Mann, 2000; Crutzen, 2002; Downie et al., 2011).

Aeolianite-palaeosol-sand sequences, which commonly characterise low- to mid-latitude, siliciclastic shallow shelf and coastal areas, reflect the dynamic interaction between the natural and anthropogenic influences. Analysis of the stratigraphical structure and accompanying sediment features (Certini and Scalenghe, 2011) enable to investigate the forcing factors that operated in this environment (Huntley et al., 1993, 1994; Rose et al., 1999; Huntley and Prescott, 2001; Preusser et al., 2002; Munyikwa, 2005; Tripaldi and Forman, 2007; Amorosi et al., 2009; Fitzsimmons et al., 2009; Roskin et al., 2011a; Brooke et al., 2014; Rowe and Bristow, 2015a, 2015b) leading to the coastal strip morphological development.

Previous studies that examined coastal areas and their response to both natural drivers and anthropogenic influences mainly focused on sheltered environments, such as estuaries and deltas, as the preservation potential within these settings is exceptionally high (e.g. Allard et al., 2009; Zecchin et al., 2009). More recently, researchers have started to examine the response of open coastlines to these same drivers, with particular emphasis given to the response of the Late Pleistocene to Holocene transgression (e.g. Zecchin et al., 2008; Yoo et al., 2014; Mendoza et al., 2014). However, these studies focused exclusively on the current offshore record, with relatively few attempts being made to combine the terrestrial and littoral components of the coastal zone (Bersezio et al., 2007; Stoker et al., 2009; Peterson et al., 2010; Cawthra et al., 2014).

Terrestrial coastal stratigraphic studies have been conducted across the Mediterranean basin, in Spain (Fornós et al., 2009; Mauz et al., 2012), Sardinia (Coltorti et al., 2010; Thiel et al., 2010), Tunisia (Mauz et al., 2009, 2012; Elmejdoub et al., 2011), Cyprus (Tsakalos, 2016) and Egypt (El-Asmar, 1994; El-Asmar and Wood, 2000). These localities are characterized by alternating Late Pleistocene aeolianites, palaeosol units and accompanying alluvial facies, and have been settled over millennia. However, these studies have mainly concentrated on the correlation between dune formation and Late Quaternary sea level oscillation, while less attention has been given to the broader coastal geomorphic response to climate, aeolian and alluvial processes, and to an even lesser extent, human impact. In addition, the units studied were usually restricted in extent, and not correlated with the adjacent terrestrial and offshore-submerged stratigraphies.

Israel’s Mediterranean coast is an ideal location for studying Late Quaternary coastal evolution for the following reasons: (1) Relative sea levels generally track eustatic sea-level changes (Sivan et al., 2001, 2004a; Galili et al., 2007), even for the last interglacial (Sivan et al., 2016); (2) Israel's coast is considered tectonically stable, at least since Marine Isotope Stage (MIS)

5e (Sivan et al., 1999; Galili et al., 2007; Mauz et al., 2013; Sivan et al., 2016), with low isostatic uplift rates of about 0.1 mm/year in the Holocene (Sivan et al., 2001; Anzidei et al., 2011; Toker et al., 2012), and about 0.05 mm/y over about the last 125 ka (Sivan et al., 2016); (3) The Late Pleistocene synoptic regime over the eastern Mediterranean was similar to the present one (Enzel et al., 2008); (4) Israel's coast has been inhabited almost continuously over the last 10,000 years (Galili and Nir, 1993; Galili et al., 1993), and thus its sediments can be potentially used for associating between human settlements and environmental changes (Sivan et al., 2004b).

1.2. Research Goals and Questions

1.2.1. Research Goal

The overall intention of the study is to achieve a deeper and more comprehensive understanding of the geomorphic changes that have occurred in the coastal zone of central Israel (Fig. 1.1 for location). Within this wide-ranging goal, the principal research aim is to investigate the combined influence of RSL and climatic and local controls on morphogenesis of this coastline over the last glacial-interglacial period. The correlation between the coastal evolution and forcing factors also enables the author to investigate the effect of human settlement on the coastal stratigraphy during the Late Holocene.

This aim is achieved by combining, extensive and diverse extant geophysical and geological datasets, with newly acquired, targeted, high-resolution shallow marine geophysical surveys with sedimentological and chronostratigraphic studies of a series of cores drilled in the Alexander-Hadera coastal lowland area adjacent to the mouths of Nahal (Stream in Hebrew; N.) Hadera and N. Alexander (Fig. 1.1c for location), all conducted by the author. These data are interpreted through a holistic approach, linking the onshore and offshore sequences, while combining geomorphology, sedimentology, stratigraphy, petrophysics, geochemistry, micro-archaeology techniques, integrated with archaeological finds and historical documentation to form a 4-D model of the terrestrial and inner-shelf coastal zone.

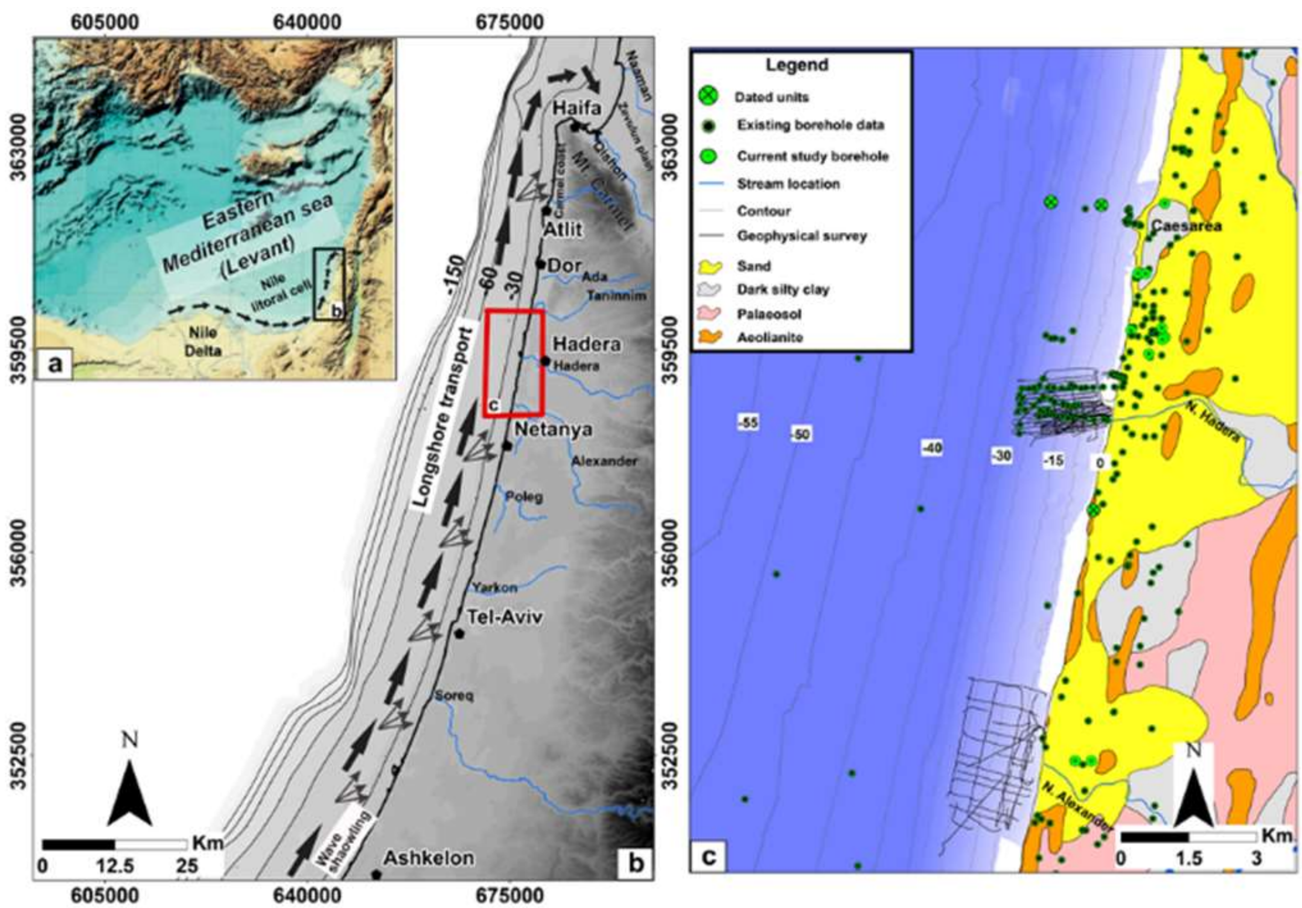

Figure 1.1: Location maps - (a) Israel, east Mediterranean, consisting of the contributors of sediments and transport regimes. (b) Location of study areas in Israel's coast. (c) Location of the new and existing data used in the current study.

1.2.2. Research questions

The specific research questions are as follows:

1. What are the late-Pleistocene to Holocene stratigraphical units found today on the shallow inner shelf of Israel, and how do these units correlate with the stratigraphy identified on the adjacent coastal plain?
2. What were the dominant depositional processes that formed the current stratigraphy of Israel's coastal area, and how did they change over time during the last 115 ka?
3. How did global (e.g., sea level) regional (e.g., climate) and local (e.g., fluvial processes) scale forcing factors, during the last regression-transgression cycle, shape the depositional, preservation and erosional patterns of these open coastal areas? and how did these factors affect the lithification and pedogenesis processes that were responsible for the formation of the Late Quaternary coastal stratigraphy ?
4. Is there evidence of human agency in the evolution of the coastal strip?

1.2.3. Strategic dataset compilations and general research methodology

In order to answer these questions a large database was compiled by the author, consisting of existing data and newly acquired datasets from the terrestrial and inner shelf area of Israel's central coast (Fig. 1.1b). This area was chosen because of: (1) The lack of previous similar studies performed in it; (2) Its location, in the centre parts of Nile littoral cell and thus useful as a case-study for most of Israel's coast; (3) In contrast to other Israeli coastal areas most of the study area's morphology and stratigraphy are yet to be heavily effected by modern infrastructure and manmade influences enabling the author to carry out this research.

The current study establishes for the first time combined marine geophysical and radiometrically dated terrestrial geological records. The amalgamation of continues relatively high resolution geophysical data of the offshore inner shelf and chrono stratigraphicaly analysed lithologies of the neighbouring terrestrial coast enable to produce a chrono-stratigraphic spatial reconstructions of the coastal zone of central Israel. These time slice reconstructions present a better understanding of the relationship between natural global to local forcing factors along with anthropogenic influenced and the paleo-environment of Israel’s coastal strip.

Existing shallow bathymetry and sub-bottom profiling data were obtained from the Israel Oceanographic and Limnological Research (IOLR). The shallow marine geophysical data were integrated with 280 boreholes gathered from published research papers and reports (supplementary). The borehole locations, elevations and lithological descriptions were modified by the author in ArcGIS 10.3.1, along with previously acquired DEM models, soil maps, rectified aerial photographs and chronostratigraphic data to produce a single geospatial database (the database construction is explained in further detail in sections 2.4.1, 3.4.1 and 4.4.1).

In order to fill the gaps the existing datasets, the author conducted new geophysical surveys and sedimentological analyses. Over 220 km of seismic profiles were acquired offshore Hadera and Alexander streams (Fig. 1c; the seismic surveying is explained in further detail in section 2.4.2). The seismic surveys were complemented by seven new cores drilled by the author in the lowland area adjacent to the Hadera and Alexander streams (coring location-selection is explained in detail in sections 3.4.2 and 4.4.2). Coring was carried out along a 10 km-long N-S transect extending to 1.5 km east of the current shoreline. Lithological description together with magnetic susceptibility (MS), particle-size distribution (PSD), total organic carbon (TOC) and inorganic carbon (IC) measurements, X-ray fluorescence (XRF) and Fourier Transform Infrared spectroscopy (FTIR) analysis was conducted by the author on the new cores (further methodological detail can be found in sections 3.4.2 and 4.4.2 respectively). These petro-sedimentological and geochemical analyses together with the radiometric dating (the full OSL and ^{14}C procedures can be found in sections 3.4.3 and 4.4.3 respectively) and correlation to the interpreted offshore stratigraphies enabled the author to reconstruct the chronostratigraphy of the coastal zone.

1.2.4. Thesis Structure

This dissertation is based upon three published peer review journals and are presented as chapters 2 - 4). Chapter 2 presents a high resolution combined geophysical and geological study conducted in the continental shelf, in depths shallower than -30 m covering a time period which spans over more than 100 ka. The study explores through a 4-D reconstruction a terrestrial area that was long exposed to changing environmental conditions, and later flooded by the sea. The chronostratigraphy is based on correlation to adjacent dated coastal and marine stratigraphical units.

Chapter 3 describes the Late Pleistocene history of the coastal lowlands of Israel that is examined through a combination of high-resolution petro-sedimentological methods and OSL ages. This approach enables the reconstruction of the palaeogeography and landscape evolution processes that occurred in this area. Then, by combining the understandings gained from the offshore geophysical surveys, which are discussed in chapter 2, and the chronostratigraphy of the lowland with earlier interpretations of the coastal cliff sequences, a 4-D reconstruction of the evolution of the coast of Israel during the last glacial-interglacial cycle was created. Furthermore, it demonstrates the influence of global to local scale forcing factors on these environments.

Chapter 4 focuses on the upper late Holocene coastal sand unit, where the continuous efforts of human populations to adapt their activities to their varying needs and changing natural environments has left anthropogenic markers in the buried sediments. These markers were analysed through cored boreholes utilizing geomorphology, sedimentology, stratigraphy, petrophysics, geochemistry, microarchaeology, archaeology and history to form an understanding of how changing settlement and subsistence patterns in the area surrounding an ancient urban centre in the central coastal plain of Israel, affected natural sediments and soils in its vicinity.

The present chapter describes the relevance and importance of the research while Chapter 5 summarises the main findings and conclusion of this research, its scientific significance and proposed future research.

1.3. Regional setting: Israel in the south-eastern Mediterranean

1.3.1. Physiographic setting of the coast of Israel

The 190 km-long coastal plain of Israel widens from about 3 km in the north to about 15 km in the south (Almagor and Hall, 1984). The continental shelf follows the same spatial pattern, widening from about 10 km in the north to about 20 km in the south (Fig. 1.1b; Almagor et al., 2000; Sade et al., 2006). The sediments that cover the shelf and coastal plain are mostly comprised of Nile derived quartz sand (Picard, 1943; Emery and Neev, 1960; Pomerancblum, 1966; Almagor et al., 2000; Zviely et al., 2009) transported to the region through longshore currents terminating at Haifa Bay (Fig. 1.1a, b; Zviely et al., 2006; Hyams-Kaphzan et al., 2008).

The morphology of the coast and immediate hinterland of Israel (Fig. 1.1b) is dominated by up to eighteen aeolianite ridges that trend, parallel-subparallel to the current coastline. These ridges, which rise above the surface of the coastal plain and (Gvirtzman et al., 1983 among others) sea floor (Mart and Belknap, 1991; Belknap and Mart, 1999; Almagor et al., 2000; Schattner et al., 2010; 2015), were formed during the late Pleistocene when sea levels were lower than present and the shelf was exposed (Mauz et al., 2013).

1.3.2. Relative sea level fluctuations in the Mediterranean and along the coast of Israel

In the Mediterranean, Rohling et al. (2014) have produced the longest (up to 5.3 Myr) continuous Mediterranean, RSL record based on $\delta^{18}O$ obtained from benthic foramenifera of deep sea core from the Gibraltar. Within this period RSL data based on coastal indications of MIS9 to MIS5 Highstands were recorded by Zazo et al. (2003, 2013) in Spain while Antonioli et al. (2004) constructed a composite sequence from Argentarola cave speleothems in western Italy consisting of five marine and four continental layers during the last 215 ka. In the south east Mediterranean coast of Israel Galili et al. (2007) and Sivan et al. (2016) reported an MIS5 Highstand. A younger, continuous record was created by Lambeck and Bard (2000) for the last 30 ka from the west Mediterranean while Lambeck and Purcell (2005) presented a GIA (Glacial Isostatic Adjustment) model for the entire Mediterranean basin extending back to the Last Glacial Maximum (LGM; about 20 ka). Based on this data-base it seems that during the last interglacial cycle the Mediterranean sea level dropped from several meters above the present mean sea level (+6 m to max +9 m) during the MIS5e to a minimum elevations of 135 m below mean sea level during the LGM. Combining long continuous records, like those of Lambeck and Bard (2000) with the Holocene Israeli RSL curve (Sivan et al., 2001) and the modern day bathymetry of the Israeli continental shelf, gives a simplistic indication of the extent of shoreline migration as a result of sea level change (Cohen-Seffer et al., 2005). Archaeological observations from the coast of Israel indicate that sea levels continued to rise until ~7 ka to ~6 ka when rates slowed considerably and the shoreline was located ~1.5 km offshore from its current location. Sea level almost reached its present elevation at ~4 ka (Sivan et al., 2001, 2004b; Anzidei et al., 2011; Toker et al., 2012), and the coastline prograded to reach its present location at ~3 ka (Kadosh et al., 2004; Cohen-Seffer et al., 2005; Zviely et al., 2006, 2007; Porat et al., 2008; Sivan et al., 2011).

1.3.3. The local coastal-shallow marine chrono-stratigraphy

The Late Pleistocene aeolianite coastal cliff of Israel, that yield ages younger than about 75 ka (Engelmann et al., 2001; Frechen et al., 2001, 2002; Porat et al., 2004; Moshier et al., 2010; Mauz et al., 2013) is overlain by a thick brown-red sandy clayey loam palaeosol (Fig. 1.2; Gvirtzman et al., 1983, 1998; Engelmann et al., 2001). This soil sequence is comprises of Nilotic derived units that differ in their lithological characteristics (Yaalon, 1997; Gvirtzman et al., 1998; Gvirtzman and Wieder, 2001; Frechen et al., 2002; Porat et al., 2004) consisting of a wide range of ages, sometimes synchronous with the aeolianite units, and sometimes younger, dating from about 87 to about 8 ka (Gvirtzman and Wieder, 2001; Frechen et al., 2002; Porat et al., 2004; Sivan and Porat, 2004; Mauz et al., 2013).

In the coastal lowlands, adjacent to the stream path and mouths, between the parallel aeolianite ridges, up to 20 m thick sequences of unconsolidated sediments overly a submerged calcareous sandstone surface (Sivan and Porat, 2004; Elyashiv, 2013). These sequences consist of Dark brown to brownish-red clayey sand to sandy clay palaeosols (Kadosh et al., 2004; Sivan and Porat, 2004; Cohen-Seffer et al., 2005; Elyashiv, 2013; Roskin et al., 2015) covered by a dark silty clay unit, rich in organic material, interpreted to originate from freshwater to brackish wetland marshes (Fig. 1.2; Galili and Weinstein-Evron, 1985; Sivan et al., 2011).

As sea level rose during the Late Pleistocene-Holocene transition, the shoreline migrated eastwards, and at about 8 ka flooded the shallow shelf (depth shallower than -20 m; Sivan et al., 2001, 2004). Nilotic sands, which were also transported shoreward, started to accumulate on the coast, covering the coastal lowland and cliff surface about 7 ka ago (Fig. 1.2; Frechen et al., 2002; Porat et al., 2004; Mauz et al., 2013; Roskin et al., 2015).

Figure 1.2: Israel's coastal morphologies and litho-stratigraphies presented from young to old.

1.3.4. Israel's climate regimes during the Late Pleistocene-Holocene

During the last 115 ka a succession of alternating drier and humid periods have been identified for the south-eastern part of the Mediterranean Sea. These climate conditions were reconstructed based on δ^{18}O values of Israel's Soreq cave speleothem (Bar-Matthews et al., 2000; 2003), δ^{18}O values of benthic foraminiferal assemblages (Almogi-Labin et al., 2009) and pollen records (Langgut et al., 2011) both acquired from deep-sea cores drilled in the eastern part of the Mediterranean Sea. The climate during the remnant MIS5e is considered to have been relatively dry followed by a humid and warm period of Sapropel S3 (85 to 75 ka) consisting of rainfall amounts which are similar to today (Cheddadi and Rossignol-Strick, 1995). Then, all through the Last Glacial period (75 to 16 ka) the climate became generally dry and cold whereas some slightly more humid fluctuations were identified between 56 and 43 ka.

The late Pleistocene to early Holocene transition is marked by three anomalous climate epochs: (i) the LGM (~23 to 19 ka) characterized by cooler, drier and windier conditions that amplify aeolian processes (i.e. dust transport) (Goodfriend and Magaritz, 1988; Bar-Matthews et al., 1997, 1999; Calvert and Fontugne, 2001). Lakes evolving in the nearby Dead Sea basin however, record an inverse pattern in which increase humidity promoted high lake stands (Bartov et al., 2002). (ii) the Bølling-Allerød (~15 to 13 ka) which was warmer and wetter (Rossignol-Strick, 1995, 1999; Bar-Matthews et al., 1997, 1999; 2003; Emeis et al., 2003). (iii) the Younger Dryas (~12.7 to 11.5 ka) characterized by cold, arid and windy conditions (Bar-Matthews et al., 2003; Roskin et al., 2011a) promoting regional aeolian activity (Bar-Matthews et al., 2003) and dust accretion on the SEM coastal plain (Yaalon, 1987; Gvirtzman and Wieder, 2001).

Since the onset of the Holocene the southeast Mediterranean climate has been characterized by dry summers and rainy winters (Eshel and Farrell, 2000; Gvirtzman and Wieder, 2001). The latitude, frequency and depth of wintertime cyclones originating in the central Mediterranean Sea, known as Cyprus Lows, are the most important controlling mechanisms on southeast Mediterranean precipitation and winds (Eshel and Farrell, 2000; Enzel et al., 2008). The early Holocene interval (~10.5 to 7 ka) is characterized by increase in wetness. This rainy time interval, which is still debated (Robinson et al., 2006; Litt et al., 2012), is one of the main factors that governed inland and desert landscape evolution in the southeast Mediterranean (Goodfriend, 1988; Bar-Matthews et al., 1996; Issar, 2004; Issar and Zohar, 2004). There is no accepted record of substantial middle to late Holocene climate change in the coastal region of the Levant. Some proxies and records in other parts of the Israeli coastal plain indicate that the middle to late Holocene climate seems to have been generally stable with regard to temperature and humidity (Ackermann et al., 2014, 2015). Conversely, interpretations from the Soreq cave speleothems (Bar-Matthews and Ayalon, 2011) and pollen records acquired from cores drilled in the Golan heights, Sea of Galilee and Dead-sea shores, covering a 220 km long north-south transact (Litt et al., 2012; Langgut et al., 2013, 2015) indicate several climate changes and oscillations.

1.4. The study area: Taninim to Alexander Stream mouths, central coast of Israel

A study area located in Israel's central coast, between Nahal (Stream in Hebrew; N.) Alexander in the south and N. Taninim in the north; and from water depth of -30 mILSD (Israel Land Survey Datum) and up to 1.5 km east from the current shoreline (Fig. 1.1 for location) was selected for conducting the research. The study area was chosen on the basis of: (1) its particular location between two streams (Taninim and Alexander; Fig. 1.1b); (2) the presence of various morphologies (aeolianite ridges, coastal dunes, marshlands and streams; Fig. 1.2), which provide the optimal conditions for studying their interplay with sea level-changes through time; (3)

indications of long anthropogenic activity from the Persian period (approx. 400 BCE; Stieglitz, 1996; Raban, 2007) until the Crusader times (1200 CE; Taxel, 2013; Avni, 2014; Ramsay and Holum, 2015) adjacent to settlements just south of the coastal parts of N. Taninim.

The physiography, environmental conditions and setting make this chosen area an ideal location for studying the eustatic, climatic and local controls on the morphogenesis of the coastal system during the Late Quaternary.

1.5. Refrences

Ackermann, O., Greenbaum, N., Ayalon, A., Bar-Matthews, M., Boaretto, E., Bruins, H.J., Cabanes, D., Horwitz, L.K., Neumann, F.H., Porat, N., Weiss, E., Maeir, A.M., 2015. Using palaeo-environmental proxies to reconstruct natural and anthropogenic controls on sedimentation rates, Tell es-Safi/Gath, eastern Mediterranean. Anthropocene 8, 70-82.

Ackermann, O., Greenbaum, N., Bruins, H., Porat, N., Bar-Matthews, M., Almogi-Labin, A., Schilman, B., Ayalon, A., Horwitz, L.K., Weiss, E., Maeir, A.M., 2014. Palaeoenvironment and anthropogenic activity in the southeastern Mediterranean since the mid-Holocene: The case of Tell es-Safi/Gath, Israel. Quaternary International 328-329, 226-243.

Allard, J., Chaumillon, E., Féniès, H., 2009. A synthesis of morphological evolutions and Holocene stratigraphy of a wave-dominated estuary: The Arcachon lagoon, SW France. Continental Shelf Research 29, 957-969.

Almagor, G., Gill, D., Perath, I., 2000. Marine Sand Resources Offshore Israel. Marine Georesources & Geotechnology 18, 1-42.

Almagor, G., Hall, J.K., 1984. Morphology of the Mediterranean Contintental Margin of Israel: A Comparative Summary and a Bathymetric Chart. Geological Survey of Israel.

Almogi-Labin, A., Bar-Matthews, M., Shriki, D., Kolosovsky, E., Paterne, M., Schilman, B., Ayalon, A., Aizenshtat, Z., Matthews, A., 2009. Climatic variability during the last ~90ka of the southern and northern Levantine Basin as evident from marine records and speleothems. Quaternary Science Reviews 28, 2882-2896.

Amorosi, A., Ricci Lucchi, M., Rossi, V., Sarti, G., 2009. Climate change signature of small-scale parasequences from Lateglacial–Holocene transgressive deposits of the Arno valley fill. Palaeogeography, Palaeoclimatology, Palaeoecology 273, 142-152.

Antonioli, F., Bard, E., Potter, E.-K., Silenzi, S., Improta, S., 2004. 215-ka History of sea-level oscillations from marine and continental layers in Argentarola Cave speleothems (Italy). Global and Planetary Change 43, 57-78.

Anzidei, M., Antonioli, F., Benini, A., Lambeck, K., Sivan, D., Serpelloni, E., Stocchi, P., 2011. Sea level change and vertical land movements since the last two millennia along the coasts of southwestern Turkey and Israel. Quaternary International 232, 13-20.

Avni, G., 2014. The Byzantine-Islamic transition in Palestine: an archaeological approach. Oxford University Press.

Bar-Matthews, M., Ayalon, A., 2011. Mid-Holocene climate variations revealed by high-resolution speleothem records from Soreq Cave, Israel and their correlation with cultural changes. The Holocene 21, 163-171.

Bar-Matthews, M., Ayalon, A., Gilmour, M., Matthews, A., Hawkesworth, C.J., 2003. Sea–land oxygen isotopic relationships from planktonic foraminifera and speleothems in the Eastern Mediterranean region and their implication for paleorainfall during interglacial intervals. Geochimica et Cosmochimica Acta 67, 3181-3199.

Bar-Matthews, M., Ayalon, A., Kaufman, A., 1997. Late Quaternary paleoclimate in the eastern Mediterranean region from stable isotope analysis of speleothems at Soreq Cave, Israel. Quaternary Research 47, 155-168.

Bar-Matthews, M., Ayalon, A., Kaufman, A., 2000. Timing and hydrological conditions of Sapropel events in the Eastern Mediterranean, as evident from speleothems, Soreq cave, Israel. Chemical Geology 169, 145-156.

Bar-Matthews, M., Ayalon, A., Kaufman, A., Wasserburg, G.J., 1999. The Eastern Mediterranean paleoclimate as a reflection of regional events: Soreq cave, Israel. Earth and Planetary Science Letters 166, 85-95.

Bar-Matthews, M., Ayalon, A., Matthews, A., Sass, E., Halicz, L., 1996. Carbon and oxygen isotope study of the active water-carbonate system in a karstic Mediterranean cave: Implications for paleoclimate research in semiarid regions. Geochimica et Cosmochimica Acta 60, 337-347.

Bartov, Y., Stein, M., Enzel, Y., Agnon, A., Reches, Z.e., 2002. Lake levels and sequence stratigraphy of Lake Lisan, the late Pleistocene precursor of the Dead Sea. Quaternary Research 57, 9-21.

Belknap, D.F., Mart, Y., 1999. Sea-level Lowstand in the east mediterranean-late pleistocen coastal Tarraces Offshore nothern Israel. Journal of Coastal Research 15, 399-412.

Ben-Israel, M., Enzel, Y., Amit, R., Erel, Y., 2015. Provenance of the various grain-size fractions in the Negev loess and potential changes in major dust sources to the Eastern Mediterranean. Quaternary Research 83, 105-115.

Bersezio, R., Giudici, M., Mele, M., 2007. Combining sedimentological and geophysical data for high-resolution 3-D mapping of fluvial architectural elements in the Quaternary Po plain (Italy). Sedimentary Geology 202, 230-248.

Brooke, B.P., Olley, J.M., Pietsch, T., Playford, P.E., Haines, P.W., Murray-Wallace, C.V., Woodroffe, C.D., 2014. Chronology of Quaternary coastal aeolianite deposition and the drowned shorelines of southwestern Western Australia – a reappraisal. Quaternary Science Reviews 93, 106-124.

Calvert, S., Fontugne, M., 2001. On the late Pleistocene-Holocene sapropel record of climatic and oceanographic variability in the eastern Mediterranean. Paleoceanography 16, 78-94.

Cawthra, H.C., Bateman, M.D., Carr, A.S., Compton, J.S., Holmes, P.J., 2014. Understanding Late Quaternary change at the land–ocean interface: a synthesis of the evolution of the Wilderness coastline, South Africa. Quaternary Science Reviews 99, 210-223.

Certini, G., Scalenghe, R., 2011. Anthropogenic soils are the golden spikes for the Anthropocene. The Holocene 21, 1269-1274.

Cheddadi, R., Rossignol-Strick, M., 1995. Improved preservation of organic matter and pollen in eastern Mediterranean sapropels. Paleoceanography 10, 301-309.

Cohen-Seffer, R., Greenbaum, N., Sivan, D., Jull, T., Barmeir, E., Croitoru, S., Inbar, M., 2005. Late Pleistocene–Holocene marsh episodes along the Carmel coast, Israel. Quaternary International 140-141, 103-120.

Coltorti, M., Melis, E., Patta, D., 2010. Geomorphology, stratigraphy and facies analysis of some Late Pleistocene and Holocene key deposits along the coast of Sardinia (Italy). Quaternary International 222, 19-35.

Crutzen, P.J., 2002. Geology of mankind. Nature 415, 23-23.

Downie, A.E., Van Zwieten, L., Smernik, R.J., Morris, S., Munroe, P.R., 2011. Terra Preta Australis: Reassessing the carbon storage capacity of temperate soils. Agriculture, Ecosystems & Environment 140, 137-147.

El-Asmar, H.M., 1994. Aeolianite sedimentation along the northwestern coast of Egypt: evidence for middle to late quaternary aridity. Quaternary Science Reviews 13, 699-708.

El-Asmar, H.M., Wood, P., 2000. Quaternary shoreline development- the northwestern coast of Egypt. Quaternary Science Reviews 19, 1137-1149.

Elmejdoub, N., Mauz, B., Jedoui, Y., 2011. Sea-level and climatic controls on late Pleistocene coastal aeolianites in the Cap Bon peninsula, northeastern Tunisia. Boreas 40, 198-207.

Elyashiv, H., 2013. The Late Pleistocene-Holocene sedimentary evolution of Zevulun Plain : focusing on the wetlands MA Thesis Faculty of Natural Sciences, Leon H. Charney School of Marine Sciences, The Dr. Moses Sreauss Dept. of Marine Geosciences, University of Haifa, Israel.

Emeis, K.C., Schulz, H., Struck, U., Rossignol-Strick, M., Erlenkeuser, H., Howell, M., Kroon, D., Mackensen, A., Ishizuka, S., Oba, T., 2003. Eastern Mediterranean surface water temperatures and $\delta18O$ composition during deposition of sapropels in the late Quaternary. Paleoceanography 18, 1005-1029.

Emery, K., Neev, D., 1960. Mediterranean beaches of Israel: Israel Geological Survey Bulletin. 26, 1-24.

Engelmann, A., Neber, A., Frechen, M., Boenigk, W., Ronen, A., 2001. Luminescence chronology of Upper Pleistocene and Holocene aeolianites from Netanya South - Sharon Coastal Plain, Israel. Quaternary Science Reviews 20, 799-804.

Enzel, Y., Amit, R., Crouvi, O., Porat, N., 2010. Abrasion-derived sediments under intensified winds at the latest Pleistocene leading edge of the advancing Sinai–Negev erg. Quaternary Research 74, 121-131.

Enzel, Y., Amit, R., Dayan, U., Crouvi, O., Kahana, R., Ziv, B., Sharon, D., 2008. The climatic and physiographic controls of the eastern Mediterranean over the late Pleistocene climates in the southern Levant and its neighboring deserts. Global and Planetary Change 60, 165-192.

Eshel, G., Cane, M.A., Farrell, B.F., 2000. Forecasting eastern Mediterranean droughts. Monthly Weather Review 128, 3618-3630.

Faust, D., Yanes, Y., Willkommen, T., Roettig, C., Richter, D., Richter, D., Suchodoletz, H.v., Zöller, L., 2015. A contribution to the understanding of late Pleistocene dune sand-paleosol-sequences in Fuerteventura (Canary Islands). Geomorphology 246, 290-304.

Fitzsimmons, K.E., Magee, J.W., Amos, K.J., 2009. Characterisation of aeolian sediments from the Strzelecki and Tirari Deserts, Australia: Implications for reconstructing palaeoenvironmental conditions. Sedimentary Geology 218, 61-73.

Fornós, J.J., Clemmensen, L.B., Gómez-Pujol, L., Murray, A.S., 2009. Late Pleistocene carbonate aeolianites on Mallorca, Western Mediterranean: a luminescence chronology. Quaternary Science Reviews 28, 2697-2709.

Frechen, M., Dermann, B., Beonigk, W., Ronen, A., 2001. luminesence chronology of the aeolianites from the section at givat olga-coastal plain of israel. Quaternary Science Reviews 20, 805-809.

Frechen, M., Neber, A., Dermann, B., Alexander, T., Boenigk, W., Raban, A., 2002. Chronostratigraphy of aeolianites fromthe Sharon Coastal Plain of Israel. Quaternary International, 31-44.

Galili, E., Dahari, U., Sharvit, J., 1993. Underwater surveys and rescue excavations along the Israeli coast. The International Journal of Nautical Archaeology 22, 61-77.

Galili, E., Nir, Y., 1993. The submerged Pre-Pottery Neolithic water well ofAtlit-Yam, northern Israel and its palaeoenviromental implications. The Holocene 3, 265-270.

Galili, E., Weinstein-Evron, M., 1985. Prehistory and paleoenvironments of submerged sites along the Carmel coast of Israel. Paleorient 11, 37-52.

Galili, E., Zviely, D., Ronen, A., Mienis, H.K., 2007. Beach deposits of MIS 5e high sea stand as indicators for tectonic stability of the Carmel coastal plain, Israel. Quaternary Science Reviews 26, 2544-2557.

Goodfriend, G.A., Magaritz, M., 1988. Palaeosols and late Pleistocene rainfall fluctuations in the Negev Desert. Nature 332, 144-146.

Gvirtzman, G., Netser, M., Katsav, E., 1998. Last-Glacial to Holocene kurkar ridges, hamra soils, and dune fields in the coastal belt of central Israel. Israel Journal of Earth Sciences 47, 27-46.

Gvirtzman, G., Shachnai, E., Bakler, N., Ilani, S., 1983. Stratigraphy of the Kukar group (Quaternary) of the coastal palin of Israel. Geological Survey of Israel, Current Research, 70-82.

Gvirtzman, G., Wieder, M., 2001. Climate of the last 53,000 years in the eastern med based on soil-sequence Stratigraphy in coastla plain Israel. Quaternary Science Reviews 20, 1827-1849.

Huntley, D., Hutton, J., Prescott, J., 1993. The stranded beach-dune sequence of south-east South Australia: a test of thermoluminescence dating, 0–800 ka. Quaternary Science Reviews 12, 1-20.

Huntley, D., Hutton, J., Prescott, J., 1994. Further thermoluminescence dates from the dune sequence in the southeast of South Australia. Quaternary Science Reviews 13, 201-207.

Huntley, D.J., Prescott, J.R., 2001. Improved methodology and new thermoluminescence ages for the dunw sequance in the south-east south Australia. Quaternary Science Reviews 20, 687-699.

Hyams-Kaphzan, O., Almogi-Labin, A., Sivan, D., Benjamini, C., 2008. Benthic foraminifera assemblage change along the southeastern Mediterranean inner shelf due to fall-off of Nile-derived siliciclastics. Neues Jahrbuch für Geologie und Paläontologie-Abhandlungen 248, 315-344.

Issar, A., Zohar, M., 2004. Climate Change-Environment and Civilization in the Middle East: Environment and Civilization in the Middle East. Springer Science & Business Media.

Issar, A.S., 2004. Climate changes during the Holocene and their impact on hydrological systems. Cambridge University Press.

Kadosh, D., Sivan, D., Kutiel, H., Weinstein-Evron, M., 2004. A late quaternary paleoenvironmental sequence from Dor, Carmel coastal plain, Israel. Palynology 28, 143-157.

Lambeck, K., Bard, E., 2000. Sea-level change along the French Mediterranean coast for the past 30,000 years. Earth and Planetary Science Letters 175, 203-222.

Lambeck, K., Purcell, A., 2005. Sea-level change in the Mediterranean Sea since the LGM: model predictions for tectonically stable areas. Quaternary Science Reviews 24, 1969-1988.

Langgut, D., Almogi-Labin, A., Bar-Matthews, M., Weinstein-Evron, M., 2011. Vegetation and climate changes in the South Eastern Mediterranean during the Last Glacial-Interglacial cycle (86 ka): new marine pollen record. Quaternary Science Reviews 30, 3960-3972.

Langgut, D., Finkelstein, I., Litt, T., 2013. Climate and the Late Bronze Collapse: New Evidence from the Southern Levant. Tel Aviv 40, 149-175.

Langgut, D., Finkelstein, I., Litt, T., Neumann, F.H., Stein, M., 2015. Vegetation and Climate Changes during the Bronze and Iron Ages (~3600–600 BCE) in the Southern Levant Based on Palynological Records. Radiocarbon 57, 217-235.

Larrasoaña, J.C., Roberts, A.P., Rohling, E.J., 2008. Magnetic susceptibility of eastern Mediterranean marine sediments as a proxy for Saharan dust supply? Marine Geology 254, 224-229.

Lindhorst, S., Betzler, C., 2016. The climate-archive dune: Sedimentary record of annual wind intensity. Geology, G38093.38091.

Litt, T., Ohlwein, C., Neumann, F.H., Hense, A., Stein, M., 2012. Holocene climate variability in the Levant from the Dead Sea pollen record. Quaternary Science Reviews 49, 95-105.

Maher, B.A., 2011. The magnetic properties of Quaternary aeolian dusts and sediments, and their palaeoclimatic significance. Aeolian Research 3, 87-144.

Mann, C.C., 2000. Earthmovers of the Amazon. Science 287, 786-789.

Mart, Y., Belknap, D.F., 1991. Origin of Late Pleistocene Submerged Marine Terraces on the outer continental shelf. Geo-Marine Letters.

Mauz, B., Elmejdoub, N., Nathan, R., Jedoui, Y., 2009. Last interglacial coastal environments in the Mediterranean–Saharan transition zone. Palaeogeography, Palaeoclimatology, Palaeoecology 279, 137-146.

Mauz, B., Fanelli, F., Elmejdoub, N., Barbieri, R., 2012. Coastal response to climate change: Mediterranean shorelines during the Last Interglacial (MIS 5). Quaternary Science Reviews 54, 89-98.

Mauz, B., Hijma, M.P., Amorosi, A., Porat, N., Galili, E., Bloemendal, J., 2013. Aeolian beach ridges and their significance for climate and sea level: Concept and insight from the Levant coast (East Mediterranean). Earth-Science Reviews 121, 31-54.

Mendoza, U., Ayres Neto, A., C. Abuchacra, R., Fernandes Barbosa, C., G. Figueiredo, A., C. Gomes, M., Belem, A.L., Capilla, R., S. Albuquerque, A.L., 2014. Geoacoustic character, sedimentology and chronology of a cross-shelf Holocene sediment deposit off Cabo Frio, Brazil (southwest Atlantic Ocean). Geo-Marine Letters 34, 297-314.

Moshier, S., Master, D., Leport, J., Wheatley, D., Felker, B., Lavigne, E., College, W., 2010. Reconstruction of the Ancient Landscapes and Paleoenvitonments of the geological foundations of the ancient seaport Ashkelon, Israel, GSA Annual Meeting & Exposition, Minneapolls, Minnesota USA.

Muhs, D.R., Bettis, I.I.I.E.A., 2003. Quaternary loess-Paleosol sequences as examples of climate-driven sedimentary extremes. Geological Society of America 370, 53-74.

Munyikwa, K., 2005. Synchrony of Southern Hemisphere Late Pleistocene arid episodes: a review of luminescence chronologies from arid aeolian landscapes south of the Equator. Quaternary Science Reviews 24, 2555-2583.

Pelle, T., Scarciglia, F., Di Pasquale, G., Allevato, E., Marino, D., Robustelli, G., La Russa, M.F., Pulice, I., 2013. Multidisciplinary study of Holocene archaeological soils in an upland Mediterranean site: Natural versus anthropogenic environmental changes at Cecita Lake, Calabria, Italy. Quaternary International 303, 163-179.

Peterson, C.D., Vanderburgh, S., Roberts, M.C., Jol, H.M., Phipps, J., Twichell, D.C., 2010. Composition, age, and depositional rates of shoreface deposits under barriers and beach plains of the Columbia River littoral cell, USA. Marine Geology 273, 62-82.

Picard, L., 1943. Structure and evolution of Palestine. Bull. Geol. Dept. Hebrew Univ., Jerusalem 4, 1-134.

Pomerancblum, M., 1966. The distribution of heavy minerals and their hydraulic equivalents in sediments of the Mediterranean continental shelf of Israel. Journal of Sedimentary Research 36.

Porat, N., Sivan, D., Zviely, D., 2008. Late Holocene embayment infill and shoreline migration, Haifa Bay, Eastern Mediterranean. Israel Journal of Earth Sciences 57, 21-31.

Porat, N., Wintle, A.G., Ritte, M., 2004. Mode and timing of kurkar and hamra formation, central coastal plain, Israel. Israel Journal of Earth Sciences 53, 13-25.

Preusser, F., Radies, D., Matter, A., 2002. A 160,000-year record of dune develop and Atmospheric Circulation in the Southern Arabia. Science 296, 2018-2020.

Raban, A., 2007. Ancient harbors of the Mediterranean, In: Artzy M, Goodman B, Gal Z (Eds.), The Harbor of Sebastos in its Roman Mediterranean context. BAR International Series, Oxford, pp. 1-48.

Ramsay, J., Holum, K., 2015. An archaeobotanical analysis of the Islamic period occupation at Caesarea Maritima, Israel. Vegetation History and Archaeobotany 24, 655-671.

Robinson, S.A., Black, S., Sellwood, B.W., Valdes, P.J., 2006. A review of palaeoclimates and palaeoenvironments in the Levant and Eastern Mediterranean from 25,000 to 5000 years BP: setting the environmental background for the evolution of human civilisation. Quaternary Science Reviews 25, 1517-1541.

Rodriguez, A.B., Simms, A.R., Anderson, J.B., 2010. Bay-head deltas across the northern Gulf of Mexico back step in response to the 8.2ka cooling event. Quaternary Science Reviews 29, 3983-3993.

Rohling, E.J., Foster, G.L., Grant, K.M., Marino, G., Roberts, A.P., Tamisiea, M.E., Williams, F., 2014. Sea-level and deep-sea-temperature variability over the past 5.3 million years. Nature 508, 477-482.

Rose, J., Meng, X., Watson, C., 1999. Palaeoclimate and palaeoenvironmental responses in the western Mediterranean over the last 140 ka: evidence from Mallorca, Spain. Journal of the Geological Society 156, 435-448.

Roskin, J., Porat, N., Tsoar, H., Blumberg, D.G., Zander, A.M., 2011. Age, origin and climatic controls on vegetated linear dunes in the northwestern Negev Desert (Israel). Quaternary Science Reviews 30, 1649-1674.

Roskin, J., Sivan, D., Shtienberg, G., Roskin, E., Porat, N., Bookman, R., 2015. Natural and human controls of the Holocene evolution of the beach, aeolian sand and dunes of Caesarea (Israel). Aeolian Research 19, 65-85.

Rossignol-Strick, M., 1995. Sea-land correlation of pollen records in the eastern Mediterranean for the glacial-interglacial transition: biostratigraphy versus radiometric time-scale. Quaternary Science Reviews 14, 893-915.

Rossignol-Strick, M., 1999. The Holocene climatic optimum and pollen records of sapropel 1 in the eastern Mediterranean, 9000–6000BP. Quaternary Science Reviews 18, 515-530.

Rowe, M.P., Bristow, C.S., 2015a. Landward-advancing Quaternary eolianites of Bermuda. Aeolian Research 19, 235-249.

Rowe, M.P., Bristow, C.S., 2015b. Sea-level controls on carbonate beaches and coastal dunes (eolianite): Lessons from Pleistocene Bermuda. Geological Society of America Bulletin 127, 1645-1665.

Sade, A.R., Hall, J.K., Amit, G., Golan, A., Gur-Arieh, L., Tibor, G., 2006. The Israel national bathymetric survey—A new look at the seafloor off Israel. Israel Journal of Earth Sciences 55, 185-187.

Sander, L., Fruergaard, M., Koch, J., Johannessen, P.N., Pejrup, M., 2015. Sedimentary indications and absolute chronology of Holocene relative sea-level changes retrieved from coastal lagoon deposits on Samsø, Denmark. Boreas 44, 706-720.

Schattner, U., Gurevich, M., Kanari, M., Lazar, M., 2015. Levant jet system—effect of post LGM seafloor currents on Nile sediment transport in the eastern Mediterranean. Sedimentary Geology 329, 28-39.

Schattner, U., Lazar, M., Tibor, G., Ben-Avraham, Z., Makovsky, Y., 2010. Filling up the shelf — A sedimentary response to the last post-glacial sea rise. Marine Geology 278, 165-176.

Sivan, D., Elyahu, D., Raban, A., 2004a. Late Pleistocene to Holocene wetlands now covered by sand, along the Carmel Coast of Israel, and their relation to Human settlement- An example from the coastal site of Dor. Journal of Coastal Research 20, 1035-1048.

Sivan, D., Greenbaum, N., Cohen-Seffer, R., Sisma-Ventura, G., Almogi-Labin, A., 2011. The origin and disappearance of the late Pleistocene–early Holocene short-lived coastal wetlands along the Carmel coast, Israel. Quaternary Research 76, 83-92.

Sivan, D., Gvirtzman, G., Sass, E., 1999. Quaternary Stratigraphy and Paleogeography of the Galilee Coastal Plain, Israel. Quaternary Research 51, 280-294.

Sivan, D., Lambeck, K., Toueg, R., Raban, A., Porath, Y., Shirman, B., 2004b. Ancient coastal wells of Caesarea Maritima, Israel, an indicator for relative sea level changes during the last 2000 years. Earth and Planetary Science Letters 222, 315-330.

Sivan, D., Porat, N., 2004. Evidence from luminescence for Late Pleistocene formation of calcareous aeolianite (kurkar) and paleosol (hamra) in the Carmel Coast, Israel. Palaeogeography, Palaeoclimatology, Palaeoecology 211, 95-106.

Sivan, D., Sisma-Ventura, G., Greenbaum, N., Bialik, O.M., Williams, F.H., Tamisiea, M.E., Rohling, E.J., Frumkin, A., Avnaim-Katav, S., Shtienberg, G., Stein, M., 2016. Eastern Mediterranean sea levels through the last interglacial from a coastal-marine sequence in northern Israel. Quaternary Science Reviews 145, 204-225.

Sivan, D., widowinski, S., Lambeck, K., Galili, E., Raban, A., 2001. Holocene sea level changes based on archeological sites off northen israel Palaeogeography, Palaeoclimatology, Palaeoecology 167, 101-117.

Stieglitz, R., 1996. Stratonos Pyrgos - MigdalSar - Sebastos: history and archaeology, In: Rabban, A., Holum, K.G. (Eds.), Caesarea Maritima - retrospective after two millennia. Brill, Leiden, pp. 593-608.

Stoker, M.S., Bradwell, T., Howe, J.A., Wilkinson, I.P., McIntyre, K., 2009. Lateglacial ice-cap dynamics in NW Scotland: evidence from the fjords of the Summer Isles region. Quaternary Science Reviews 28, 3161-3184.

Taxel, I., 2013. The Byzantine-early Islamic transition on the Palestinian coastal plain: a re-evaluation of the archaeological evidence. Semitica et Classica, 73-106.

Thiel, C., Coltorti, M., Tsukamoto, S., Frechen, M., 2010. Geochronology for some key sites along the coast of Sardinia (Italy). Quaternary International 222, 36-47.

Toker, E., Sivan, D., Stern, E., Shirman, B., Tsimplis, M., Spada, G., 2012. Evidence for centennial scale sea level variability during the Medieval Climate Optimum (Crusader Period) in Israel, eastern Mediterranean. Earth and Planetary Science Letters 315-316, 51-61.

Tripaldi, A., Forman, S.L., 2007. Geomorphology and chronology of Late Quaternary dune fields of western Argentina. Palaeogeography, Palaeoclimatology, Palaeoecology 251, 300-320.

Tsakalos, E., 2016. Geochronology and exoscopy of quartz grains in environmental determination of coastal sand dunes in SE Cyprus. Journal of Archaeological Science: Reports 7, 679-686.

Woods, W.I., 1995. Comments of the Black Earths of Amazonia, Papers and Proceedings of Applied Geography Conferences. APPLIED GEOGRAPHY CONFERENCES, pp. 159-166.

Yaalon, D.H., 1987. Saharan dust and desert loess: effect on surrounding soils. Journal of African Earth Sciences (1983) 6, 569-571.

Yaalon, D.H., 1997. Soils in the Mediterranean region- what makes them diffrent? Catena 28, 157-169.

Yoo, D.G., Kim, S.P., Chang, T.S., Kong, G.S., Kang, N.K., Kwon, Y.K., Nam, S.L., Park, S.C., 2014. Late Quaternary inner shelf deposits in response to late Pleistocene–Holocene sea level changes: Nakdong River, SE Korea. Quaternary International 344, 156-169.

Zazo, C., Goy, J.L., Dabrio, C.J., Bardají, T., Hillaire-Marcel, C., Ghaleb, B., González-Delgado, J.-Á., Soler, V., 2003. Pleistocene raised marine terraces of the Spanish Mediterranean and Atlantic coasts: records of coastal uplift, sea-level highstands and climate changes. Marine Geology 194, 103-133.

Zazo, C., Goy, J.L., Dabrio, C.J., Lario, J., González-Delgado, J.A., Bardají, T., Hillaire-Marcel, C., Cabero, A., Ghaleb, B., Borja, F., Silva, P.G., Roquero, E., Soler, V., 2013. Retracing the Quaternary history of sea-level changes in the Spanish Mediterranean–Atlantic coasts: Geomorphological and sedimentological approach. Geomorphology 196, 36-49.

Zecchin, M., Baradello, L., Brancolini, G., Donda, F., Rizzetto, F., Tosi, L., 2008. Sequence stratigraphy based on high-resolution seismic profiles in the late Pleistocene and Holocene deposits of the Venice area. Marine Geology 253, 185-198.

Zecchin, M., Brancolini, G., Tosi, L., Rizzetto, F., Caffau, M., Baradello, L., 2009. Anatomy of the Holocene succession of the southern Venice lagoon revealed by very high-resolution seismic data. Continental Shelf Research 29, 1343-1359.

Zhou, X., Sun, L., Huang, W., Liu, Y., Jia, N., Cheng, W., 2014. Relationship between magnetic susceptibility and grain size of sediments in the China Seas and its implications. Continental Shelf Research 72, 131-137.

Zviely, D., Kit, E., Klein, M., 2007. Longshore sand transport estimates along the Mediterranean coast of Israel in the Holocene. Marine Geology 238, 61-73.

Zviely, D., Kit, E., Rosen, B., Galili, E., Klein, M., 2009. Shoreline migration and beach-nearshore sand balance over the last 200 years in Haifa Bay (SE Mediterranean). Geo-Marine Letters 29, 93-110.

Zviely, D., Sivan, D., Ecker, A., Bakler, N., Rohrlich, V., Galili, E., Boarreto, E., Klein, M., Kit, E., 2006. Holocene evolution of the Haifa Bay area, Israel, and its influence on ancient tell settlements, The Holocene, pp. 849-861.

2. Late-Pleistocene evolution of the continental shelf of central Israel, a case study from Hadera

Gilad Shtienberg, Justin K. Dix, Nicolas Waldmann, Yizhaq Makovsky, Arik Golan, and Dorit Sivan, 2016. Late-Pleistocene evolution of the continental shelf of central Israel, a case study from Hadera. Geomorphology 261, 200-211 (dx.doi.org/10.1016/j.geomorph.2016.03.008; Published).

<u>Contribution statement</u>

G. Shtienberg jointly conceived the study, designed the offshore geophysical survey and terrestrial drillings with D. Sivan and J. Dix. Collection and integration of existing borehole records, topographic and geophysical data was undertaken by G. Shtienberg. The offshore survey was carried out by G. Shtienberg with A. Golan while the drilling was conducted by G. Shtienberg under the direction of D. Sivan. Seismic processing was performed by Y. Makovsky and the interpretation was done by G. Shtienberg under the guidance of J. Dix and N. Waldmann. Sedimentological interpretation was conducted by G. Shtienberg under the guidance of D. Sivan and J. Dix. The manuscript was drafted and edited by G. Shtienberg with review contributions from D. Sivan, J. Dix, N. Waldmann and Y. Makovsky.

2.1. Abstract

Sea-level fluctuations are a dominant mechanism that control coastal environmental changes through time. This is especially the case for the successive regressions and transgressions over the last interglacial cycle, which have shaped the deposition, preservation and erosion patterns of unconsolidated sediments currently submerged on continental shelves. The current study focuses on creating an integrated marine and terrestrial geophysical and litho-stratigraphic framework of the coastal zone of Hadera, north-central Israel. This research presents a case study, investigating the changing sedimentological units in the study area. Analysis suggest these represent various coastal environments and were deposited during times of lower than present sea level and during the later stages of the Holocene transgression.

A multi-disciplinary approach was applied by compiling existing elevation raster grids, bathymetric charts, one hundred lithological borehole data-sets, and a 110 km-long sub-bottom geophysical survey. Based on seismic stratigraphic analysis, observed geometries, and reflective appearances, six bounding surfaces and seven seismic units were identified and characterized. These seismic units have been correlated with the available borehole data to produce a chronologically constrained lithostratigraphy for the area. This approach allowed us to propose a relationship between the lithological units and sea-level change and thus enable the reconstruction of Hadera coastal evolution over the last ~100 ka. This reconstruction suggests that the stratigraphy is dominated by lowstand aeolian and fluvial terrestrial environments, subsequently transgressed during the Holocene. The results of this study provide a valuable framework for future national strategic shallow-water infrastructure construction and also for the possible locations of past human settlements in relation to coastal evolution through time.

Key words

Shallow geophysics; Continental shelf; Late Pleistocene-Holocene sequence; Israel; Coastal and marine geology

2.2. Introduction

The “coastal” zone, which encompasses both current terrestrial and marine environments, frequently contains sedimentary sequences which can provide detailed records of changing depositional environments and ecosystems in response to climate change and sea-level fluctuations. Prior studies that have examined these coastal areas and their response to past sea level and climate change have largely focused on sheltered environments such as estuaries and deltas, as the preservation potential within these settings is exceptionally high (e.g. Belknap and Kraft, 1985; Allard et al., 2009; Zecchin et al., 2009). More recently researchers have started to examine the response of open coastlines to these same drivers, with particular focus on the response to the Late Pleistocene to Holocene transgression (e.g. Zecchin et al., 2008; Yoo et al., 2014; Mendoza et al., 2014). However, these latter studies have focused exclusively on the current offshore record with relatively few attempts being made to tie together the terrestrial and littoral components of the coastal zone (Bersezio et al., 2007; Stoker et al., 2009; Peterson et al., 2010; Twichell et al., 2010; Vanderburgh et al., 2010; Anderson et al., 2014; Cawthra et al., 2014). The partial mapping and dating of open coastline shallow shelf sediments and the complexities in correlating to onshore equivalents, posed difficulties to fully understand the global and local factors shaping and altering the shallow marine areas (Bates et al., 2007; Hampson and Storms, 2008).

This paper focuses on a case study, from the open coastline of central Israel and attempts to combine data from both the marine and terrestrial components of its coastal zone. The Israeli coast (Fig. 2.1) suits this kind of study as: it is micro-tidal (± 0.40 m) (Emery and Neev, 1960; Davis and Hayes, 1984; Golik and Rosen, 1999); its continental shelf is characterized by a relatively narrow (10 to 23 km) and moderately steep (0.5° to 0.8°) strip of mostly unconsolidated sediments that have been largely supplied by a single dominant source since the Pliocene (the Nile River e.g. Emery and Bentor, 1960; Neev et al., 1976; Almagor and Hall, 1984; Almagor, 1993; Stanley and Warne, 1998); it is considered tectonically stable since MIS5e (Sivan et al., 1999; Galili et al., 2007; Mauz et al., 2013), with low isostatic rates of 0.1 mm/year, at least in the Holocene (Sivan et al., 2001; Anzidei et al., 2011; Toker et al., 2012); there is currently little known about the timing and extent of the shallow shelf subsurface stratigraphy.

Inquiry of the shallow shelf stratigraphy is achieved through a combination of dense offshore sub-bottom profiles, bathymetry (from water depth of -5 to -30 m), topography data and onshore and offshore cores. The integration and analysis of these data-sets allows the generation of a time-lapse palaeo-environmental reconstruction for the last ~100 ka in the area of Hadera on the central Israeli coast. In addition to providing a detailed case study of coastal change for an open coast setting, this work also provides insight into the process of change in an area that is currently undergoing rapid onshore and offshore infrastructure development. Finally, the knowledge gained from this research also benefits archeologists in evaluating locations suited for finding ancient settlements now submerged under the sea bed.

2.3. Regional setting

The width of Israel's coastal plain varies from a few hundred meters, in its northern parts up to 15 km south of Mt. Carmel (Almagor and Hall, 1984). The morphology of the coast and immediate hinterland of Israel (Fig. 2.1b) is dominated by up to eighteen aeolianite ridges that trend, parallel-subparallel to the current 190 km-long relatively straight coastline. These ridges, which are identified both onshore and offshore (Neev et al., 1978; Almagor et al., 2000; Frechen et al., 2001, 2002, 2004; Sivan and Porat, 2004; Sivan et al., 2004a; Schattner et al., 2010), were formed during the late Pleistocene when sea levels were lower than present and the shelf was exposed (Mauz et al., 2013). The Nile littoral cell system (Emery and Neev, 1960; Pomerancblum, 1966; Davis et al., 2012) supplied quartz-rich sands (with minor litho- and bio-clasts) from the Nile Delta to the Levant shelf (shallower then 40 m water depth). Wave- and wind-induced currents subsequently transported these sediments landward and once on the beach, these sands were blown inland to accumulate on the coastal plain as a series of shore-parallel dunes. Through the dissolution of carbonate skeletal debris within the sand by meteoric waters and its precipitation as calcite cement, the dunes underwent lithification to create the sandstone aeolianites, known locally as Kurkar (Yaalon, 1967; Gavish and Friedman, 1969; Almagor et al., 2000; Mauz et al., 2013). The number and size of these ridges diminishes northward and only three are found onshore west of Mount Carmel (Michelson, 1970; Sneh et al., 1998).

The trough regions between these parallel Kurkar ridges are filled with up to ~20 m thick sequences of unconsolidated sediments. These sediments include additional Nilotic derived aeolian sediments which pedogenized under different climatic conditions (Yaalon, 1997; Gvirtzman et al., 1998; Gvirtzman and Wieder, 2001) to orange silty sand and brown clayey silty sand (locally known as Hamra and Brown-Palaeosol units respectively). These soils are covered by wetland dark silty clays and/or aeolian sand (Gvirtzman et al., 1998; Kadosh et al., 2004, Sivan and Porat; 2004; Sivan et al., 2004a, 2011, Zviely et al., 2006).

While the topmost surface of the Pleistocene Kurkar unit has been chronologically constrained to between ~101 and ~50 ka (Engelmann et al., 2001; Frechen et al., 2004; Sivan and Porat, 2004; Sivan et al., 2004a; Zviely et al., 2006; Roskin et al., 2015) there is no spatial pattern to the varying ages of the Kurkar ridges and the relationships between them and former sea-level changes have still not been properly established (Sivan and Porat, 2004; Mauz et al., 2013). Most of our understanding of the Kurkar, its chronology and morphology, comes from studies carried out on exposed terrestrial outcrops, leaving the extent and ages of the offshore submerged Kurkar mostly unknown. Offshore, the Kurkar has only been sporadically mapped by seismic profiling (Neev et al., 1978; Belknap and Mart, 1999; Almagor et al., 2000; Schattner et al., 2010) and even more limited sea floor observations carried out by ROVs and side scan sonar (Mart and Belknap, 1991; Belknap and Mart, 1999).

The overlying Hamra and Brown-Palaeosol units have been shown to have a wide range of ages, from ~87 to ~55 ka and ~50 to ~11 ka respectively (Frechen et al., 2001, 2004; Gvirtzman and Wieder, 2001; Cohen-Seffer et al., 2005; Roskin et al., 2015), so are sometimes synchronous with the Kurkar's formation (Sivan and Porat, 2004) and sometimes younger. These two units contain various sub-units and hiatuses, which probably indicate long exposure to pedogenic processes, hence impeding proper lateral chronostratigraphical correlations (Sivan and Porat, 2004). In the coastal areas of north and central Israel the Hamra and Brown-Palaeosol units reach a maximum thickness of 8 m. Particle size and hue values change spatially and temporally, apparently following the palaeotopography (Sivan and Porat, 2004) and/or dictated by phases of wet/dry palaeoclimate (Neev et al., 1978; Wieder et al., 1997; Yaalon, 1997; Gvirtzman et al., 1998).

A dark silty clay unit, rich in organic material, interpreted to originate from freshwater to brackish wetland marshes, unconformably overlies the Hamra/Brown-Palaeosol sequence (Galili and Weinstein-Evron, 1985; Sivan et al., 2011). Dating of this unit onshore and in two shallow offshore core locations in southern and north-central Israel (Fig. 2.1), reveals that the wetlands prevailed between 14.4 to 8.4 cal. kyr BP (Neev et al., 1978; Sivan et al., 1999, 2004a; Porat et al., 2003a). The creation of these wetlands and the underlying erosional unconformity of the Hamra/Brown-Palaeosol units may be related to a combination of early Holocene wet climate conditions, sand dune obstruction of fluvial outlets due to increasing sedimentation rates, as well as the indirect effects of sea-level rise on groundwater levels (Kadosh et al., 2004; Cohen-Seffer et al., 2005; Sivan et al., 2011).

Rohling et al. (2014) have produced the longest (up to 5.3 Myr) continuous Mediterranean, eustatic, sea-level record based on $\delta^{18}O$ from carbonate microfossils, whilst Lambeck and Purcell (2005) present a GIA model for the Mediterranean that extends back to the Last Glacial Maximum (LGM; about 20 ka). All other Israeli relative sea-level curves only cover the Holocene (e.g. Sivan et al., 2001). A simplistic reconstruction based on the Rohling et al. (2014) sea level data and the modern day bathymetry of the Israeli continental shelf (used as a lowstand land surface proxy) can give an indication of the extent of shoreline migration over the last ~100 ka. From ~100 ka sea levels dropped from -30 m to a minimum of -135 m during the LGM. Accordingly the shoreline migrated seaward from 3 km at ~100 ka to ~10 km offshore at the LGM. Since the LGM, global sea levels have risen dramatically, reaching ~35 m below present MSL by the beginning of the Holocene. Archaeological observations from the coast of Israel indicate that sea levels continued to rise until ~6 ka to ~7 ka when rates of sea level rise slowed considerably and the shoreline was located ~3 km offshore from its current location. Sea level almost reached its present elevation at ~4 ka (Sivan et al., 2001, 2004b; Anzidei et al., 2011; Toker et al., 2012), and the coastline prograded to reach its present location at ~3 ka (Kadosh et al., 2004; Cohen-Seffer et al., 2005; Zviely et al., 2006, 2007; Porat et al., 2008; Sivan et al., 2011).

The Nile-sediment fluxes responsible for the Kurkar ridges have continued to operate throughout the Holocene and are still dominant today (Ronen et al., 2005; Zviely et al., 2006). Currently, the rates of sand supplied by wind- and wave-induced longshore currents gradually decrease northwards and end in the Haifa Bay depositional sink (Fig. 2.1a; Inman and Jenkins, 1984; Zviely et al., 2006). The initiation and timing of current wind-induced coastal sand build-up is based on luminescence and radiocarbon ages of *in situ* land snails and relative age estimations from archaeological relicts. Dates sampled offshore (Porat et al., 2003b; Goodman-Tchernov et al.,

2009) and in Israel's central coastal plain suggest that the coastal sand unit accumulated since ~6 ka (Fig. 2.1; Engelmann et al., 2001; Frechen et al., 2001; Kadosh et al., 2004; Roskin et al., 2015). The connection between coastal landscape, sedimentological characteristics and human occupation has been determined for the Caesarea-Atlit (Fig. 2.1) coast, during the Pre-Pottery Neolithic B period (that ends at ~8 ka) and the Chalcolithic period (ending ~ 5.1 ka) when humans settled on the dried dark silty clay, while later in the Middle Bronze age IIA period, (~4 ka), they settled on the aeolianite ridges (Galili and Nir, 1993; Galili et al., 1997; Sivan et al., 2004a, 2011).

The area offshore of Hadera was found suitable for conducting a case study aimed at verifying the influence of sea-level changes on an open coastal sedimentary sequence. Moreover, the area is suitable for investigating the relationship between topography, and hydrology with the coastline evolution on the basis of: (1) its particular location between two streams (Taninim and Alexander; Fig. 2.1b), (2) the inclusion of various morphologies (Kurkar ridges, coastal dunes, marshlands and stream), which provide the optimal conditions for studying their interplay with sea level-changes through time.

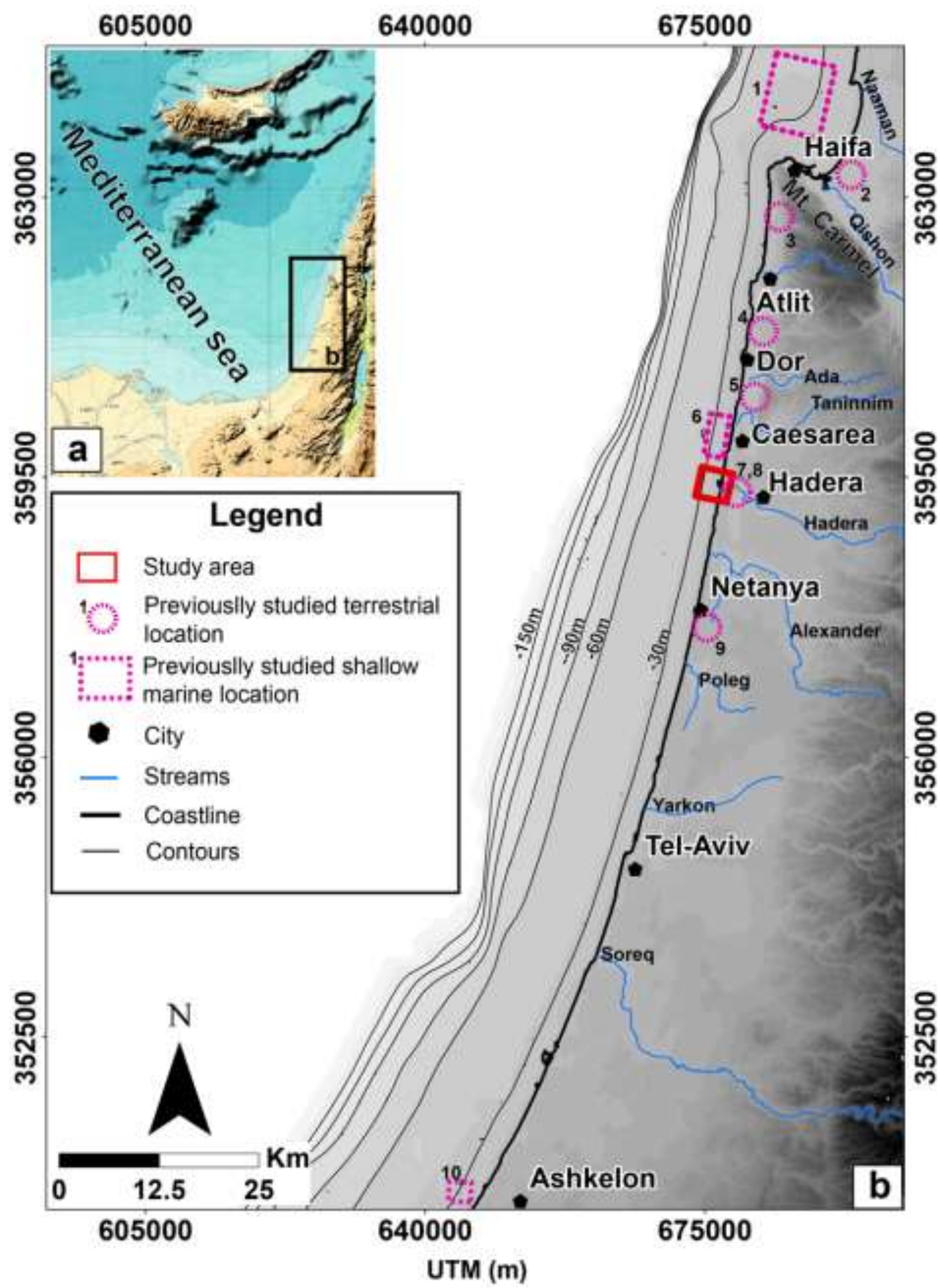

Figure 2.1: Location maps of Israel in SE Mediterranean (1a) and the relevant studies conducted in Israel's coastal and shallow shelf. The black square demonstrates the location of Fig. 1b (1b); The red square represents the study area; the numbered dashed purple circle represent previously studied zones on the terrestrial side; the numbered purple dashed square represents previously studied zones in the shallow shelf area. The previously studied zones are described in the following papers according to their numbering: (1) Schattner et al. (2010); (2) Zviely et al. (2007); (3) Galili and Weistein-Evron (1985); (4) Kadosh et al. (2004); Sivan et al. (2004a); (5) Cohen-Seffer et al. (2005); Sivan et al. (2011); (6) Neev et al. (1978); Goodman-Tchernov et al. (2009); (7) Roskin et al. (2015); (8) Frechen et al. (2001); (9) Engelmann et al. (2001); and (10) Porat et al. (2003a).

2.4. Methods

2.4.1. Compilation of existing datasets

Existing shallow bathymetry, sub-bottom profiling and borehole data (both geotechnical and lithological) were collected from governmental offices, academic institutes and commercial companies. The bathymetric and sub-bottom profiling measurements were undertaken by the Israeli Oceanographic and Limnological Research (IOLR) in 2007 on board of the *RV Adva,* which was equipped by the following devices: a single-beam Odom Echotrack Df-3200 MK2 echo-sounder operating at 209 kHz frequency; and a Datasonic CAP-6600 chirp sub-bottom profiler operating in the frequency range of 2 to 7 kHz with a shot interval of 0.25 sec and a vertical resolution of 0.15 m. A Trimble differential GPS provided navigation at horizontal precisions <1 m (Golan, 2007). The measurements were generally conducted in the E to W direction and consisted of 13 lines perpendicular to the coast, spaced 50 m apart and two shore normal lines extending from elevations of -2 to -28 m (Fig. 2.2), relative to the Israel Land Survey Datum (mILSD).

One hundred terrestrial and offshore boreholes were also made available for the purposes of this study. These were acquired in different surveys since the 1970s ranging in depths from 5 to 50 m below the drilling surface. Out of the 100 boreholes, 40 were drilled offshore on behalf of the Israel Electric Corporation between 1978 and 1980 (see Fig. 2.2 for location).

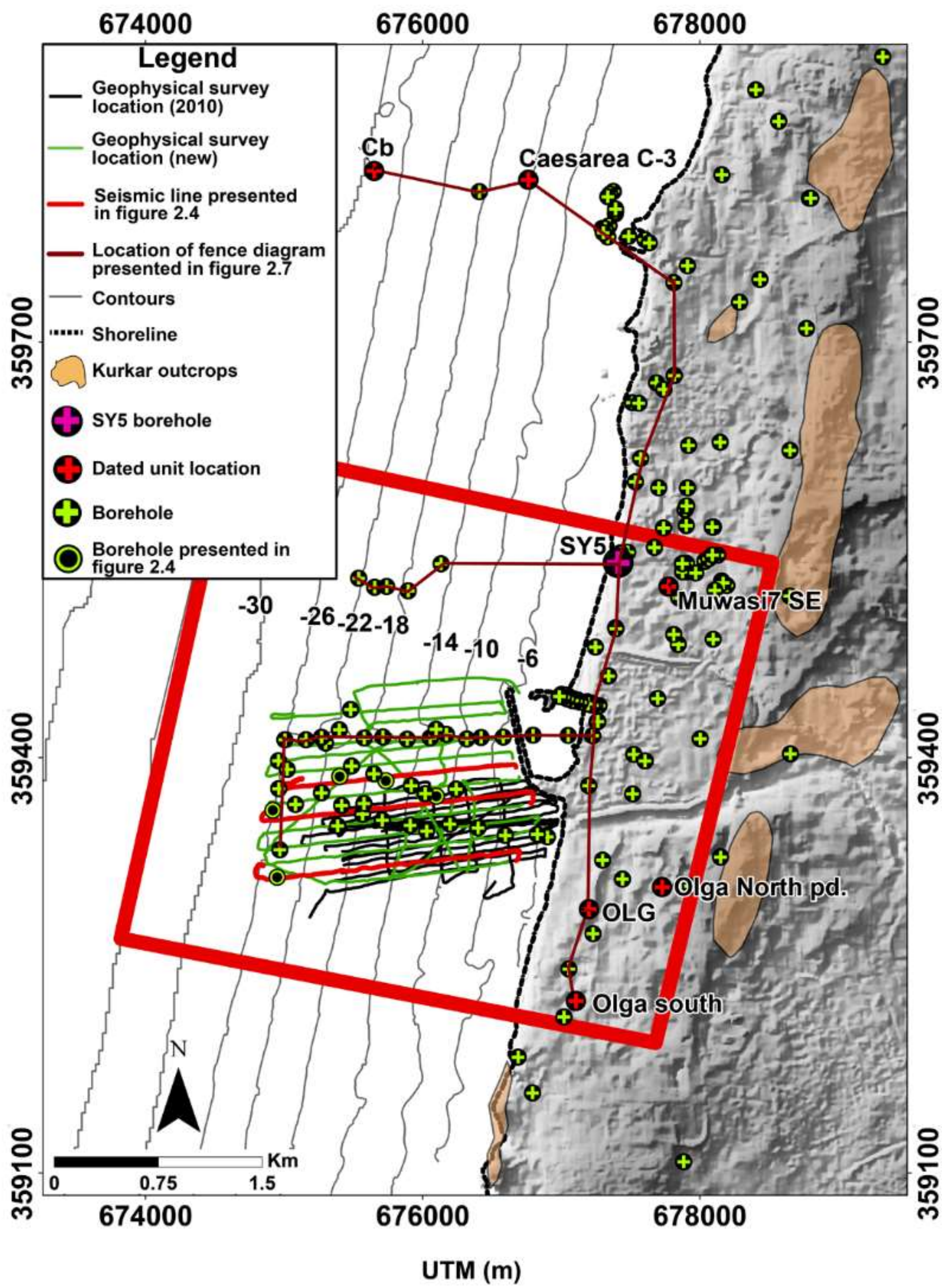

Figure 2.2: Enlargement of the study area showing the location of the boreholes and seismic data. The black circles with a red cross are the locations of dated units from previous studies which include: Cb (Neev et al., 1978), Caesarea C-3 (Goodman-Tchernov et al., 2009), Muwasi 7Se, Olga North bp. Olga south (Roskin et al., 2015), OLG (Frechen et al., 2001). The black circle with the purple cross is the location of borehole SY5; for analysis see Fig. 2.8.

2.4.2. Newly acquired datasets

In order to fill the gaps in the extent of the existing datasets, new geophysical and sedimentological datasets were obtained. The survey was conducted on board *RV Adva* using the equipment and acquisition parameters from the 2010 survey. Over 110 km of seismic profiles were acquired in an area encompassing ~34 km^2. The survey grid consisted of 15 lines perpendicular to the coastline, spaced 100 m apart extending from -4 to -27 mILSD. Spatial referencing were added and interpretation of the seismic profiles were performed in Paradigm and Petrel software packages. Constant velocities of 1500 m/s and 1750 m/s were considered for seawater and unconsolidated sediment, respectively. These are based on published results of a refraction survey, which was conducted in the Hadera's shallow shelf (Almagor and Nir, 1977; Nir, 1979). Both the existing and newly acquired datasets were integrated into a single geospatial database using ArcGIS.

The seismic survey was complemented by core SY5, which retrieved 9.6 m of sediments using a Geo-probe 6620DT direct push corer device 1 km north of Hadera harbor onshore at an elevation of 1.2 mILSD (Fig. 2.2 for location). The borehole location and elevation were measured using a Proflex 500 DGPS with precisions of 1 and 5 cm respectively. The constant datum used through the study enabled to efficiently connect the various datasets and seamlessly link between the shallow shelf and coastal zone. Following drilling operations, core SY5 was transported to the University of Haifa for storage at 4 ˚C. Following this step, the core was sectioned lengthwise for visual lithological description and further sedimentological measurements. Samples for granulometry and Total Carbon (IC/TOC) were retrieved from the main lithological units. The samples were to later be measured using a Malvern laser diffraction particle-size analyzer and a

Primacs^{SLC} TOC Analyzer at the Basin Analysis and Petrophysical Laboratory (PetroLab), the University of Haifa.

2.5. Results

2.5.1. Seismic stratigraphy

The seismic stratigraphic analysis of the shallow continental shelf offshore Hadera reveals seven seismic units:

2.5.1.1. Acoustic Basement (AB)

The acoustic basement (Fig. 2.3a) is characterized by a seismically transparent unit with no internal reflectors, topped by an irregular, uneven and rugged set of reflections (S1; Fig 2.4), which extends over the entire study area from elevations of -4 m to -28 mILSD and dips westwards at ~1.4˚ (Figs. 2.3a, 2.4). A ~N-S striking elongate structural high is recognized at elevations of -24 to -26 mILSD and at a distance of ~1.4 km parallel to the current coastline (Fig. 2.5). This morphological feature has a maximum width of 200 m, with crests that are sitting higher than 8 m above the surrounding surface topography. The main axis of this structure is perpendicularly dissected by five ~3 m deep troughs at water depths of -24 to -26 mILSD.

2.5.1.2. Unit F1

Unit F1 is characterized by an acoustically transparent to semi-transparent seismic facies, occasionally intercalated by low amplitude, high frequency chaotic discontinuous reflections (Fig. 2.3b). The unit thickness varies between 0 to 6 m (Fig. 2.4), and its top is bounded by three high to medium amplitude reflections, marking three irregular surfaces (S2, S3 and S4; Fig. 2.4). The combined surface of F1 (S2, S3 and S4; Fig 2.5) dips westward at an angle of ~1° with an identifiable 400 m wide topographical high which covers the S1's ridge-resembling feature (Figs. 2.4, 2.5). The crest is situated 1.4 km west and parallel to the present shoreline (Fig. 2.5) and has a morphology that dips 2.5° westward. The morphological high divides the surface into two main sloping (< 0.5°) depressions that are located 1 km and 2.1 km from the shoreline with elevations of -25 mILSD and -28 mILSD, respectively. F1 is thickest in the northern trough and is thinnest directly above the surface S1 ridge and 300 m from the present day coastline (Fig. 2.6).

2.5.1.3. Unit F2

Unit F2 (Fig. 2.3c) consists of acoustically semi-transparent and discontinuous low-to-medium amplitude, and occasional high frequency and chaotic, reflections. This seismic unit is bounded between S2 and S5 below and above, respectively, and its thickness varies by up to 3 m. F2 is truncated in the eastern, up slope direction by units F3 (Figs. 2.4b, c) and F4 while the elevation of its top ranges from -30 to -32 mILSD in the westernmost edge of the survey area.

2.5.1.4. Unit F3

Unit F3 (Fig. 2.3d) is found in the northern parts of the survey (Fig. 2.6), and consists of high amplitude, continuous sub-horizontal reflectors and sub-parallel, west-trending clinoforms (Fig. 2.4a-d). F3 represent a lens-shape progradated infill package, toplapping the S5 and downlapping surface S3 (Fig. 2.4). The base of F3 (S3) is truncated landwards by the base of unit F5 (S4). The thickness of the facies varies between 0 and 5 m, being thicker in the southern parts of the S3 depression at elevations of -29 mILSD while it is thinnest above the S1 morphological high at elevations of -17 mILSD and 1250 m from the present day coastline (Fig. 2.6).

2.5.1.5. Unit F4

Unit F4 (Fig. 2.3e) is found only in the southern parts of the survey, and consists of mostly chaotic high amplitude and low frequency reflections (Fig. 2.4e, f). Overall it appears to represent a lens-shape prograded infill package, toplapping the S5 and downlapping surface S3 (Fig. 2.4). The base of F4 (S3) is truncated landwards by the base of Unit F5 (S4). The thickness of the unit varies between 4 and 7 m, being thicker in the southern parts of the S3 depression with elevations of -30 mILSD and thinnest above the S3 morphological high at elevations of -17 mILSD and 1300 m from the present day coastline (Fig. 2.6).

2.5.1.6. Unit F5

Unit F5 (Fig. 2.3f) consists of several continuous sub-horizontal sub-parallel reflections which onlap S4 seawards and toplap S5 landward (Fig. 2.4). These reflections are shoreward bounded by weak to moderate discontinuities and chaotic reflectivity. F5 appears to represent a thin lens-shaped prograded sedimentary fill, which is confined at the bottom by S4. F5 is generally dipping ~0.8˚ seaward, its thickness varies between 0.5 and 4 m, thickest above S1 eastern depression and thinnest above S1 ridge and in its southern and northern boundaries (Figs. 2.5, 2.6).

2.5.1.7. Unit F6

Unit F6 (Fig. 2.3g) is characterized by continuous, medium amplitude, medium frequency, sub-horizontal and sub-parallel reflectors. The reflections onlap the unit's lower boundary S5 shoreward; S5 truncates previously deposited sediments of units 4 and 5 (Fig. 2.4). S5 extends up to 2.1 km from the present shoreline, with elevation ranging between -5 mILSD adjacent to the shoreline to -26 mILSD in its westernmost stretch (Fig. 2.5). The surface has a general westward dip of 0.8˚. F6 thickness varies between 1 and 5 m, is thickest in its northern boundary and at water depths larger than 17 m (Fig. 2.6).

Facies F6 is confined at the top by surface S6 which corresponds to the present-day sea floor. The S6 surface (Fig. 2.5) is generally dipping 0.9º west and its elevation ranges from 0 to -28 mILSD in the westernmost edge of the survey areas. A west-trending linear depression, up to 250 m wide and 3 m deep, is evident at elevations of -7 to -25 mILSD offshore Hadera's power plant harbor (Figs. 2.5, 2.6).

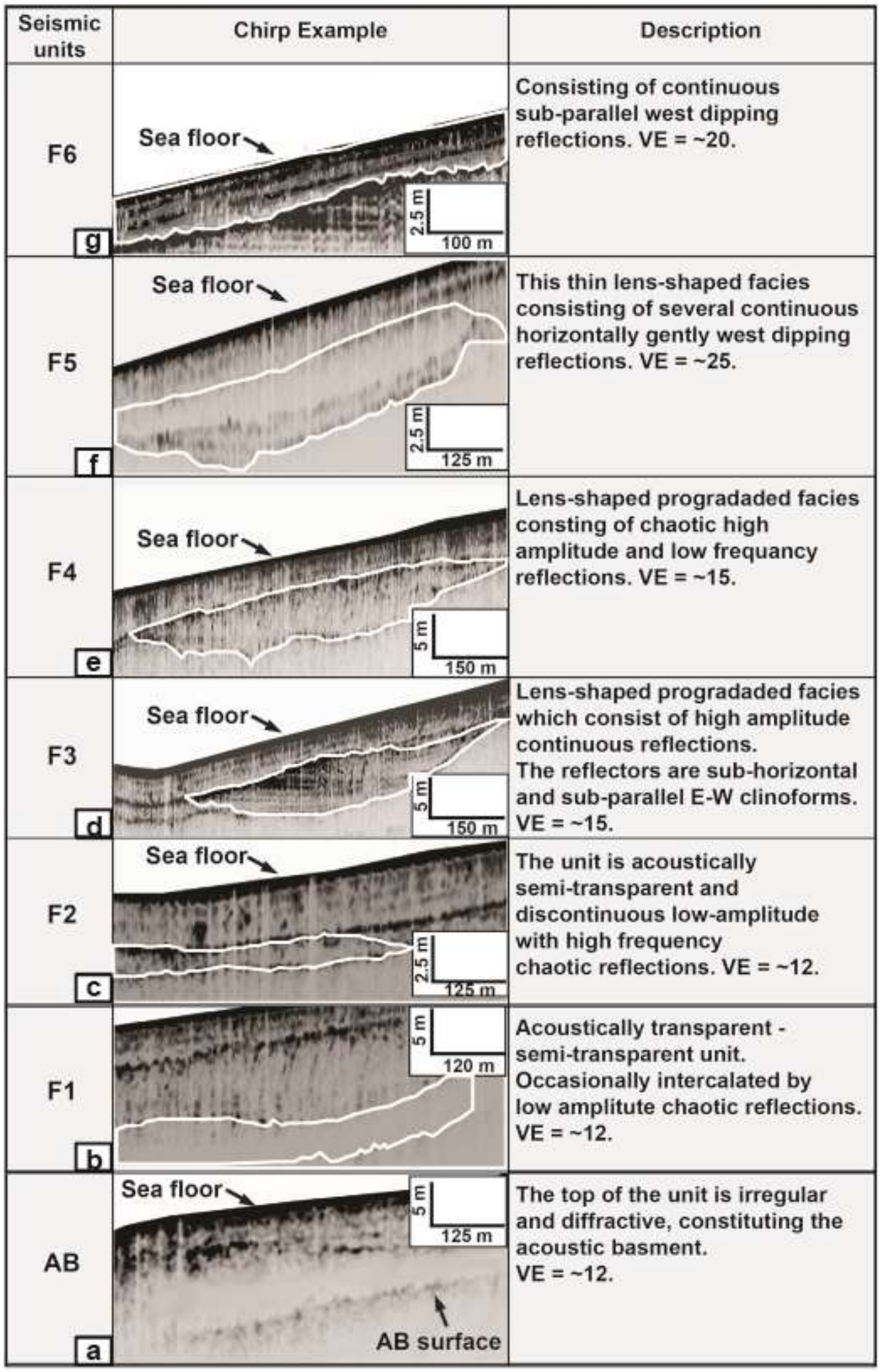

Figure 2.3: Acoustic units identified from the chirp data acquired in Hadera. The facies are highlighted by a white polygon. Horizontal and vertical scales are shown for each example.

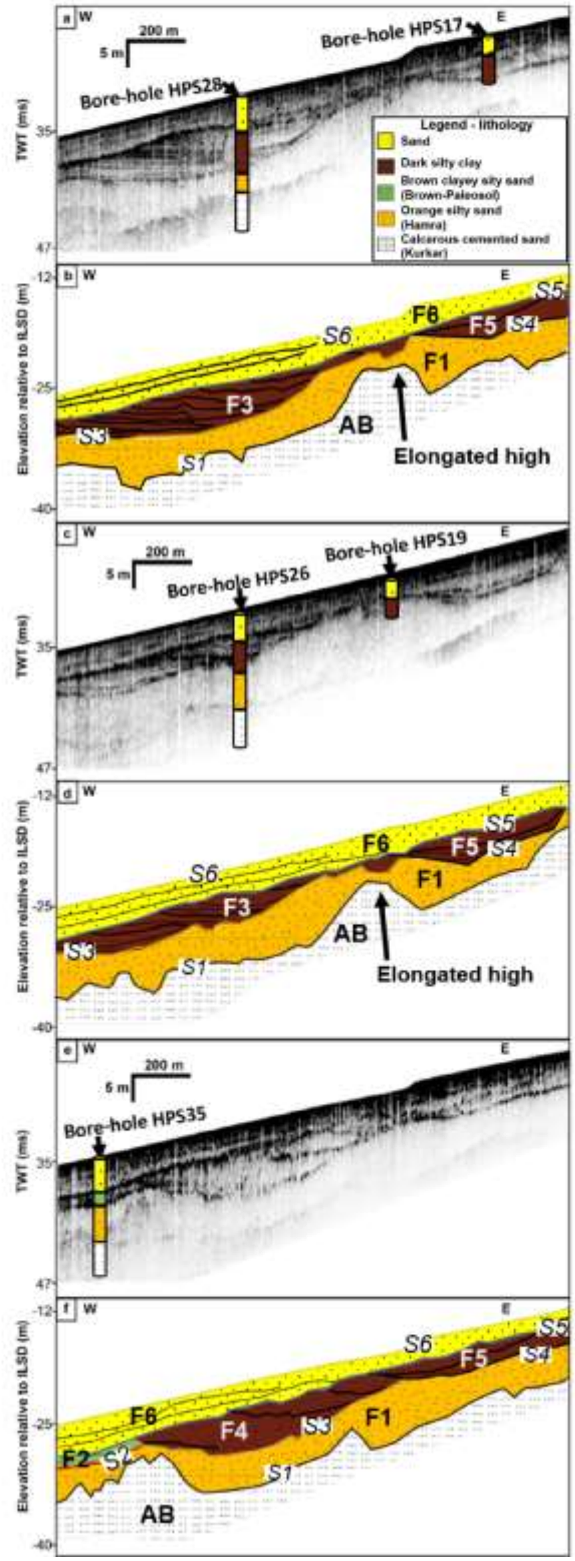

Figure 2.4: Hadera's shallow coastal shore-normal seismic sections (a, c and e) and their interpretation (b, d and f) which was done on the basis of boreholes HPS19, HPS26, HPS35, HPS17 and HPS28. The location of the seismic section and boreholes is displayed in Fig. 2.2.

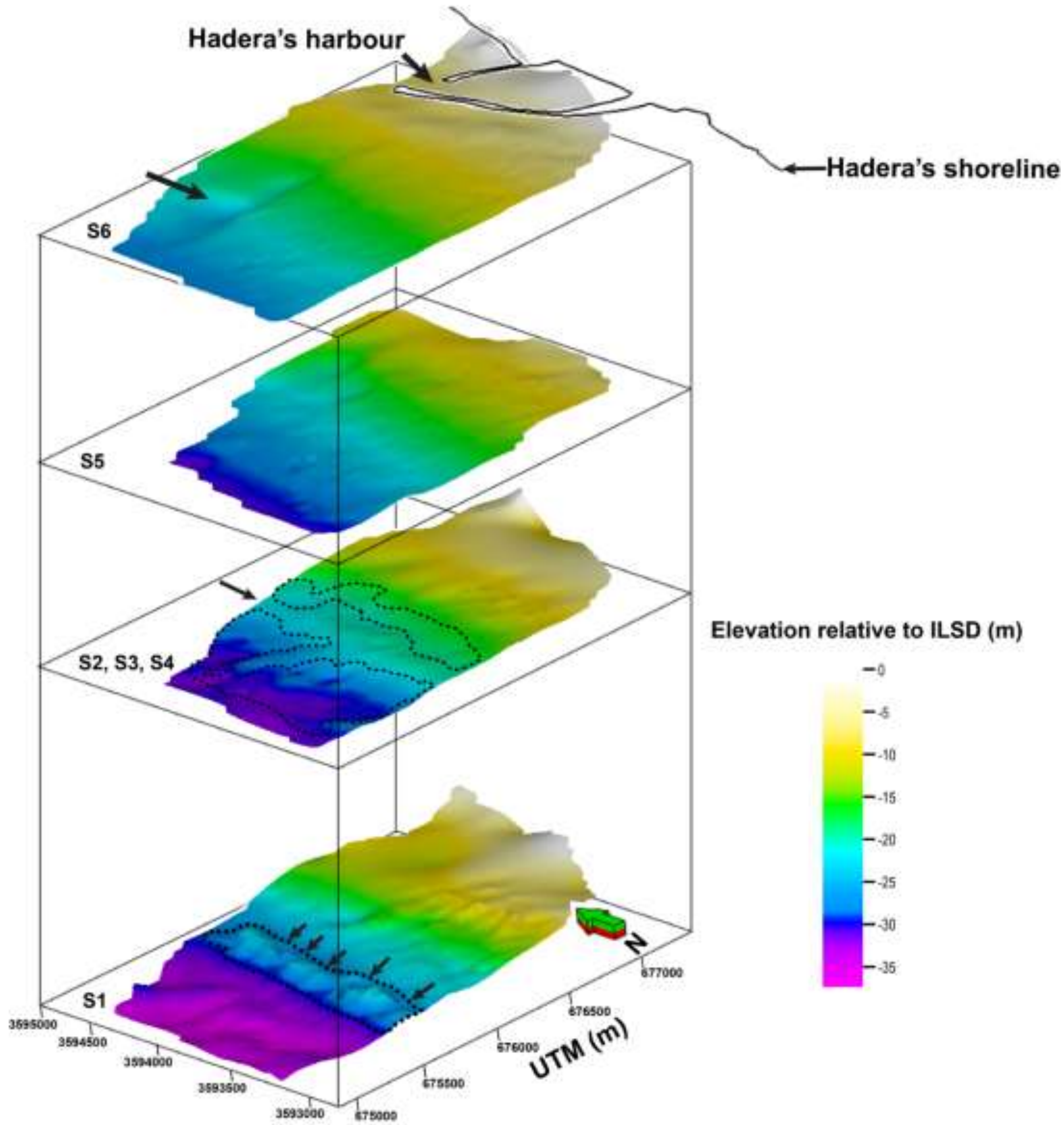

Figure 2.5: Elevation map of the seismic unit surfaces and counterpart features. The elongated-high and five cutting troughs of surface S1 are annotated by a dashed polygon and arrows respectively. The topographical high of the combined surface S2, S3 and S4 is marked by an arrow while the two bordering depressions are annotated by dashed polygons. The west trending linear morphological depression of surface S6 is highlighted by an arrow.

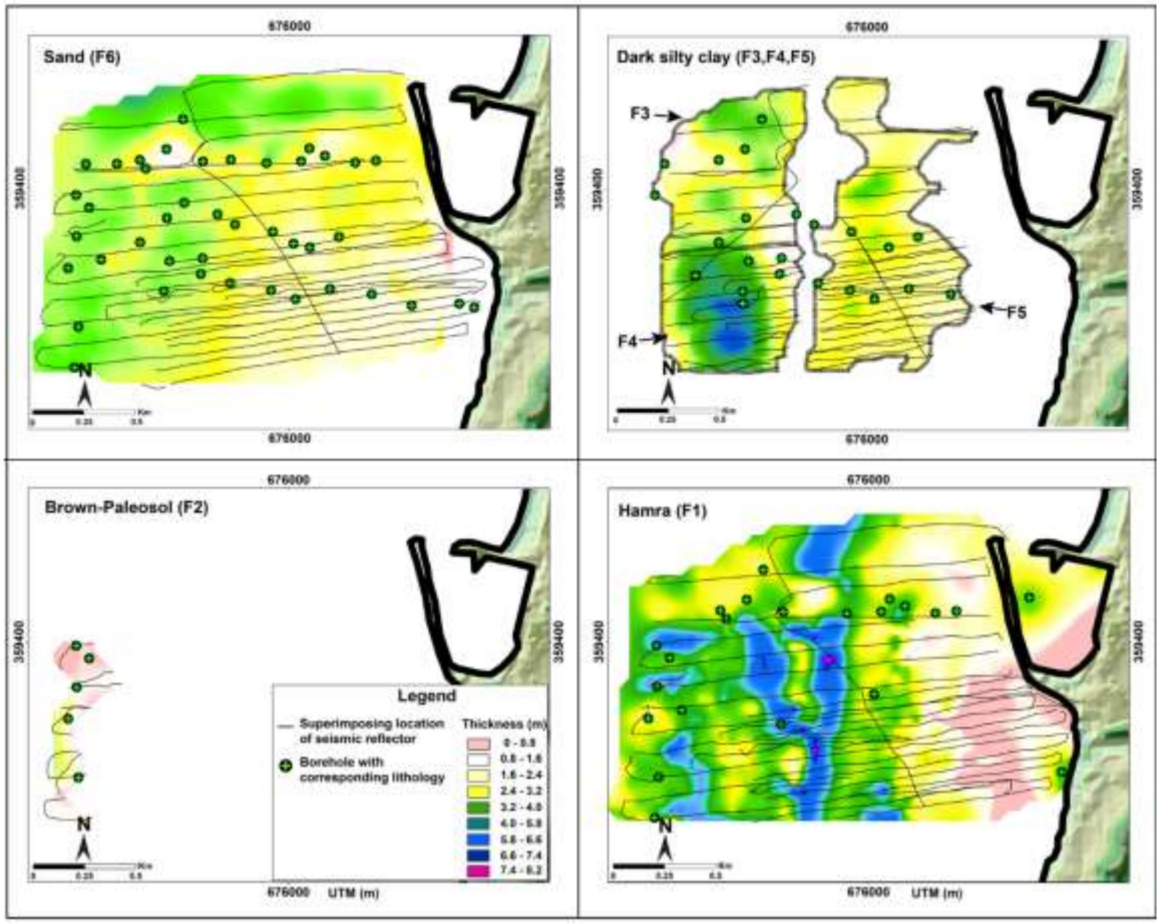

Figure 2.6: Isopach map of Hadera's seismic litho-stratigraphies. Each surface is presented with its corresponding seismic reflector and matching borehole-lithology. The litho-facies are presented from young (top left) to old (bottom right).

2.5.2. Lithostratigraphy

Up to five litho-stratigraphic units (Kurkar, Hamra, Brown-Palaeosol, dark silty clay and sand) are identified in both the N-S and E-W sections, inferred from the available borehole data (location of fence diagram is presented in Fig. 2.2), which range from 12 to -14 mILSD and from 12 to -40 mILSD, respectively (Fig. 2.7). The surface of the Kurkar is evident in most of the boreholes and reveals an uneven surface with topographic highs and lows both onshore and offshore Hadera.

Stratigraphic analysis reveals that the thickest unconsolidated sedimentary units occupy the depressions in between the Kurkar ridges, while they are thinnest on top of the Kurkar highs (Fig. 2.7). The Hamra facies, which is identified in most of the boreholes, covers the Kurkar and has a thickness that ranges from 1 to 8 m. In the boreholes the topography of the Hamra surface mirrors that of the Kurkar throughout the study zone. The Hamra is, in turn, covered by a 1 to 3 m-thick Brown-Palaeosol unit in the western parts of the area, between -22 and -26 mILSD and in a few zones in the vicinity of the shoreline. In the western parts of the study area, from a depth of -28 to -20 mILSD, the dark silty clay facies is seen deposited on top of the Hamra and/or Brown-Palaeosol, varying in thickness between 2 to 6 m. Onshore the unit is scarce and is only seen in one section. A sandy facies covers the identified units onshore and offshore at times also including shell fragments or finer (silt) fractions. The sand unit is evident from elevations of -26 to 11 mILSD, with thicknesses varying between 1 to 7 m.

All five litho-stratigraphic units are present in core SY5 (Fig. 2.8). The sedimentological description and corresponding properties are described for each unit:

- The lowermost unit the Kurkar, starting at -8.2 mILSD and reaching the borehole’s bottom, is composed of fine bright yellow (Fig. 2.8a) sand mixed with small size Kurkar clasts (Fig. 8f). Inorganic carbon values decrease upward and rang between 2 to 4 % (Fig. 2.8g). These characteristics and the elevation of the Kurkar unit in nearby onshore and offshore boreholes (Fig. 2.7) led to the identification of this unit.

- Overlying the Kurkar is a Hamra unit which is composed of an orange fine silty sand (Fig. 2.8a, b, e, f). The unit is 1.2 m thick (-8.2 to -7 mILSD) and is homogenous with high fractions of sand (Fig. 2.8f). These characteristics and the elevation of the Hamra unit in nearby boreholes located onshore and offshore (Fig. 2.7) was used for its identification.

- Covering the Hamra is a Brown-Palaeosol unit which consists of a dark brown clayey silty sand. The unit is 3.2 m thick (-7 to -3.8 mILSD: Figs. 2.8b, c, e), mostly homogenous and has relatively higher fractions of silt and clay (Fig. 2.8f). However, between -5.3 to -4.8 m depth (ILSD), thin yellowish sand layers are evident (Fig. 2.8a, f). Root remains are detected between -5.3 to -4.6 m (ILSD). These characteristics and the elevation of the palaeosol unit in nearby boreholes located onshore and offshore (Fig. 2.7) led to the unit's identification.

- Overlying the palaeosol is a 0.5 m thick (-3.8 to -3.3 mILSD) grey-dark grey clayey silty sand with a few yellow 1-3 cm sand patches. Sediment composition of clay and silt fractions is lower than 35 % (Fig. 2.8f) while fractions of organic carbon range between 0.2 to 0.8 % (Fig. 8g). The identification of this unit was based on these characteristics along with the elevation of a similar characterized unit located in onshore and in offshore boreholes (Fig. 2.7).

- Covering the dark silty clay is a 4.3 m thick grayish yellow sand unit with scattered bivalve fragments spotted between 0.8 and -0.3 mILSD. Inorganic carbon values decrease downward ranging between 1 to 3.5 % (Fig. 2.8g). From depths of -1.8 (ILSD) m the unit becomes less homogenous consisting of finer grain fractions and sand aggregates (Fig. 2.8a, f, d). From -2.5 mILSD, the unit's dampness increases, and it gradually becomes water saturated. This unit is also evident in various neighboring boreholes both onshore and offshore.

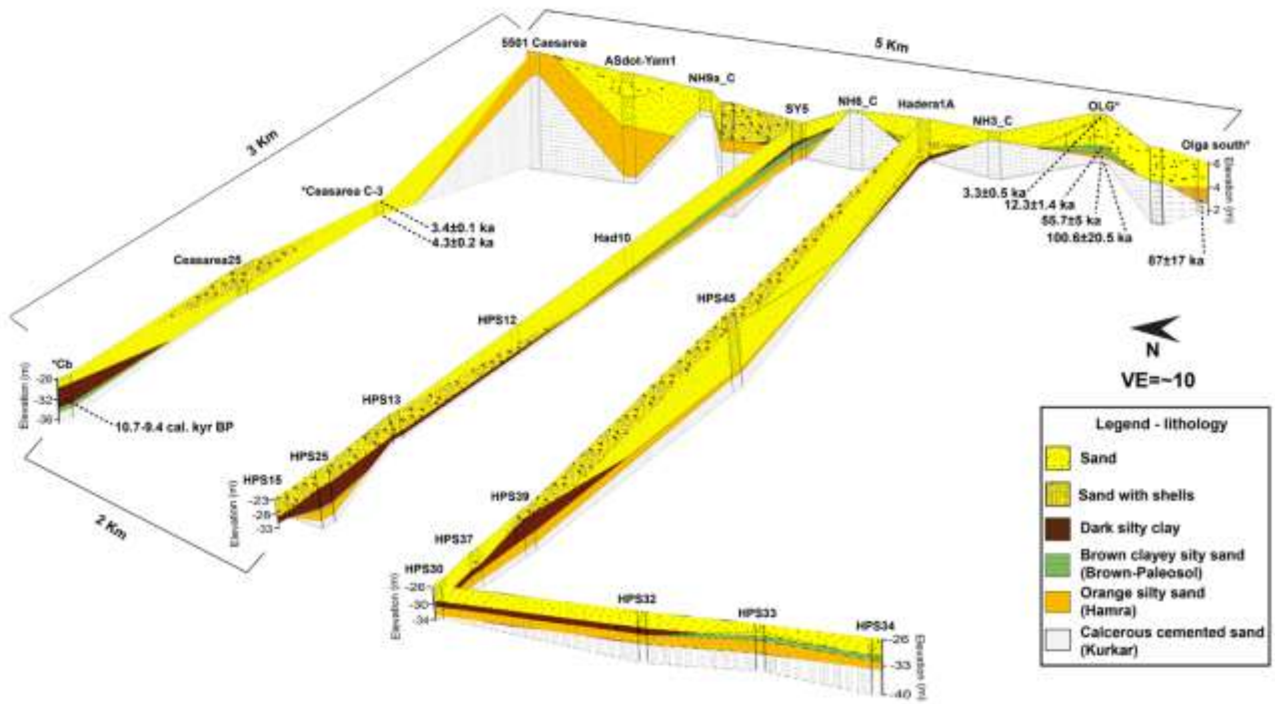

Figure 2.7: Fence diagram presenting the litho-stratigraphies of Hadera coastal and shallow shelf area according to borehole lithology and core SY5. Boreholes in which the lithologies have been dates in previous studies are marked with *. These include: Cb (Neev et al., 1978), Caesarea C-3 (Goodman-Tchernov et al., 2009), Olga south (Roskin et al., 2015), OLG (Frechen et al., 2001). The location of the boreholes is displayed in Fig. 2.2.

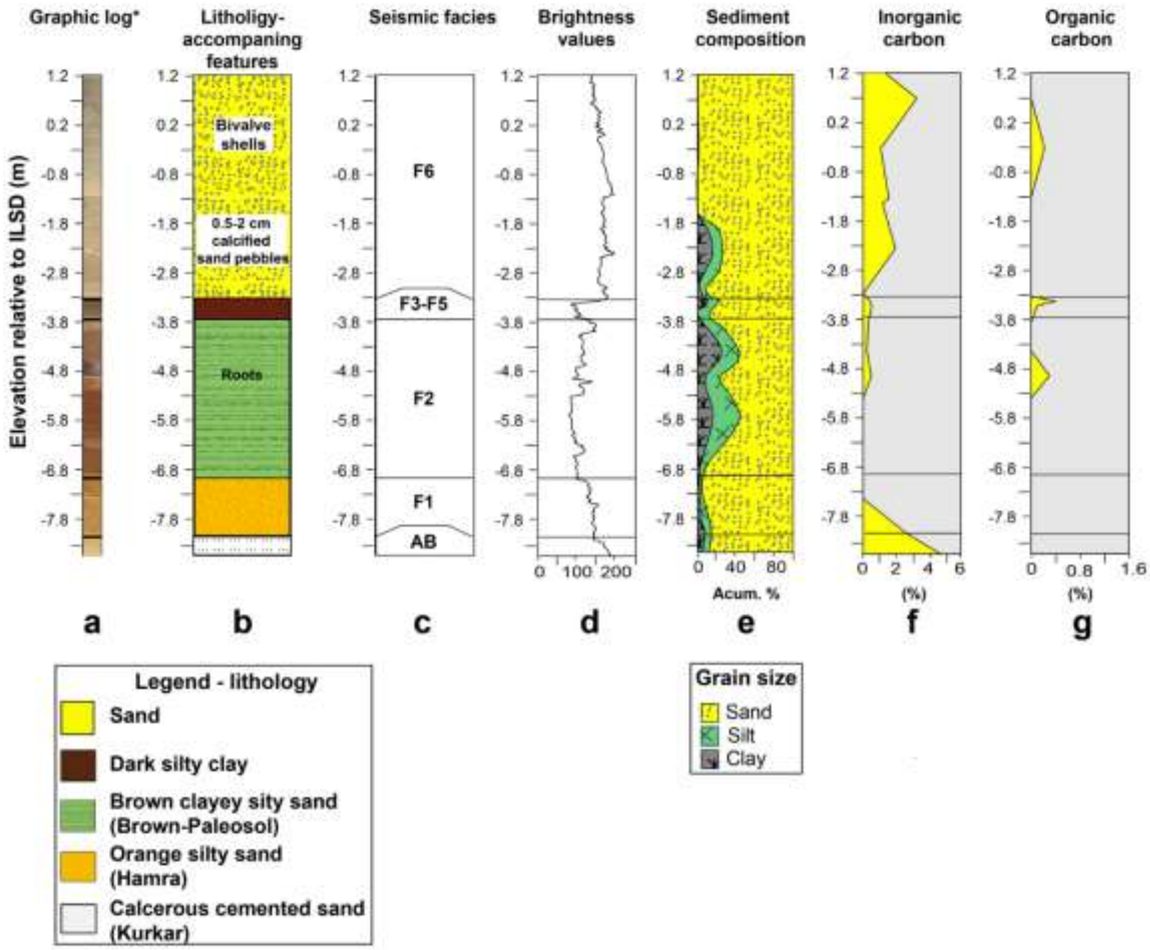

Figure 2.8: Borehole SY5 (location is displayed in Fig. 2.2) with lithology description, accompanying features, analogous seismic facies, graphic analysis (a - d), sedimentological and geochemical results (e - g).

2.5.3. Sedimentological and stratigraphical interpretation

The seismic units were correlated with the stratigraphy and lithology based on the geometrical relations between the different units, their respective seismic facies, the morphological features identified on coastal outcrops, litho-stratigraphical relations and the sedimentological correspondence with the boreholes. The lithological description of the acoustic basement surface and the six seismic units are presented from bottom to top, as follows:

The morphology of the acoustic basement S1 surface resembles the elevation differences, dipping angles, irregularity and shore parallel direction of the Kurkar, as observed on the adjacent coast (Gvirtzman et al., 1998; Sivan et al., 2004a; Frechen et al., 2001: Fig. 2). These morphological characteristics also match those of Kurkar as interpreted from a *uniboomer* seismic section by Neev et al. (1978) in water depths of 5 to 35 m offshore Caesarea (~2.5 km north of Hadera; Fig. 2.1). Moreover, this surface is identified and directly correlated to the seismic sections in 22 offshore boreholes. Taken together, this evidence leads to the identification of the acoustic basement as the top of the Kurkar surface.

Over the entire study area, the Kurkar is directly overlain by seismic unit F1. This seismic unit is penetrated by 12 boreholes all of which show Hamra sediments at this depth (Fig. 2.6). Covering the Hamra, from water depths of -26 to -28 mILSD, is a 2 m thick lens-shape unit (Fig. 6) which is directly sampled by 5 boreholes, and can be correlated to the bordering coastal area sequences (Fig. 2.6). Thus seismic unit F2 correlates to the Brown-Palaeosol unit.

Three lens-shaped fill units (F3, F4 and F5) cover the Hamra and truncate the Brown-palaeosol unit in the western boundary of the study area. These seismic units F3, F4 and F5 are all identified as dark silty clay units based on depth correspondences of these three units' surfaces in 23 boreholes. Units F3 and F4 display similar morphologies, thicknesses and lithology throughout the correlated boreholes. However, marked differences of reflectivity geometries are observed between unit F3 in the north and unit F4 in the south (Fig. 2.3). While the southern sections (F4; Fig. 2.6) consist of chaotic low-amplitude reflections (Fig. 2.4e), the northern ones (F3; Fig. 2.6) consist of subparallel sub-horizontal high amplitude reflections (Fig. 4a). These dissimilarities suggest different depositional mechanisms for the similar silty clay sediments. Finally, the topmost unit (F6), when correlated with 40 boreholes is identified as a sandy unit with minor shells and silty sands components (Fig. 2.6).

2.6. Discussion

2.6.1. Chronological framework

The correlation between the litho-stratigraphical units and previously dated sequences (Figs. 2.2, 2.7) also allows a chronology to be assigned to the described units. The deepest and oldest detectable surface identified across the entire study area is the top of the Kurkar sequence. The Kurkar surface, on the terrestrial side and in the shallow offshore, has been dated between ~101 and ~50 ka (Gvirtzman et al., 1998; Frechen et al. 2001; Porat et al., 2003a; Sivan and Porat, 2004; Zviely et al., 2006). These ages represent the depositional age of the sand, which occurred before and during the lithification process (Yaalon, 1967; Gavish and Friedman, 1969; Sivan and Porat, 2004). Based on these dates, and the Kurkar ages obtained in Hadera's coastal area (for location see Fig. 2.7; Frechen et al., 2001; Roskin et al., 2015) we hypothesize a similar chronology for the submerged Kurkar surface (Table 2.1).

A Hamra unit overlies the Kurkar and, in the western parts, is overlain by a Brown-Palaeosol sequence (Fig. 2.4). The correlation of these units to the onshore Hamra and Brown-Palaeosol (Figs. 2.7, 2.8) suggests that the units were deposited between ~87 to ~55 ka for the Hamra and between ~50 to ~11 ka for the Brown-Palaeosol (Table 2.1). As discussed by Sivan and Porat (2004), the wide age ranges for these units suggest that the Hamra and Palaeosol were deposited laterally over time with no direct association to sea levels. Although no direct dating has been carried out offshore, the extent and boundaries of the Hamra and Brown-Palaeosol can be clearly delineated in the seismic surveys and corresponding boreholes (Figs. 2.4, 2.6).

Overlying the Hamra unit and truncating the western Brown-Palaeosol boundary are two dark silty clay units, which are interpreted as representing wetland units (F3/F4 and F5; Figs. 2.4, 2.5, 2.6). The western and eastern lens-shaped seismic units are characterized as different wetland facies based on their seismic facies appearances, thickness, elevations differences and depositional environments which are divided by a topographic high. These facies stratigraphicaly corresponds to the coastal-wetland silty clays located in the Carmel coast (Fig. 2.1b) described by Kadosh et al. (2004), Sivan et al. (2004a), Cohen-Seffer et al. (2005), and Sivan et al. (2011). The base of the western wetland unit (F3/F4) is correlated to a wetland facies sampled in core Cb, 2.5 km north of the study area (Fig. 2.7), which was dated to 10.7 to 9.4 cal. kyr BP. This correlation is proposed due to the corresponding sub-bottom topography, stratigraphy, equivalent distance from the present-day shoreline (~2 km) and elevation (base elevation of -32 m ILSD) discussed by Neev et al. (1978). The inner seismic reflections of the wetland deposits are cut at the unit's top (Fig. 2.4) indicating that the surface of the western (F3/F4) and eastern (F5) units mark an erosional unconformity. Taking into account the sea-level curve of the Mediterranean from the LGM to present times (Fig. 2.9; Sivan et al., 2004b), and the elevations of the ravinement surfaces which extend from -28 to -12 mILSD, it is proposed that the wetland units eroded between ~9 ka and ~8 ka (Table 2.1). Nilotic sand (F6) was transported landward and deposited on top of the dark silty clay units (F3/F4 and F5; Figs. 2.4, 2.9). OSL chronologies sampled offshore Caesarea in equivalent water depths (Reinhardt et al., 2006; Goodman-Tchernov et al., 2009) and also onshore Hadera (Frechen et al., 2001; Roskin et al., 2015) indicate that sand stabilization started ~6 ka. The ages leave a time gap of ~2000 years between the wetland drying phase and the beginning sand deposition. It is most probable that the sand started to accumulate in these areas during the transgression (now ranging between -28 m to -15m) ~8 ka. However, since the area was subjected to high energy, which characterizes the surf zone, the sand was bleached due to sunlight exposer causing the age values to be younger.

Table 2.1: Dated litho-facies in the Israel's north-central coastal and its adjacent shallow marine area (see Figs. 2.1b, 2.2 for location). The unit elevation values are compared to Israel Land Survey Datum ILSD.

Borehole and reference	Unit/lithology of sample	Depth of unit compared to ILSD		Age range (ka)	
		Top	Bottom	Top	Bottom
Muwasi BB (5)	Sand	1		3.3±0.1*	
Caesarea c-3 (2)	Sand	-15.8	-16.1	3.4±0.1*	4.3±0.2*
Muwasi 7SE (5)	Sand	3.4	2.5	0.86±0.1*	4.8±0.7*
OLG (1)	Sand	16.8	15	3.3±0.5*	5.3±0.7*
MAM-B (5)	Dark silty clay	-8	-9.3	8.7 – 9.0 cal	9.2 – 9.5 cal
Cb-Ceasarea (3)	Dark silty clay	-32		9.4 – 10.7 cal	
MAM-B (4)	Brown clayey silty sand (Brown-Palaeosol)	-10.4	-11.4	11.1 – 11.2 cal	23.6 – 24 cal
OLG (1)	Brown clayey silty sand (Brown-Palaeosol)	8.8	4.8	12.3±1.4**	50.5±9**
OLG (1)	Orange silty sand (Hamra)	7.1	2.1	55.7±5**	
Olga South (5)	Orange silty sand	2.6	1.6		87±17*
OLG (1)	Calcareous cemented sand	5.5	4.3	54.7±9.1**	100.6±20.5**
MAM-B (4)	Calcareous cemented sand	-12		59.6±5.2*	
Olga North pd. (5)	Calcareous cemented sand	0.4		92±18*	
MAM-A (4)	Calcareous cemented sand	-12		101±11*	

* - OSL dates
** - IRSL dates
cal - ^{14}C calibrated dates
Referenced Chrono-stratigraphy data: (1) Frechen et al., 2001; (2) Goodman-Tchernov et al., 2009; (3) Neev et al., 1978; (4) Cohen-Seffer et al., 2005; (5) Roskin et al., 2015.

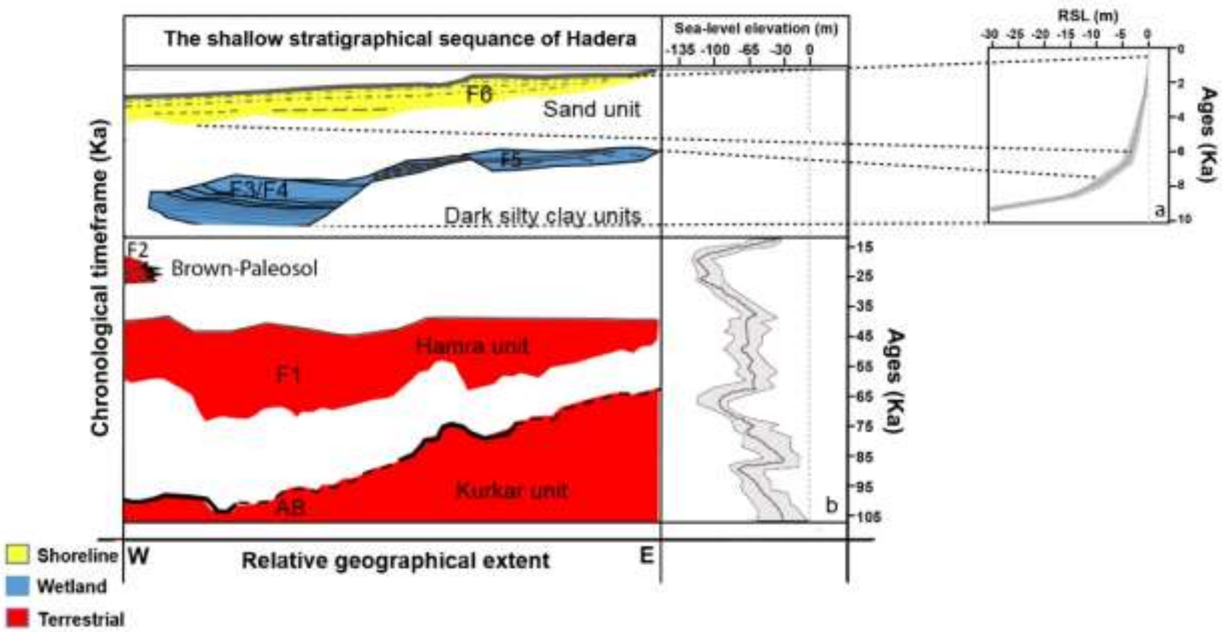

Figure 2.9: Wheeler diagram of Hadera shallow coastal shelf stratigraphical sequence. The stratigraphical units are displayed according to their depositional environment, depositional epoch, location and sea-level fluctuations. The deposition period and sea-level changes are presented in relative time. Please note that there is a time overlap for the Kurkar (AB) Hamra (F1) and palaeosol units (F2) and a hiatus between the wetland episode (~11 to ~8 ka) and the beginning sand deposition (~6 ka). The interglacial is demonstrated for the early Holocene (a) (after Sivan et al., 2001) and the last 105,000 years (b) (after Rohling et al., 2014). The envelope for both pots (shading) demonstrates the upper and lower limits.

2.6.2. Palaeogeographical reconstruction of the ancient drainage system

The top of the Kurkar and Hamra surfaces shows clear indications of a lowstand drainage system (Fig. 2.10). The channel locations were computed using the ArcGIS Hydrology toolset. The calculation modeled the hydrological flow for the interpolated submerged unit surfaces. The procedure was done in four steps: (1) identification and sink filling; (2) flow direction calculation; (3) calculating the flow accumulation; and (4) creation of the stream network. Location in which the paths could be the result of interpolation artifacts are marked by a dashed line.

The Kurkar and Hamra palaeo-drainage systems correlates in direction and channel width (3 to 5 m) to the adjacent Hadera stream (Fig. 2.10). The Hadera stream is one of the most substantial coastal rivers in Israel (Lichter et al., 2011). The stream extends more than 50 km long with a drainage basin that covers an area of approximately 600 km^2. As a result of the construction of Hadera’s power plant in the 1980’s the stream’s natural path was altered and its route was moved south, a few hundred m from its natural route (Fig. 2.10). The Kurkar and Hamra drainage system begins about 300 m from the present-day coastline and unlike the current coastal system possibly consisted of 6 and 5 paths respectively both trending in E-W directions. Then, 1.5 km from the modern shoreline, the three southern creeks of the Kurkar unite to one route, while the Hamra’s two northern and three southern creeks unite, forming two main routes.

Further, the greatest accumulations of the overlying dark silty clay sediments are found in the deepest topographic lows of this incised Hamra surface and near the palaeo-drainage intersections (Fig. 2.10c). This spatial correlation would suggest that the Hadera stream played a major role in contributing depositing material into these wetlands during the early Holocene. We also hypothesize that the reflection geometries of the fill units (F3/F4) differ between the northern and southern (Figs. 2.3, 2.4) areas because of the differences in the proximity to the drainage system channels (Fig. 2.10). The unstructured facies located in the southern parts is interpreted to be related to higher fluvial energy and continuous supply of homogenous fine material. The western located acoustically well layered geometry results from lower energy draping of these sediments in this wetland environment. Thus, Hadera's palaeo-stream affected the sedimentary depositional patterns of the western and eastern wetlands.

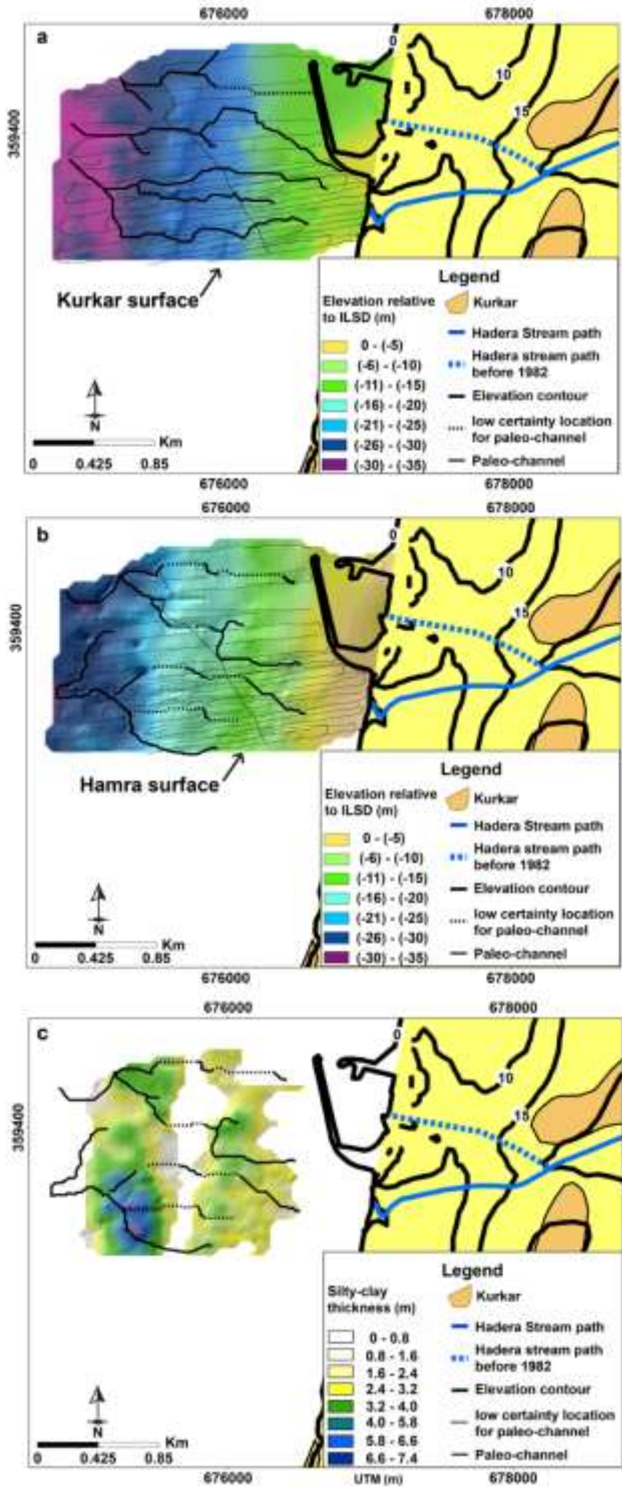

Figure 2.10: Late Pleistocene to Early Holocene palaeo-drainage system of Hadera (grey line). The drainage system was computed for the Kurkar (AB surface; a) and Hamra (F1 surface; b); and is presented against the dark silty clay isopach layer (F3-F5; c).

2.6.3. Palaeoenvironmental evolution

As a result of lower sea levels throughout most of the study's timeframe (between ~100 and ~9 ka), Hadera's offshore area was exposed and the shoreline was located between ~3 and ~13 km to the west of its present location (Almagor et al., 2000; Waelbroeck et al., 2002; Lambeck and Purcell, 2005; Hughes et al., 2013). In the final stages of the transgression (between ~9 and ~3 ka) the study area was flooded by the rising sea (Sivan et al., 2001; 2004a; Porat et al., 2008). The sea-level transgression shaped the deposition, preservation and erosion patterns of unconsolidated sediments and altered the currently submerged morphological features at Hadera.

The Kurkar surface was lithified between ~101 and ~50 ka in a terrestrial environment on the exposed shelf (Fig. 2.9). After its cementation the irregular surface was subjected to atmospheric and fluvial (Hadera palaeo-stream path; Fig. 2.10) erosion which made it rugged and channelized (Friedman, 1964; Yaalon, 1967; Gavish and Friedman, 1969; Schattner et al., 2010).

Following the Kurkar’s formation, Nilotic-based aeolian sediments infilled the Kurkar depressions and eventually covered its peaks (Figs. 2.4, 2.7) (Gvirtzman and Wieder, 2001; Sivan and Porat, 2004; Cohen-Seffer at al., 2005). The sand was later pedogenized in an oxidizing environment, in which the Hamra evolved (Gvirtzman et al., 1998; Sivan and Porat, 2004) reaching thicknesses of up to ~8 m. The boundary between the Hamra and the Brown-Palaeosol is acoustically distinguished (Figs. 2.3a, 2.4). The distinctive soil-sequence boundaries are hypothesized to be linked to alteration in deposition of finer material as seen in Hadera’s borehole based litho-stratigraphy (Fig. 2.7) and sedimentological analysis of SY5 (Fig. 2.8). The two units were pedogenized under different climatic conditions which resulted in finer material variations and differences in hue, and carbonate content (Yaalon, 1997; Gvirtzman et al., 1998; Gvirtzman and Wieder, 2001).

During the early Holocene (~10.5 to ~8 ka), sea-levels rose from ~ -45 to ~ -15 m (Fig. 2.9; Fairbanks, 1989; Bard et al., 1990, 1996; Lambeck and Bard, 2000; Sivan et al., 2001; Lambeck and Chappell., 2001; Sivan et al., 2004b; Berné et al., 2007) and the Israeli shoreline migrated ~1.5 km shoreward. Over this timeframe, four probable contributing factors led to the formation of Hadera's wetlands (Figs. 2.4, 2.6):

1. The coastal groundwater was elevated as a response to the sea-level rise and its shoreward migrating trend. The high levels of the aquifer flooded the topographic lows of the Hamra unit (Sivan et al., 2011).
2. The shelf flooding reduced the stream gradient, which consequently reduced the stream drainage energy.
3. Drainage was obstructed by growing volumes of Nilotic sediments transported shoreward as a result of the transgressing sea.
4. Wetter and warmer conditions occurred between 10.5 to 7.5 ka (Bar-Matthews et al., 2003), which consequently induced an increase in stream flow conditions that swamped the lowland areas.

At around ~8 ka, the rising sea flooded the eastern-most part of the wetlands. Nilotic sand was transported shoreward and started to accumulate on the wetland surface by ~6 ka. During this time wave and wind induced currents transported the sand to the shoreline and it was windblown inland. Then, by ~4 ka, when the shoreline reached its current location (Sivan et al., 2001) sand was windblown up to 2.5 km inland (Roskin et al., 2015) later to form Hadera’s sand dune field.

2.7. Conclusion

This is the first high resolutions combined geophysical and geological study to be conducted along the open coast of Israel (< 30 m) that combines marine and terrestrial data and which covers a time period which spans over more than 100 ka. The combination of continuous marine seismic data with core data drilled on land enables a 4-D reconstruction (including the time dimension) of an area that was long exposed to changing environmental conditions, and later was flooded by the sea.

The chronostratigraphy is based on correlation to adjacent dated coastal and marine stratigraphical units. The reconstruction revealed that the stratigraphy of this area is dominated by aeolian and fluvial processes operating during sea level lowstands. Only later, during the Holocene, is the landscape directly affected by a marine transgression, and the landward approaching shorelines. The units overlying the Pleistocene Kurkar were deposited in three environments: 1) the oldest Hamra/palaeosol units were deposited and pedogenized in a terrestrial environment over the course of thousands of years; 2) the early Holocene's wetland-silty clay units were deposited in a calm, fresh to brackish, water environment with increasing siltation in response to rising sea levels; and 3) the Nilotic sand unit, which was deposited in a shallow marine environment over the last 8,000 years.

The coastal changes recorded from the open coastline environment at Hadera contrast with the previous studies undertaken in more sheltered embayments on the Israeli coast (i.e Haifa Bay: Zviely et al., 2006; Porat et al., 2008). In these enclosed areas the rapid transgression during the early part of the Holocene led to rapid onshore migration of the coastline, reaching a maximum of 3 km inland of the modern-day coastline at ~4 ka. Then, once sea levels reached its current position and in response to the Nile-sediment input from the west, and local wetland and fluvial sediment input from the east, the coastline progradated until retreating back to its current position by ~2 ka. This late phase progradation is absent from the Hadera section which is characterized by continuous transgression until ~4 ka when it reached its present location.

The understanding gained from the study will serve as an analogue to other shallow marine and adjacent coastal environments that have formed under similar conditions (e.g. open sea, with sand supply source etc.). This reconstruction can also be of use for archaeological and engineering purposes. Archaeologists can use the 4-D litho-stratigraphical mapping for targeting ancient habitation which changed according to the (now submerged) surface lithology, distance from palaeo-water sources and rising sea levels. A connection between wetland sequences and ancient settlement having already been established in Israel's central coastal area, suggests that there is high archaeological potential offshore. Finally, engineers can make use of such high-resolution subsurface data for future infrastructure planning intended to be built/buried in or on the shelf's shallow subsurface. These include marines and harbours, gas pipes, electricity cables and communication network.

Acknowledgments

The authors like to thank the Ministry of National Infrastructure for funding the research (research grant no. 221-17-032) and also gratefully acknowledge support from the Sir Maurice and Lady Hatter Fund of the Leon Recanati Institute for Maritime Studies (RIMS), University of Haifa. Nimer Taha and Or Bialik are both thanked for helping with the sedimentological analyses. Dina Dagan from ben Gurion University and, Joel Roskin, Silas Dean and Guy Sisma-Ventura from the University of Haifa are acknowledged for their help in the field. The authors would like to thank Paradigm, Schlumberger and IHS for granting academic licenses for Seismic processing software as well as Petrel and Kingdom Suite for Seismic Interpretation software. Improvements of earlier versions of the manuscript by anonymous reviewers and by Editor-in-Chief (Prof. Andrew James Plater) are truly appreciated.

2.8. References

Allard, J., Chaumillon, E., Féniès, H., 2009. A synthesis of morphological evolutions and Holocene stratigraphy of a wave-dominated estuary. The Arcachon lagoon, SW France. Continental Shelf Research 29, 957-969.

Almagor, G., Nir, Y., 1977. Detailed bathymetric and shallow seismic survey off the site for the M. D. Electric Station near Hadera. Israel Geological Survey, Report GSI/1/77, Jerusalem.

Almagor, G., Hall, J.K., 1984. Morphology of the Mediterranean continental margin of Israel. Geological Survey of Israel 77, pp. 31.

Almagor, G., 1993. Continental slope processes off northern Israel and southernmost Lebanon and their relation to onshore tectonics. Marine Geology 112, 151-169.

Almagor, G., Gill, D., Perath, I., 2000. Marine Sand Resources Offshore Israel. Marine Georesources & Geotechnology 18, 1-42.

Anderson, J.B., Wallace, D.J., Simms, A.R., Rodriguez, A.B., Milliken, K.T., 2014. Variable response of coastal environments of the northwestern Gulf of Mexico to sea-level rise and climate change: Implications for future change. Marine Geology 352, 348-366.

Anzidei, M. Antonioli, F. Benini, A. Lambeck, K. Sivan, D. Serpelloni, E., Stocchi, P., 2011. Sea-level change and vertical land movements since the last two millennia along the coasts of southwestern Turkey and Israel. Quaternary International 232, 1-20.

Bard, E., Hamelin, B., Fairbanks, R.G., 1990. U-Th ages obtained by mass spectrometry in corals from Barbados: sea level during the past 130,000 years. Nature 346, 456-458.

Bard, E., Hamelin, B., Arnold, M., Montaggioni, L., Cabioch, G., Faure, G., Rougerie, F., 1996. Deglacial sea-level record from Tahiti corals and the timing of global meltwater discharge. Nature 382, 241-244.

Bar-Matthews, M., Ayalon, A., Gilmour, M., Matthews, A., Hawkesworth, C.J., 2003. Sea–land oxygen isotopic relationships from planktonic foraminifera and speleothems in the Eastern Mediterranean region and their implication for paleorainfall during interglacial intervals. Geochimica et Cosmochimica Acta 67, 3181-3199.

Bersezio, R., Giudici, M., Mele, M., 2007. Combining sedimentological and geophysical data for high-resolution 3-D mapping of fluvial architectural elements in the Quaternary Po plain (Italy). Sedimentary Geology 202, 230-248.

Bates, M.R., Richard Bates, C., Briant, R.M., 2007. Bridging the gap: a terrestrial view of shallow marine sequences and the importance of the transition zone. Journal of Archaeological Science 34, 1537-1551.

Belknap, D.F., Kraft, J.C., 1985. Influence of antecedent geology on stratigraphic preservation potential and evolution of Delaware's barrier systems. Marine Geology 63, 235-262.

Belknap, D.F., Mart, Y., 1999. Sea-level Lowstand in the east Mediterranean-late Pleistocene coastal Terraces Offshore northern Israel. Journal of Coastal Research 15, 399-412.

Berné, S., Jouet, G., Bassetti, M.A., Dennielou, B., Taviani, M., 2007. Late Glacial to Preboreal sea-level rise recorded by the Rhône deltaic system (NW Mediterranean). Marine Geology 245, 65-88.

Cawthra, H.C., Bateman, M.D., Carr, A.S., Compton, J.S., Holmes, P.J., 2014. Understanding Late Quaternary change at the land–ocean interface: a synthesis of the evolution of the Wilderness coastline, South Africa. Quaternary Science Reviews 99, 210-223.

Cohen-Seffer, R., Greenbaum, N., Sivan, D., Jull, T., Barmeir, E., Croitoru, S., Inbar, M., 2005, Late Pleistocene-Holocene marsh episodes along the Carmel coast, Israel. Quaternary International 140-141, 103-120.

Davis, R.A., Hayes, M.O., 1984. What is a wave dominant coast? Marine Geology 60, 313-329.

Davis, M., Matmon, A., Rood, D. H., Avnaim-Katav, S., 2012. Constant cosmogenic nuclide concentrations in sand supplied from the Nile River over the past 2.5 m.y. Geology 40, 359-362.

Emery, K.O., Bentor, Y.K., 1960. The continental shelf of Israel. Geological Survey Israel Bulletin 26, 25-41.

Emery, K.O., Neev, D., 1960. Mediterranean beaches of Israel. Geological Survey Israel Bulletin 26, 1-24.

Engelmann, A., Neber, A., Frechen, M., Boenigk, W., Ronen, A., 2001. Luminescence chronology of upper Pleistocene and Holocene aeolianites from Netanya South-Sharon coastal plain, Israel. Quaternary Science Reviews 20, 799-804.

Fairbanks, R.G., 1989. A 17, 000-year glacio-eustatic sea level record: influence of glacial melting rates on the Younger Dryas event and deep-ocean circulation. Nature 342, 637-642.

Frechen, M., Dermann, B., Boenigk, W., Ronen, A., 2001. Luminescence chronology of aeolianites from the section at Givat Olga Coastal Plain of Israel. Quaternary Science Reviews 20, 805-809.

Frechen, M., Neber, A., Dermann, B., Tsatskin, S. Boenigk, W., Ronen, A., 2002. Chronostratigraphy of aeolianites from the Sharon Coastal Plain of Israel. Quaternary International 89, 31-44.

Frechen, M., Neber, A., Tsatskin, A., Boenigk, W., Ronen, A., 2004. Chronology of Pleistocene sedimentary cycles in the Carmel Coastal Plain of Israel. Quaternary International 121, 41-52.

Friedman, G.M., 1964. Early diagenesis and lithification in carbonate sediments. Journal of Sedimentary Research 34, 777-813.

Galili, E., Weinstein-Evron, M., 1985. Prehistory and palaeoenvironments of submerged sites along the Carmel Coast of Israel. Pale´orient 11, 37-51.

Galili, E., Nir, Y., 1993. The submerged Pre-Pottery Neolithic water well of Atlit-Yam, Northern Israel, and its paleoenvironmental implications. The Holocene 3, 265-270.

Galili, E., Stanley, D.J., Sharvit, Y., Weinstein-Evron, M., 1997. Evidence for Earliest Olive-Oil Production in Submerged settlements off the Carmel Coast, Israel. Journal of archaeological Science 24, 1141-1150.

Galili, E., Zviely, D., Ronen, A., Mienis, H.K., 2007. Beach deposits of MIS 5e high sea stand as indicators for tectonic stability of the Carmel coastal plain, Israel. Quaternary Science Reviews 26, 2544-2557.

Gavish, E., Friedman, G.M., 1969. Progressive diagenesis in Quaternary to Late Tertiary carbonate sediments: sequence and time scale. Journal of Sedimentary Research 39, 980-1006.

Golan, A., 2007. Shallow geophysical survey in Hadera. IOLR Report H2/2007. 19 pp. (In Hebrew).

Golik, A., Rosen, S.D., 1999. Management of the Israeli coastal sand resources. Israel Oceanographic and Limnological Research, Report H 28/98 submitted to the Mediterranean Action Plan and the Ministry of Environment, Israel 70 pp.

Goodman-Tchernov, B.N., Dey, H.W., Reinhardt, E.G., McCoy, F., Mart, Y., 2009. Tsunami waves generated by the Santorini eruption reached Eastern Mediterranean shores. Geology 37, 943-946.

Gvirtzman, G., Netser, M., Katsav, E., 1998. Last-Glacial to Holocene Kurkar ridges, hamra soils, and dune fields in the coastal belt of central Israel. Israel Journal of Earth Sciences 47, 27-46.

Gvirtzman, G., Wieder, M., 2001. Climate of the last 53,000 years in the eastern Mediterranean, based on soil-sequence stratigraphy in the coastal plain of Israel. Quaternary Science Reviews 20, 1827-1849.

Hampson, G.J., Storms, E.A., 2008. Geomorphological and sequence stratigraphic variability in wave-dominated, shoreface-shelf parasequences. Sedimentology 50, 667-701.

Hughes, P.D., Gibbard, P.L., Ehlers, J., 2013. Timing of glaciation during the last glacial cycle: evaluating the concept of a global 'Last Glacial Maximum' (LGM). Earth-Science Reviews 125, 171-198.

Inman, D.L., Jenkins, S.A., 1984. The Nile littoral cell and man's impact on the coastal zone of the southeastern Mediterranean. In: ASCE Proceedings of the 19th Conference on Coastal Engineering, Houston, TX, pp. 1600-1617.

Kadosh, D., Sivan, D., Kutiel, H., Weinstein-Evron, M., 2004. A late quaternary paleoenvironmental sequence from Dor, Carmel coastal plain, Israel. Palynology 28, 143-157.

Lambeck, K., Bard, E., 2000. Sea-level change along the French Mediterranean coast for the past 30,000 years. Earth and Planetary Science Letters 175, 203-222.

Lambeck, K., Chappell, J., 2001. Sea level change through the last glacial cycle. Science 292, 679-686.

Lambeck, K., Purcell, A., 2005. Sea-level change in the Mediterranean Sea since the LGM: model predictions for tectonically stable areas. Quaternary Science Reviews 24, 1969-1988.

Lichter, M., Klein, M., Zviely, D., 2011. Dynamic morphology of small south-eastern Mediterranean river mouths: a conceptual model. Earth Surface Processes and Landforms 36, 547-562.

Mart, Y., Belknap, D.F., 1991. Origin of Late Pleistocene Submerged Marine Terraces on the outer continental shelf. Geo-Marine Letters 11, 66-70.

Mauz, B., Hijma, M.P., Amorosi, A., Porat, N., Galili, E., Bloemendal, J., 2013. Aeolian beach ridges and their significance for climate and sea level: Concept and insight from the Levant coast (East Mediterranean). Earth-Science Reviews 121, 31-54.

Mendoza, U., Ayres Neto, A.C., Abuchacra, R., Fernandes Barbosa, C.G., Figueiredo, A.C., Gomes, M., Belem, A.L., Capilla, R., Albuquerque, A.L., 2014. Geoacoustic character, sedimentology and chronology of a cross-shelf Holocene sediment deposit off Cabo Frio, Brazil (southwest Atlantic Ocean). Geo-Marine Letters 34, 297-314.

Michelson, H., 1970, The geology of the Carmel coast. MSc thesis, the Hebrew University, Jerusalem. 61 pp. (In Hebrew).

Neev, D., Almagor, G., Arad, A., Ginzburg, A., Hall, J.K., 1976. The geology of the southern Mediterranean Sea. Geological Survey Israel Bulletin 68, 1-47.

Neev, D., Shachnai, E., Hall, J.K., Bakler, N., Ben Avraham, Z., 1978. The young (post Lower Pliocene) geological history of the Caesarea Structure. Israel Journal of Earth-Sciences 27, 43-64.

Nir, Y., 1979. Detailed bathymetric and shallow seismic survey off the site for the M. D. Electric Station near Hadera. Israel Geological Survey, Report GSI/1/79, Jerusalem.

Peterson, C.D., Vanderburgh, S., Roberts, M.C., Jol, H. M., Phipps, J., Twichell, D.C., 2010. Composition, age, and depositional rates of shoreface deposits under barriers and beach plains of the Columbia River littoral cell, USA. Marine Geology 273, 62-82.

Pomerancblum, M., 1966. The distribution of heavy minerals and their hydraulic equivalents in sediments of the Mediterranean continental shelf of Israel. Journal of Sedimentary Research 36, 162-179.

Porat, N., Avital, A., Frechen, M., Almogi-Labin, A., 2003a. Chronology of upper Quaternary offshore successions from the southeastern Mediterranean Sea, Israel. Quaternary Science Reviews 22, 1191-1199.

Porat, N., Wintle, A.G., Ritte, M., 2003b. Mode and timing of Kurkar and Hamra formation, central coastal plain, Israel. Israel Journal of Earth Sciences 53, 13-25.

Porat, N., Sivan, D., Zviely, D., 2008. Late Holocene embayment and sedimentological infill processes in Haifa Bay, SE Mediterranean. Israel Journal of Earth Sciences 57, 21-31.

Reinhardt, E.G., Goodman, B.N., Boyce, J. I., Lopez, G., van Hengstum, P., Rink, W.J., Mart, Y., Raban, A., 2006. The tsunami of 13 December AD 115 and the destruction of Herod the Great's harbor at Caesarea Maritima, Israel. Geology 34, 1061-1064.

Rohling, E.J., Foster, G. L., Grant, K.M., Marino, G., Roberts, A.P., Tamisiea, M.E., Williams, F., 2014. Sea-level and deep-sea-temperature variability over the past 5.3 million years. Nature 508, 477-482.

Ronen, A., Golik, A., Neber, A., Tsatskin, A., Boenigk, W., Beiles, A., 2005. Pleistocene and Holocene pattern of sand migration along the Mediterranean littoral of Israel. Israel Journal of Earth Sciences 54, 187-198.

Roskin, J., Sivan, D., Shtienberg, G., Roskin, E., Porat, N., Bookman, R., 2015. Natural and human controls of the Holocene evolution of the beach, aeolian sand and dunes of Caesarea (Israel). Aeolian Research 19, 65-85.

Schattner, U., Lazar, M., Tibor, G., Ben-Avraham, Z., Makovsky, Y., 2010. Filling up the shelf - A sedimentary response to the last post-glacial sea rise. Marine Geology 278, 165-176.

Sivan, D., Gvirtzman, G., Sass, E., 1999. Quaternary stratigraphy and paleogeography of the Galilee coastal plain, Israel. Quaternary Research 51, 280-294.

Sivan, D. Wdowinski, S. Lamback, K. Galili, E., Raban, A., 2001. Holocene sea-level changes along the Mediterranean coast of Israel, based on archaeological observations and Numerical model. Palaeogeography, Palaeoclimatology and Palaeoecology 167, 101-117.

Sivan, D., Eliyahu, D., Raban, A., 2004a. Late Pleistocene to Holocene wetlands now covered by sand, along the Carmel Coast, Israel, and their relation to human settlement: an example from Dor. Journal of Coastal Research 20, 1035-1048.

Sivan, D., Lambeck, K., Toueg, R., Raban, A., Porath, Y., Shirman, B., 2004b. Ancient coastal wells of Caesarea Maritima, Israel, an indicator for relative sea level changes during the last 2000 years. Earth and Planetary Science Letters 222, 315-330.

Sivan, D., Porat, N., 2004. Late Pleistocene contemporaneous formation of calcareous aeolianite (Kurkar) and paleosol (Hamra) in the Carmel coast, Israel. Palaeogeography, Palaeoclimatology, Palaeoecology 211, 95-106.

Sivan, D., Greenbaum, N., Cohen-Seffer, R., Sisma-Ventura, G., Almogi-Labin, A., 2011. The origin and disappearance of the late Pleistocene–early Holocene short-lived coastal wetlands along the Carmel coast, Israel. Quaternary Research 76, 83-92.

Sneh, A. Y., Bartov, Rosensaft, M., 1998. Geological map of Israel, 1:200,000, 4 sheets. Israel Geological Survey.

Stanley, D.J., Warne, A.G., 1998, Nile Delta in its destruction phase. Journal of Coastal Research 14, 795-825.

Stoker, M.S., Bradwell, T., Howe, J.A., Wilkinson, I.P., McIntyre, K., 2009. Late glacial ice-cap dynamics in NW Scotland: evidence from the fjords of the Summer Isles region. Quaternary Science Reviews 28, 3161-3184.

Toker, E., Sivan, D., Stern, E., Shirman, B., Tsimplis, M., Spada, G., 2012. Evidence for centennial scale sea-level variability during the Medieval Climate Optimum (Crusader Period) in Israel, eastern Mediterranean. Earth and Planetary Science Letters 315-316, 51-61.

Twichell, D.C., Cross, V. A., Peterson, C.D., 2010. Partitioning of sediment on the shelf offshore of the Columbia River littoral cell. Marine Geology 273, 11-31.

Vanderburgh, S., Roberts, M., Peterson, C., Phipps, J., Herb, A., 2010. Transgressive and regressive deposits forming the barriers and beachplains of the Columbia River Littoral Cell, USA. Marine Geology 273, 32-43.

Waelbroeck, C., Labeyrie, L., Michel, E., Duplessy, J.C., McManus, J., Lambeck, K., Balbon, E., Labracherie, M., 2002. Sea-level and deep water temperature changes derived from benthic foraminifera isotopic records. Quaternary Science Reviews 21, 295-305.

Wieder, M., Gvirtzman, G., Netzer, M., 1997. Origin of clayey soils on aeolian dust in the central coastal plain of Israel. In: Shoba, S., Gerasimova, M., Miedema, R. (Eds.), Soil Micromorphology: Diversity, Diagnostics, Dynamics. IWMSM, Moscow - Wageningen, pp. 196-203.

Yaalon, D.H., 1967. Factors affecting the lithification of eolianite and interpretation of its environmental significance in the coastal plain of Israel. Journal of Sedimentary Research 37, 1189-1199.

Yaalon, D.H., 1997, Soils in the Mediterranean region: what makes them different? Catena 28, 157-169.

Yoo, D.G., Kim, S.P., Chang, T.S., Kong, G.S., Kang, N.K., Kwon, Y.K., Nam, S.L., Park, S.C., 2014. Late Quaternary inner shelf deposits in response to late Pleistocene–Holocene sea level changes: Nakdong River, SE Korea. Quaternary International 344, 156-169.

Zecchin, M., Baradello, L., Brancolini, G., Donda, F., Rizzetto, F., Tosi, L., 2008. Sequence stratigraphy based on high-resolution seismic profiles in the late Pleistocene and Holocene deposits of the Venice area. Marine Geology 253, 185-198.

Zecchin, M., Brancolini, G., Tosi, L., Rizzetto, F., Caffau, M., Baradello, L., 2009. Anatomy of the Holocene succession of the southern Venice lagoon revealed by very high-resolution seismic data. Continental Shelf Research 29, 1343-1359.

Zviely, D., Sivan, D., Ecker, A., Bakler, N., Rohrlich, V., Galili, E., Boaretto, E., Klein, M., Kit, E., 2006. Holocene evolution of the Haifa Bay area, Israel, and its influence on ancient tell settlements. The Holocene 16, 849-861.

Zviely, D., Kit, E., Klein, M., 2007. Longshore sand transport estimates along the Mediterranean coast of Israel in the Holocene. Marine geology 238, 61-73.

3. New perspectives on coastal landscape reconstruction during the Late Quaternary: A test case from central Israel

Gilad Shtienberg , Justin K. Dix, Joel Roskin, Nicolas Waldmann, Revital Bookman, Or M. Bialik, Naomi Porat, Nimer Taha and Dorit Sivan, 2017. New perspectives on coastal landscape reconstruction during the Late Quaternary: A test case from central Israel. Palaeogeography, Palaeoclimatology, Palaeoecology 468, 503-519 (http://dx.doi.org/10.1016/j.palaeo.2016.12.045; Published).

Contribution statement

G. Shtienberg jointly conceived the study, designed the terrestrial drillings with D. Sivan and J. Dix. Collection and integration of existing borehole records, topographic and spatial data was undertaken by G. Shtienberg. The drilling was conducted by G. Shtienberg under the direction of D. Sivan with the help of J. Roskin while sedimentological analysis was conducted by G. Shtienberg under the direction of D. Sivan and N. Taha. OSL Dating was completed by G. Shtienberg under the guidance of N. Porat. Sedimentological data integration and interpretation was completed by G. Shtienberg under the supervision of D. Sivan and J. Dix. The manuscript was drafted and finalised by G. Shtienberg with editing contributions from D. Sivan, J. Dix, N. Waldmann, R. Bookman, J Roskin and O. Bialik.

3.1. Abstract

The stratigraphic architecture of coastal plains is determined by the interactions between local (e.g. fluvial processes and topography), regional (e.g. climate) and global (e.g. sea level) forcing factors, primarily during the Late Quaternary Period. Detailed stratigraphic and sedimentological analyses of boreholes, cored between coastal ridges in the lowlands, coupled with optically stimulated luminescence (OSL) dating, and integrated with existing onshore and offshore databases, has enabled a 4-D reconstruction of the evolution of the coast of Israel during the last glacial-interglacial cycle. This model revealed that Nilotic-sourced littoral sand, intermittently transported inland by wind, has either been lithified into aeolianite or pedogenized into orange – brown palaeosol from about 100 ka to 8 ka. Dark silty clay wetlands were deposited between the aeolian coastal ridges adjacent to streams which cut the Israeli coastal plain and flow westward, from the Last Glacial Maximum until the onset of the Holocene. These units are topped by beach and aeolian quartz sand dated from 6.6 to 0.1 ka. Diachronous thicknesses and lithological dissimilarities were identified between the sections studied and previous reports on adjacent coastal aeolianite ridges. Streams were found to be a dominant control on the stratigraphical composition and related facies architecture due to fluvial-induced erosion. Consequently, the relief variations between the lowland and cliff controlled aeolian pedogenesis as well as alluvial processes from about 80 to 5 ka. Climate, mainly influenced by precipitation and dust input, induced pedogenic processes; while sea level lowstand during the Last Glacial Maximum is shown to have hindered sediment deposition in the shallow offshore, which in turn affected aeolian transport, reducing sediment accumulation on the palaeo-coastal plain. The palaeoenvironmental model presented in the current study serves as an example for understanding the evolution of similar low-latitude siliciclastic-rich low-gradient shelf-coastal areas during the last glacial-interglacial cycle. Furthermore, it demonstrates the influence of local to global forcing factors on these environments.

Keywords

Stratigraphic architecture; Eastern Mediterranean; Coastal lowlands, Aeolianite cliff; Quaternary-landscape evolution; Siliciclastic sequence

3.2. Introduction

During the Quaternary, relative sea level (RSL) fluctuations have had a major influence on the sedimentary archives of continental shelves and the adjacent coastal plains. The effect of sea-level on accommodation space is one of the major influences on aggradation and erosion, and hence on the distribution of sediments across the shelves. Additional interconnected factors operating at all scales, such as tides, waves, storms, precipitation, sediment input and vegetation cover, also play important roles in the depositional and erosional phases that shape the litho-stratigraphic architecture. Moreover, local processes, such as stream-courses, modify pre-existing depositional patterns and induce irregular erosion patterns, while local relief variations affect soil formation processes (Dan et al., 1968; Paton et al., 1995; Yaalon, 1997).

Aeolianite-palaeosol-sand sequences, which are characteristic of low latitude, siliciclastic shallow shelf and coastal areas, reflect this dynamic interaction between accommodation space, sediment supply and climate changes (Hearty, 2007; Brooke et al., 2003; Bateman et al., 2004; Zazo et al., 2005; Faust et al., 2015). Consequently, detailed chronostratigraphic study can potentially reveal changes in the environmental conditions during the Quaternary (Huntley et al., 1993, 1994; Rose et al., 1999; Huntley and Prescott, 2001; Preusser et al., 2002; Munyikwa, 2005; Tripaldi and Forman, 2007; Amorosi et al., 2009; Fitzsimmons et al., 2009; Roskin et al., 2011a; Brooke et al., 2014; Rowe and Bristow, 2015a, 2015b). Coastal stratigraphic studies have been conducted across the Mediterranean basin, in Spain (Fornós et al., 2009; Mauz et al., 2012), Sardinia (Coltorti et al., 2010; Thiel et al., 2010), Tunisia (Mauz et al., 2009, 2012; Elmejdoub et al., 2011), Cyprus (Tsakalos, 2016) and Egypt (El-Asmar, 1994; El-Asmar and Wood, 2000). These are characterized by alternating Late Pleistocene aeolianites, palaeosol units and accompanying alluvial facies. These studies have mainly focused on the correlation between dune formation and Late Quaternary sea level oscillation, while less attention has been given to the coastal geomorphic response to climate, aeolian and alluvial processes. Furthermore, the studied units were usually site-specific, and not correlated with the adjacent terrestrial and submerged stratigraphies.

The Late Quaternary coastal palaeogeography of Israel has been studied since the 1940s in an attempt to correlate the coastal outcrop stratigraphy with transgressive and regressive sea level phases (Avnimelech, 1950). Later works concentrated on radiometric (luminescence and radiocarbon) ages for the central coastal aeolianite cliff sequences which yield ages younger than about 75 ka (Engelmann et al., 2001; Frechen et al., 2001, 2002; Porat et al., 2004; Moshier et al., 2010; Mauz et al., 2013). Hardly any attention has been paid to the submerged stratigraphy and to the sequences of lowlands located between coastal ridges. These locations potentially include palaeosols containing valuable climate indicators, and useful evidence for reconstructing past environments (Gvirtzman and Wieder, 2001; Zazo et al., 2005; Fitzsimmons et al., 2009). The relatively short time-frame attributed to the exposed sequences; the paucity of adequate subsurface chronostratigraphic studies; the absence of correlation of the coastal cliffs to the nearby lowland areas (Fig. 3.1c, d); and the lack of connection of the inner shelf to the coastal stratigraphy, have all hindered detailed reconstruction of the stratigraphic architecture of coastal areas and the investigation of the dominant long-term factors that affect the evolution of the coastal landscape.

The present study investigates the eustatic, climatic and local controls on the morphogenesis of the coastal system during the Late Quaternary of a selected study area located in central Israel (Fig. 3.1 for location). The findings are correlated in a wider environmental and climatic perspective, enabling the construction of an evolutionary model of the coastal environment over the last glacial-interglacial period. These goals were achieved through high-resolution sedimentological and chronostratigraphic studies of seven cores drilled in the Alexander-Hadera lowland area adjacent to the mouths of Nahal (Stream in Hebrew; N.) Hadera and N. Alexander (Fig. 3.1 for location). The new data were integrated with an existing detailed onshore and offshore database. The study area was selected based on: (1) the inclusion of various morphologies (aeolian dune system, sand sheets, wetlands and streams), which provide the optimal conditions for studying the interplay of these morphologies with sea level over time; (2) the sensitivity of the stream valleys to climate (precipitation) and hydrological influences (floods); (3) previous studies of the stratigraphic architecture of both the adjacent terrestrial (Neber, 2002) and inner shelf (Shtienberg et al., 2016) environments; and (4) radiometrically-dated sequence of the coastal cliff section (Frechen et al., 2002).

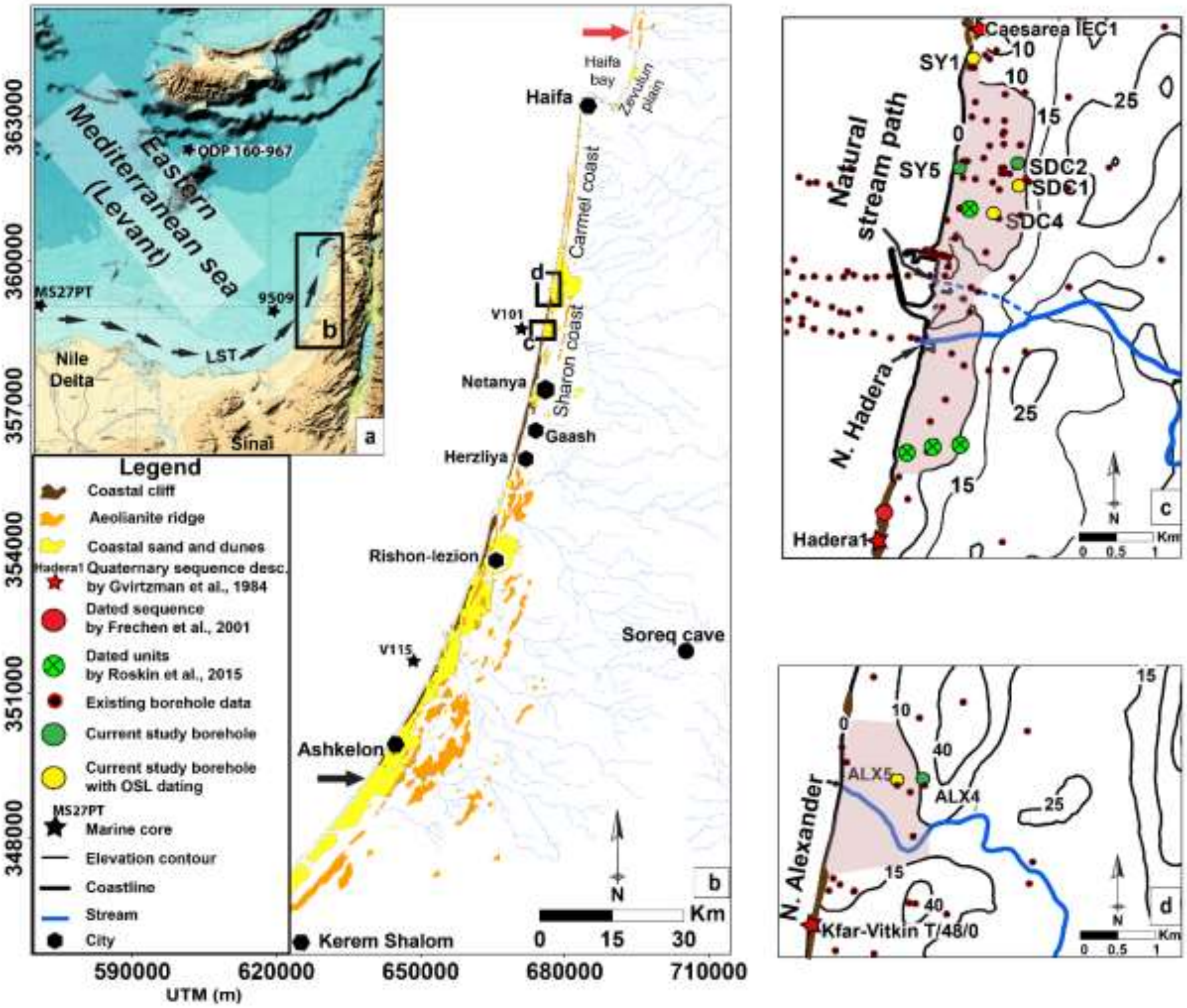

Figure 3.1: The regional and sedimentological context of the studied area in the SE Mediterranean: (a) Location map of the study area in the south-eastern Mediterranean, showing the Nile littoral cell, longshore transport (LST) and existing marine drilling locations; (b) The sand sheets and Late Pleistocene aeolianite ridges of Israel’s coastal plain. The wider parts of the coastal plain and coastal shelf are at the south (black arrow), while the narrow areas are at the north (red arrow); (c) Zoom into the Hadera area with existing logs, dated units and current study drilling location conducted in the 'lowland' area (grey polygon); and (d) Zoom into Alexander area with existing logs and current study drilling location conducted in the 'lowland' area (grey polygon).

3.3. Regional setting

Israel's Mediterranean coastal plain is an ideal location for studying Late Quaternary coastal evolution. Relative sea levels of the Mediterranean Sea generally track eustatic sea-level changes (Lambeck and Bard, 2000; Galili et al., 2007; Sivan et al., 2016), and it is hypothesised that the Late Pleistocene synoptic regime over the Mediterranean was similar to the present (Enzel et al., 2008). Israel's coast is considered tectonically stable, at least since Marine Isotope Stage (MIS) 5e (Sivan et al., 1999; Galili et al., 2007; Mauz et al., 2013; Sivan et al., 2016), with low isostatic uplift rates of about 0.1 mm/year in the Holocene (Sivan et al., 2001; Anzidei et al., 2011; Toker et al., 2012), and about 0.05 mm/y over about the last 125 ka (Sivan et al., 2016).

The 190 km-long coastal plain of Israel widens from about 3 km in the north to about 15 km in the south (Almagor and Hall, 1984). The continental shelf follows the same spatial pattern, widening from about 10 km in the north to about 20 km in the south (Fig. 3.1b), with the shelf break situated at water depths of 80 to 130 m below mean sea level (bmsl; Almagor et al., 2000; Sade et al., 2006). The sediments that cover the shelf and coastal plain mostly comprise of Nile derived quartz sand 1 to 9 m thick (Fig. 3.1a, b; Picard, 1943; Emery and Neev, 1960; Pomerancblum, 1966; Neev et al., 1978; Zviely et al., 2009; Davis et al., 2012; Almagor et al., 2000; Zviely et al., 2006; Schattner et al., 2010, 2015; Roskin et al., 2016; Shtienberg et al., 2016). This allogenic material is transported to the region through longshore currents, and is mostly deposited at water depths shallower than 40 m bmsl. The sand flux diminishes northwards and terminates at Haifa Bay (Fig. 3.1b for location) (Zviely et al., 2006; Hyams-Kaphzan et al., 2008).

During the Quaternary, wave- and wind-induced currents transported these sediments landwards to the beach, from where they were windblown inland to form sand sheets and sand dunes (Fig. 3.1b; Gvirtzman et al., 1998; Porat et al., 2004). The dunes later fossilized through dissolution of carbonate by meteoric waters and calcite cementation, forming calcareous aeolianite sandstone ridges (locally known as *kurkar*; Fig. 3.1b; Yaalon, 1967; Gavish and Friedman, 1969; Almagor et al., 2000). Up to eighteen aeolianite ridges trending parallel–sub-parallel to the shoreline rise above the surface of the coastal plain and the relatively flat sea-bed (Almagor et al., 2000; Mauz et al., 2013; and references therein). The relationship between the spatial and temporal patterns of the coastal ridges and past sea-level changes is still not well established (Sivan and Porat, 2004; Mauz et al., 2013, Shtienberg et al., 2016) due to the absence of an RSL curve, dating resolution and radiometric errors.

The Late Pleistocene aeolianite coastal ridges of Israel, located up to 3 km east of the present shoreline, are overlain by a thick brown-red sandy clayey loam soil (Chromic Luvisol) locally known as *hamra* (Gvirtzman et al., 1983, 1998; Engelmann et al., 2001). This soil sequence comprises sub-units that differ in their lithological characteristics (Frechen et al., 2002; Porat et al., 2004). These palaeosol sub-units have a wide range of ages, sometimes synchronous with the aeolianite ridges, and sometimes younger, dating from about 87 to about 8 ka (Gvirtzman and Wieder, 2001; Frechen et al., 2002; Porat et al., 2004; Sivan and Porat, 2004; Mauz et al., 2013).

Unlike the beach ridge sequence chronology, the coastal lowland sequences adjacent to the stream path and mouths have not been studied in detail. Boreholes drilled in the Carmel coast and Zevulun Plain lowlands (Fig. 3.1b), reveal calcareous sandstone units down to 15 m below the present surface, dated to 101 ± 11 and 131 ± 16 ka (Sivan and Porat, 2004; Elyashiv, 2013) respectively, which are older than the base aeolianite of the coastal cliff (Engelmann et al., 2001; Frechen et al., 2002; Porat et al., 2004). Dark brown to brownish-red clayey sand to sandy clay palaeosols uncomfortably overlay the sandstone units in the Carmel coast and Zevulun Plain lowlands. These sandy soils range from about 92 ka to about 8 ka, and contain hiatuses within units that are yet to be explored (Kadosh et al., 2004; Sivan and Porat, 2004; Cohen-Seffer et al., 2005; Elyashiv, 2013; Roskin et al., 2015).

As sea level rose during the Holocene, the shoreline migrated eastwards, flooding the shallow shelf (depth shallower than -20 m) at about 8 ka (Sivan et al., 2001, 2004). Nilotic sand started to accumulate on the coast, and covered the coastal ridges and lowland palaeosols at about 7 ka (Engelmann et al., 2001; Frechen et al., 2001; Porat et al., 2004). At about 3 ka, sea level stabilized at approximately the present mean sea level (MSL; Sivan et al., 2001, 2004). During this time, the ridge that currently marks the shoreline was eroded, forming coastal cliffs which exposed its internal architecture (Katz and Mushkin, 2013).

3.4. Methods

3.4.1. Compilation of existing datasets

Previously acquired stratigraphic, chronostratigraphic, geomorphic and spatial data from the study area were integrated into a single geospatial database using ArcGIS 10.3.1. Existing borehole data were collected from published research papers and reports (Fig. 3.1c; supplementary). The borehole compilation locations, elevations, and lithological descriptions were modified in ArcGIS tables. Existing DEM models (4 × 4 m bin size), soil maps, rectified aerial photographs and chronostratigraphic data of the study area were also uploaded to the ArcGIS database. Based on the relevant lithological data, the submerged calcareous sandstone top stratum topography was mapped using the ArcGIS *Topo to Raster* module (Fig. 3.2).

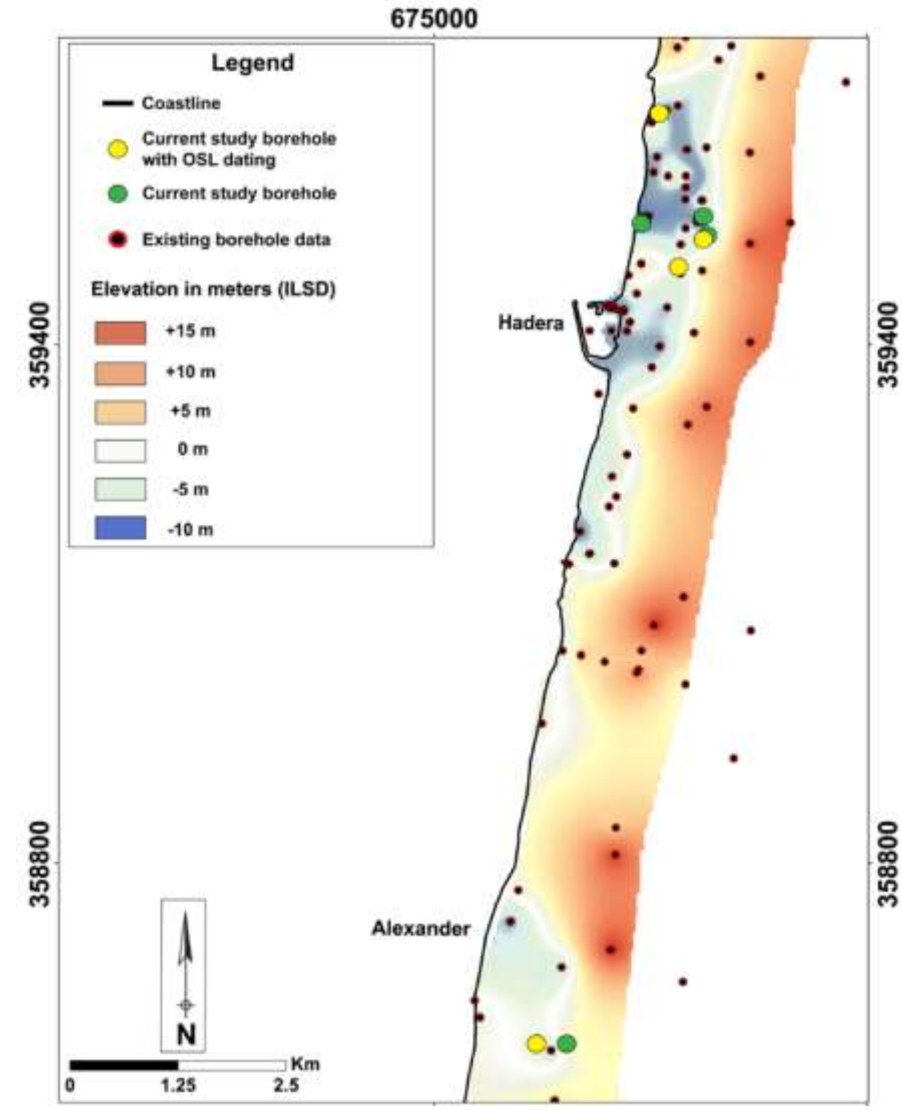

Figure 3.2: Reconstructed topography of the Late Pleistocene calcareous sandstone surface of various dates based on existing log data. The current study drillings (yellow and green circles) were carried out in the reconstructed lowland areas of Hadera and Alexander.

3.4.2. New borehole drillings and petro-sedimentological analyses

In the current study, the locations of new drillings, all in the lowland areas, were chosen, based on a reconstructed shallow top calcareous sandstone surface (Fig. 3.2). Coring was conducted along a 10 km-long N-S transect extending to 1.5 km east of the current shoreline by a Geo-probe 6620DT direct push corer. Locations and elevations of seven continuous cores penetrating down to 15 m were measured using a Proflex 500 RTK-GPS with precisions of XY = ±1 cm and Z = ±5 cm respectively (Fig. 3.1c, d). Magnetic susceptibility (MS) and density were measured every 2 cm for each core. The measurements were conducted using a Geotek multi-sensor core logger equipped with a Bartington loop sensor, compatible for small diameter cores, producing a 0.565 kHz magnetic field.

The boreholes were sectioned lengthwise and logged, including Munsell colours. Brightness values ranging from 0 to 254 were assigned for each pixel though digital photography based on its colour appearance. Particle-size distribution (PSD) was carried out on 300 samples from the seven cores. The measurements, with a particle range of 0.02–2000 µm, were conducted with a Beckman Coulter LS 13 320 laser diffraction particle size analyzer. Total organic carbon (TOC) and inorganic carbon (IC) measurements were conducted on 210 freeze-dried sediment samples of 0.2 g. TOC and IC were measured using a PrimacsSLC TOC analyzer. X-ray fluorescence (XRF) analysis was undertaken on 60 samples from Boreholes SY1 and ALX5, using the EX-310LC(ED) instrument, in an excitation voltage of 35 kV, with an 8 mm diameter beam. Faunal analysis was carried out on 30 selected samples from Borehole ALX5. Samples of 10 g dry weight were washed over a 63 mm sieve and dried. Sub-samples of 5 g were subjected to palaeontological analysis by Dr. Avnaim-Katav. Pollen analysis of ten samples was carried out by Dr. Langgut at the Laboratory of Archaeobotany and Ancient Environments, Tel Aviv University. Thin sections of the basal unit were analysed using an Olympus BX53-P petrographic microscope. Their structures and diagenetic features were classified, described and interpreted following Wright and Tucker (1991) ,Wright (1992), Adams and Mackenzie (1998).

3.4.3. Optically stimulated luminescence (OSL) dating

Sixteen OSL samples were taken from Boreholes SY1, SDC1, SDC4 and ALX5 (Fig. 3.3c, d). The samples were prepared and measured at the Luminescence Laboratory of the Geological Survey of Israel, Jerusalem. Quartz grains (125–150 µm) were extracted using routine laboratory procedures under subdued orange light (Davidovich et al., 2012). After wet-sieving to the desired grain size, carbonates were dissolved with 8 % HCl. The rinsed and dried samples were passed through a Frantz magnetic separator to remove heavy minerals, undissolved carbonates, and most feldspars. A 40-min rinse in 40 % hydrofluoric acid (HF) dissolved any remaining feldspars and etched the quartz grains, followed by rinsing in 16 % HCl overnight to remove any fluorides which may have precipitated.

OSL measurements were carried out on a refurbished Risø DA-12 or DA-20 TL/OSL reader equipped with an integral ^{90}Sr β source, with dose rates of 2.8 Gy/min or 2.3 Gy/min, respectively. Stimulation was achieved with blue LEDs, and detected through 7 mm U-340 filters. The SAR protocol of Murray and Wintle (2000) was used to determine the equivalent dose (De). Preheat and cut heat temperatures of 260 °C and 220 °C were selected respectively, after dose recovery tests showed that with such preheats known doses can be recovered to within 95 %. Individual aliquots (13 to 20 for each sample) were measured, and the average De errors were calculated using the unweighted mean and standard deviation. OSL ages are presented as thousands of years (ka) before 2015.

The sixteen OSL ages obtained in this study are considered reliable (Table 3.1), with bright and rapidly decaying OSL signals, recycling ratios within 5 % of unity, little recuperation and no feldspar contamination. De distributions are mostly tight (over-dispersion values from 8 % to 25

%), indicating that the samples were well bleached at the time of deposition. The ages are in stratigraphic order within errors, and are consistent within each unit (Fig. 3.4).

Table 3.1: Current study boreholes- optically stimulated luminescence (OSL) laboratory data and ages.

Site, Core name, and Sample	Lithological unit/facies	Sample depth relative to ILSD (m)	Moisture (%)	Grain size (μm)	K (%)	U (ppm)	Th (ppm)	Ext. α (μGy/a)	Ext. β (μGy/a)	Ext. γ (μGy/a)	Cosmic (μGy/a)	Total dose (μGy/a)	No. of discs	OD (%)	De (Gy)	**Age (ka)**
Alexander (ALX5)																
ALX-1	F5/a	1.8	6	125-180	0.25	0.35	0.74	1	221	127	189	538±11	18/18	15.7	1.9±0.3	**3.6±0.5**
ALX-2	F5/a	1	14	125-180	0.14	0.77	1.2	2	193	153	174	522±15	20/20	12.3	3.4±0.4	**6.6±0.9**
ALX-3	F4	0.35	22	74-210	0.76	1.60	8.7	7	744	623	158	1531±63	17/18	11.7	16.5±2.1	**10.8±1.4**
ALX-4	F4	0	21	74-210	0.74	1.61	8.5	7	738	619	154	1518±63	18/18	18.3	15.6±3	**10.3±2.0**
ALX-5	F4	-1.2	22	74-210	0.90	1.83	8.7	7	845	672	134	1658±69	18/18	17.4	35.1±6.5	**21±4**
ALX-6	F3	-1.7	18	74-210	0.78	1.52	6.8	6	739	568	130	1443±53	18/18	24.5	52±13	**36±9**
ALX-7	F3	-2	16	74-210	0.84	1.20	5.8	5	735	521	127	1388±50	14/14	23.8	49.8±11.2	**36±8**
ALX-8	F3	-2.2	10	90-150	0.86	1.08	4.7	5	758	496	120	1378±51	14/14	17.8	59.7±11.7	**43±9**
ALX-9	F3	-2.5	16	90-150	0.81	0.95	4.2	4	658	426	115	1202±43	18/18	10.7	50.6±5.7	**42±5**
ALX-10	F3	-2.8	14	125-180	0.58	0.70	2.8	3	479	304	111	897±34	18/18	15.3	52.1±6.9	**58±8**
Hadera-1 (SDC1)																
HAD-33	F2	0.4	17	125-180	0.42	0.53	1.96	2	337±23	214±13	91±4	644±27	13/14	24.2	45.8±11.2	**71±18**
Hadera-2 (SDC4)																
HAD-34	F1	4	16	125-180	0.45	0.56	1.99	2	362±24	226±14	112±6	702±28	13/14	20.9	73±15	**104±22**
HAD-35	Bu	3.3	10	125-150	0.19	0.65	0.91	2	212±15	146±8	105±5	466±18	14/14	21.5	61±14	**131±31**
Sdot-Yam (SY1)																
HAD-36	F3	-2.4	17	125-180	0.32	0.44	1.64	2	264±14	172±10	65±3	502±18	18/18	14.3	26±3.8	**52±8**
HAD-37	F3	-2.9	15	125-180	0.37	0.47	1.92	2	308±16	200±12	62±3	572±20	17/18	14.8	27.5±4.4	**48±8**
HAD-38	F3	-3.2	13	90-150	0.55	0.96	4.18	4±1	524±28	384±24	60±3	973±37	17/18	10.4	46.2±5.3	**48±6**

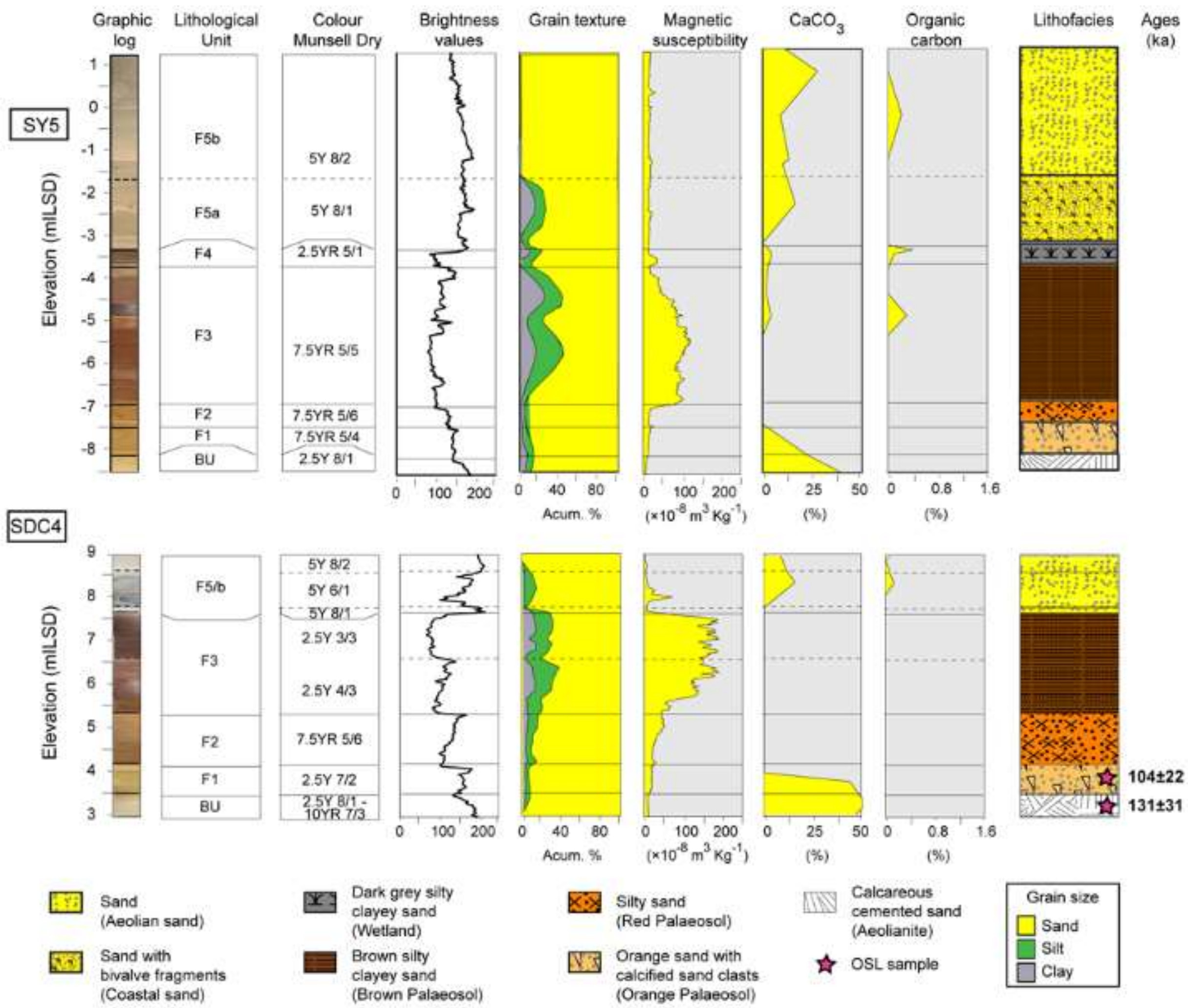

Figure 3.3a, b, c: Boreholes SY5, SDC4, SY1, ALX4, ALX5, SDC2 and SDC1 (location displayed in Fig. 1) with lithological unit classification, colour description (Munsell colour chart), brightness analysis (0 to 254; Campbell, 1996), sedimentological, MS, geochemical results, lithological interpretation and OSL sampling location and ages along the core. XRF analyses were conducted in Boreholes SY1 and SY5 for Fe and Al.

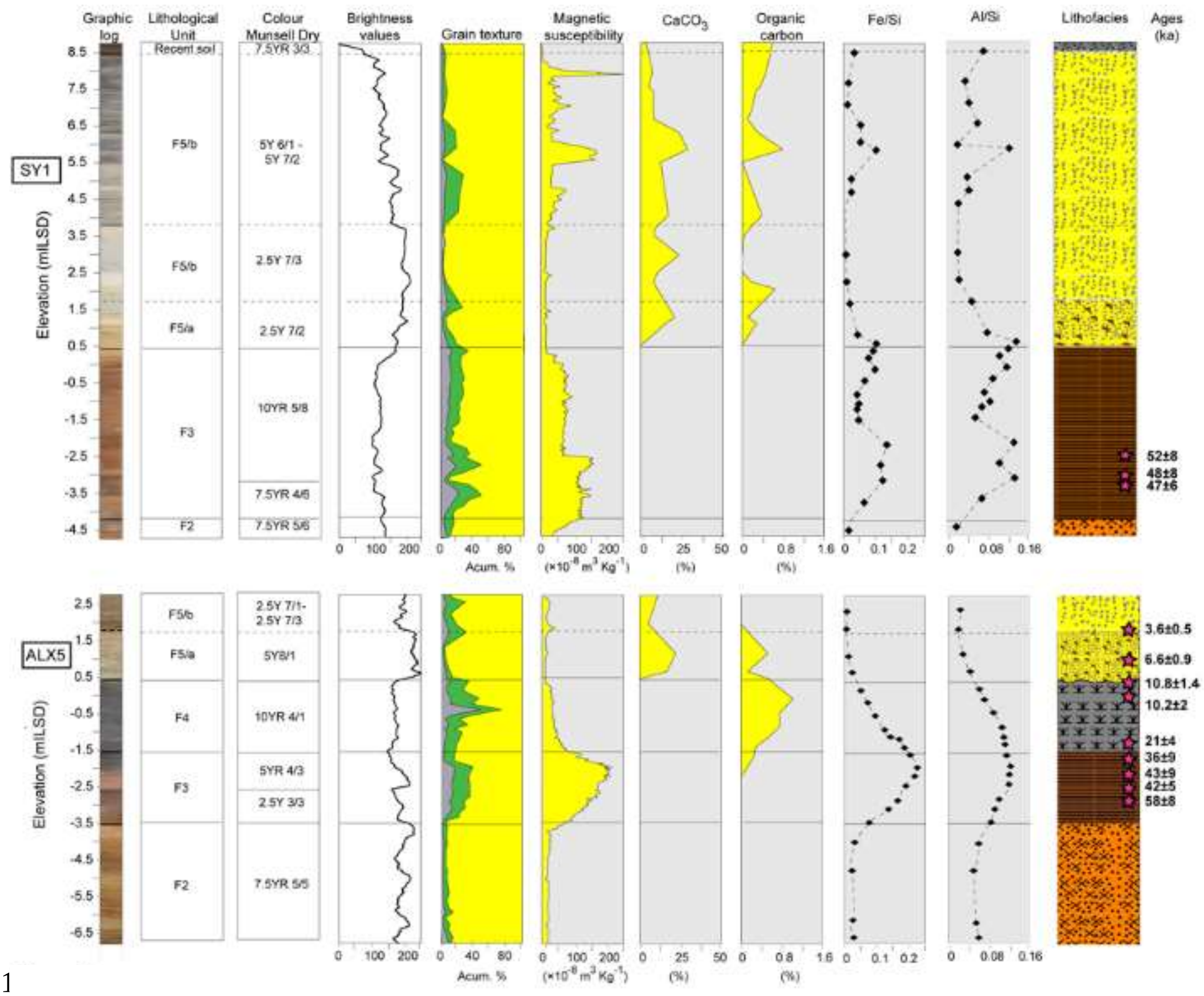

Figure 3.3 (continued)

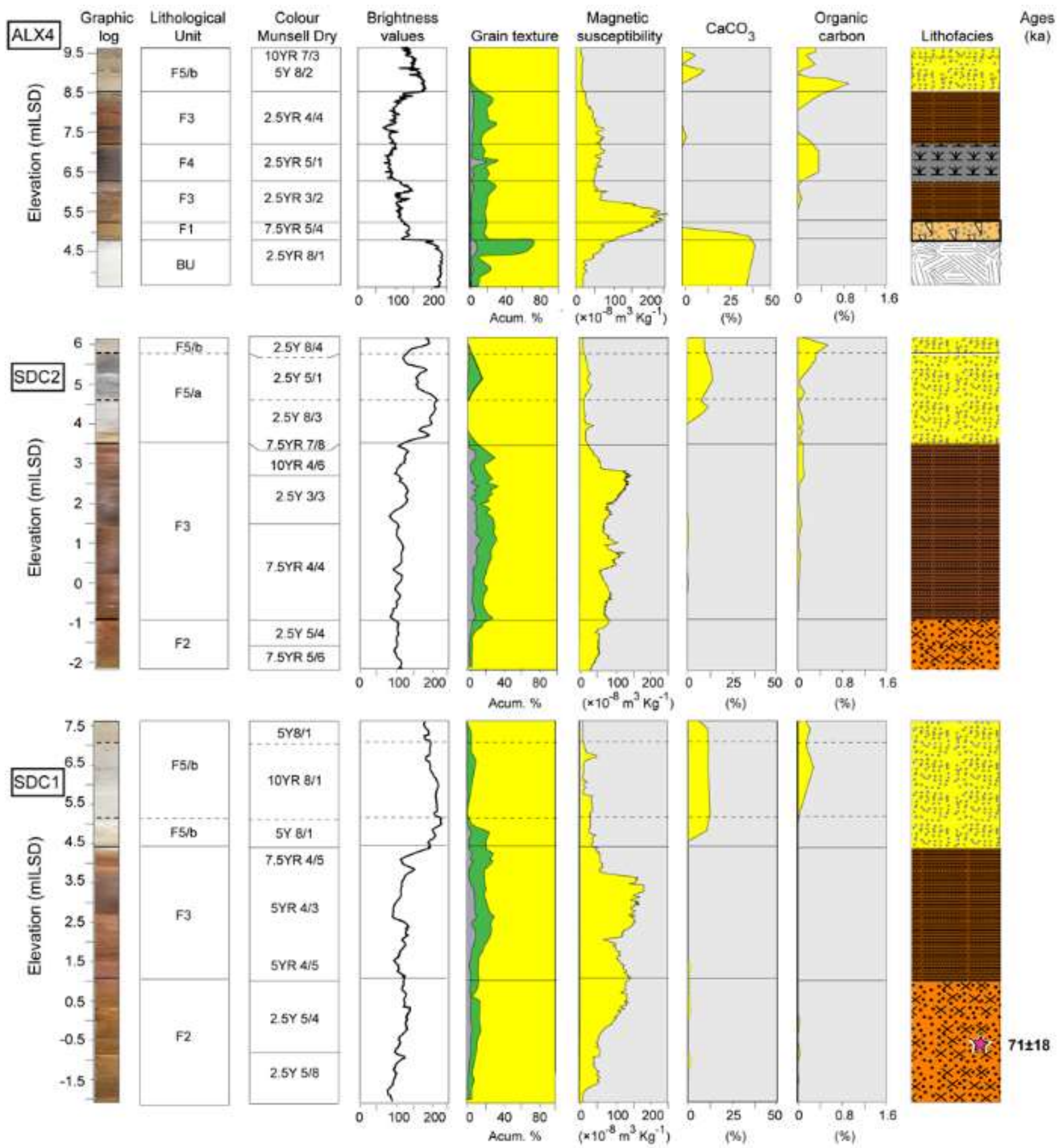

Figure 3.3 (continued)

3.5. Results

The sedimentary sequence of the Alexander-Hadera lowland (Fig. 3.1c, d) consists of five Units (F1-F5), which unconformably overlie the basal unit (Fig. 3.3). The lithological classification of each unit was obtained through integration of the morphological and sedimentological database. Correlation between units was based on morphological features, thickness, elevations, litho-stratigraphical relations, sedimentological and petrophysical similarities:

3.5.1. Basal Unit (BU)

The top 0.5 m of the basal unit of the sequence was reached in Boreholes SDC4, SY5 and ALX4 (Figs. 3.1, 3.3a, c). The upper parts of this unit, whose elevations range from -8.3 to +4.8 relative to the Israel Land Survey Datum (mILSD), are characterized as indurated-brittle cemented sand, while it is identified colour ranges from light reddish grey to dull yellow orange. The unit is dated by OSL in Core SDC4 to 130 ± 31 ka (Table 3.1; Fig. 3.3a).

Samples from Boreholes SDC4 and SY5, retrieved 5 cm beneath the unit's surface, were examined in thin sections. Samples display well sorted, sub-angular to sub-rounded quartz grains coated by brownish micrite carbonate, while pore space is also filled by micrite. Shell fragments, benthic foraminifera (*Ammonia parkinsoniana*, Miliolid) and red algae (*Amphiroa* sp.: Appendix 3.1) were found solely in Borehole SY5. Based on the micromorphology of the quartz grains and the lack of substantial marine microfauna remains, this basal unit is interpreted as the calcareous sandstone aeolianite surface.

A tentative interpretation (due to sparse spatial sampling) of the buried calcareous sandstone surface (Basal Unit) reveals two depressions (Fig. 3.2). The northern one, near N. Hadera, covers an area of 3.4 km^2, and consists of three 6 km-long N-S sub-basins parallel to the shoreline. The basins range from +10 to -10 mILSD, and stretch up to 1.3 km inland from the present shoreline. The southern basin, adjacent to N. Alexander, covers an area of 1.4 km^2, and is an oval depression with its long axis oriented NE-SW. It ranges from elevations of +14 to -6 mILSD, and stretches up to 1.4 km inland from the present shoreline.

3.5.2. Unit F1

Overlying the Basal Unit is Unit F1, identified in Boreholes SDC4, ALX4 and SY5, with the texture of a sandy loam, with a thickness ranging from 0.4 to 0.8 m (Fig. 3.3). The surface elevation ranges from -7.5 to +5.3 mILSD, and is characterized as a sediment with irregularly-shaped hard calcareous cemented sand pebbles. The size and abundance of the pebbles decreases upward from 1 cm, and they are absent at the top of the unit. Colour ranges from dull brown to light orange. F1 is defined as an Orange Palaeosol unit containing no microfauna or pollen, and is OSL-dated in Core SDC4 to 104 ± 22 ka (Table 3.1; Fig. 3.3).

3.5.3. Unit F2

Unit F2 lies conformably on Unit F1 (seen in Boreholes SDC4 and SY5: Fig. 3.3). Its thickness varies from 1 to 3.5 m, while surface elevations range from -4.3 to +5.1 mILSD. Colour ranges from light reddish brown to bright brown, while grain texture becomes finer upwards, and ranges between loamy sand and sandy loam. Elemental analyses show relatively low concentrations of Fe and Al, which increase toward the top of the unit. These concentration variations correlate with the changing MS values silt and clay content (Fig. 3.3b). F2, which is defined as the Red Palaeosol unit, contains no microfauna or pollen. This unit is OSL-dated in Core SDC1 to 71 ± 18 ka (Table 3.1; Fig. 3.3).

3.5.4. Unit F3

Unit F3, which occurs in all the boreholes studied, conformably overlies Unit F2 (Fig. 3.3). Its thickness varies from 1.8 to 4.5 m, while its surface elevations range from -4 to +7.8 mILSD. Grain texture and colour range between sandy clayey loam and sandy loam and dark reddish brown to brown respectively. Elemental analysis shows relatively high concentrations of Fe and Al, which again correlate with the fluctuating MS values and silt and clay content (Fig. 3.3b). F3 contains no microfauna or pollen, and is interpreted as a Brown Palaeosol unit. Its age is constrained by seven samples from two cores ranging from 58 ± 8 to 36 ± 9 ka (Table 3.1; Fig. 3.3b).

3.5.5. Unit F4

Unit F4 conformably overlies the Unit F3 in Boreholes SY5 and ALX5 (Fig. 3.3), while in Borehole ALX4 it is situated in between two lithofacies of the Brown Palaeosol unit. The unit thickness varies from 0.5 to 2 m, while its surface elevations range from -3.4 to +7 mILSD. The unit's grain texture ranges between clay and sandy clay loam, while colour ranges between yellowish-grey and brownish-grey. Elemental analysis conducted in Borehole ALX5 shows a decreasing trend in concentrations of Fe and Al compared to F3, which are in agreement with MS values (Fig. 3.3b). F4 is homogeneous, and microfauna and pollen are absent, except for Borehole ALX5, where *Zannichellia palustris* seeds were identified, suggesting a brackish marsh environment. These characteristics led to the understanding that the F4 dark silty clay was deposited in wetlands. The wetland unit presents three OSL ages: 21 ± 4 ka, 10.2 ± 2 ka and 10.8 ± 1.4 ka, which were sampled from the bottom, 20 cm below the surface and from the surface of the unit respectively (Table 3.1; Fig. 3.3). The ages sampled in the upper part of the unit overlap within measurement errors.

3.5.6. Unit F5

The topmost unit (F5) is found in all of the boreholes. F5 overlies Unit F4 in Boreholes ALX5 and SY5, while in SDC1, SDC2, SY1 and ALX4 (Fig. 3.3) it covers Unit F3. The unit's thickness ranges from 1.3 to 8 m, and its surface elevation ranges from +1.2 to +9.6 mILSD. Unit F5 grain texture ranges from sand to sandy loam, and consists of two identified sub-lithological units, described from bottom to top in Appendix 3.2.

1. Sub-unit F5a is identified in Boreholes ALX5, SY5 and SY1. The facies colour ranges between yellowish-light grey and greyish-yellow. Elemental analysis shows decreasing concentrations up the section of Fe and Al that are generally lower than in Units F3 and F4 (Fig. 3.3b). The sub-unit elevations range from -2.5 to +1.2 m ILSD, accompanied at times by soft cemented sand aggregates. Bivalve shell and shell fragments are evident throughout. This relatively poorly sorted sub-unit is identified as beach sand, and was dated by OSL in Core ALX5 to 6.6 ± 0.9 ka (Table 3.1; Fig. 3.3).
2. Sub-unit F5b is found in all of the boreholes in the current study, and is partly accompanied by land snails. Its thickness ranges from 0.2 to 7 m, while the facies sediment colour ranges between grey and pale yellow. In Boreholes SY1, SDC2, SDC4 and SDC1 pottery remains are evident in several sediment horizons, while small glass remains (less than 0.5 cm), bone fragments, micro-charcoal and lithic fragments of chalk (less than 1 cm) also occur in SY1. Elemental analysis conducted in Borehole SY1 shows varying concentrations of Fe and Al, peaking at +5.5 mILSD, in agreement with MS values (Fig. 3.3b). This relatively well-sorted sub-unit is interpreted as aeolian sand, and was dated by OSL in Core ALX5 to 3.6 ± 0.5 ka (Table 3.1; Fig. 3.3).

Unit F5 as a whole is interpreted as an unconsolidated beach aeolian sand unit.

3.6. Discussion

3.6.1. Depositional environments of the coastal lowlands

The Hadera-Alexander sedimentological units consist mainly of quartz sand in various forms: at the base of the sequence as a lithified calcareous sandstone, while the overlying unconsolidated units have undergone pedogenesis, forming loams of various types. These units have been covered since the Mid-Holocene by windblown sand (Figs. 3.4, 3.5a, d; Roskin et al., 2015). Based on these units, four depositional environments – terrestrial (soils), wetland (clay loam), beach (sand) and aeolian – were identified:

1. Terrestrial – These units include the three palaeosols F1, F2 and F3, barren of fauna and pollen, consisting of orange to brown loamy sand to silty clayey sand, with MS values of 50–250 ($\times 10^{-8}$ m^3 kg^{-1}) and low $CaCO_3$ content (Fig. 3.3). The MS values correlate with the varying silt-clay percent and ferro-magnetic minerals, which point to fine aeolian dust, deposited by rain into the unconsolidated and porous sand profile, driving the pedogenic processes (Gvirtzman and Wieder, 2001; Tsatskin et al., 2008, 2015). $CaCO_3$ content is derived from shell fragments which have been transported inland from the coastal zone/beach. The extent of the pedogenesis process determines the concentration of $CaCO_3$; the longer the process of pedogenesis, the lower is the concentration of $CaCO_3$ as seen in the profile as a result of carbonate dissolution due to leaching (Dan et al., 1968; Yaalon, 1997; Porat et al., 2004; Tsatskin and Ronen, 1999). Based on the high sand content (higher than 70 %) and their associated ages, these palaeosols are presumed to have been formed in the relatively moderate to flat topography of the coastal plain a few hundred metres to several kilometres from the palaeo-coastline when sea level was lower, during most of the last glacial-interglacial period (100 to 8 ka).

2. Wetland – This unit includes the wetland Facies F4, which consists of organic (about 1 %) clay to sandy clay loam sediments which are $CaCO_3$-free. Although the unit contains no microfauna or pollen, *Zannichellia palustris* seeds were identified. These sedimentological properties and the aquatic plant seeds support the interpretation of these sediments being deposited in a brackish marsh environment, while the lack of palaeontological and palynological remains, together with the extended episode of the unit's existence (21 to 10 ka), suggest prolonged exposure of the sediment to aerial conditions and oxidation.
3. Beach – These sediments include the beach Facies F5a, consisting of poorly-sorted coarse to fine quartz sand (Appendix 3.2), bivalve shell fragments, allochthonous benthic microfauna and scarce red algae remains, indicating high wave energy of surf zone to the coastline environment. The unit elevations range from -2.5 to +1.2 mILSD.
4. Aeolian – These sediments include sand Facies F5b, and consist of fine well-sorted round quartz sand (Appendix 3.2), with terrestrial land snail shell fragments, devoid of other fauna. These characteristics suggest sediments that were windblown inland, creating terrestrial sand sheets. Within this facies some horizons include additional features (e.g. potsherds, bone remains and greyish hues). These horizons are probably of anthropogenic origin (Porath, 1975; Roskin et al., 2015); however, further study is required to establish this hypothesis.

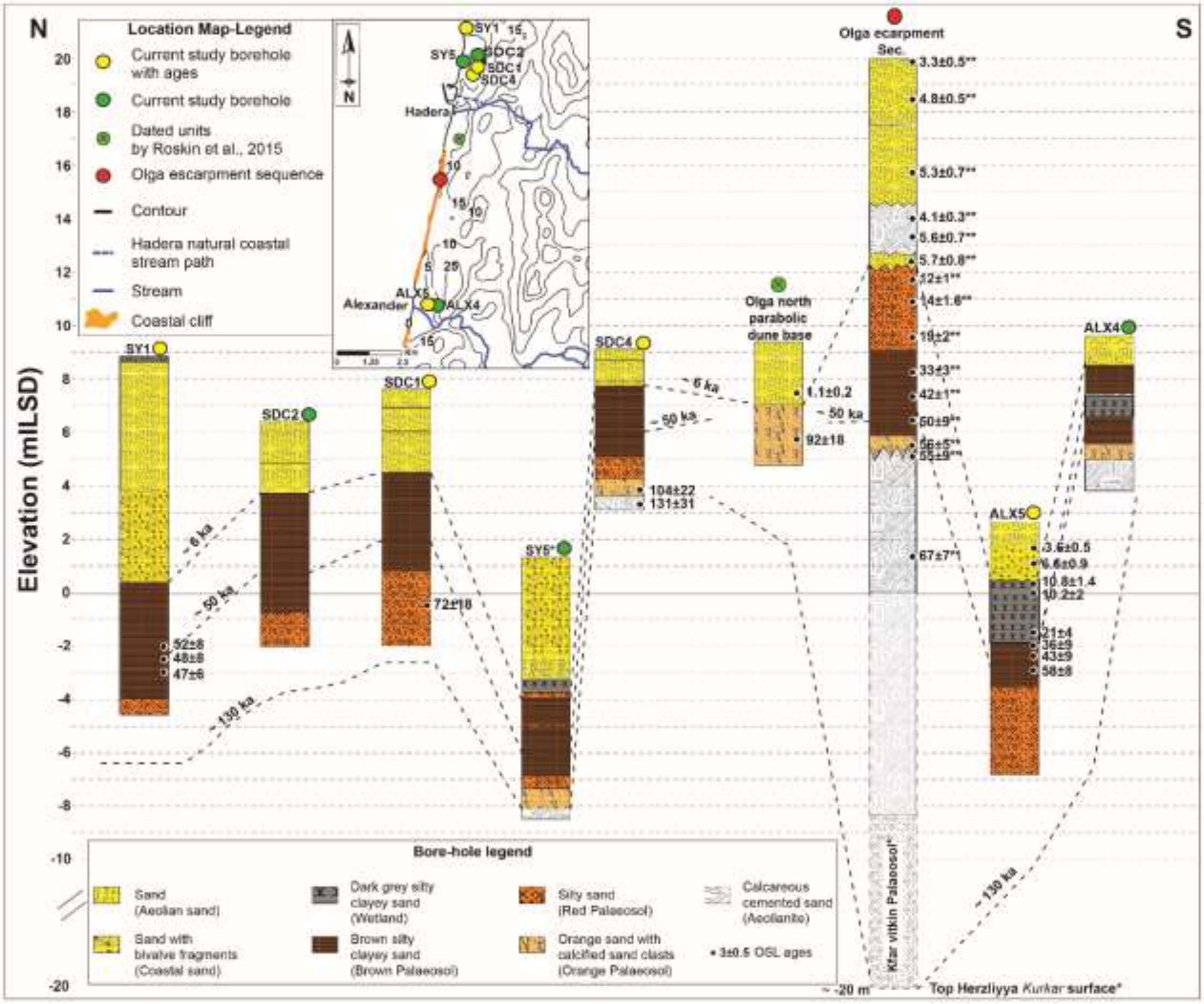

Figure 3.4: The current study borehole lithofacies and accompanied ages (see supplemental map for locations) are represented from north to south against the dated Olga coastal cliff sequence (Frechen et al., 2001, 2002) and Olga north parabolic dune base borehole (Roskin et al., 2015). The litho-chronology is about 6 ka (sandbase), about 50 ka (middle of Brown Palaeosol unit) and about 130 ka (top of the calcareous sandstone basal unit) and are projected and indicated by dashed lines. Since the Olga cliff sequence did not extended lower than 0 mILSD, and chronologically reached about 67 ka, the subsurface elevation of the basal units are estimated based on Gvirtzman et al. (1983). These submerged units (Kfar Vitkin palaeosol and Herzliyya *kurkar*) are indicated with mottled grey.

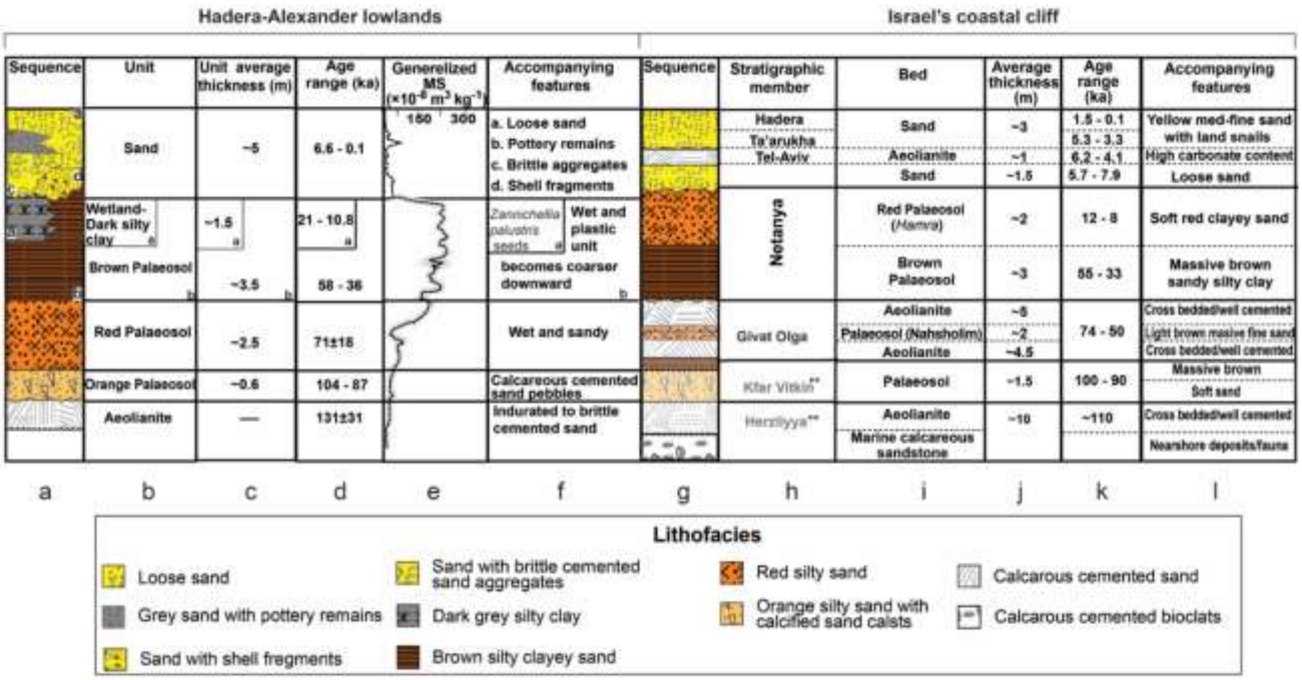

Figure 3.5: Comparison between a composite of sequences of the Hadera-Alexander lowland area and the Israel coastal cliff; (a) The generalized lithofacies of the lowland sequence; (b) unit; (c) average thickness; (d) unit age range; (e) generalized MS values; (f) accompanying features, and with the supplementary previously published data of Roskin et al. (2015). The generalized cliff sequence was computed through the integration of the thickness and ages from Engelmann et al. (2001); Frechen et al. (2001); Frechen et al. (2002); Neber (2002); Porat et al. (2004); Moshier et al. (2010); and Mauz et al. (2013). Since the generalized cliff sequences did not extended below the surface, the subsurface elevations of the basal units (marked by two asterisks) are estimated based on Gvirtzman et al. (1983) (Givat Olga *kurkar*, Kfar Vitkin palaeosol and Herzliyya *kurkar*), and are shown with mottled grey symbols; (g) The generalized lithofacies of the coastal cliff sequence; (h) stratigraphic member; (i) bed; (j) average thickness; (k) unit age range; (l) accompanying features.

3.6.2. Coastal lowland and coastal cliff chronostratigraphic correlation

The coastal lowland sequence which was studied here in detail for the first time can be correlated with the coastal cliff sequence (Fig. 3.5) located along most of Israel's shore from Ashkelon to the Carmel coast (Fig. 3.1b). The correlation is based on the lithological description, petro-sedimentological characteristics, accompanying features, and a stratigraphic position comparison of our new OSL ages with published ages (Gvirtzman et al., 1983, 1998; Engelmann et al., 2001; Frechen et al., 2001, 2002; Gvirtzman and Wieder, 2001; Neber, 2002; Porat et al., 2004; Tsatskin et al., 2009; Moshier et al., 2010; Mauz et al., 2013). This correlation suggests that the coastal lowlands are dominated by palaeosol units with little if any aeolianites, while the coastal ridge sections consist primarily of aeolianites interbedded by palaeosols.

The basal unit (BU) of the studied sequence dates to 131 ± 30 ka (Table 3.2). Relying on the field description, sedimentological analyses (Fig. 3.3) and micromorphology (Appendix 3.1), we propose that this calcareous sandstone unit was deposited in a beach-terrestrial environment. Based on this age range, the stratigraphical position and features of the units can be correlated with the upper terrestrial facies of Herzliyya *kurkar* (i.e., 98 ± 6 ka; Mauz et al., 2013), which was found at elevations ranging from a few metres above ILSD on the Carmel coast to about -75 mILSD in southern Israel (Fig. 3.1b; Gvirtzman et al., 1983; Frechen et al., 2004).

Overlying the Herzliyya *kurkar* is the Orange Palaeosol (F1), dated to about 104 ± 22 ka (Fig. 3.3a). A similar facies, with corresponding sedimentological appearances (hue, lithology, grain size, $CaCO_3$ and accompanying irregularly-shaped calcareous cemented sand nodules), has been identified 2 km south of Borehole SDC4 and dated to 87 ± 17 ka (Roskin et al., 2015). Based on this age range, the stratigraphical position of the units (Gvirtzman et al., 1983) and features can be correlated with the Kfar Vitkin palaeosol (Gvirtzman et al., 1998; Frechen et al., 2004), which was found at elevations ranging from about +8 mILSD to about -70 mILSD (Fig. 3.1b; Gvirtzman et al., 1998; Frechen et al., 2004; Tsatskin et al., 2009). There are differences between the two units, with F1 having lower silt and clay concentrations and lower MS values than the Kfar Vitkin palaeosol (Mauz et al., 2013). These sedimentological differences are proposed to be a result of relief differences and slope angle variations between the two areas, leading to lateral erosion of sediments in the sloping areas and re-deposition in the depression (Dan et al., 1968; Yaalon, 1997; Tsatskin et al., 2009).

The Orange Palaeosol unit is covered by the Red Palaeosol (F2), which is dated to about 71 ± 18 ka (Fig. 3.3c). During the depositional time of the Red Palaeosol parent material, from 80 to 55 ka, sand was deposited on the coastal plain of Israel in a thickness ranging from 2 to 40 m (Zilberman et al., 2007; Roskin et al., 2013), forming dunes and sand sheet complexes. Since stream energies were greater during periods of low sea levels, mainly due to higher gradients and incisions (Suter and Berryhill, 1985; Anderson et al., 1996; Blum and Tōrnqvist, 2000 and ref. therein), the streams limited sand deposition in their channels, consequently transporting the sand back to the coastline where it was deposited. The sand removal from the stream outlets and dune build-up over the rest of the area led to the formation of the lowlands (Fig. 3.1c, d). Moreover, the synchronous deposition of the dune-sand sheet complex (up to 40 m) and the slow sand sheet accumulation in the coastal lowland (up to 4 m) led to the concurrent development of the coastal ridges Givat Olga Member (aeolianites interbedded by Nahsholim Palaeosol; Gvirtzman et al., 1983, 1998) and lowland Red Palaeosol (Figs. 3.5, 3.6; Frechen et al., 2002; Mauz et al., 2013).

The Red Palaeosol is overlain by a dark reddish-brown to brown unit with sandy clayey loam to sandy loam grain texture (F3). This Brown Palaeosol consists of high Fe and Al concentrations, which are in agreement with fluctuating MS values, and is dated to between 58 ± 8 and 36 ± 9 ka (Figs. 3.3, 3.4). The carbonate percentage, particle size, MS and chronology of the Brown Palaeosol are comparable to the lower coastal cliff Netanya palaeosol sub-unit (Fig. 3.5; Gvirtzman and Wieder, 2001). The upper sub-units of the Netanya palaeosol are dated from 12 to 8 ka at varying elevations ranging from +10 mILSD to about +40 mILSD in an N-S section from the Sharon coast to Ashkelon in the south (Figs. 3.1b, 3.5; Gvirtzman et al., 1983; 1998; Frechen et al., 2002; Porat et al., 2004; Mauz et al., 2013). Even though the top of the lowland Netanya palaeosol was not dated in this study (Appendix 3.3) the unit's surface was dated in a similar geomorphic location south of Rishon-Lezion (Fig. 3.1b) to 8.6 ± 2.5 ka (Roskin et al., 2016).

In several boreholes adjacent to the stream paths, a dark silty-clay deposit (F4) was identified covering the Brown Palaeosol. This wetland facies, dated from 21 ± 4 to 10 ± 2 ka, was also identified along the Carmel coast (Kadosh et al., 2004; Cohen-Seffer et al., 2005; Sivan et al., 2011 among others) adjacent to stream systems but was not detected on the higher coastal ridge sequence (Fig. 3.4).

The topmost unit identified in the lowlands consists of four sandy units deposited from 6.6 to 0.1 ka (Fig. 3.6; Roskin et al., 2015) which correspond closely to three aeolian units deposited on the coastal ridges (6.2 to 0.1 ka): Hadera; Ta'arukha sand; and the Tel-Aviv *kurkar* (Gvirtzman et al., 1983).

Table 3.2: Age comparison between Alexander-Hadera lowland and generalized coastal cliff sequence.

Hadera-Alexander generalized lowland units	Lithology	Lowland Ages (ka)	Israel's generalized coastal cliff stratigraphic member	Lithology	Coastal cliff ages (ka)
Sand	Loose sand Grey sand	*0.12±0.05*[1] *0.86±0.1*[1]	Hadera Ta'arukha	Loose sand	*0.2±0.02*[3a] *5.3±0.7*[3a]
	Brittle cemented sand aggregates	*3.3±0.5*[1] **3.6±0.5**	*Kurkar* Tel-Aviv	Calcareous cemented sand	*4.1±0.3*[3a] *6.2±0.7*[3a]
	Sand with bioclasts	**4.3±0.9** **6.6±0.9**		Sand with land snails	*5.7±0.8*[3a] *7.9±0.2*[2]
Wetland dark silty clay	Clay-Sandy clayey loam	**10.8±1.4** **10.2±2** **21±4**	Netanya palaeosol	Sandy loam	*8±0.4*[4] *12±1*[3a] *14±2*[3a] *19±2*[3a]
Brown Palaeosol	Sandy clayey loam	**36±9** **43±9** **52±8** **48±8** **47±6** **58±8**	Netanya palaeosol	Sandy clayey loam	*33±3*[3a] *51±9*[3a] *56±5*[3a]
Red Palaeosol	Sandy loam	**71±18**	Givat Olga	Calcareous cemented sand	*50±4*[3a] *56±4*[2]
				Palaeosol	*55±5*[3a]
				Calcareous cemented sand	*74±8*[4]
Orange Palaeosol	Sandy loam with calcareous nodules	*87±17*[1] *92±18*[1] **104±22**	Kefar Vitkin Palaeosol	Sandy loam with calcareous nodules	*80±5*[3] *84±4*[3]
Aeolianite	Calcareous cemented sand	**131±31**	*Kurkar* Herzeliyya	Calcareous cemented sand	*98±6*[3]

Ages annotated in Bold were dated in the current study.

[a] IRSL ages of K-feldspars. The ages were obtained 15 to 20 years ago using IR50, and were not corrected for anomalous fading. The true ages could be as much as 20 to 30 % older (Thomsen et al., 2008).

References: (1) Roskin et al., 2015 (2) Mauz et al., 2013 (3) Engelmann et al., 2001; Frechen et al., 2001; 2002; Porat et al., 2004 (4) Moshier et al., 2010.

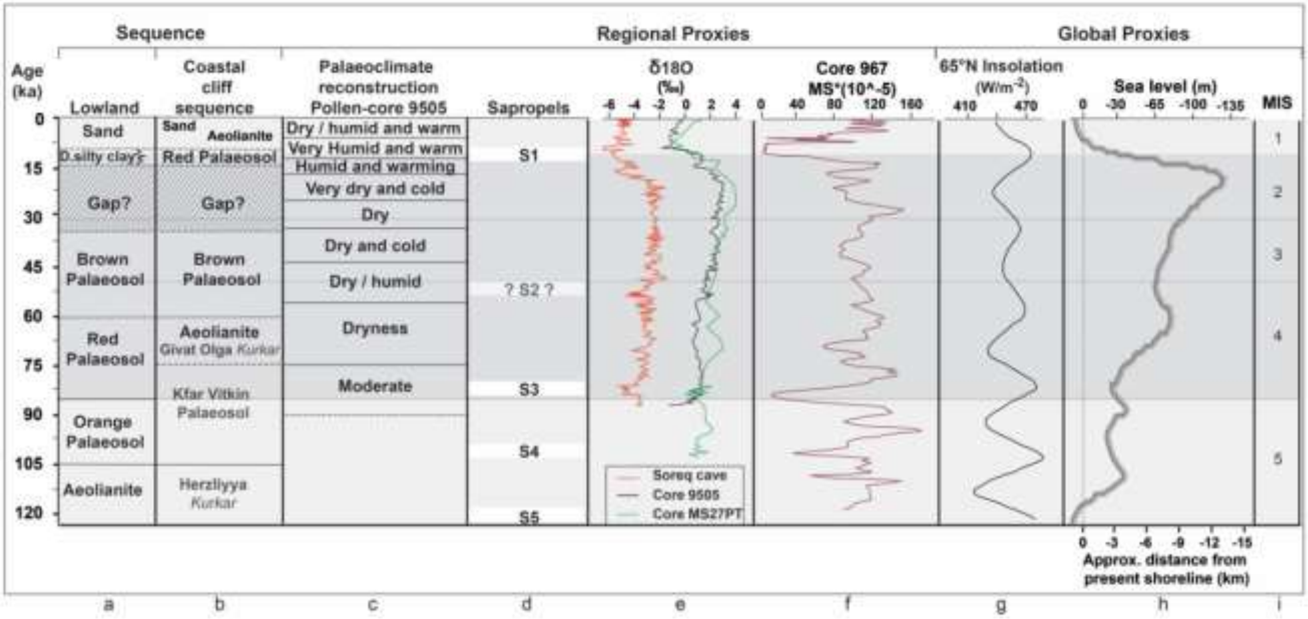

Figure 3.6: Comparison between a composite of sequences of Hadera-Alexander lowland, Israel coastal cliff, palaeoclimate records of the region and global proxies. (a) The generalized lowland chronostratigraphy (b) The generalized coastal cliff chronostratigraphy of Israel computed from Engelmann et al. (2001); Frechen et al. (2001); Frechen et al. (2002); Neber (2002); Porat et al. (2004); Moshier et al. (2010); Mauz et al. (2013). Since the generalized cliff sequences were not studied below the surface, the subsurface elevation of the basal unit is estimated based on Gvirtzman et al. (1983) (Givat Olga *kurkar*, Kfar Vitkin palaeosol and Herzliyya *kurkar*), and is indicated by semi-transparent symbols; (c) Palaeoclimate reconstruction based on Core 9505 (Langgut et al., 2011); (d) Sapropel accumulation periods; (e) Soreq cave speleothem record as a proxy for precipitation and runoff (Bar-Matthews et al., 2003), and deep sea record as a proxy for Levantine sea response to global ice accumulation (Almogi-Labin et al., 2009; Revel et al., 2010); (f) MS values computed from ODP Core 160-967 used as a proxy for Saharan dust supply. This correlation is proposed for the last interglacial because of the correspondence between high MS values and dry periods, and low MS values with periods of wet climate (Larrasoaña et al., 2008); (g) Insolation at 65°N (Imbrie et al., 1984); (h) Global sea level stack (Spratt and Lisiecki, 2015) against approximated distance from present shoreline; (i) Marine Isotope stages.

3.6.3. Global to regional-scale triggering forces influencing the formation of the coastal stratigraphy

The reconstructed chronostratigraphy for the lowlands and coastal cliff can be linked to both global and regional environmental proxies, in order to highlight the triggering and driving forces that shaped the Israel coastal evolution over the last 110 ka. In the following sections the contribution of global sea-level, together with regional climate, is discussed.

3.6.3.1. Low sea levels and their controls on sedimentation gaps

From about 110 ka to the Middle Holocene, the continental shelf was partly-fully exposed due to lower than present sea levels (Fig. 3.6). The common parent material of the last glacial-interglacial coastal sequence of Israel and the relatively continuous ages (Figs. 3.4, 3.5) suggest that the longshore transport of sand from the Nile Delta to the coastal zone was fairly continuous during most of the period studied. Nevertheless, both the lowland and coastal cliff sequences highlight a possible depositional time gap in the Netanya palaeosol from about 33 to 12 ka (Figs. 3.5, 3.6). The disruption in sand accumulation is supported by various studies from across the southern (Zilberman et al., 2007; Roskin et al., 2011a), central (Gvirtzman et al., 1998; Gvirtzman and Wieder, 2001; Sivan and Porat, 2004) and northern (Zviely et al., 2006; Elyashiv, 2013) Israeli coastal plain, in which only a single age of 19 ± 2 ka was obtained by Frechen et al. (2001), sampled from a coastal ridge in central Israel. Global eustatic sea level curves (Spratt and Lisiecki, 2015), regional eustatic sea level proxy records (Anzidei et al., 2011; Rohling et al., 2014), local RSL data (Sivan et al., 2001) and erosive unconformity from subsurface profiles (Schattner et al., 2010, 2015) suggest that this gap is associated with the LGM lowstand (33 to 15 ka), and then from 15 to 12 ka during the rapid RSL rise.

During the lowstand, sea level ranged from -85 to -130 mILSD, and the shoreline was situated below the shelf-break (Fig. 3.6i). The shelf-break curvature – exceeding 1 º – (Almagor et al., 2000) and its ridged surface (Schattner et al., 2010, 2015) served as a further barrier to easterly aeolian transportation of sand (Posamentier et al., 1992; Mauz et al., 2013; Shtienberg et al., 2016). A depositional gap of aeolian sediments during lower sea level phases has been described for other Mediterranean coastal areas, and even beyond it. These included Egypt (El-Asmar, 1994; El-Asmar and Wood, 2000), Tunisia (Mauz et al., 2009; Elmejdoub et al., 2011) southern Spain (Zazo et al., 2008) and the Canary Islands (von Suchodoletz, et al., 2010), occurring from 70 ka in the Mediterranean and from 30 ka in the Canary Islands to Mid-Holocene. The longer hiatuses in sedimentation documented in the northern coasts of Egypt (shelf-break curvature 0.15 º) and northern Tunisia (0.1 º) are presumed to be the result of the shallower coastal profile, compared to Israel's shelf bathymetry (0.5 º) (Almagor et al., 2000; Sade et al., 2006; Amante and Eakins, 2009).

At the end of the LGM (about 20 to 19 ka), sea level rose rapidly, reaching -85 m by 15 ka (Fig. 3.6h; Lambeck and Purell, 2005). As a result of the fast transgression (Waelbroeck et al., 2002; Rohling et al., 2014; Spratt and Lisiecki 2015), accommodation space outpaced sediment supply, hindering sand deposition on the coastal plain until 12 ka.

<u>3.6.3.2. Regional processes affecting pedogenesis</u>

The environment of deposition and post-depositional changes on Israel's coastal plain have inevitably been affected by climate change. Such regional processes are identified in the sediments of both the lowland coastal plain and the coastal cliffs. These sediments pedogenised into Netanya palaeosol across most of Israel's coastal plain (Fig. 3.5; Gvirtzman et al., 1983; Gvirtzman and

Wieder, 2001; Neber, 2002; Tsatskin et al., 2008). The MS values (80–250 $\times 10^{-8}$ m^3 kg^{-1}), which are high compared to the other units found in the Quaternary sequence, and the red-dark brown hues are the result of continuous enrichment by aeolian dust and illuviation of the clay's associated magnetic iron-rich minerals (Fig. 3.3b), e.g. smectite (Dan et al., 1968). These petro-sedimentological characteristics are temporally associated with regional climate proxies that include lower $\delta^{18}O$ values and oak types (Fig. 3.6c - f; Bar-Matthews et al., 2003; Revel et al., Langgut et al., 2011), suggesting relatively wetter climatic conditions during pedogenesis (Yaalon; 1997; Tsatskin and Ronen, 1999; Gvirtzman and Wieder, 2001). These wetter climatic conditions, coaeval with Sapropel S2, also enhanced pedogenesis across the Canary Islands, which were influenced by fluctuations in the Saharan dust supply, and are reflected in changes in environmental conditions in the northwest African region (Bozzano et al., 2002). For example, a clay-rich, brown-red palaeosol with high MS values was formed throughout Lanzarote, dated from 55 to 30 ka (von Suchodoletz et al., 2010).

3.6.4. Evolution of the coastal plain of Israel during the Late Quaternary

During MIS5e, sea level was 1 to 7 m higher than at present (Fig. 3.6i; Galili et al., 2007; Hearty et al., 2007; Kopp et al., 2009, 2013; Rohling et al., 2014; Dutton et al., 2015; Spratt and Lisiecki, 2015; Sivan et al., 2016). Based on the reconstructed topography of the Late Pleistocene calcareous sandstone surface (Fig. 3.2), together with Boreholes Caesarea IEC1; Hadera 1, Kfar Vitkin T/48/0 (Fig. 3.1c, d), and the elevation of the Herzliyya *kurkar* surface along Israel's coastal plain (Gvirtzman et al., 1983), we propose that over this period inland flooding occurred, creating an irregular coastline with estuaries, bays and headlands (Fig. 3.7a). Based on a simplified reconstruction combining sea level data from Spratt and Lisiecki (2015) and modern-day bathymetry of the Israeli continental shelf (Hall, 1994), the approximate distance from present shoreline is shown in Fig. 3.6h from 115 ka onward.

From about 110 to 80 ka, sea level fluctuated by magnitudes of about ±25 m, while the shoreline was located up to 5 km westward (Fig. 3.6h). Nilotic sand, which continued to be deposited on the palaeo-shores (present day offshore) of Israel, was windblown inland, dispersing on the palaeo-coastal plain. The aeolian sand covered the basal aeolianite (BU) as a thin (about 1 to 2 m thick) sand sheet (Fig. 3.7b), in some areas leaving the surface exposed for long periods. The sedimentological characteristics of the Orange palaeosol, consisting of light orange sandy loam with hard calcareous cemented irregularly-shaped sand pebbles, the size and abundance of which decrease from the bottom to the top of the unit, were identified in the Hadera–Alexander lowland (Fig. 3.1c, d) and on the Carmel coast (Frechen et al., 2004; Tsatskin et al., 2009; Roskin et al., 2015). These characteristics suggest that the basal aeolianite surface (BU) partly weathered back to its parent material (C horizon). The weathered aeolianite material and newly deposited Nilotic quartz sand pedogenised to form Kfar Vitkin Palaeosol. In the Carmel coast this unit has a red–dark red colour, high MS values and higher silt and clay contents (Fig. 3.3; Frechen et al., 2004; Tsatskin et al., 2009; Mauz et al., 2013). The ages of the unit correlate to similar dark red silty clayey palaeosols that formed on the northern coasts of Egypt and Tunisia (El-Asmar and Wood, 2000; Elmejdoubet al., 2011, who propose their connection with the wetter climate of Sapropel 3) (Fig. 3.6).

Between 80 and 55 ka, sand accumulated across the coastal plain, covering the Kfar Vitkin Palaeosol (Fig. 3.7c). Deposition was limited close to the stream outlets, eventually resulting in sand sheets only 2 m thick. Following stabilization at about 55 ka, the sand unit close to the streams slowly pedogenised into the Red Palaeosol (Figs. 3.5, 3.6, 3.7c). The pedogenesis process was controlled by the interaction of dust accumulations and precipitation. The source of the dust that accumulated on the coastal plain of Israel was either solely or jointly supplied by the wide exposed shelf, Sahara deserts (Enzel et al., 2008), or the north of the Sinai-Negev dune field (Ben-David, 2003; Crouvi et al., 2012). The post-depositional pedogenic process took place during wetter periods, enabling hydrolytic weathering of silicate minerals and leaching of dispersed clay minerals in the soil profile. The process ended when sand deposition exceeded the pedogenic process, resulting in the burial of the soil, and leading to a new pedogenetic cycle (Yaalon, 1967, 1997; Tsatskin et al., 1999; Gvirtzman and Wieder, 2001; Mauz et al., 2013). Due to the low to moderate silty-clay content, the light hues contain relatively low concentrations of Fe, Al, and the MS values of the Red Palaeosol. This unit is interpreted as a moderately developed palaeosol (Fig. 3.3b). We propose that the Red Palaeosol is the outcome of the relatively dry conditions which prevailed between 80 and 55 ka, in light of the relatively constant aeolian dust supply during the formation of the three lowland palaeosol units from 80 to 25 ka (Fig. 3.6c - e; Cheddadi and Rossignol-Strick, 1995; Larrasoaña et al., 2008). In other locations, distant from the stream paths, dune-sand sheet complexes up to 40 m thick were deposited, eventually forming the lower exposed units of the present-day shore-parallel ridges (i.e. Givat Olga member; Figs. 3.5, 3.7c; Gvirtzman et al., 1998; Engelmann et al., 2001; Mauz et al., 2013).

The regressing sea level reached about -65 mILSD by 55 ka, and from about 55 to 35 ka it fluctuated by about ±10 m (Fig. 3.6h; Waelbroeck et al., 2002; Rohling, 2014). During this time of RSL stability, windblown quartz sediments covered Israel's palaeo-coastal plain (Fig. 3.7d) by an average thickness of about 3.5 m (Fig. 3.5a). Based on a correlation conducted across most of Israel's coastal plain and in two shallow shelf locations (depth shallower than -40 mILSD) located offshore, the southern (Ashkelon; Porat et al., 2003) and central (Hadera; Shtienberg et al., 2016) coasts of Israel, it is evident that this sand sheet pedogenised into Netanya Palaeosol (Gvirtzman et al., 1983; Gvirtzman and Wieder, 2001; Neber, 2002; Tsatskin et al., 2008). The sedimentological and petrophysical characteristics of Netanya Palaeosol suggest a unit which is fully pedogenised (Yaalon, 1997; Gvirtzman and Wieder, 2001) along most of the palaeo-coastal plain of Israel. Regional climate proxies indicate that the pedogenesis of the Netanya palaeosol occurred during an alternating relatively wet climate that prevailed from about 55 to 45 ka, and dry climate from about 45 to 35 ka (Fig. 3.6; Cita et al., 1977; Cheddadi and Rossignol-Strick, 1995; Revel et al., 2010). These changing climate periods were accompanied by a relatively constant dust accumulation (Enzel et al., 2008), interpreted from the MS values (Fig. 3.6) of the Ocean Drilling Program ODP 160-976 (see location in Fig. 3.1b; Larrasoañaet al., 2008).

A rapid drop in sea level occurred from about 35 ka to 20 ka, when sea level fell from about -85 mILSD to a minimum of about -135 mILSD (Rohling et al., 2014), resulting in shoreline migration from about 11 km to about 14 km offshore (Fig. 3.6h). The regressing coastline was accompanied by increased windiness and dry and cold conditions, which continued until about 16 ka (Fig. 3.6; Bar-Matthews et al., 2000; McGee et al., 2010; Revel et al., 2010; Roskin et al., 2011a, 2011b). Much like the coastal areas of northern Tunisia (Elmejdoub et al., 2011) and the Huelva coast in south-western Spain (Zazo et al., 2005), the low sea level and climate conditions left the coast and exposed shelf sediment starved, inducing an erosional hiatus.

At the end of the LGM, sea level rapidly rose, (Fig. 3.6h; Waelbroeck et al., 2002; Lambeck and Purell, 2005; Spratt and Lisiecki 2015), hindering sand deposition on the coastal plain unit until 12 ka. A dark-grey silty clay facies was identified adjacent to the streams in the Alexander and Hadera lowlands (Figs. 3.3, 3.7e), indicating wetlands. These wetlands resemble, in their location and age, the wetlands on the coast and the shallow shelf of southern (Porat et al., 2003), central (Neev et al., 1978; Kadosh et al., 2004; Sivan et al., 2011; Shtienberg et al., 2016), and northern (Avnaim-Katav et al., 2012; Elyashiv et al., 2016) Israel. As suggested by Sivan et al., (2011), Elyashiv et al. (2016) and Shtienberg et al., (2016), such units were deposited on the coastal plain as a result of stream overflows affected by rising sea level and a wetter climate, which changed from about 15 ka, as a result of the extreme insolation values (Fig. 3.6c, d; Bar-Matthews et al., 2000; Revel et al., 2010; Langgut et al., 2011).

During the Pleistocene-Holocene transition, sea level transgression rates slowed (Fig. 3.6h; Lambeck and Bard, 2000), and the palaeo-shoreline was located about 3 km offshore of its current position (Fig. 3.6h). Consequently, sediment transport recommenced from the Nile Delta by the longshore currents and was carried landward by the wind. The depositing sand pedogenized to form the upper sub-units of Netanya Palaeosol identified on the coastal ridges and lowlands, dated from 12 to 8 ka (Fig. 3.5; Gvirtzman and Wieder, 2001; Porat et al., 2004; Roskin et al., 2016). The earliest documented deposition of the upper, unconsolidated, sand is about 8 ka (Fig. 3.5; Gvirtzman and Wieder, 2001; Mauz et al., 2013), and is proposed to be the result of two contributing factors: (a) erosion of the Nile Delta as a result of the rising sea levels, consequently increasing the sediment discharge to the Levantine basin (Fig. 3.6h; Stanley and Warne, 1998; Revel et al., 2010); and (b) closer coastlines and slower sea level rise. The high sediment discharge hypothesis is supported by higher sedimentation rates of 55 cm/ka and 110 cm/ka calculated from the deep-sea Cores 9505 and MS27PT (Fig. 3.1a; Revel et al., 2010; Langgut et al., 2011), respectively, and higher fluxes of up to 180 cm/ka in the shallow marine Cores V115, V101, located 1.5 km seaward from the current shoreline in a water depth of -30 m (Fig 3.1b; Mor-Federman, 2012). In addition, the shoreline reached about 1.5 km offshore from its present position (Fig. 3.6h).

Archaeological observations from the coast confirm that sea level continued to rise during the early stages of the Holocene until c. 6 to 7 ka, when transgression slowed considerably. Then, at about 6 to 4 ka, as sea level and the coastline almost reached their present elevation and location (Fig. 3.6; Sivan et al., 2001, 2004; Anzidei et al., 2011; Toker et al., 2012), the volumes of windblown sand which accumulated along the coast increased (Roskin et al., 2015 and ref. therein). The initiation and timing of the current wind-induced beach sand build-up is dated to 5 ka in the shallow shelf by Porat et al. (2003), Reinhardt et al. (2006), Goodman-Tchernov et al. (2009), and on the coast mainly by Roskin et al. (2015).

A 1.5 m-thick bioclastic sand facies (Figs. 3.3, 3.4), found in the current study in the lowland area of the Alexander stream, was dated to between about 6.6 and 3.3 ka (Table 3.2). Based on its location, elevation range (+1.3 to +0.3 mILSD), the relatively high percentage of the bioclasts, and the covering aeolian sand unit, we suggest that in the stream outlets the sea penetrated inland and created estuaries (Appendix 3.2). In these areas the coastline reached about 1 km inland at about 4 ka (Raban and Galili, 1985), and progradated to its current position at about 3 ka. These late Holocene embayments resemble, on a smaller scale, those described in Haifa Bay and the Zevulun Plain (Fig. 3.1; Zviely et al., 2006; Porat et al., 2008; Elyashiv et al., 2016). From 6 to 4 ka, a sequence of bioclastic sand 1 to 3 m thick was deposited along most of Israel's coastal cliff. This bioclastic sand eventually calcified to aeolianite (Tel Aviv *kurkar*) (Fig. 3.7f; Gvirtzman et al., 1998; Frechen et al., 2002; Porat et al., 2004), although its formation has yet to be properly examined. As the sea level and coastline position stabilized, greater volumes of sand were windblown inland (Fig. 3.7f). The aeolian sand overlaid the lowland areas around the estuaries, and created ridges reaching a thickness of up to 7 m (Fig. 3.3; Roskin et al., 2015).

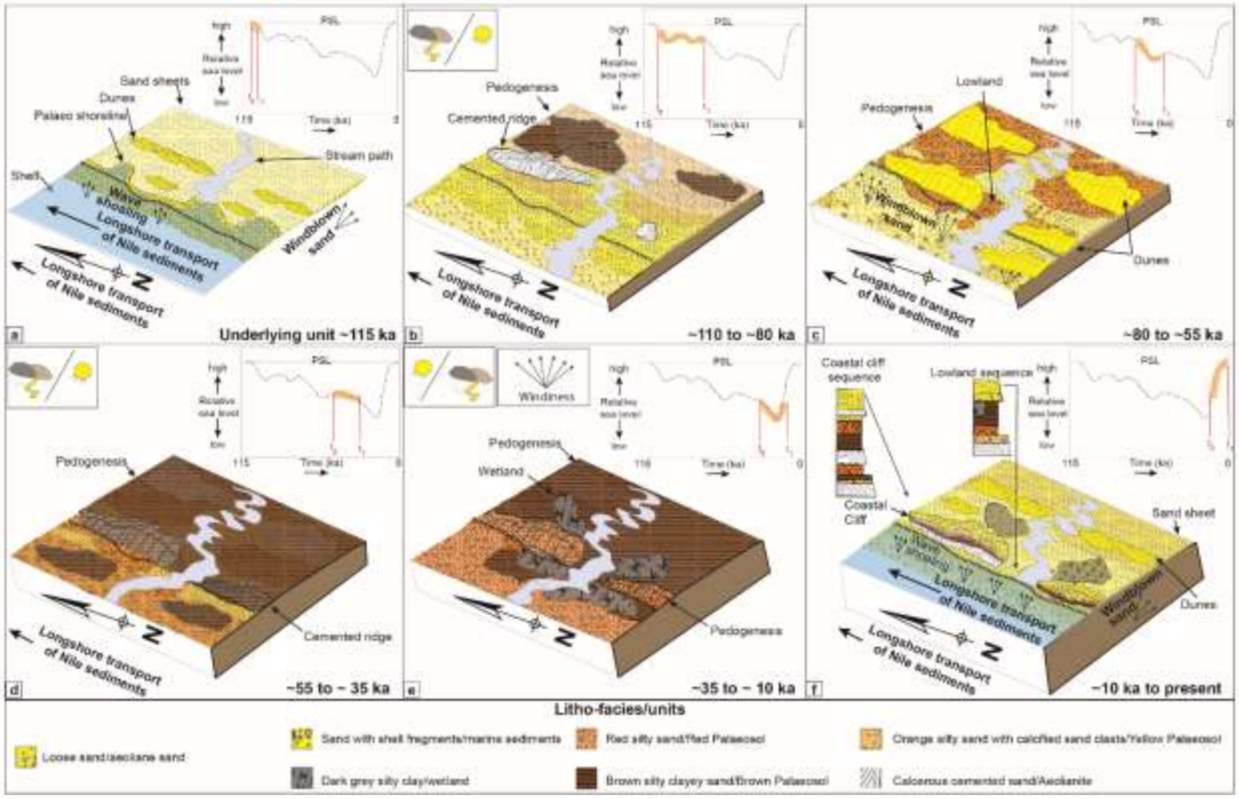

Figure 3.7: Schematic models (not to scale) of the Late Quaternary evolution of Israel's coastal plain from Ashkelon to the Carmel coast. The evolution is portrayed through six periods: (a) about 115 ka; (b) about 115 to 80 ka; (c) about 80 to 55 ka; (d) about 55 to 35 ka; (e) about 35 ka to 10 ka; (f), and about 10 ka to the present. Sea level, climate patterns and sediment transport are also shown in their appropriate period. The present shoreline location is shown as a thick dotted line.

3.7. Conclusions

For the first time the Late Pleistocene history of the coast lowlands of Israel has been examined through a combination of high-resolution petro-sedimentological methods and OSL ages, enabling reconstruction of the palaeogeography and landscape evolution processes. The coastal reconstruction, combined with earlier interpretations of the coastal cliff sequences, reveal that over the last glacial-interglacial cycle the stratigraphy of the coastal plain of Israel was dominated mainly by aeolian, and to a lesser extent, fluvial, processes. The variation in lithology and facies captures six sedimentation cycles and three post-deposition processes (weathering, lithification and pedogenesis).

The conclusions from this study are:

1. The chronological association between the lowland and coastal cliff sequences reveals dissimilarities in lithologies over time. We propose that these differences, which often occur over distances smaller than 1 km, are the result of local factors, such as the ancient topography and locations of stream courses, which subsequently affected the depositional/erosional rate and soil-forming processes. As a result, two aeolianite units that exist in the coastal cliff are missing in the lowland sequence, and are replaced by thicker and more developed palaeosol units.
2. The fluvial system location did not change considerably from about 80 to 5 ka. However, the streams had a profound influence on the stratigraphical composition and related facies, due to fluvial induced erosion which shaped the evolving topography. Consequently, the relief variations between the lowland and cliff controlled aeolian, pedogenesis, and alluvial processes.
3. Correlation between sea-level fluctuations over the last interglacial and the coastal sedimentological sequence shows no distinct influence of sea level on the deposition and formation of the coastal sequence – apart from two periods: during the LGM lowstand (33 to 15), and from 15 to 12 ka. We suggest that a gap in deposition of about 20 ka was caused by the low RSL from 33 to 15 ka, which prevented sediments from reaching the palaeo-coastal plain, while from 15 to 12 ka the rapid transgression outpaced sedimentation supply to the coast.
4. The Holocene sand unit started to accumulate at about 8 ka on the shallow shelf and coastal plain, reaching a thickness of up to 10 m. We propose that the fast coastal build-up was a result of the erosion of the Nile Delta by the rising sea, and the transgressing shorelines which transported higher fluxes of sand closer to the present shoreline.

The Late Pleistocene landscape evolution described here presents a relevant example for other similar coastal areas across the southern parts of the Mediterranean basin that consist of lowland-ridge morphologies with relatively flat to moderately steep shelf and coast, comprising aeolianites, palaeosol units and alluvial facies, supplied with siliciclastic sediments and desert dust from the Sahara. Such areas include the northern coasts of Egypt, Libya and Tunisia (El-Asmar and Wood, 2000; Mauz et al., 2009, 2012; Elmejdoub et al., 2011). The model could also fit, to some degree, other areas with similar silicate-based lithologies and stratigraphic architecture influenced by Saharan dust deposits. Atlantic westerlies and monsoon circulation are responsible for advecting precipitation in the Mediterranean area in winter. These include the Atlantic shores of south-western Spain (i.e., Huelva and the Gulf of Cadiz; Zazo et al., 2005, 2008) and the Canary Islands (i.e., Lanzarote; von Suchodoletz et al., 2010).

Acknowledgments

The authors gratefully acknowledge support from the University of Haifa, the Leon H. Charney School of Marine Sciences, and the Maurice and Lady Hatter Fund of the Leon Recanati Institute for Maritime Studies (RIMS) at the University of Haifa. We thank Dina Dagan Begun of Ben Gurion University of the Negev and Silas Dean, Benny Bechor and Dr. Guy Sisma-Ventura of the University of Haifa for their vital help in the field. We thank Dr. Avnaim-Katav of the University of Haifa and Dr. Langgut of Tel Aviv University for the palaeontological and pollen analyses. Inga Boianju for preparing the samples for OSL dating, and Dina Stiber and Olga Berlin for chemical analyses, and Jonathan J. Gottlieb of the University of Haifa for preparing the thin sections. Improvements of earlier versions of the manuscript by anonymous reviewers and by Editor-in-Chief (Dr. Paul Hesse) are truly appreciated.

3.8. References

Adams, A.E., MacKenzie, W.S., 1998. A color atlas of carbonate sediments and rocks under the microscope. Manson Publishing Ltd., London, UK.

Almagor, G., Hall, J.K., 1984. Morphology of the Mediterranean Contintental Margin of Israel: A Comparative Summary and a Bathymetric Chart. Geological Survey of Israel.

Almagor, G., Gill, D., Perath, I., 2000. Marine Sand Resources Offshore Israel. Marine Georesources & Geotechnology 18, 1-42.

Amante, C., Eakins, B.W., 2009. ETOPO1 1 arc-minute global relief model: procedures, data sources and analysis. US Department of Commerce, National Oceanic and Atmospheric Administration, National Environmental Satellite, Data, and Information Service, National Geophysical Data Center, Marine Geology and Geophysics Division Colorado.

Amorosi, A., Ricci Lucchi, M., Rossi, V., Sarti, G., 2009. Climate change signature of small-scale parasequences from Lateglacial–Holocene transgressive deposits of the Arno valley fill. Palaeogeography, Palaeoclimatology, Palaeoecology 273, 142-152.

Anderson, J.B., Abdulah, K., Sarzalejo, S., Siringan, F., Thomas, M., 1996. Late Quaternary sedimentation and high-resolution sequence stratigraphy of the east Texas shelf. Geological Society, London, Special Publications 117, 95-124.

Anzidei, M., Antonioli, F., Benini, A., Lambeck, K., Sivan, D., Serpelloni, E., Stocchi, P., 2011. Sea level change and vertical land movements since the last two millennia along the coasts of southwestern Turkey and Israel. Quaternary International 232, 13-20.

Avnaim-Katav, S., Almogi-Labin, A., Sandler, A., Sivan, D., Porat, N., Matmon, A., 2012. The chronostratigraphy of a quaternary sequence at the distal part of the nile littoral cell, Haifa Bay, Israel. Journal of Quaternary Science 27, 675-686.

Avnimelech, M., 1950. The Geological History of the Yarkon Valley and its Influence on Ancient Settlements. Israel Exploration Journal 1, 77-83.

Bar-Matthews, M., Ayalon, A., Gilmour, M., Matthews, A., Hawkesworth, C.J., 2003. Sea–land oxygen isotopic relationships from planktonic foraminifera and speleothems in the Eastern Mediterranean region and their implication for paleorainfall during interglacial intervals. Geochimica et Cosmochimica Acta 67, 3181-3199.

Bateman, M.D., Holmes, P.J., Carr, A.S., Horton, B.P., Jaiswal, M.K., 2004. Aeolianite and barrier dune construction spanning the last two glacial–interglacial cycles from the southern Cape coast, South Africa. Quaternary Science Reviews 23, 1681-1698.

Ben-David, R., 2003. Changes in desert margin environments during the climate changes of the Upper Quaternary. Unpublished Ph. D. thesis, Hebrew University of Jerusalem.

Blum, M.D., Tōrnqvist, T.E., 2000. Fluvial responses to climate and sea-level change: a review and look forward. Sedimentology 47, 2-48.

Bozzano, G., Kuhlmann, H., Alonso, B., 2002. Storminess control over African dust imput to the Moroccan Atlantic margin (NW Africa) at the time of maxima boreal summer insolation- a record of the last 220 kyr. Palaeogeography, Palaeoclimatology, Palaeoecology 183, 155-168.

Brooke, B.P., Woodroffe, C.D., Murray-Wallace, C.V., Heijnis, H., Jones, B.G., 2003. Quaternary calcarenite stratigraphy on Lord Howe Island, southwestern Pacific Ocean and the record of coastal carbonate deposition. Quaternary Science Reviews 22, 859-880.

Brooke, B.P., Olley, J.M., Pietsch, T., Playford, P.E., Haines, P.W., Murray-Wallace, C.V., Woodroffe, C.D., 2014. Chronology of Quaternary coastal aeolianite deposition and the drowned shorelines of southwestern Western Australia – a reappraisal. Quaternary Science Reviews 93, 106-124.

Campbell, J.B., 1996. Introduction to Remote Sensing. Virginia Polytechnic Institute and State University. Taylor & Francis Ltd. London, England.

Cheddadi, R., Rossignol-Strick, M., 1995. Improved preservation of organic matter and pollen in eastern Mediterranean sapropels. Paleoceanography 10, 301-309.

Cita, M.B., Vergnaud-Grazzini, C., Robert, C., Chamley, H., Ciaranfi, N., d'Onofrio, S., 1977. Paleoclimatic record of a long deep sea core from the eastern Mediterranean. Quaternary Research 8, 205-235.

Cohen-Seffer, R., Greenbaum, N., Sivan, D., Jull, T., Barmeir, E., Croitoru, S., Inbar, M., 2005. Late Pleistocene–Holocene marsh episodes along the Carmel coast, Israel. Quaternary International 140-141, 103-120.

Coltorti, M., Melis, E., Patta, D., 2010. Geomorphology, stratigraphy and facies analysis of some Late Pleistocene and Holocene key deposits along the coast of Sardinia (Italy). Quaternary International 222, 19-35.

Crouvi, O., Schepanski, K., Amit, R., Gillespie, A.R., Enzel, Y., 2012. Multiple dust sources in the Sahara Desert: The importance of sand dunes. Geophysical Research Letters 39, n/a-n/a.

Dan, J., Yaalon, D.H., Koyumdjisky, H., 1968. Catenary Soil Relationships In Israel, 1. The Netanya catena on coastal dunes of the sharon. Geoderma 2, 95-120.

Davidovich, U., Porat, N., Gadot, Y., Avni, Y., Lipschits, O., 2012. Archaeological investigations and OSL dating of terraces at Ramat Rahel, Israel. Journal of Field Archaeology 37, 192-208.

Davis, M., Matmon, A., Rood, D.H., Avnaim-Katav, S., 2012. Constant cosmogenic nuclide concentrations in sand supplied from the Nile River over the past 2.5 my. Geology 40, 359-362.

Dutton, A., Carlson, A.E., Long, A.J., Milne, G.A., Clark, P.U., DeConto, R., Horton, B.P., Rahmstorf, S., Raymo, M.E., 2015. Sea-level rise due to polar ice-sheet mass loss during past warm periods. Science 349, aaa4019.

El-Asmar, H.M., 1994. Aeolianite sedimentation along the northwestern coast of Egypt: evidence for middle to late quaternary aridity. Quaternary Science Reviews 13, 699-708.

El-Asmar, H.M., Wood, P., 2000. Quaternary shoreline development- the northwestern coast of Egypt. Quaternary Science Reviews 19, 1137-1149.

Elmejdoub, N., Mauz, B., Jedoui, Y., 2011. Sea-level and climatic controls on late Pleistocene coastal aeolianites in the Cap Bon peninsula, northeastern Tunisia. Boreas 40, 198-207.

Elyashiv, H., 2013. The Late Pleistocene-Holocene sedimentary evolution of Zevulun Plain: focusing on the wetlands MA Thesis Faculty of Natural Sciences, Leon H. Charney School of

Marine Sciences, The Dr. Moses Sreauss Dept. of Marine Geosciences, University of Haifa, Israel.

Elyashiv, H., Bookman, R., Zviely, D., Avnaim-Katav, S., Sandler, A., Sivan, D., 2016. The interplay between relative sea-level rise and sediment supply at the distal part of the Nile littoral cell. The Holocene 26, 248-264.

Emery, K., Neev, D., 1960. Mediterranean beaches of Israel: Israel Geological Survey Bulletin. 26, 1-24.

Engelmann, A., Neber, A., Frechen, M., Boenigk, W., Ronen, A., 2001. Luminescence chronology of Upper Pleistocene and Holocene aeolianites from Netanya South - Sharon Coastal Plain, Israel. Quaternary Science Reviews 20, 799-804.

Enzel, Y., Amit, R., Dayan, U., Crouvi, O., Kahana, R., Ziv, B., Sharon, D., 2008. The climatic and physiographic controls of the eastern Mediterranean over the late Pleistocene climates in the southern Levant and its neighboring deserts. Global and Planetary Change 60, 165-192.

Faust, D., Yanes, Y., Willkommen, T., Roettig, C., Richter, D., Richter, D., Suchodoletz, H.v., Zöller, L., 2015. A contribution to the understanding of late Pleistocene dune sand-paleosol-sequences in Fuerteventura (Canary Islands). Geomorphology 246, 290-304.

Fitzsimmons, K.E., Magee, J.W., Amos, K.J., 2009. Characterisation of aeolian sediments from the Strzelecki and Tirari Deserts, Australia: Implications for reconstructing palaeoenvironmental conditions. Sedimentary Geology 218, 61-73.

Fornós, J.J., Clemmensen, L.B., Gómez-Pujol, L., Murray, A.S., 2009. Late Pleistocene carbonate aeolianites on Mallorca, Western Mediterranean: a luminescence chronology. Quaternary Science Reviews 28, 2697-2709.

Frechen, M., Dermann, B., Beonigk, W., Ronen, A., 2001. luminesence chronology of the aeolianites from the section at givat olga-coastal plain of israel. Quaternary Science Reviews 20, 805-809.

Frechen, M., Neber, A., Dermann, B., Alexander, T., Boenigk, W., Raban, A., 2002. Chronostratigraphy of aeolianites fromthe Sharon Coastal Plain of Israel. Quaternary International, 31-44.

Frechen, M., Neber, A., Tsatskin, A., Boenigk, W., Ronen, A., 2004. Chronology of Pleistocene sedimentary cycles in the Carmel Coastal Plain of Israel. Quaternary International 121, 41-52.

Galili, E., Zviely, D., Ronen, A., Mienis, H.K., 2007. Beach deposits of MIS 5e high sea stand as indicators for tectonic stability of the Carmel coastal plain, Israel. Quaternary Science Reviews 26, 2544-2557.

Gavish, E., Friedman, G.M., 1969. Progressive diagenesis in Quaternary to Late Tertiary carbonate sediments: sequence and time scale. Journal of Sedimentary Research 39, 980-1006.

Goodman-Tchernov, B.N., Dey, H.W., Reinhardt, E.G., McCoy, F., Mart, Y., 2009. Tsunami waves generated by the Santorini eruption reached Eastern Mediterranean shores. Geology 37, 943-946.

Gvirtzman, G., Shachnai, E., Bakler, N., Ilani, S., 1983. Stratigraphy of the Kurkar Group (Quaternary) of the coastal plain of Israel. Geological Survey of Israel, Current Research 1984, 70-82.

Gvirtzman, G., Netser, M., Katsav, E., 1998. Last-Glacial to Holocene kurkar ridges, hamra soils, and dune fields in the coastal belt of central Israel. Israel Journal of Earth Sciences 47, 27-46.

Gvirtzman, G., Wieder, M., 2001. Climate of the last 53,000 years in the eastern med based on soil-sequence Stratigraphy in coastla plain Israel. Quaternary Science Reviews 20, 1827-1849.

Hall, J.K., 1994. Bathymetric chart of the eastern Mediterranean Sea. Geologic Structure of the Northen Mediterranean (Cruise 5 of the Akademic Nikolaj Strakhov).

Hearty, P.J., Hollin, J.T., Neumann, A.C., O'Leary, M.J., McCulloch, M., 2007. Global sea-level fluctuations during the Last Interglaciation (MIS 5e). Quaternary Science Reviews 26, 2090-2112.

Huntley, D., Hutton, J., Prescott, J., 1993. The stranded beach-dune sequence of south-east South Australia: a test of thermoluminescence dating, 0–800 ka. Quaternary Science Reviews 12, 1-20.

Huntley, D., Hutton, J., Prescott, J., 1994. Further thermoluminescence dates from the dune sequence in the southeast of South Australia. Quaternary Science Reviews 13, 201-207.

Huntley, D.J., Prescott, J.R., 2001. Improved methodology and new thermoluminescence ages for the dunw sequance in the south-east south Australia. Quaternary Science Reviews 20, 687-699.

Hyams-Kaphzan, O., Almogi-Labin, A., Sivan, D., Benjamini, C., 2008. Benthic foraminifera assemblage change along the southeastern Mediterranean inner shelf due to fall-off of Nile-derived siliciclastics. Neues Jahrbuch für Geologie und Paläontologie-Abhandlungen 248, 315-344.

Kadosh, D., Sivan, D., Kutiel, H., Weinstein-Evron, M., 2004. A late quaternary paleoenvironmental sequence from Dor, Carmel coastal plain, Israel. Palynology 28, 143-157.

Katz, O., Mushkin, A., 2013. Characteristics of sea-cliff erosion induced by a strong winter storm in the eastern Mediterranean. Quaternary Research 80, 20-32.

Kopp, R.E., Simons, F.J., Mitrovica, J.X., Maloof, A.C., Oppenheimer, M., 2009. Probabilistic assessment of sea level during the last interglacial stage. Nature 462, 863-867.

Kopp, R.E., Simons, F.J., Mitrovica, J.X., Maloof, A.C., Oppenheimer, M., 2013. A probabilistic assessment of sea level variations within the last interglacial stage. Geophysical Journal International 193, 711-716.

Lambeck, K., Bard, E., 2000. Sea-level change along the French Mediterranean coast for the past 30,000 years. Earth and Planetary Science Letters 175, 203-222.

Lambeck, K., Purcell, A., 2005. Sea-level change in the Mediterranean Sea since the LGM: model predictions for tectonically stable areas. Quaternary Science Reviews 24, 1969-1988.

Langgut, D., Almogi-Labin, A., Bar-Matthews, M., Weinstein-Evron, M., 2011. Vegetation and climate changes in the South Eastern Mediterranean during the Last Glacial-Interglacial cycle (86 ka): new marine pollen record. Quaternary Science Reviews 30, 3960-3972.

Larrasoaña, J.C., Roberts, A.P., Rohling, E.J., 2008. Magnetic susceptibility of eastern Mediterranean marine sediments as a proxy for Saharan dust supply? Marine Geology 254, 224-229.

Mauz, B., Elmejdoub, N., Nathan, R., Jedoui, Y., 2009. Last interglacial coastal environments in the Mediterranean–Saharan transition zone. Palaeogeography, Palaeoclimatology, Palaeoecology 279, 137-146.

Mauz, B., Fanelli, F., Elmejdoub, N., Barbieri, R., 2012. Coastal response to climate change: Mediterranean shorelines during the Last Interglacial (MIS 5). Quaternary Science Reviews 54, 89-98.

Mauz, B., Hijma, M.P., Amorosi, A., Porat, N., Galili, E., Bloemendal, J., 2013. Aeolian beach ridges and their significance for climate and sea level: Concept and insight from the Levant coast (East Mediterranean). Earth-Science Reviews 121, 31-54.

McGee, D., Broecker, W.S., Winckler, G., 2010. Gustiness: The driver of glacial dustiness? Quaternary Science Reviews 29, 2340-2350.

Mor-Federman, T., 2012. Chemical Characterization and Provenance Study of the Israeli Inner Shelf's Holocene Sediments. MS.c thesis Marine Geo-Sciences. The University of Haifa (in Hebrew, English abstract), Haifa.

Moshier, S., Master, D., Leport, J., Wheatley, D., Felker, B., Lavigne, E., College, W., 2010. Reconstruction of the Ancient Landscapes and Paleoenvitonments of the geological foundations of the ancient seaport Ashkelon, Israel, GSA Annual Meeting & Exposition, Minneapolls, Minnesota USA.

Munyikwa, K., 2005. Synchrony of Southern Hemisphere Late Pleistocene arid episodes: a review of luminescence chronologies from arid aeolian landscapes south of the Equator. Quaternary Science Reviews 24, 2555-2583.

Murray, A.S., Wintle, A.G., 2000. Luminescence dating of quartz using an improved single-aliquot regenative-dose protocol. Radiation Measurments 32, 57-73.

Neber, A., 2002. Sedimentological properies of Quternary deposits on the Central coastline of Israel. Unpublished Ph.D. Dissertation, Department of Archaeology,University of Haifa, Israel.

Neev, D., Schanai, E., Hall, J.K., Bakler, N., Ben-Avraham, Z., 1978. The Young (Post Loewr Pliocene) Geological History of the Caesarea. Israel Journal of Earth Sciences 28, 43-46.

Paton, T.R., Humphreys, G.S., Mitchell, P.B., 1995. Soils: a new global view. Yale University Press, New Haven and London.

Picard, L., 1943. Structure and evolution of Palestine. Bull. Geol. Dept. Hebrew Univ., Jerusalem 4, 1-134.

Pomerancblum, M., 1966. The distribution of heavy minerals and their hydraulic equivalents in sediments of the Mediterranean continental shelf of Israel. Journal of Sedimentary Research 36.

Porat, N., Avital, A., Frechen, M., Almogi-Labin, A., 2003. Chronology of upper Quaternary offshore successions from the southeastern Mediterranean Sea, Israel. Quaternary Science Reviews 22, 1191-1199.

Porat, N., Wintle, A.G., Ritte, M., 2004. Mode and timing of kurkar and hamra formation, central coastal plain, Israel. Israel Journal of Earth Sciences 53, 13-25.

Porat, N., Sivan, D., Zviely, D., 2008. Late Holocene embayment infill and shoreline migration, Haifa Bay, Eastern Mediterranean. Israel Journal of Earth Sciences 57, 21-31.

Porath, Y., 1975. The Gardens of Caesarea. Qadmoniot, 30-31.

Posamentier, H.W., Allen, G.P., James, D.P., Tesson, M., 1992. Forced regressions in a sequence stratigraphic framework: concepts, examples, and exploration significance (1). AAPG Bulletin 76, 1687-1709.

Preusser, F., Radies, D., Matter, A., 2002. A 160,000-year record of dune develop and Atmospheric Circulation in the Southern Arabia. Science 296, 2018-2020.

Raban, A., Galili, E., 1985. Recent maritime archaeological research in Israel-A preliminary. International Journal of Nautical Underwater Exploration 14, 321-356.

Reinhardt, E.G., Goodman, B.N., Boyce, J.I., Lopez, G., van Hengstum, P., Rink, W.J., Mart, Y., Raban, A., 2006. The tsunami of 13 December A.D. 115 and the destruction of Herod the Great's harbor at Caesarea Maritima, Israel. Geology 34, 1061.

Revel, M., Ducassou, E., Grousset, F.E., Bernasconi, S.M., Migeon, S., Revillon, S., Mascle, J., Murat, A., Zaragosi, S., Bosch, D., 2010. 100,000 Years of African monsoon variability recorded in sediments of the Nile margin. Quaternary Science Reviews 29, 1342-1362.

Rohling, E.J., Foster, G.L., Grant, K.M., Marino, G., Roberts, A.P., Tamisiea, M.E., Williams, F., 2014. Sea-level and deep-sea-temperature variability over the past 5.3 million years. Nature 508, 477-482.

Rose, J., Meng, X., Watson, C., 1999. Palaeoclimate and palaeoenvironmental responses in the western Mediterranean over the last 140 ka: evidence from Mallorca, Spain. Journal of the Geological Society 156, 435-448.

Roskin, J., Porat, N., Tsoar, H., Blumberg, D.G., Zander, A.M., 2011a. Age, origin and climatic controls on vegetated linear dunes in the northwestern Negev Desert (Israel). Quaternary Science Reviews 30, 1649-1674.

Roskin, J., Tsoar, H., Porat, N., Blumberg, D.G., 2011b. Palaeoclimate interpretations of Late Pleistocene vegetated linear dune mobilization episodes: evidence from the northwestern Negev dunefield, Israel. Quaternary Science Reviews 30, 3364-3380.

Roskin, J., Sivan, D., Shtienberg, G., Roskin, E., Porat, N., Bookman, R., 2015. Natural and human controls of the Holocene evolution of the beach, aeolian sand and dunes of Caesarea (Israel). Aeolian Research 19, 65-85.

Roskin, J., Sivan, D., Bookman, R., Porat, N., Shtienberg, G., 2016. Beach buildup and coastal aeolian sand incursions off the Nile cell during the Holocene Poster presented in the annual IGRG Congress; the University of Haifa, 33.

Rowe, M.P., Bristow, C.S., 2015a. Landward-advancing Quaternary eolianites of Bermuda. Aeolian Research 19, 235-249.

Rowe, M.P., Bristow, C.S., 2015b. Sea-level controls on carbonate beaches and coastal dunes (eolianite): Lessons from Pleistocene Bermuda. Geological Society of America Bulletin 127, 1645-1665.

Sade, A.R., Hall, J.K., Amit, G., Golan, A., Gur-Arieh, L., Tibor, G., 2006. The Israel national bathymetric survey—A new look at the seafloor off Israel. Israel Journal of Earth Sciences 55, 185-187.

Schattner, U., Lazar, M., Tibor, G., Ben-Avraham, Z., Makovsky, Y., 2010. Filling up the shelf – A sedimentary response to the last post-glacial sea rise. Marine Geology 278, 165-176.

Schattner, U., Gurevich, M., Kanari, M., Lazar, M., 2015. Levant jet system—effect of post LGM seafloor currents on Nile sediment transport in the eastern Mediterranean. Sedimentary Geology 329, 28-39.

Shtienberg, G., Dix, J., Waldmann, N., Makovsky, Y., Golan, A., Sivan, D., 2016. Late-Pleistocene evolution of the continental shelf of central Israel, a case study from Hadera. Geomorphology 261, 200-211.

Sivan, D., Gvirtzman, G., Sass, E., 1999. Quaternary Stratigraphy and Paleogeography of the Galilee Coastal Plain, Israel. Quaternary Research 51, 280-294.

Sivan, D., Widowinski, S., Lambeck, K., Galili, E., Raban, A., 2001. Holocene sea level changes based on archeological sites off northen israel Palaeogeography, Palaeoclimatology, Palaeoecology 167, 101-117.

Sivan, D., Lambeck, K., Toueg, R., Raban, A., Porath, Y., Shirman, B., 2004. Ancient coastal wells of Caesarea Maritima, Israel, an indicator for relative sea level changes during the last 2000 years. Earth and Planetary Science Letters 222, 315-330.

Sivan, D., Porat, N., 2004. Evidence from luminescence for Late Pleistocene formation of calcareous aeolianite (kurkar) and paleosol (hamra) in the Carmel Coast, Israel. Palaeogeography, Palaeoclimatology, Palaeoecology 211, 95-106.

Sivan, D., Greenbaum, N., Cohen-Seffer, R., Sisma-Ventura, G., Almogi-Labin, A., 2011. The origin and disappearance of the late Pleistocene–early Holocene short-lived coastal wetlands along the Carmel coast, Israel. Quaternary Research 76, 83-92.

Sivan, D., Sisma-Ventura, G., Greenbaum, N., Bialik, O.M., Williams, F.H., Tamisiea, M.E., Rohling, E.J., Frumkin, A., Avnaim-Katav, S., Shtienberg, G., Stein, M., 2016. Eastern Mediterranean sea levels through the last interglacial from a coastal-marine sequence in northern Israel. Quaternary Science Reviews 145, 204-225.

Spratt, R.M., Lisiecki, L.E., 2015. A Late Pleistocene sea level stack. Climate of the Past Discussions 11, 3699-3728.

Stanley, D.J., Warne, A.G., 1998. Nile Delta in its destruction phase. Journal of Coastal Research 14, 794-825.

von Suchodoletz, H., Oberhänsli, H., Hambach, U., Zöller, L., Fuchs, M., Faust, D., 2010. Soil moisture fluctuations recorded in Saharan dust deposits on Lanzarote (Canary Islands) over the last 180ka. Quaternary Science Reviews 29, 2173-2184.

Suter, J.R., Berryhill Jr, H.L., 1985. Late Quaternary shelf-margin deltas, northwest Gulf of Mexico. AAPG Bulletin 69, 77-91.

Thiel, C., Coltorti, M., Tsukamoto, S., Frechen, M., 2010. Geochronology for some key sites along the coast of Sardinia (Italy). Quaternary International 222, 36-47.

Thomsen, K.J., Murray, A.S., Jain, M., Bøtter-Jensen, L., 2008. Laboratory fading rates of various luminescence signals from feldspar-rich sediment extracts. Radiation Measurements 43, 1474-1486.

Toker, E., Sivan, D., Stern, E., Shirman, B., Tsimplis, M., Spada, G., 2012. Evidence for centennial scale sea level variability during the Medieval Climate Optimum (Crusader Period) in Israel, eastern Mediterranean. Earth and Planetary Science Letters 315-316, 51-61.

Tripaldi, A., Forman, S.L., 2007. Geomorphology and chronology of Late Quaternary dune fields of western Argentina. Palaeogeography, Palaeoclimatology, Palaeoecology 251, 300-320.

Tsakalos, E., 2016. Geochronology and exoscopy of quartz grains in environmental determination of coastal sand dunes in SE Cyprus. Journal of Archaeological Science: Reports 7, 679-686.

Tsatskin, A., Ronen, A., 1999. Micromorphology of a Mousterian paleosol in aeolianites at the site Habonim, Israel. Catena 34, 365-384.

Tsatskin, A., Gendler, T.S., Heller, F., Ronen, A., 2008. Near-surface paleosols in coastal sands at the outlet of Hadera stream (Israel) in the light of archeology and luminescence chronology. Journal of Plant Nutrition and Soil Science 171, 524-532.

Tsatskin, A., Gendler, T.S., Heller, F., Dekman, I., Frey, G.L., 2009. Towards understanding paleosols in Southern Levantine eolianites: Integration of micromorphology, environmental magnetism and mineralogy. Journal of Mountain Science 6, 113-124.

Tsatskin, A., Sandler, A., Avnaim-Katav, S., 2015. Quaternary subsurface paleosols in Haifa Bay, Israel: A new perspective on stratigraphic correlations in coastal settings. Palaeogeography, Palaeoclimatology, Palaeoecology 426, 285-296.

Waelbroeck, C., Labeyrie, L., Michel, E., Duplessy, J.C., McManus, J., Lambeck, K., Balbon, E., Labracherie, M., 2002. Sea-level and deep water temperature changes derived from benthic foraminifera isotopic records. Quaternary Science Reviews 21, 295-305.

Wright, C.I., Tucker, M.E., 1991. Calcretes. Blackwell Scientific Publications, Oxford, UK.

Wright, V., 1992. A revised classification of limestones. Sedimentary Geology 76, 177-185.

Yaalon, D.H., 1967. Factors affecting the lithification of eolianite and interpretation of its environmental significance in the coastal plain of Israel. Journal of Sedimentary Research 37, 1189-1199.

Yaalon, D.H., 1997. Soils in the Mediterranean region- what makes them diffrent? Catena 28, 157-169.

Zazo, C., Mercier, N., Silva, P.G., Dabrio, C.J., Goy, J.L., Roquero, E., Soler, V., Borja, F., Lario, J., Polo, D., de Luque, L., 2005. Landscape evolution and geodynamic controls in the Gulf of Cadiz (Huelva coast, SW Spain) during the Late Quaternary. Geomorphology 68, 269-290.

Zazo, C., Mercier, N., Lario, J., Roquero, E., Goy, J.-L., Silva, P.G., Cabero, A., Borja, F., Dabrio, C.J., Bardají, T., Soler, V., García-Blázquez, A., Luque, L.d., 2008. Palaeoenvironmental evolution of the Barbate–Trafalgar coast (Cadiz) during the last ~140 ka: Climate, sea-level interactions and tectonics. Geomorphology 100, 212-222.

Zilberman, E., Porat, N., Roskin, J., 2007. The middle to Late-Pleistocene sand sheet sequence of Kerem Shalom, western Negev – an archive of coastal sand incursion. Geological Survey of Israel GSI/13/2007, 23p.

Zviely, D., Sivan, D., Ecker, A., Bakler, N., Rohrlich, V., Galili, E., Boarreto, E., Klein, M., Kit, E., 2006. Holocene evolution of the Haifa Bay area, Israel, and its influence on ancient tell settlements, The Holocene, pp. 849-861.

Zviely, D., Kit, E., Rosen, B., Galili, E., Klein, M., 2009. Shoreline migration and beach-nearshore sand balance over the last 200 years in Haifa Bay (SE Mediterranean). Geo-Marine Letters 29, 93-110.

Appendices:

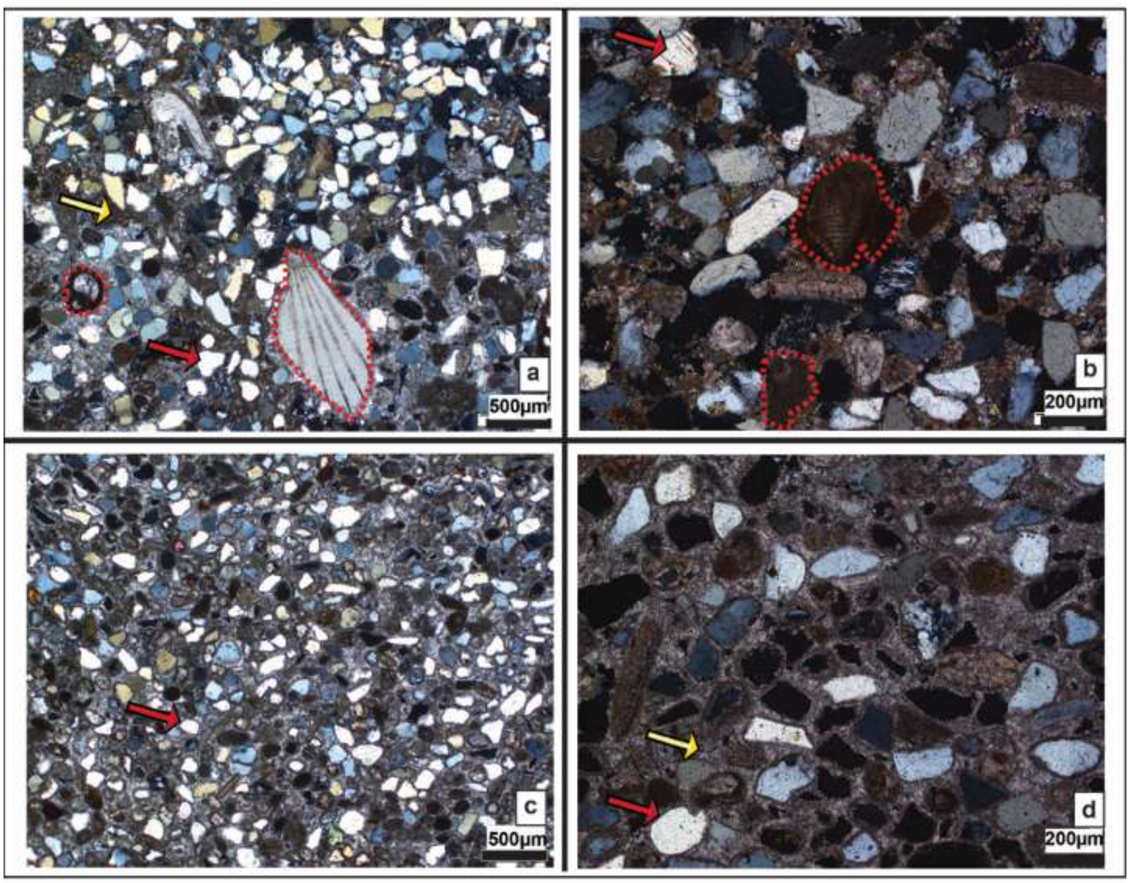

Appendix 3.1: Thin-section representation of calcareous sandstone samples SY5 (a, b) and SDC4 (c, d). Skeletal features are SY5 (dashed red polygons), micritic cement (yellow arrows) and quartz grain areas (red arrows).

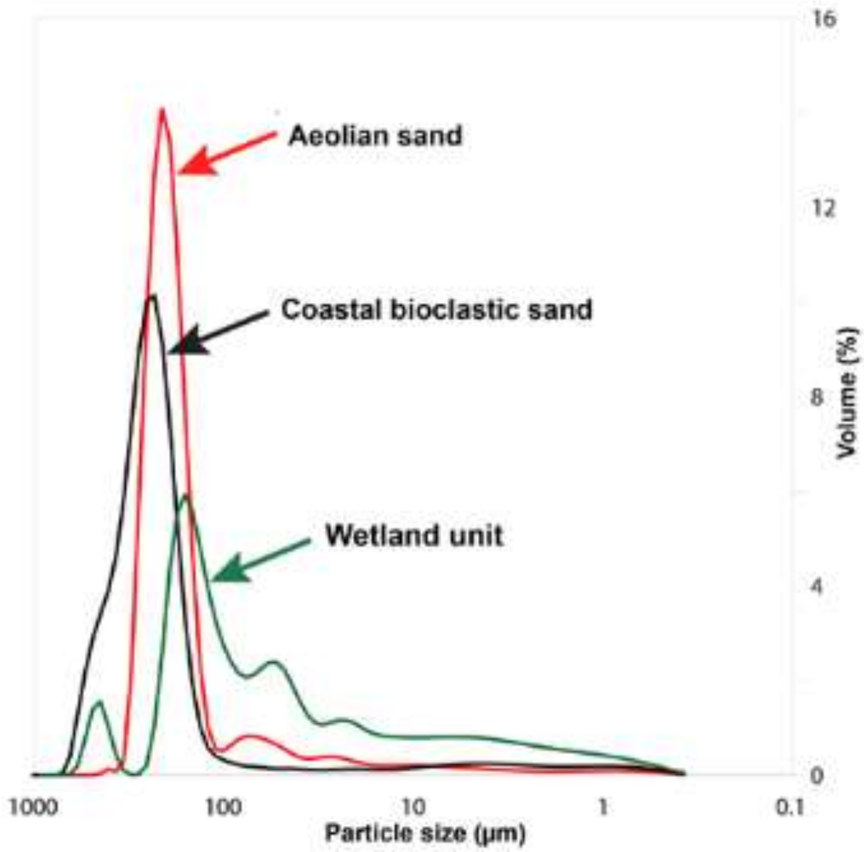

Appendix 3.2: Average particle size distribution in Borehole ALX5, presenting the top aeolian sand, bioclastic sand and wetland units. Each curve was created from six samples which represent the three environments.

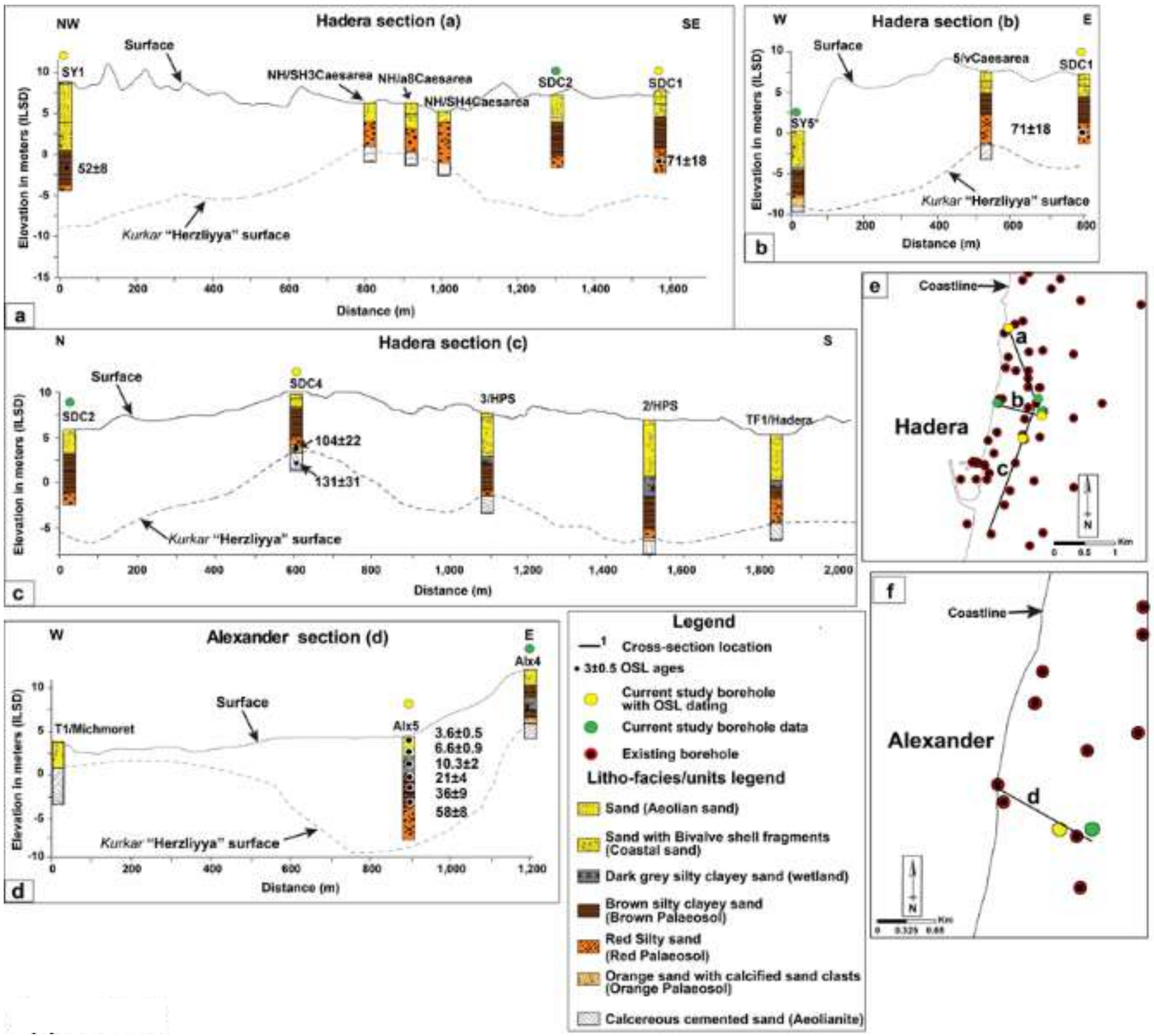

Appendix 3.3: The modern topography of Hadera-Alexander (extracted from a 4×4m DEM) versus the basal calcareous sandstone topography, corresponding borehole and current study OSL ages along (a) NW-SE transect in Hadera (b) W-E transect in Hadera (c) N-S transact in Hadera (d) W-E transect in Alexander. The Hadera and Alexander transect and borehole locations are shown in maps (e) and (f) respectively.

4. Anthropogenic overprints on natural coastal aeolian sediments, a case study from the periphery of ancient Caesarea, Israel

Gilad Shtienberg, Justin K. Dix, Ruth Shahack-Gross, Assaf Yasur-Landau, Joel Roskin, Revital Bookman, Nicolas Waldmann, Sariel Shalev and Dorit Sivan, 2017. Anthropogenic overprints on natural coastal aeolian sediments: a study from the periphery of ancient Caesarea, Israel. Anthropocene 19, 22-34 (DOI: http://dx.doi.org/10.1016/j.ancene.2017.08.004, Published).

Contribution statement

G. Shtienberg jointly conceived the study, designed the terrestrial drillings with D. Sivan and J. Dix. Collection and integration of existing borehole records, topographic, spatial data historical and archaeological records was undertaken by G. Shtienberg. The drilling was conducted by G. Shtienberg under the direction of D. Sivan with the help of J. Roskin while sedimentological analysis was completed by G. Shtienberg under the direction of R. Shahack-Gross. Sedimentological data integration with archaeological records and interpretation was done by G. Shtienberg with the support of D. Sivan, J. Dix, R. Shahack-Gross and A. Yasur-Landau. The manuscript was drafted and finalised by G. Shtienberg with editing contributions from D. Sivan, J. Dix, R Shahack-Gross, A. Yasur-Landau, J. Roskin R. Bookman N. Waldmann and S. Shalev.

4.1. Abstract

Near surface sediment stratigraphy associated with ancient human settlements can potentially reveal the complex history of human impact. This study explores such impacts in the area around ancient Caesarea, a well-known Roman to Early Islam period metropolis in the central coastal plain of Israel, with analysis of human-induced macro-features and microscopic remains found in buried sediments. We retrieved these anthropogenic markers through boreholes and analysed them with sedimentological and radiometric dating techniques, integrated with archaeological and historical records. The analysis identified a refuse deposit comprising two grey loamy sand artefact-bearing facies bedded between late Holocene aeolian sand. One anthropogenic facies represents an urban garbage mound and the other may be an agricultural pedo-sediment, both dated to the Roman to Early Islamic periods. The grey pedo-sediment, contained in three boreholes in the lowlands south of Caesarea, covers an area of at least 1.4 km^2. Apparently improved in terms of soil fertility, we postulate that the pedo-sedimentis the outcome of composting enrichment of the soil for agriculture. Taking advantage of the high coastal freshwater aquifer in the study area, we propose that the pedo-sediment represents buried agricultural plots. The comprehensive, multi-disciplinary approach demonstrated in this study of cored sediments outside ancient human settlements is among the few in the coastal area of the southern Levant. It could be relevant to other archaeological sites in the Mediterranean and elsewhere around the world.

Keywords

Eastern Mediterranean; pedo-sediment, anthropogenic traces; Islamic period, Caesarea hinterlands, aeolian coastal sand.

4.2. Introduction

For millennia, humans have manipulated soils for habitation purposes, leading to changes in the physical and chemical properties (Bouma and Hole, 1971; Hole, 1974; Nicosia and Devos, 2014). Therefore, a complex history of human impact on the environment is accruing in sediments and soils. Extensive archaeological and paleoenvironmental research has increased the understanding that significant human perturbations to the landscape occurred throughout hominin evolution, most significantly with the advent of agriculture (Sandor et al., 1990; Certini and Scalenghe, 2011; Zeder, 2011).

In the southeast Mediterranean coastal region, the Holocene period is characterized by ongoing interaction between natural processes and human activities (Bar-Yosef, 1975; Galili and Nir, 1993; Galili et al., 1993; Godfrey-Smith et al., 2003). Anthropogenic activities that have affected the environment include site construction, animal domestication, wood/charcoal burning and cultivation of crops. Human activity has left distinct traces in soils such as macroscopic artefacts: pottery, stone tools, architecture and bone remains. Microscopic evidence of human activity includes livestock dung spherulites, ash and micro-charcoal, phytoliths (plant-made minerals which may be preserved in soils and sediments) and enrichment of certain elements (i.e., phosphorous and sulphur) (Weiner, 2010). Techniques used to identify anthropogenic impacts in soils are usually applied to settlement sites and rarely to cultivated hinterlands (Smejda et al., 2017).

This study focuses on the area to the south of ancient Caesarea, Israel (32°30’0” N, 34°53’30” E), a well-known Roman to Crusader period (31 BCE to 1265 CE) urban centre. The continuous efforts of the local population to adapt their activities to both their varying needs and changing natural environments has resulted in human-induced landscape changes, giving rise to a complex cause-effect phenomena (Ackermann et al., 2014, 2015). This study investigates the effect of human settlement on the proximate environment, outside the settlement itself, through analysis of anthropogenic markers present within the local sediment stratigraphy. We identified markers through a combination of sedimentological, petrophysical, geochemical, chronological and microarchaeological analyses conducted on four boreholes. Integration of these new data with extant topographical data, borehole records, established chronology, archaeological finds and historical documentation, resulted in a spatially extensive interpretation of changing settlement and subsistence patterns in the area.

4.3. The study area

The study area is located in the Caesarea lowlands (Shtienberg et al., 2017), situated in the centre of the 190 km-long coastal plain of Israel (Fig. 4.1a, b). The study area extends up to 1.5 km east from the Mediterranean Sea between Hadera Stream to the south and Caesarea to the north. South of Haifa Bay, the coastal plain of Israel is dominated by Nile-derived quartz sand deposits attaining thicknesses of 1 to 9 m (Neev et al., 1978; Almagor et al., 2000; Zviely et al., 2006; Schattner et al., 2010; Roskin et al., 2015, 2017; Shtienberg et al., 2016). Longshore currents transported this allogenic material to the region throughout the Quaternary period (Fig. 4.1a; Picard, 1943; Emery and Neev, 1960; Pomerancblum, 1966; Zviely et al., 2009; Davis et al., 2012). Wave- and wind-induced currents transported the sediments to the beach, and wind carried them inland to form sand sheets and dunes (Fig. 4.1b). The quartz sand eventually formed the Late Pleistocene sequence consisting of alternating aeolianites (cemented dune sand locally known as `*kurkar*') and red-brown silty clayey sandy loams (Palaeosols) overlain by loose sand sheets and dunes (Fig. 4.1b; Yaalon, 1967; Yaalon and Dan, 1967; Gvirtzman et al., 1998; Frechen et al., 2002; Sivan and Porat, 2004; Mauz et al., 2013). Aeolianites in the vicinity of Caesarea are chronologically constrained between approximately 115 and 50 thousand years ago (ka; Engelmann et al., 2001; Frechen et al., 2004; Sivan and Porat, 2004; Sivan et al., 2004; Mauz et al., 2013; Shtienberg et al., 2017). The overlying palaeosol units, reaching a maximum thickness of 8 m, date from roughly 100 to 8 ka (Gvirtzman and Wieder, 2001; Frechen et al., 2001; Roskin et al., 2015; Shtienberg et al., 2017), indicating they are sometimes synchronous with aeolianite formation (Sivan and Porat, 2004) and sometimes younger. As sea level rose during the Late Pleistocene-Holocene transition, the shoreline migrated eastwards, flooding the shallow shelf (depth shallower than -20 m) c. 8 ka (Sivan et al., 2001, 2004). The Nilotic sands accumulated on the coast, initially covering the palaeosol surface c. 7 ka (Frechen et al., 2002; Porat et al., 2004; Mauz et al., 2013; Shtienberg et al., 2017). By 1.2 to 1.1 ka, the sand reached its easternmost extent in the Caesarea hinterland and stabilized shortly afterwards (Roskin et al., 2015).

The study area experiences a sub-humid Mediterranean climate characterized by a hot, dry summer season (June to September) and a cool, rainy winter season (December to February). The mean temperature in January and August is 12 ºC and 26 ºC, respectively. The rainy season generally lasts from October to May, with a mean annual rainfall of 500–600 mm (Israel Meteorological Service, 2011). This climate regime has generally prevailed during the last 3,000 years with only modest fluctuations (Bar-Matthews et al., 2003; Revel et al., 2010; Langgut et al., 2011; Ellenblum, 2012) and thus is relevant to the historical periods discussed in this study. Vegetation cover mainly consists of Mediterranean garrigue and maquis vegetation (Danin, 2005) that likely contributed to the stabilization of sands and dunes (Levin, 2013; Roskin et al., 2015).

In the vicinity of Caesarea (Fig. 4.1c), the earliest historical settlement is attributed to the Persian period at approximately 400 BCE (Raban, 2007). Known as “Straton’s Tower” (Stieglitz, 1996), the settlement was completely rebuilt during the reign of Herod the Great and renamed Caesarea in honour of the Roman Emperor Augustus Caesar (Patrich, 2001; Porath, 2002; Reinhardt and Raban, 2008; Roskin et al., 2015). Throughout the Roman and Byzantine periods (31 BCE to 640 CE), the city functioned as a provincial metropolis (Reinhardt and Raban, 1999, 2008; Goodman-Tchernov and Austin, 2015). Caesarea reached its maximum extent (1.2 km^2) by the 5^{th} and 6^{th} centuries CE, housing a population of 25,000 to 35,000 (Holum, 2011). During the late Roman to Byzantine period, a lively export and import trade passed through Caesarea's harbor. Local markets included agricultural products such as wheat, dates, rice and cumin cultivated in the city's territory (Habas, 1996; Holum, 2009). Caesarea was conquered by the Muslim Rashidun army under 'Amr ibn al-'As's leadership during the 7th century CE; however, the population did not decrease significantly. Furthermore,archaeobotanical and historical evidence suggest that Islamic Caesarea significantly invested in local agriculture (Holum, 2011). During the 11th Century CE, Caesarea was taken by the Crusaders, resulting in decline of the city, reduction of population, and a change of settlement pattern from urban to rural (Taxel, 2013; Avni, 2014; Ramsay and Holum, 2015).

Although few known archaeological sites (i.e. farming complexes and irrigation systems) surround Caesarea (Fig. 4.2; Olami et al., 2005; Ad, 2009), Roman, Byzantine and Islamic period glass and pottery remains are scattered on the sand surface (Fig. 4.2e). These remains cover rectangular to square areas defined by low sand berms (Fig 4.2c, d) that may be associated with Mawasi agriculture (Porath, 1975), a traditional-farming practise that takes advantage of the coastline's high fresh water table (Tsoar and Zohar, 1985).

Based on historical documentation of Caesarea's urban development and findings in nearby cities, we hypothesized that areas to the south of Caesarea were cultivated to support the urban population during its prime, from the Roman-Byzantine period until Early Islamic times. This study tests the hypothesis by investigating the following questions:

1. Is there an environmental signature within the sediments of Caesarea's hinterland that is compatible with extensive agricultural activity?
2. Was active cultivation present throughout the Roman period to the Crusader period?

3. Assuming the city was supported by an agricultural hinterland, how did cultivation take place in the nutrient-deprived, sandy sediments characterized by poor water adhesion properties?

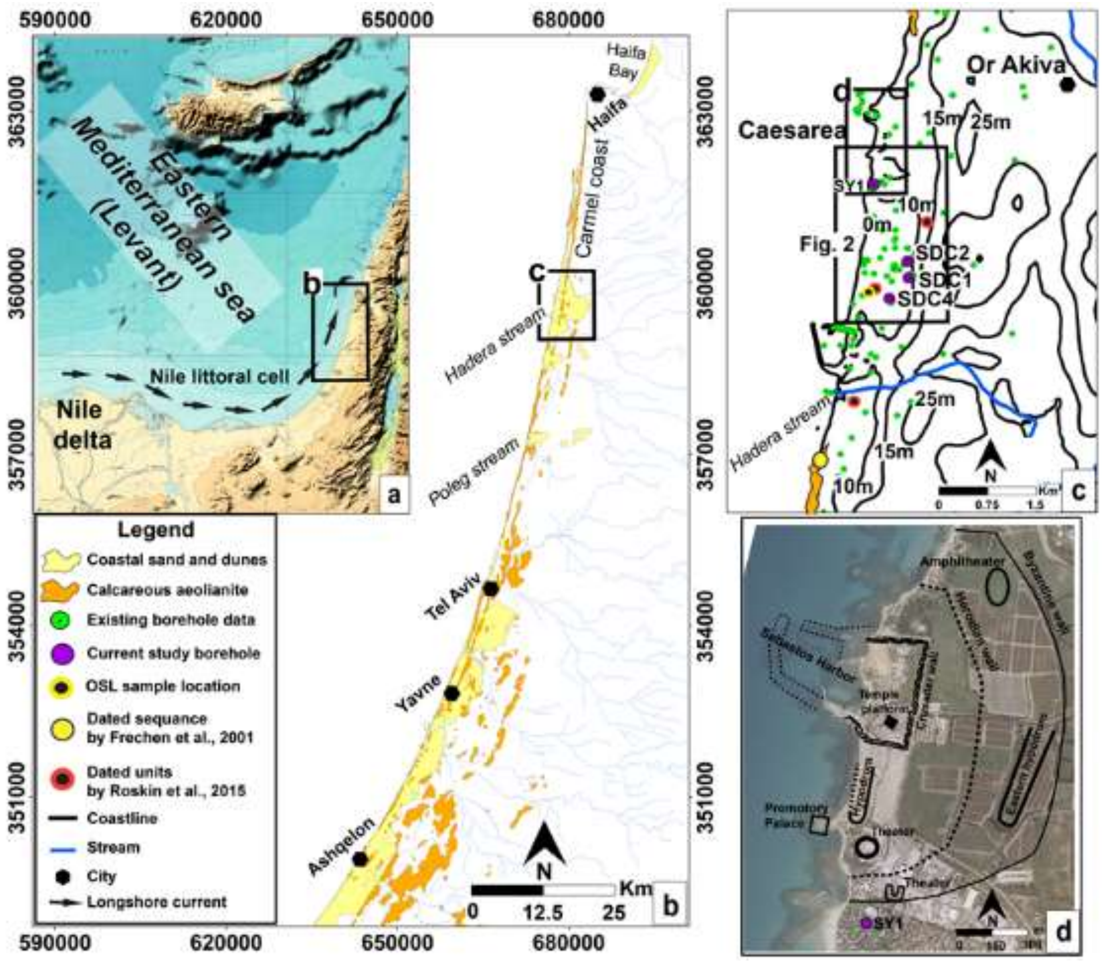

Figure 4.1: Regional and sedimentological context of the study area. (a) Map of the southeast Mediterranean illustrating the Nile littoral cell and longshore transport responsible for accumulation of sand along the eastern Mediterranean Israeli coast. (b) Detailed map showing sand sheets and Late Pleistocene aeolianite ridges typical to Israel's coastal plain and the river systems flowing toward the coastal area. (c) Map of the Caesarea area (study site) marking previously published and current boreholes along with dated unit locations. (d) Map of Caesarea (32°30'0" N, 34°53'30" E) annotating the previously excavated site and harbour ruins (modified after Reinhardt and Raban, 2008) in relation to borehole SY1 on a rectified aerial photograph from 2016.

4.4. Materials and Methods

In order to answer the research questions, we combined detailed analyses of four new boreholes with a large extant database of cores taken across the area for both academic and industrial purposes.

4.4.1. Compilation of existing data sets

We compiled published logs from 70 existing boreholes (Fig. 4.1c; supplements) and converted the borehole locations, elevations, and lithological descriptions to a common coordinate system (WGS84-UTM 36N) and vertical datum (Israel Land Survey Datum; ILSD) system in ArcGIS. The ArcGIS database also contained existing digital elevation models (DEMS; 4 × 4 m bin size), soil maps, rectified aerial photographs and chronostratigraphic data. We generated topographic and isopach surface for each facies and mapped to a bin size of 25 × 25 m through interpolation, using the ArcGIS *Topo to Raster* module (Fig. 4.3). This procedure uses an iterative finite difference interpolation technique that allows the fitted DEM to follow abrupt changes in terrain, such as streams, ridges and cliffs.

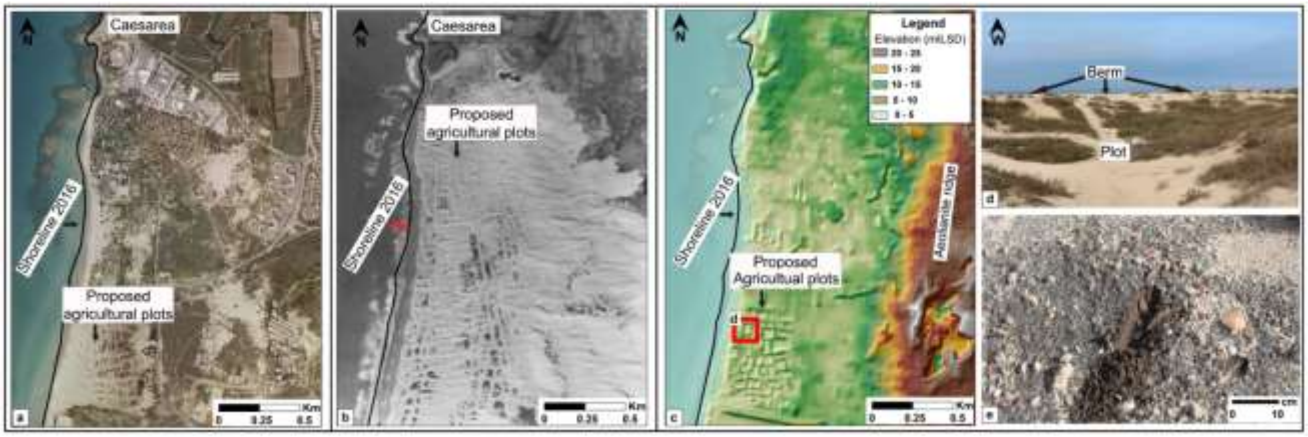

Figure 4.2: Site morphology of the coastal area south of Caesarea. The site location is displayed in Figure 4.1c (a) Rectified aerial photograph (Orthophoto) from 2016 annotating the northern boundary of the agricultural plots. (b) Rectified aerial photograph from 1946 annotating the northern boundary of the agricultural plots. (c) DEM of the coastal area south of the northern boundary of the agricultural hinterland and southern aeolianite ridge. (d) Photograph of an agricultural plot surrounded by berms. The location is displayed in Figure 4.2c (red rectangle). (e) Grey sand rich with sherds, marble, seashells and glass covering the berm surface.

4.4.2. New borehole drilling and petro-sedimentological analyses

We chose the locations of the new boreholes based on interpretation of the ground model developed from extant logs, focusing on horizons with high potential of anthropogenic activity as indicated by anecdotal records of artefacts (Fig. 4.3c). Coring was completed with a Geo-probe 6620DT vibrocorer in the high potential zones up to 1.5 km inland of the Mediterranean Sea. We measured the locations and elevations of the four boreholes using a Proflex 500 RTK-GPS with precision of ± 1 cm and ± 5 cm, respectively (Fig. 4.1c). The cores were then sectioned lengthwise to describe colour (Munsell colour chart) and lithology. Digital photographic analysis of the sediments assigned brightness values ranging from 0 to 254 for each pixel.

We measured magnetic susceptibility (MS) and density of the cores at every 2 cm. The measurements were made by a Geotek multi-sensor core logger equipped with a Bartington loop sensor compatible with small diameter cores. Using a Beckman Coulter LS 13 320 Laser diffraction Particle Size Analyzer, we carried out particle size distribution (PSD) analysis on 95 samples prepared by consolidating representative sediments of the four main lithofacies that were identified. Petrographic observations were made using an Olympus BX53-P petrographic microscope, following Wright and Tucker (1991),Wright (1992) and Adams and Mackemzie (1998). Total organic carbon (TOC) and inorganic carbon (IC) of 75 freeze-dried sediment samples were measured with a PrimacsSLC TOC Analyzer. X-ray fluorescence (XRF) analysis was completed on 90 samples using the EX-310LC(ED) instrument in an excitation voltage of 35 kV with beam diameter of 8 mm. The raw element values were then normalized to silica values, a dominant element in Israel's coastal sediments, to enable relative difference assessment for each sub-unit sample (Revel et al., 2010; Box et al., 2011).

We determined the mineralogical composition of the identified litho-facies through Fourier Transform Infrared spectroscopy (FTIR) analysis using a Nicolet iS5 FTIR spectrometer and ‘‘Omnic’’ software. After homogenization by grinding, bulk sediment samples were prepared using the KBr method. The Interpretation of the mineralogical composition was based on reference libraries.

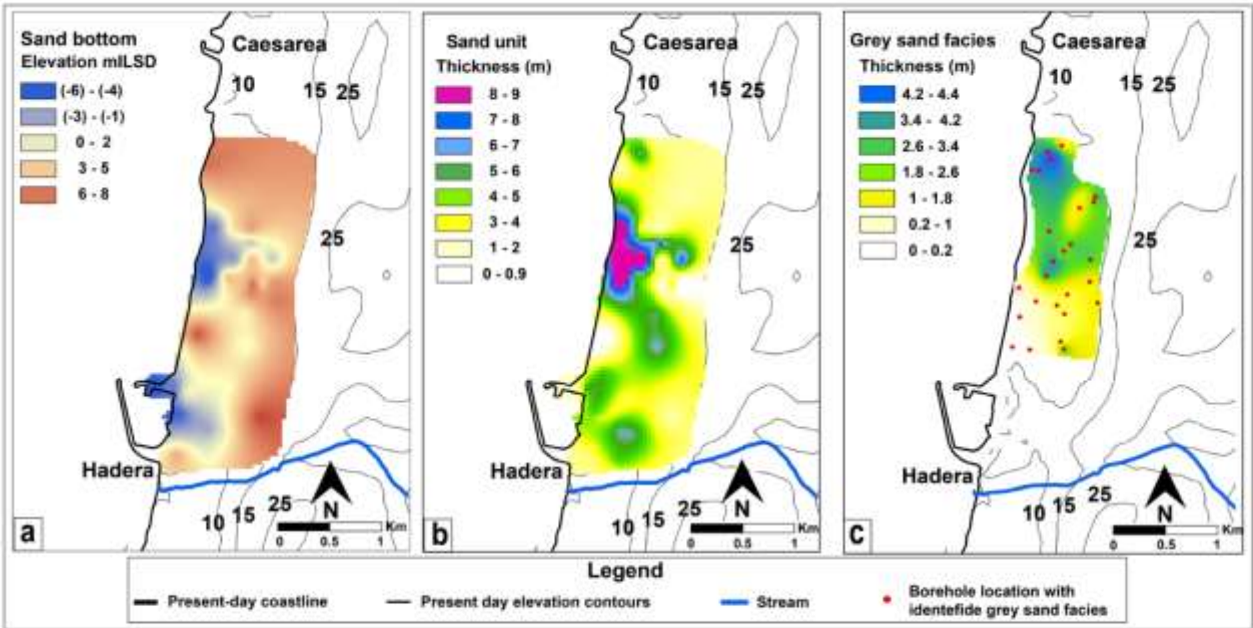

Figure 4.3: Elevation and thickness maps. (a) The bottom elevation of the yellow sand facies. (b) The thickness of the entire sandy unit (c) The thickness of the grey sand facies interpolated from the presented boreholes (red dot). Note that the grey sand facies covers a large area south and southeast of Caesarea, with the thickest part located closest to the ancient city walls.

4.4.3. Dating

4.4.3.1. Optically Stimulated Luminescence

One optically stimulated luminescence (OSL) sample was prepared and measured at the Luminescence Laboratory of the Geological Survey of Israel, Jerusalem. Quartz grains (125–150 µm) were extracted using routine laboratory procedures under subdued orange light (Davidovich et al., 2012), following single aliquot regenerative-dose (SAR) protocol. Further data on OSL procedures performed on aeolian sand by the Geological Survey of Israel can be found in Shtienberg et al., 2017. OSL ages are presented in thousands of years (ka) before 2015 (Table 4.2).

.

4.4.3.2. Radiocarbon

Four samples (one bone and three wood fragments) were ^{14}C-dated using the Accelerator Mass Spectrometry (AMS) technique (Table 4.2; Fig. 4.1c). The samples were selected following pre-screening using FTIR spectroscopy. Samples were pre-treated, graphitized and measured at the Poznan radiocarbon laboratory in Poznan, Poland. The ages obtained are given as ^{14}C age ± 1σ year before present (BP), and the calibrated ranges for ± 1σ and ± 2σ in years BP, according to the convention in Stuiver and Polach (1977). Radiocarbon dates were calibrated using the IntCal 13 atmospheric curve (Reimer et al., 2009) and OxCal version 4.2.3© (Ramsey and Lee, 2013).

Table 4.1: Optically stimulated luminescence (OSL) laboratory data and age with corresponding lithological facies, sample depth relative to ILSD (m) and sample location (UTM). The sample was measured in 2-mm aliquots. The De and error on De were calculated using unweighted mean and standard deviation. The sample shows recycling ratios within 5 % of 1.0 and negligible recuperation and IR signals. Aliquots used: the number of aliquots used for the average De out of the aliquots measured.

Sample name	Est. moisture (%)	Facies grain size (μm)	Elev. (mILSD)	location (UTM 36N)	K (%)	U (ppm)	Th (ppm)	Ext. α (μGy/a)	Ext. β (μGy/a)	Ext. γ (μGy/a)	Cosmic (μGy/a)	Total dose (μGy/a)	No. of discs	OD (%)	De (Gy)	**Age (ka)**
HAD-90	3	Grey clayey sand 90-125	4	677775 3595235	0.39	0.57	1.24	2	367	211	176	757±20	18/19	21	0.64±0.09	**0.85±0.11**

Table 4.2: Radiocarbon ages of the four samples from the cores SY1 and SDC1 at different depths: the bone remains and wood fragments both retrieved from a grey sand at depths of 6.5 and 5.5 m respectively. The ages are given as ^{14}C age ± 1s year BP, and the calibrated ranges for ± 1 s and ± 2 s in years BP, according to the convention in Stuiver and Polach (1977).

Core	Lab no.	Elev. (mILSD)	Location (UTM 36N)	Material	^{14}C age ±1σ year BP uncal.	Calibrated range ± 1σ year BP	Calibrated range ±2σ year BP
SY1	Poz-83568	6.5	677740 3596659	Bone remains in grey sand unit	1280 ± 30 BP	1335 (40.8%) 1295 1275 (27.4%) 1249	1354 (95.4%) 1242
SY1	Poz-83569	4.7	677740 3596659	Wood fragments in grey sand unit	Modern	64 (68.2%) 60	66 (95.4%) 58
SY1	Poz-83571	4.5	677740 3596659	Wood fragments in grey sand unit	Modern	64 (68.2%) 60	66 (95.4%) 58
SDC1	Poz-83570	6.8	678109 3595207	Wood fragments in grey sand unit	Modern	64 (68.2%) 60	66 (95.4%) 57

4.5. Results

The stratigraphy of the area to the south of Caesarea consists of two main units: F1 and F2 (Table 4.3; Figs. 4.4, 4.6), which can be divided into one and four facies, respectively. The lithological characteristics of each unit and correlations between the boreholes were described through integration of their sedimentological properties with mineralogy, petrographic microscopy and elemental composition.

4.5.1. Unit F1

Unit F1 is found in all four cores. It is composed of approximately 65 % sand, 25 % silt, and 10 % clay. F1 consists of very low values (<0.1%) of $CaCO_3$ and TOC. Brightness values vary from 70 to 150, while colour is dark reddish brown to dull brown (2.5YR3/3 to 7.5YR4/5). MS values range from 60 to 150 $\times 10^{-8}$ m^3 Kg^{-1} (Fig. 4.4). Microscopically, F1 comprises well-sorted, sub-rounded to rounded quartz grains within a groundmass of reddish brown clay, and is barren of phytoliths (Fig. 4.5a). Mineralogically, it is composed of quartz and clay. The unit is relatively enriched in the elements P, Fe, Al, Ti, Zn and Sr (analysed in core SDC2) compared to the unit immediately above it, facies F2a (Fig. 4.6). Based on the relatively high MS values, hue, granulometry ratios and microscopic features this unit is interpreted as a palaeosol.

4.5.2. Unit F2

Unit F2 unconformably lies over unit F1 and consists of four facies: F2a, F2b (1-3), F2c and F2d (Fig. 4.4).

4.5.2.1. Facies F2a

Facies F2a is found in all four cores (Fig. 4.4). It is composed of roughly 85 % sand, 10% silt, and 5 % clay. $CaCO_3$ concentrations range between 0 to 20 %, and TOC values are higher than unit F1 (< 0.8 %). Brightness values vary from 150 to 220, and colour is pale yellow to light grey (2.5Y 8/1 to 5Y8/2). MS values range from 25 to 50 $\times 10^{-8}$ m^3 Kg^{-1}. F2a consists of well-sorted, sub-rounded quartz grains and bioclasts, including bivalve shells, land snail fragments and foraminifera species of the family Textulariidae. No phytoliths were evident (Fig. 4.5b). Elemental concentrations in F2a (analysed in cores SY1, SDC1 and SDC2) are the lowest compared to F1 and facies of F2b and F2c (Fig. 4.6). The mineral composition of F2a includes quartz, aragonite and calcite from sand, shell and microfossil remains, respectively (Fig. 4.4). Based on the facies, granulometry ratios, hues and microscopic features this facies is interpreted as aeolian sand.

4.5.2.2. Facies F2b

Facies F2b is identified in borehole SY1 south of ancient Caesarea, and includes three sub-facies (F2b1; F2b2; F2b3) that are separated by facies F2a (Fig. 4.4). These facies are all greyish in colour:

1. Sub-facies F2b1 is 1.2 m thick and consists of about 80 % sand, 15 % silt and 5 % clay. $CaCO_3$ concentrations range from 0 % to 20 %, while TOC values are as high as 0.4 %. F2b1 has a brightness value of 150, and colour is light greyish yellow (2.5Y 7/3). MS values mostly range from 50 to 80 $\times 10^{-8}$ m^3 Kg^{-1}. Phytoliths, pottery remains, 1 cm calcareous sandstone clasts, wood pieces, shell and glass fragments (> 1 cm) are present throughout this poorly-sorted sub-facies (Fig. 4.5b, c, f1-2). F2b1 mainly consists of quartz, calcite and aragonite with the carbonated phosphate mineral hydroxylapatite identified 0.15 m above its base (Fig. 4.4).

Hydroxylapaite is a major component of bone, but may also form diagenetically following composting processes (Weiner, 2010). Elemental analysis shows high concentrations of P, Fe, Ca, Ti and Pb compared to F2a, peaking about 0.4 m from the sub-facies surface (Fig. 4.6). Two wood fragments sampled 0.1 and 0.35 m below the sub-facies surface were radiocarbon dated to 1960 with a probability of 95 % (Table 4.2). These two samples and a third wood fragment collected in facies F2c likely represent modern vegetation roots that penetrated deep into the subsurface (Kutiel et al., 2016). Based on the elemental and mineral composition, hues and microscopic and macroscopic features this sub-facies is interpreted to be an anthroposol.

2. Sub-facies, F2b2 is 1 m thick and is composed of 80 % sand, 15 % silt, and 5 % clay. $CaCO_3$ concentrations range from 12 % to 25 %, and TOC values fluctuate from 0.2 % to 0.8 %. Brightness values are around110, and colour is light grey (10Y 7/1). MS values mostly range from 50 to 180 $\times 10^{-8}$ m^3 Kg^{-1}, peaking 0.6 m below the sub-facies surface (Fig. 4.4). The sub-facies is poorly-sorted with pottery remains, 1 cm calcareous sandstone clasts and shells present throughout. Bone fragments were identified 0.2-0.3 m below the F2b2 surface (Fig. 4.5b). F2b2 consists of quartz, calcite and carbonated hydroxylapatite minerals. Microscopically, it was found to contain micritic calcite that resembles wood ash (Shahack-Gross and Ayalon, 2013), phytoliths and micro-charcoal fragments. Quartz grains appear to be less frequent than in the overlying upper section (Fig. 4.5b, c). Concentrations of P, Fe, Al, Ca, Ti, Zn, Cu, and Pb are highest in F2b2 compared to all other sub-facies and facies across the boreholes. Elemental concentrations peak 0.6 m below the sub-facies surface (Fig. 4.6). A 1.5 × 1.5 cm bone fragment found in F2b2 was dated between 1354 and 1242 calibrated years BP (Table 4.2; Fig. 4.6), i.e., the Early Islamic period. Based on the elemental and mineral composition, hues and microscopic and macroscopic features this sub-facies is interpreted as e an anthroposol.

3. Sub-facies F2b3 is 1.5 m thick. It is composed of approximately 90 % sand, and 0 % silt. The $CaCO_3$ concentration of is about 8 %, while TOC values range from 0.3 % to 0.6 %. Brightness values are 150, and colour varies from light grey to yellowish grey (10Y 7/2 to 2.5Y 5/1).MS values mostly range from 80 to 250 $\times10^{-8}$ m^3 Kg^{-1} (Fig. 4.4). We identified small pottery remains (> 2 cm; Fig. 4.5f), 1 cm calcareous sandstone clasts, land snail and bivalve shell fragments throughout this poorly-sorted sub-facies. Minerals identified in F2b3 include quartz, calcite, aragonite and carbonated hydroxylapatite. Microscopically, the sub-facies consists of micritic calcite (ash), phytoliths and micro-charcoal fragments (Fig. 4.5b, c). Concentrations of P, S, Fe, Al, Ti and Pb are comparatively high. A peak was identified for Ca, Zn and Cu at 0.3 m below F2b3's surface (Fig. 4.6). Based on elemental and mineral composition, hues and microscopic and macroscopic features this sub-facies is interpreted to be an anthroposol.

4.5.2.3. Facies F2c

Facies F2c is identified in boreholes SDC1, SDC2, SDC4, covering unit F2a with thicknesses of 1 to 2 m. It is composed of roughly 85 % sand, and 15 % silt. $CaCO_3$ concentrations are between 5 % and 12 %, while TOC values fluctuate from 0 % to 0.4 %. Brightness values vary from 130 to 200, and colour is yellowish grey to light grey (2.5Y 5/1 to 10YR 8/1). MS values mostly range from 30 to 80 $\times10^{-8}$ m^3 Kg^{-1} (Fig. 4.4). Microscopic examination identified traces of phytoliths and subrounded quartz grains surrounded by dark microsparitic calcite (Fig. 4.5d). We identified pottery fragments, 0.5 cm calcareous sandstone clasts, shell and land snail fragments, wood remains and small glass fragments (> 1 cm) throughout the facies. F2c is relatively well sorted and consists of quartz, aragonite, calcite and carbonated hydroxylapatite minerals. Elemental concentrations of P, S, Fe, Al, Ca, Ti, Zn, Sr and Pb are higher compared to F2a but lower compared to F2b. One OSL age (sample HAD-90; Table 4.1) dated F2c to 0.85 ± 0.11 ka (1165 ±

110 CE – the Crusader period). The sample was collected 200 m east of the Mediterranean Sea, 0.7 m below the facies surface (Fig. 4.7). A wood fragment sampled 0.15 m below the F2c surface in borehole SDC1 was dated to 1960 with a probability of 95 % (Table 4.2). Based on the elemental and mineral composition, hues and microscopic and macroscopic features this facies is interpreted to be an anthroposol.

4.5.2.4. Facies F2d

F2d is the topmost facies in boreholes SDC1, SDC2 and SDC4 (Fig. 4.4). It is composed of about 95 % sand and ~5 % silt. $CaCO_3$ concentrations range from 6 % to 15 %, while TOC values fluctuate between 0 % and 0.6 %. Brightness values vary from 180 to 200, and colour is light grey to pale yellow (5Y 8/1 to 5Y8/4). MS values mostly range from 15 to 25 $\times10^{-8}$ m^3 Kg^{-1}. F2d consists of well-sorted, sub-rounded quartz grains sometimes accompanied by land snail shell fragments. F2d is free of sherds, calcareous sandstone clasts, glass fragments and barren of phytoliths wood ash and micro-charcoal. Elemental concentrations in cores SDC1 and SDC2 resemble those of F2a and are comparatively lower than concentrations measured in unit F1 and facies F2b and F2c (Fig. 4.6). Mineralogically, F2d is composed of quartz, aragonite and calcite from sand and shell remains greater than 0.5 cm (Fig. 4.4). Based on the granulometry ratios, hues and microscopic features this facies is interpreted as aeolian sand.

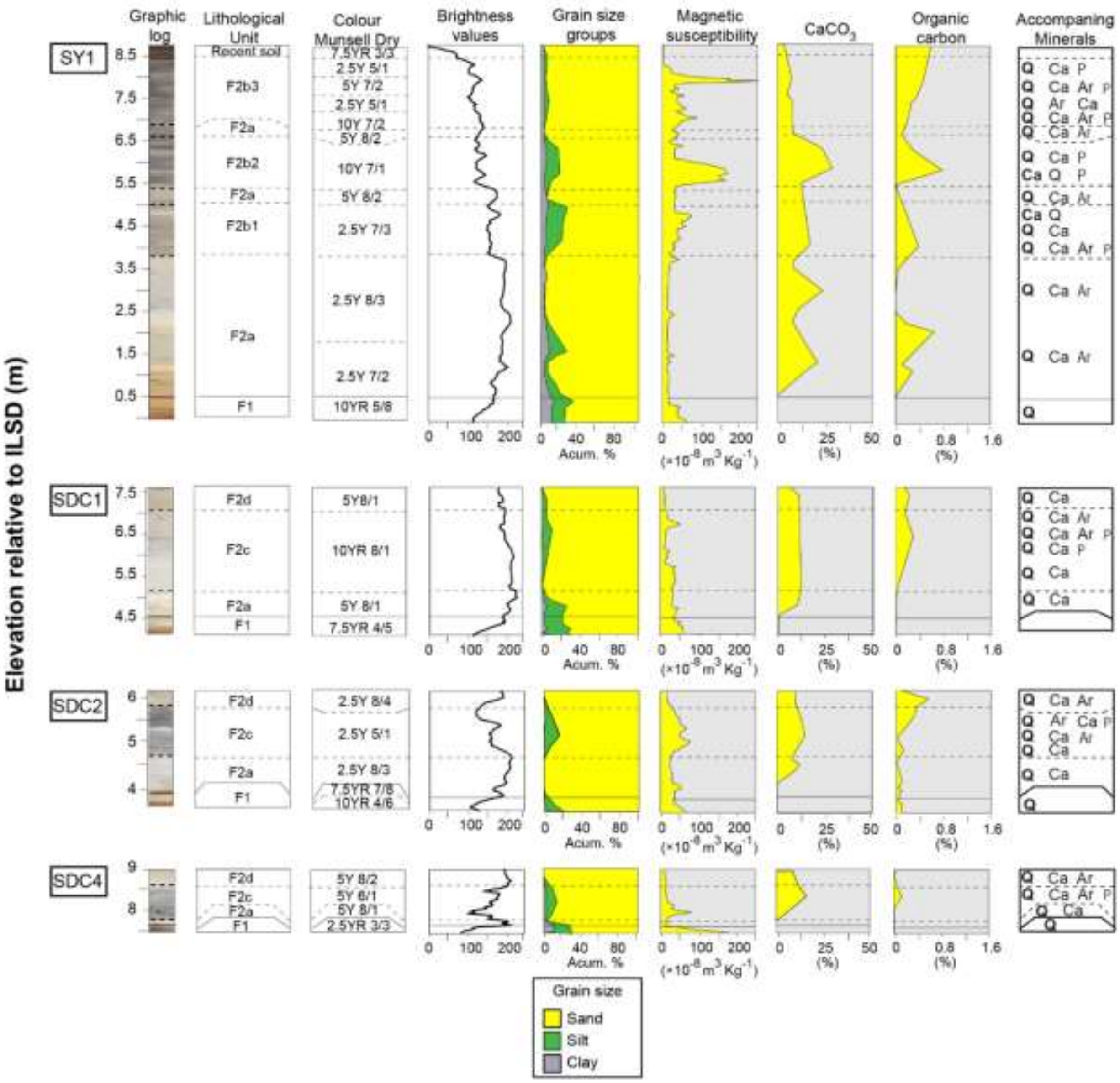

Figure 4.4: Detailed information obtained from boreholes SY1, SDC1, SDC2 and SDC4. Note that grey lithological units seem to correspond with increased silt levels, increased magnetic susceptibility, and presence of phosphate-containing minerals.

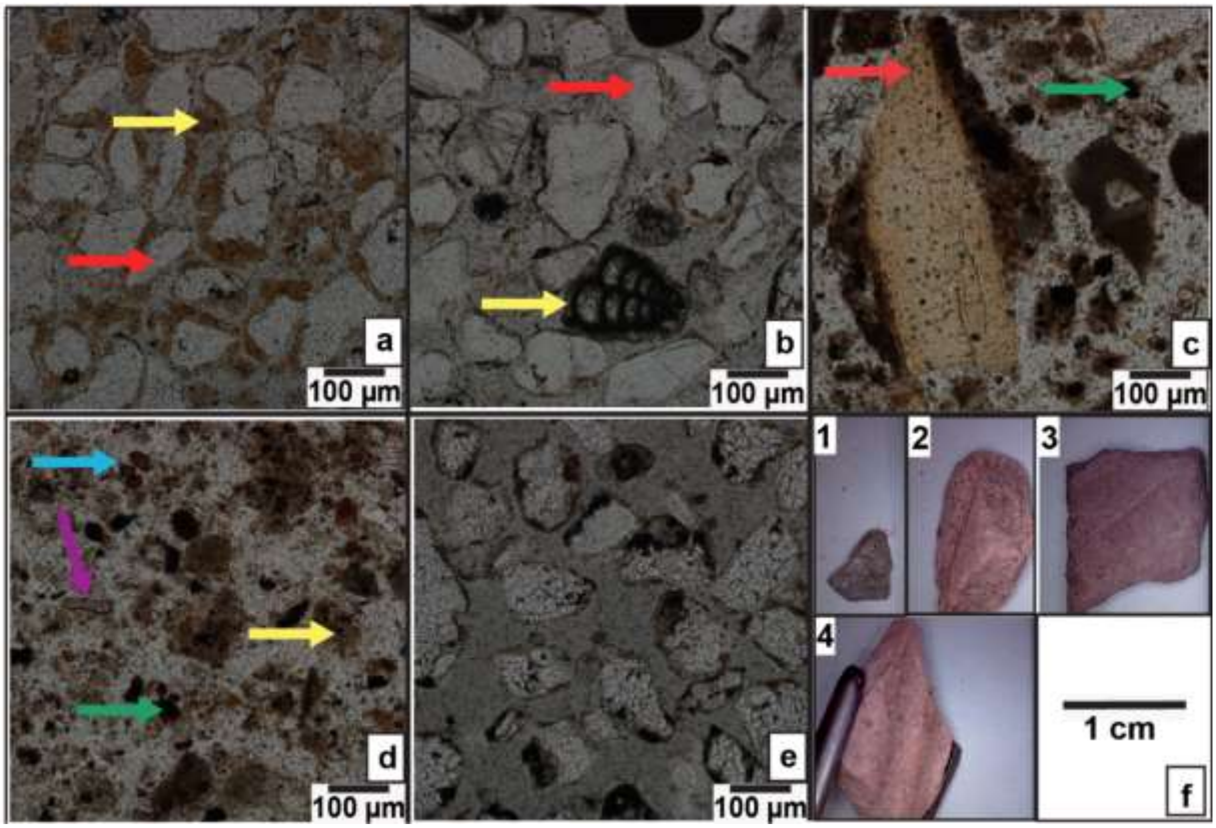

Figure 4.5: Microscopic features in thin section (a-e) and macroscopic finds (f). (a) Unit F1 (palaeosol). Subrounded quartz grains (red arrow) within a groundmass of reddish-brown clay. (b) Subunit F2d (yellow sand). Subrounded quartz grains (red arrow) and skeleton of the foraminifer Textulariidae sp. (yellow arrow) testifying to the aeolian origin of this unit. (c) Subunit F2b (grey sand) with abone fragment and micro-charcoal fragments (red arrow). (d) Subunit F2b (grey sand). Low quantities of quartz grains associated with abundant micro-charcoal fragments (green arrow), phytoliths (purple arrow), pollen grains (blue arrow) and micritic calcite resembling wood ash (yellow arrow). (e) Unit F2c (grey sand). Quartz grains partly surrounded by dark microsparitic calcite. (f) Glass (1) and pottery remains (2-4) which were identified throughout subunits F2b and F2c. Note that artefacts and microscopic remains indicating human activity are primarily identified in the grey sand subunit F2b.

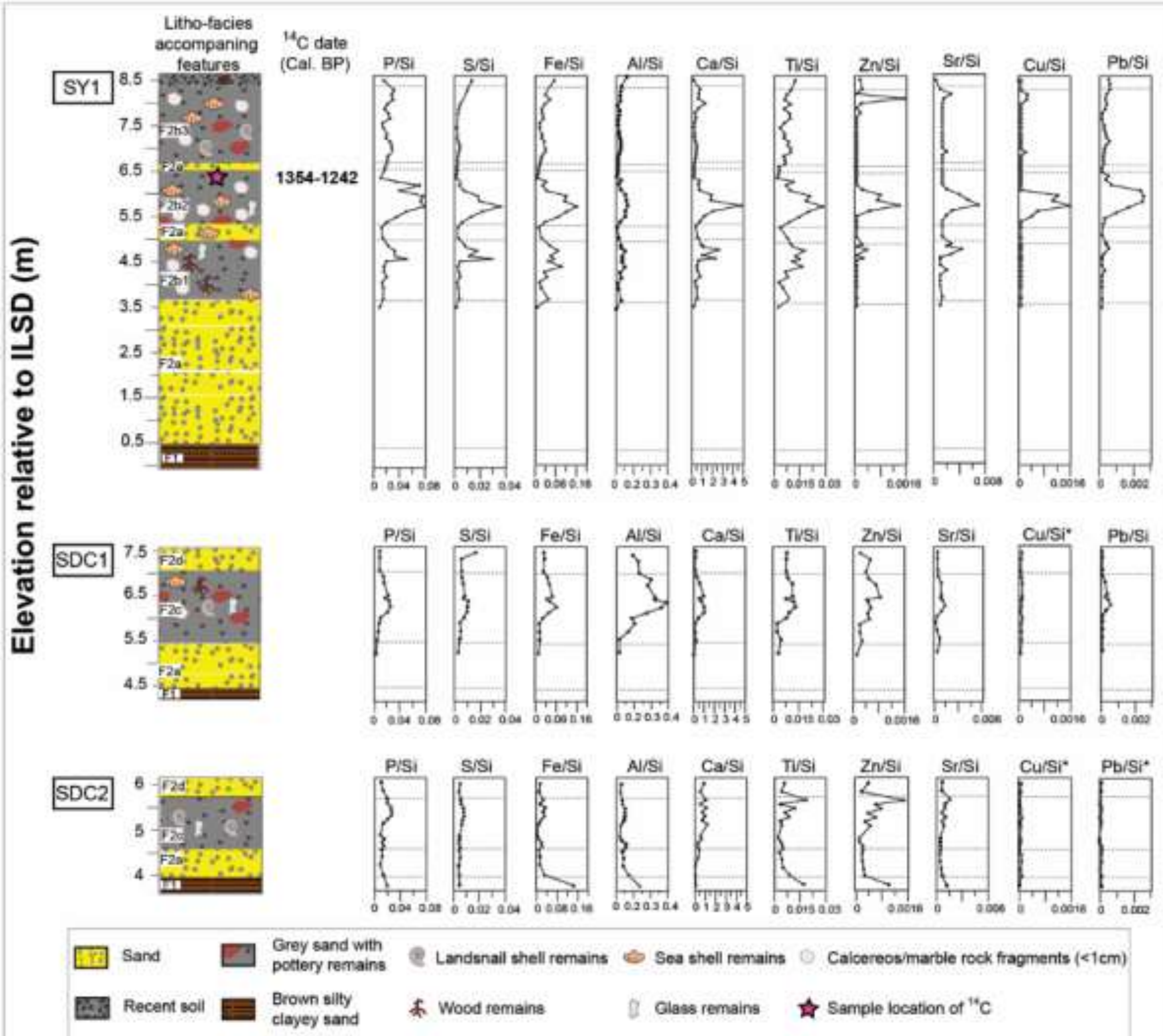

Figure 4.6: Relative elemental concentrations (all normalized relative to silicon concentrations) measured in boreholes SY1, SDC1 and SDC2. The various lithofacies are presented along with macroscopic remains found within them. A bone (borehole SY1) fragment yielded radiocarbon date that is presented here as well, corresponding to the Early Islamic period. Note that the trace elements values for Cu in borehole SDC1 and Cu and Pb in borehole SDC2 (marked by asterisk) were lower than the detection capabilities of the EX-310LC(ED) instrument.

4.6. Discussion

We combined detailed analyses of four newly acquired boreholes with a chronologically constrained ground model generated from extant datasets to answer questions regarding the nature of human-landscape activity in the hinterland to the south of Caesarea.

4.6.1. Palaeo-topography spatial variability and chrono-stratigraphy

The base lithology underlying the study area consists of aeolianites and palaeosols that range between elevations of -4 to +7.8 mILSD (Fig. 4.3a). We identified four sand facies (Figs. 4.1c, 4.6; Table 4.3) overlying the basal topography (Fig. 4.7; Table 4.3). Sand accumulations up to 9 m thick (Fig. 4.3a) fill the base topographic lows while the thinnest accumulations, about 0.5 m thickness, overlay topographic highs.

OSL (Roskin et al., 2015) and infrared stimulated luminescence (IRSL; Frechen et al., 2002) techniques dated the lower aeolian sand facies (F2a) to 5.9 – 3.3 ka (Fig. 4.7). F2a covers most of the basal topography between Hadera and Caesarea (Fig. 4.1c). Based on these ages and previous studies conducted on the north central coast of Israel (Kadosh et al., 2004; Porat et al., 2004; Cohen-Seffer et al., 2005; Mauz et al., 2013; Shtienberg et al., 2017), the initial aeolian sand incursion and stabilisation of the coastal landscape occurred around 3885 ± 900 BCE (Fig. 4.7), i.e. the Chalcolithic period.

Overlying F2a is a grey coloured, artefact-containing pedo-sediment (facies F2b and F2c; Table 4.3) that was mapped (Figs. 4.1c, 4.3c) throughout the southern parts of Caesarea's lowlands (Shtienberg et al., 2017). This grey sand is identified in the vicinity of high sand berms (Fig. 4.2), covering an area of 1.4 km^2 that extends up to 3 km south of the city boundaries. These facies thin with distance from Caesarea. The results of this study indicate these facies are chronologically constrained between 662 CE and 1165 ± 110 CE, i.e., Early Islamic to Crusader period (Table 4.3). These results are supported by a previously published OSL date of 1165 ± 110 CE from the dune field located 3 km south of the city (Fig. 4.7; Roskin et al., 2015).

The anthropogenic sand facies F2b and F2c are covered by yellow aeolian sand (F2d) that was deposited after 1165 ± 110 CE, i.e., the Crusader period. During the Crusader period, the city of Caesarea was under constant attack, resulting in declining human presence in the area south of Caesarea (Porath, 2000). The decrease in human activity caused re-establishment of vegetation and sand stabilization. Based on ages from the same facies on the adjacent coastal plain and coastal escarpment (Fig. 4.1c; Frechen et al., 2001; Salmon, 2013; Roskin et al., 2015), we propose that the upper sand (F2d) was deposited and stabilized from 1365 ± 160 CE until present. This combined chronology is consistent with the archaeological and historical timelines of ancient Caesarea (Table 4.3).

Table 4.3: Characterisation and age chronology of the sedimentological unit identified in the current study from the surface downward**.**

Unit	Facies	Sub-facies	Grain texture	Accompanying features	Unit interpretation	OSL (ka)	Cal. ^{14}C age (BP)	Historical date (BCE/CE)	Cultural period	Reference (ages)
F2	F2d	-	Sand	Subrounded quartz grains, land snail fragments	Sand	present to 0.65 ± 0.16		present to 1365 ± 160 CE	Israel - Mameluke - Ottoman Empire	Frechen et al., 2001; Salmon, 2013; Roskin et al., 2015
	F2c	-	Loamy sand	Subrounded quartz grains surrounded with dark microsparitic calcite, pottery remains, 0.5 cm calcareous sandstone rocks, shell and land snail fragments, glass remains	Anthropogenic sand	0.85 ± 0.11; 0.86 ± 0.1		1165 ± 110 CE; 1155 ± 100 CE	Crusader	Current study; Roskin et al., 2015
	F2b	3	Sand	1 cm calcareous sandstone rocks, land snail and shell fragments, wood ash, micro charcoal	Anthropogenic sand					
		2	Loamy sand	Phytoliths, sherds, 1 cm calcareous sandstone rocks, wood pieces, shells, bone pieces, wood ash, micro charcoal, glass fragments	Anthropogenic sand		1354 – 1242	774 – 662 CE	Early Islamic	Current study
		1	Loamy sand	Phytoliths, sherds, 1 cm calcareous sandstone rocks, wood pieces, shells glass fragments	Anthropogenic sand					
	F2a	-	Sand	Subrounded quartz grains shell and land snail fragments, microfossil remains	Sand	3.3 ± 0.5 to 5.9 ± 0.9		1285 ± 500 to 3885 ± 900 BCE	Chalcolithic - Bronze age	Frechen et al., 2002; Kadosh et al., 2004; Porat et al., 2004; Cohen-Seffer et al., 2005; Mauz et al., 2013; Roskin et al., 2015; Shtienberg et al., 2017
F1	-	-	Sandy loam	Subrounded to rounded quartz grains and groundmass of reddish-brown clay	Palaeosol (unit upper constrain)	7.7 ± 1.2		~6000 BCE	Neolithic	Gvirtzman and Wieder, 2001; Roskin et al., 2016

4.6.2. Anthropogenic activity in the outskirts of ancient Caesarea

The grey facies F2b and F2c have a typical anthropogenic pedo-sediments composition previously identified in prehistoric (Shahack-Gross et al., 2004) and historic (Regev et al., 2015) sites. The composition of F2b and F2c reflects the past presence of organic matter and/or bones; ash, micro-charcoal and high MS values corresponding with fire; plant phytoliths; and macroscopic artefacts such a pottery and glass. Due to their size (< 2 cm), the macroscopic artefacts do not enable further investigation. All of these features indicate a strong human presence associated with these horizons.

The two anthropogenic grey facies, F2b and F2c, slightly differ from one another. Facies F2c, found in three cores (Figs. 4.6 and 4.7) seems to exhibit less anthropogenic impact than facies F2b, found only in core SY1. The difference is more evident when comparing F2c to sub-facies F2b2, as F2b2 contains lower concentrations of man-made elements and micro-remains such as phytoliths and ash.

By contrast, the bounding sand facies (F2a and F2d) are clearly of aeolian origin and lack signatures of human activity. The two facies have the lowest concentrations of elements other than Si and Ca and the lowest MS values recorded in this study (below 50×10^{-8} m^3 Kg^{-1}). The characteristics of F2a and F2d do not suggest evidence of fire (Gvirtzman and Wieder, 2001; Tsatskin et al., 2008) or human, animal or cultivation activity.

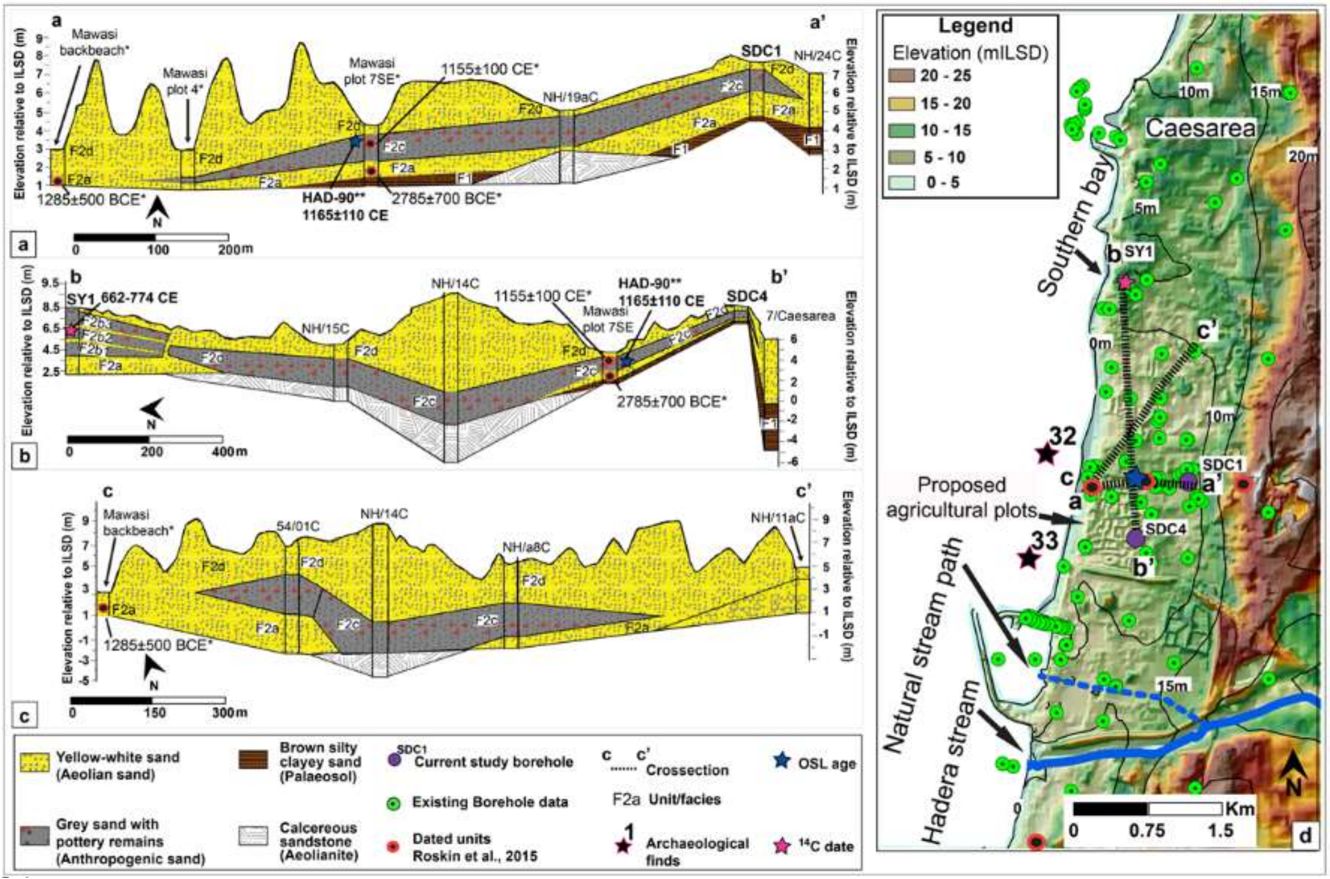

Figure 4.7: Chronostratigraphic cross sections in the Hadera-Caesarea coastal area (a-c) based on previous lithological and OSL data (marked with a star) published in Roskin et al. (2015) as well as lithological and radiocarbon data from t study. Refer to (d) to follow cross sections in space. The modern topography of Hadera-Caesarea was extracted from a 4×4m DEM. Archaeological sites located in the study area (black stars in d) are marked with a site number linked to the IAA survey: http://www.antiquities.org.il/survey/new/. Note that OSL dates determine the date of last exposure to sunlight, while radiocarbon dates indicate the time of death of organic matter.

4.6.2.1. The dumping site

The thickness of facies F2b (approximately 4 m), along with the internal separation by thin units of natural aeolian sand (F2a), indicates repeated activity in the same locality. Two options can explain such an assemblage of macroscopic and microscopic artefacts outside of a settlement: (a) repeated human habitation with intermittent abandonment phases, and (b) repeated garbage disposal activity with intermittent abandonment phases. The absence of architecture, combined with the placement of Facies F2b outside the walls of Roman-Byzantine Caesarea (Fig. 4.1d), argues against the first option. The topography of facies F2b (Fig. 4.6b, 4.d), roughly 4 m higher than its surroundings, implies that this facies is in the form of a 0.07 km^2 mound (Fig. 4.3b, c). Thus, the topography of facies F2b indicates this accumulation may be a garbage dump.

Previous excavations have identified ancient dumps in several old cities throughout Israel. One such garbage accumulation is located in the Early Roman city of Jerusalem (Bar-Oz et al., 2013). The ancient dump in Jerusalem is rich in pottery, bone, shells, plant remains, grey building debris, coins and glass. Large garbage dumps are also known in the vicinity of Byzantine-Early Islamic (6^{th}-9^{th} centuries CE) cities in the Negev region of southern Israel. Preliminary observations in excavations at the ancient Negev cities of Elusa, Shivta and Nessana highlight the grey-coloured appearance of these dumps (Shahack-Gross, pers. observations). An older garbage heap in the Iron Age city of Megiddo in northern Israel is also composed of grey-coloured sediments where carbonated hydroxylapatite, phytoliths, dung spherulites and ash (along with macroscopic artefacts of pottery, bones and stones) are abundant. This Iron Age trash heap consists of several superimposed beds, indicating repeated garbage disposal activity (Shahack-Gross et al., 2009). The appearance and properties of facies F2b sediments resemble those of garbage mounds found in other cities in the southern Levant region of the Eastern Mediterranean, further evidence that facies F2b represents a garbage mound associated with ancient Caesarea (Fig. 4.3c).

A bone fragment obtained from the middle of facies F2bprovides a temporal constraint of 662 to 774 CE. Therefore, dumping started before this date, possibly even during the Roman period. High Pb concentrations are present below the level of the dated bone fragment (Figs. 4.5, 4.6), and high lead concentrations are generally associated with Roman period activities (Rosen and Galili, 2007). The dated bone fragment is overlain by approximately 2 m of facies F2b sediments, indicating that the garbage mound also operated after 720 CE. At 740 CE, the Muslims took control over Caesarea following a seven-year siege, a conquest that did not lead to large-scale destruction and abandonment (Avni, 2014). The continued use of the dumping site after the Islamic conquest appears to be represented at the top of facies F2b.

Consideration of the spatial and temporal characteristics of the landfill can assist with identifying probable users of the dumping site. This apparent urban dumping site operated 0.5 km south of the ancient wall of Byzantine Caesarea (Fig. 4.1d) and a few hundred meters east of the southern Bay of Caesarea. The Bay of Caesarea was a hub of maritime activity (Fig. 4.7d) that included an anchorage and a pier set in the natural bay (Galili et al., 1993) in addition to a Byzantine docking site and ship cargo remains (sites 33 and 32; Fig. 4.7d). Therefore, users of the dumping site likely included city inhabitants and anchorage workers.

4.6.2.2. Modified agricultural sand south of Caesarea

Facies F2c presents a different formation process then F2b. The facies extends over a larger area in comparison to facies F2b and is thinner (reaching a maximum thickness of about 3 m; Fig. 4.3c). Facies F2c is somewhat less anthropogenically impacted in terms of elemental concentrations and macroscopic and microscopic artefacts (Fig. 4.5d). F2c is located 0.2 km from the coastline and extends up to 1.5 km landward (Fig. 4.7d), covering an area of 1.4 km^2 with an overall volume of about 4.8 km^3. F2c does not exhibit evidence of widespread architecture. Comparison of the underlying and overlaying natural aeolian sand units demonstrates that facies F2c has the following characteristics: (i) higher organic content; (ii) higher P, S and Ca concentrations, (iii) the presence of phytoliths, and (iv) calcitic-clay coatings surrounding the quartz sand grains.

Based on these observations, we postulate that facies F2c represents a pedo-sediment that is the outcome of aeolian sand fertilised to be suited for agricultural use. We propose that the higher organic content and elevated elemental concentrations are the result of composting practices. The compost itself may have been domestic or urban trash, which explains the presence of pottery, glass and rock fragments. The calcitic-clay coatings may indicate incipient pedogenesis (compared with the clay coatings around the quartz sand in the palaeosol; Fig. 4.5a, e). Such composting practices could change the barren coastal aeolian sand into a fertile sediment suited for agricultural use (Tsoar and Zohar, 1985; Ward and Summers, 1993; Blume and Leinweber, 2004). Moreover, composting added silt (Fig. 4.4; Table 4.3) to the original sand, which enhanced the water adhesion properties of the sediment. Historical reuse of organic-rich material for agricultural composting has been documented in other regions throughout the Mediterranean and the Middle East, including Crete, Greece, Egypt and Iraq, dating as far back as the third millennium (Wilkinson, 1989; Bull et al., 2001). The low number of phytoliths found in the pedo-sediment means they cannot be used for further interpretation or statistical analysis. The existence of phytoliths, however, may be a by-product of the original compost, as they are abundant in the garbage deposits identified in facies F2b.

Overall, facies F2c is interpreted as the remains of agricultural fields that supported ancient Caesarea several of centuries before 1165 ± 110 CE (Fig. 4.7a, c; Table 4.3). This interpretation is supported by historical and archaeological records. During the Roman and perhaps most of the Byzantine period, there was little attempt to conduct agricultural intensification of the immediate countryside of Caesarea (Safrai, 2003). Agricultural produce may have poured to the city not only from its port, but from villages as far as the Carmel coast to the north and east of Poleg Stream to the south (Fig. 4.1b; Holum, 2016). Only in the late Byzantine or the Early Islamic period was there an active attempt to improve the fertility of the sand around Caesarea for more intensive agriculture. These actions were perhaps aimed at making the huge metropolis less dependent on imports and long supply lines resulting from the politically volatile conditions of the 6th and 7th centuries CE (e.g., the 6th century revolts of the Samaritans). Three types of archaeological evidence found near Caesarea have led researchers to suggest that agricultural plots surround the area: (a) grey sediments in rectangular shapes, (b) excavations of farmhouses and farming complexes, (c) botanical analyses of finds from Caesarea.

Porath (1975) was the first to propose that the area south of Caesarea was the focus of an intensive agricultural effort conducted by the central authorities of the city. He identified raised plots with a 0.5 to 0.7 m thick layer of grey sediment consisting of sherds, building refuse and shreds. He interpreted these plots as Mawasi agriculture (Fig. 4.7), as the grey sediment was situated just above the high coastal fresh water table, probably allowing natural subsurface watering by capillary rise (Warren, 1871; Tsoar and Zohar, 1985; Sánchez and Cuellar, 2016). Excavations near Or-Akiva (Fig. 4.1b) led Ad (2009) to suggest that the coastal agricultural system extended up to 3 km east of Caesarea. Ad proposed this hypothesis due to the presence of a similar grey-coloured sand deposit containing sherds, coins, construction materials and possibly trash remains. The trash remains may have been brought from Caesarea in order to improve the cultivation properties of the sediment. In addition, the Or-Akiva excavations contained farming complexes with a well, water dividing channels, delineation walls and a threshing floor. The archaeological evidence for agricultural intensification near Caesarea is also supported by rich archaeobotanical finds from Caesarea itself. The majority of weed and wild species found within the assemblage of edible plants are common components of field cultivation (Ramsay and Holum, 2015).

The archaeological finds and historical documentation combined with radiometric ages obtained in this study show that Caesarea had a large agricultural system that dates to the Islamic period. Dating of the pottery remains and Fatimid quarter coins excavated in the field area and archaeobotanical finds from Caesarea suggest that the fields operated throughout early Islamic times. These dated artefacts and archaeobotanical samples are supported by historical descriptions from Early Islamic period writers that praise the agricultural produce of the city (Avni, 2014; Ramsay and Holum, 2015). Other sources point out that even after the Crusader conquest, and during the 12^{th} century until the battle of Hattin (1101-1087 CE), Caesarea was still involved in agricultural production of wheat, olives, citrus and figs (Prawer, 1972; Ramsay and Holum, 2015). Recent work has identified similar grey sand units between eroded berms in the Yavne dune field (Fig 4.1) along the southern coast of Israel (Roskin and Taxel, 2017). The grey units in this location have early 12^{th} century OSL ages similar to those found in the Caesarea fields. Yavne's grey sand also displays slightly improved fertility (phosphate, potassium, nitrogen and calcium carbonate concentrations) relative to the underlying sand, suggesting an anthropogenic enrichment of ash and refuse. The Yavne finds suggests a similar and contemporaneous attempt to improve agricultural productivity during the Early Islamic period in the Israeli sandy coastal plain.

4.7. Conclusion

This paper provides a detailed holistic study of sediments from the southern hinterland of Caesarea, Israel in order to explore the impact of an urban settlement on its periphery. Combining sedimentological and micro-archeological analyses of recently acquired borehole data with existing topographic, chronology, log-lithology, archaeological finds and historical documentations enables the following conclusions to be made:

1. We identified two different facies of anthropogenically influenced sediments.
   a. An urban garbage mound, characterised by a dark grey sediment containing the highest copper, lead and phosphate ratios found in this study, along with the presence of ash, micro-charcoal and macroscopic artefacts such as pottery and glass.
   b. A cultivated 1 to 3 m thick grey pedo-sediment covering an area of 1.4 km^2, identified by the presence of higher organic content, phosphate, sulphur and calcite ratios compared to underlying and overlying natural sand, along with plant phytoliths.

The ability to differentiate between anthroposols through the holistic approach presented in this study could be used in future research to reveal past uses of landscapes and soils.

2. During the early Islamic period, inhabitants of Caesarea enriched the nutrient deprived sediments south of the city by adding domestic or urban refuse. These composting practices changed the barren coastal aeolian sand into a fertile pedo-sediment with water adhesion properties better suited for agricultural use.
3. The burial of the agricultural pedo-sediment, signifying the end of the cultivation period, dates to the Crusade period. This chronology agrees with historical evidence of the decline and abandonment of Caesarea.

This study shows the potential for studying hinterlands of urban centres through analysis of sediment cores in addition to conventional archaeological work that typically focuses on excavation of settlements. It is likely that sites with similar anthropogenic pedo-sediments are present along the coast of Israel. Because such sites have not yet been explored through the methodologies used in this research, it is unclear whether fertilizing sandy sediments was pioneered in Caesarea or if it was part of a wider (possibly earlier) phenomenon. The holistic approach presented here may present new possibilities to increased understanding of the impact of human societies on the environment.

Acknowledgments

The authors gratefully acknowledge support from the University of Haifa, the Helmsley Charitable Trust Mediterranean Sea Research Center, and also Maurice and Lady Hatter Fund of the Leon Recanati Institute for Maritime Studies (RIMS) at the University of Haifa. Dina Dagan Begun of Ben Gurion University of the Negev and Silas Dean, Benny Bechor and Dr. Guy Sisma-Ventura of the University of Haifa are thanked for their vital help in the field. We also thank Dr. Or M. Bialik and Dr. Nimer Taha from the University of Haifa for their help in the sedimentological and geochemical analyses. Jonathan J. Gottlieb from the University of Haifa is thanked for preparation of thin sections.

4.8 References

Ackermann, O., Greenbaum, N., Ayalon, A., Bar-Matthews, M., Boaretto, E., Bruins, H.J., Cabanes, D., Horwitz, L.K., Neumann, F.H., Porat, N., Weiss, E., Maeir, A.M., 2015. Using palaeo-environmental proxies to reconstruct natural and anthropogenic controls on sedimentation rates, Tell es-Safi/Gath, eastern Mediterranean. Anthropocene 8, 70-82.

Ackermann, O., Greenbaum, N., Bruins, H., Porat, N., Bar-Matthews, M., Almogi-Labin, A., Schilman, B., Ayalon, A., Horwitz, L.K., Weiss, E., Maeir, A.M., 2014. Palaeoenvironment and anthropogenic activity in the southeastern Mediterranean since the mid-Holocene: The case of Tell es-Safi/Gath, Israel. Quaternary International 328-329, 226-243.

Ad, U., 2009. Or-Akiva: Remains of a Farming Complex and Irrigation System from the End of the Byzantine–Beginning of the Early Islamic Periods in the Agricultural Hinterland of Caesarea. Atiqot 61, 49-60 (in Hebrew).

Adams, A.E., MacKenzie, W.S., 1998. A color atlas of carbonate sediments and rocks under the microscope. Manson Publishing Ltd., London, UK.

Almagor, G., Gill, D., Perath, I., 2000. Marine Sand Resources Offshore Israel. Marine Georesources & Geotechnology 18, 1-42.

Avni, G., 2014. The Byzantine-Islamic transition in Palestine: an archaeological approach. Oxford University Press.

Bar-Oz, G., Bouchnik, R., Weiss, E., Weissbrod, L., Bar-Yosef Mayer, D.E., Reich, R., 2013. “Holy Garbage”: A Quantitative Study of the City-Dump of Early Roman Jerusalem. Levant 39, 1-12.

Bar-Matthews, M., Ayalon, A., Gilmour, M., Matthews, A., Hawkesworth, C.J., 2003. Sea–land oxygen isotopic relationships from planktonic foraminifera and speleothems in the Eastern Mediterranean region and their implication for paleorainfall during interglacial intervals. Geochimica et Cosmochimica Acta 67, 3181-3199.

Bar-Yosef, O., 1975. The Epi-paleolithic in Palestine and Sinai, In: Marks, A.E. (Ed.), Problems in prehistory: North Africa and the Levant. SMU Press, Dallas, Texas pp. 363-378.

Blume, H.-P., Leinweber, P., 2004. Plaggen Soils: landscape history, properties, and classification. Journal of Plant Nutrition and Soil Science 167, 319-327.

Bouma, J., Hole, F.D., 1971. Soil structure and hydraulic conductivity of adjacent virgin and cultivated pedons at two sites: A Typic Argiudoll (silt loam) and a Typic Eutrochrept (clay). Soil Science Society of America Journal 35, 316-319.

Box, M.R., Krom, M.D., Cliff, R.A., Bar-Matthews, M., Almogi-Labin, A., Ayalon, A., Paterne, M., 2011. Response of the Nile and its catchment to millennial-scale climatic change since the LGM from Sr isotopes and major elements of East Mediterranean sediments. Quaternary Science Reviews 30, 431-442.

Bull, I., Phillip PB, Richard PE, 2001. An Organic Geochemical Investigation of te Practice of Manuring at a Minoan Site on Pseira Island, Crete. Geoarchaeology 16, 223-242.

Certini, G., Scalenghe, R., 2011. Anthropogenic soils are the golden spikes for the Anthropocene. The Holocene 21, 1269-1274.

Cohen-Seffer, R., Greenbaum, N., Sivan, D., Jull, T., Barmeir, E., Croitoru, S., Inbar, M., 2005. Late Pleistocene–Holocene marsh episodes along the Carmel coast, Israel. Quaternary International 140-141, 103-120.

Danin, A., 2005. The sandy areas of Caesarea, a rare situation of alpha and beta diversity linked by plant succession. Israel Journal of Plant Sciences 53, 247-252.

Davis, M., Matmon, A., Rood, D.H., Avnaim-Katav, S., 2012. Constant cosmogenic nuclide concentrations in sand supplied from the Nile River over the past 2.5 my. Geology 40, 359-362.

Ellenblum, R., 2012. The collapse of the eastern Mediterranean: climate change and the decline of the East, 950-1072. Cambridge University Press.

Emery, K., Neev, D., 1960. Mediterranean beaches of Israel: Israel Geological Survey Bulletin. 26, 1-24.

Engelmann, A., Neber, A., Frechen, M., Boenigk, W., Ronen, A., 2001. Luminescence chronology of Upper Pleistocene and Holocene aeolianites from Netanya South - Sharon Coastal Plain, Israel. Quaternary Science Reviews 20, 799-804.

Frechen, M., Dermann, B., Beonigk, W., Ronen, A., 2001. luminesence chronology of the aeolianites from the section at givat olga-coastal plain of israel. Quaternary Science Reviews 20, 805-809.

Frechen, M., Neber, A., Dermann, B., Alexander, T., Boenigk, W., Raban, A., 2002. Chronostratigraphy of aeolianites fromthe Sharon Coastal Plain of Israel. Quaternary International, 31-44.

Frechen, M., Neber, A., Tsatskin, A., Boenigk, W., Ronen, A., 2004. Chronology of Pleistocene sedimentary cycles in the Carmel Coastal Plain of Israel. Quaternary International 121, 41-52.

Galili, E., Dahari, U., Sharvit, J., 1993. Underwater surveys and rescue excavations along the Israeli coast. The International Journal of Nautical Archaeology 22, 61-77.

Galili, E., Nir, Y., 1993. The submerged Pre-Pottery Neolithic water well ofAtlit-Yam, northern Israel and its palaeoenviromental implications. The Holocene 3, 265-270.

Godfrey-Smith, D.I., Vaughan, K.B., Gopher, A., Barkai, R., 2003. Direct luminescence chronology of the Epipaleolithic Kebaran site of Nahal Hadera V, Israel. Geoarchaeology 18, 461-475.

Goodman-Tchernov, B.N., Austin, J.A., 2015. Deterioration of Israel's Caesarea Maritima's ancient harbor linked to repeated tsunami events identified in geophysical mapping of offshore stratigraphy. Journal of Archaeological Science: Reports 3, 444-454.

Gvirtzman, G., Netser, M., Katsav, E., 1998. Last-Glacial to Holocene kurkar ridges, hamra soils, and dune fields in the coastal belt of central Israel. Israel Journal of Earth Sciences 47, 27-46.

Gvirtzman, G., Wieder, M., 2001. Climate of the last 53,000 years in the eastern med based on soil-sequence Stratigraphy in coastla plain Israel. Quaternary Science Reviews 20, 1827-1849.

Habas, E., 1996. The Halachic status of Caesarea as reflected in the Talmudic literature, In: Raban A, KG, H. (Eds.), Caesarea Maritima: a retrospective after two millennia, Brill, Leiden, pp. 454-475.

Hole, F., 1974. Wild soils of the Pine-Popple Rivers basin. Transactions of the Wisconsin Academy of Sciences, Arts, and Letters.

Holum, K.G., 2009. Et dispositione civitatis in multa eminens: Comprehending the urban plan of 4th century Caesarea. Man near a Roman arch. The Israel Exploration Society, Jerusalem, 187-207.

Holum, K.G., 2011. Caesarea Palaestinae: a paradigmatic transition. Shaping the Middle East. Jews, Christians, and Muslims in an Age of Transition, 400-800.

Holum, K.G., 2016. Caesarea Palaestinae: City and Countryside in Late Antiquity: City and Countryside in Late Antiquity, In: Patrich, J., Peleg-Barkat, O., Ben-Yosef, E. (Eds.), Arise, Walk Through the Land. Studies in the Archaeology and History of the Land of Israel in Memory of Yizhar Hirschfeld on the Tenth Anniversary of his Demise. Israel Exploration Society, Jerusalem, pp. 1-16.

Israel Meteorological Service, 2011. Climate Atlas, http://www.ims.gov.il/IMS/CLIMATE/ClimaticAtlas/RainMaps.htm (16.02.15) (in Hebrew).

Kadosh, D., Sivan, D., Kutiel, H., Weinstein-Evron, M., 2004. A late quaternary paleoenvironmental sequence from Dor, Carmel coastal plain, Israel. Palynology 28, 143-157.

Kutiel, P. B., Katz, O., Ziso-Cohen, V., Divinsky, I., Katra, I., 2016. Water availability in sand dunes and its implications for the distribution of Artemisia monosperma. Catena, 137, 144-151.

Langgut, D., Almogi-Labin, A., Bar-Matthews, M., Weinstein-Evron, M., 2011. Vegetation and climate changes in the South Eastern Mediterranean during the Last Glacial-Interglacial cycle (86 ka): new marine pollen record. Quaternary Science Reviews 30, 3960-3972.

Levin, N., 2013. The Palestine exploration fund map (1871–1877) of the holy land as a tool for analysing landscape changes: the coastal dunes of Israel as a case study. The Cartographic Journal.

Mauz, B., Hijma, M.P., Amorosi, A., Porat, N., Galili, E., Bloemendal, J., 2013. Aeolian beach ridges and their significance for climate and sea level: Concept and insight from the Levant coast (East Mediterranean). Earth-Science Reviews 121, 31-54.

Neev, D., Schanai, E., Hall, J.K., Bakler, N., Ben-Avraham, Z., 1978. The Young (Post Loewr Pliocene) Geological History of the Caesarea. Israel Journal of Earth Sciences 28, 43-46.

Nicosia, C., Devos, Y., 2014. Urban dark earth, Encyclopedia of Global Archaeology. Springer, pp. 7532-7540.

Olami, Y., Sender, S., Oren, E., 2005. Map of Binyamina. Israel Antiquities Authority, Jerusalem.

Patrich, J., 2001. The carceres of the Herodian hippodrome/stadium at Caesarea Maritima and connections with the Circus Maximus. Journal of Roman Archaeology 14, 269-283.

Picard, L., 1943. Structure and evolution of Palestine. Bull. Geol. Dept. Hebrew Univ., Jerusalem 4, 1-134.

Pomerancblum, M., 1966. The distribution of heavy minerals and their hydraulic equivalents in sediments of the Mediterranean continental shelf of Israel. Journal of Sedimentary Research 36.

Porat, N., Wintle, A.G., Ritte, M., 2004. Mode and timing of kurkar and hamra formation, central coastal plain, Israel. Israel Journal of Earth Sciences 53, 13-25.

Porath, Y., 1975. The Gardens of Caesarea. Qadmoniot, 30-31.

Porath, Y., 2000. Caesarea–1994–1999. Hadashot Arkheologiyot: Excavations and Surveys in Israel (in Hebrew), 34-40.

Porath, Y., 2002. The water-supply to Caesarea: a re-assessment, In: Amit D, Hirschfeld Y, J, P. (Eds.), JOURNAL OF ROMAN ARCHAEOLOGY-SUPPLEMENTARY SERIES, pp. 104-129.

Prawer, J., 1972. The Latin Kingdom of Jerusalem: European Colonialism in the middle Ages Weidenfeld, London.

Raban, A., 2007. Ancient harbors of the Mediterranean, In: Artzy M, Goodman B, Gal Z (Eds.), The Harbor of Sebastos in its Roman Mediterranean context. BAR International Series, Oxford, pp. 1-48.

Ramsay, J., Holum, K., 2015. An archaeobotanical analysis of the Islamic period occupation at Caesarea Maritima, Israel. Vegetation History and Archaeobotany 24, 655-671.

Ramsey, C.B., Lee, S., 2013. Recent and planned developments of the program OxCal. Radiocarbon 55, 720-730.

Regev, L., Cabanes, D., Homsher, R., Kleiman, A., Weiner, S., Finkelstein, I., Shahack-Gross, R., 2015. Geoarchaeological Investigation in a Domestic Iron Age Quarter, Tel Megiddo, Israel. Bulletin of the American Schools for Oriental Research (BASOR) 374, 135-157.

Reimer, P.J., Baillie, M.G., Bard, E., Bayliss, A., Beck, J.W., Blackwell, P.G., Bronk, R.C., Buck, C.E., Burr, G.S., Edwards, R.L., 2009. IntCal09 and Marine09 radiocarbon age calibration curves, 0-50,000 years cal BP. Radiocarbon 51, 1111-1150.

Reinhardt, E.G., Raban, A., 1999. Destruction of Herod the Great’s harbor at Caesarea Maritima, Israel-Geoarchaeological evidance. Geology 27, 811-814.

Reinhardt, E.G., Raban, A., 2008. Site formation and stratigraphic development of Caesarea's ancient harbor, In: Holum, K., Stabler, J., Reinhardt, E. (Eds.), Caesarea Reports and Studies: Excavations 1995–200, pp. 155-182.

Revel, M., Ducassou, E., Grousset, F.E., Bernasconi, S.M., Migeon, S., Revillon, S., Mascle, J., Murat, A., Zaragosi, S., Bosch, D., 2010. 100,000 Years of African monsoon variability recorded in sediments of the Nile margin. Quaternary Science Reviews 29, 1342-1362.

Rosen, B., Galili, E., 2007. Lead Use on Roman Ships and its Environmental Effects. International Journal of Nautical Archaeology 36, 300-307.

Roskin, J., Sivan, D., Bookman, R., Porat, N., Shtienberg, G., 2016. Beach buildup and coastal aeolian sand incursions off the Nile cell during the Holocene Poster presented in the annual IGRG Congress; the University of Haifa, 33.

Roskin, J., Sivan, D., Shtienberg, G., Roskin, E., Porat, N., Bookman, R., 2015. Natural and human controls of the Holocene evolution of the beach, aeolian sand and dunes of Caesarea (Israel). Aeolian Research 19, 65-85.

Roskin, J., Sivan, D., Shtienberg, G., Porat, N., Bookman, R., 2017. Holocene beach build up and coastal aeolian sand incursions off the Nile littoral cell. In EGU General Assembly Conference Abstracts 19, 2391.

Roskin, J., Taxel, I., 2017. Early Islamic inter-settlement agroecosystems in coastal sand, Yavneh dunefield, eastern Mediterranean coast, Israel, In: EGU General Assembly Conference Abstracts 19, 844.

Safrai, Z., 2003. The Economy of Roman Palestine. Routledge.

Salmon, Y., 2013. A Second Millennium Geo-archaeological and Palaeo-environmental Study of the Nami Region: An Integrated Approach to a Coastal and Maritime Study, The Department of Maritime Civilizations. The University of Haifa.

Sánchez, R., Cuellar, M., 2016. Coastal interdune agroecosystems in the Mediterranean: a case study of the Andalusian navazo. Agroecology and Sustainable Food Systems 40, 895-921.

Sandor, A., Gersper, P.L., Hawley, J.W., 1990. Prehistoric agricultural terraces and soils in the Mimbres area, New Mexico. World Archaeology 22, 70-86.

Schattner, U., Lazar, M., Tibor, G., Ben-Avraham, Z., Makovsky, Y., 2010. Filling up the shelf — A sedimentary response to the last post-glacial sea rise. Marine Geology 278, 165-176.

Shahack-Gross, R., Ayalon, A., 2013. Stable carbon and oxygen isotopic compositions of wood ash: an experimental study with archaeological implications. Journal of Archaeological Science 40, 570-578.

Shahack-Gross, R., Berna, F., Karkanas, P., Weiner, S., 2004. Bat guano and preservation of archaeological remains in cave sites. Journal of Archaeological Science 31, 1259-1272.

Shahack-Grass, R., Gafri, M., Finkelstein, I., 2009. Identifying threshing floors in the archaeological record: a test case at Iron Age Tel Megiddo, Israel. Journal of Field Archaeology 34, 171-184.

Shtienberg, G., Dix, J.K., Roskin, J., Waldmann, N., Bookman, R., Bialik, O.M., Porat, N., Taha, N., Sivan, D. New perspectives on coastal landscape reconstruction during the Late Quaternary: A test case from central Israel. Palaeogeography, Palaeoclimatology, Palaeoecology 468, 503-519.

Shtienberg, G., Dix, J., Waldmann, N., Makovsky, Y., Golan, A., Sivan, D., 2016. Late-Pleistocene evolution of the continental shelf of central Israel, a case study from Hadera. Geomorphology 261, 200-211.

Sivan, D., Lambeck, K., Toueg, R., Raban, A., Porath, Y., Shirman, B., 2004. Ancient coastal wells of Caesarea Maritima, Israel, an indicator for relative sea level changes during the last 2000 years. Earth and Planetary Science Letters 222, 315-330.

Sivan, D., Porat, N., 2004. Evidence from luminescence for Late Pleistocene formation of calcareous aeolianite (kurkar) and paleosol (hamra) in the Carmel Coast, Israel. Palaeogeography, Palaeoclimatology, Palaeoecology 211, 95-106.

Sivan, D., Widowinski, S., Lambeck, K., Galili, E., Raban, A., 2001. Holocene sea level changes based on archeological sites off northen israel Palaeogeography, Palaeoclimatology, Palaeoecology 167, 101-117.

Smejda, L., Hejcman, M., Horak, J., Shai, I., 2017. Ancient settlement activities as important sources of nutrients (P, K, S, Zn and Cu) in Eastern Mediterranean ecosystems–The case of biblical Tel Burna, Israel. Catena, 156, 62-73.

Stieglitz, R., 1996. Stratonos Pyrgos - MigdalSar - Sebastos: history and archaeology, In: Rabban, A., Holum, K.G. (Eds.), Caesarea Maritima - retrospective after two millennia. Brill, Leiden, pp. 593-608.

Stuiver, M., Polach, H.A., 1977. Discussion; reporting of C-14 data. Radiocarbon 19, 355-363.

Taxel, I., 2013. The Byzantine-early Islamic transition on the Palestinian coastal plain: a re-evaluation of the archaeological evidence. Semitica et Classica, 73-106.81. Tsartsidou, G., Lev-Yadun, S., Efstratiou, N., Weiner, S., 2008. Ethnoarchaeological study of phytolith assemblages from an agro-pastoral village in Northern Greece (Sarakini): development and application of a Phytolith Difference Index. Journal of Archaeological Science 35, 600-613.

Tsatskin, A., Gendler, T.S., Heller, F., Ronen, A., 2008. Near-surface paleosols in coastal sands at the outlet of Hadera stream (Israel) in the light of archeology and luminescence chronology. Journal of Plant Nutrition and Soil Science 171, 524-532.

Tsoar, H., Zohar, Y., 1985. Desert Dune Sand and its Potential for Modern Agricultural Development, in: Desert Development Springer, Netherland, pp. 184-200.

Ward, S.C., Summers, R.N., 1993. Modifying sandy soils with the fine residue from bauxite refining to retain phosphorus and increase plant yield. Fertilizer Research, 151-156.

Warren, C., 1871. The Plain of Philistia. Palestine Exploration Quarterly 3, 82-96.

Weiner, S., 2010. Microarchaeology: beyond the visible archaeological record. Cambridge University Press.

Wilkinson, T.J., 1989. Extensive Sherd Scatters and Land Use Intensity: Some Recent Results. Journal of Field Archaeology 16, 31-46.

Wright, V., 1992. A revised classification of limestones. Sedimentary Geology 76, 177-185.

Wright, C.I., Tucker, M.E., 1991. Calcretes. Blackwell Scientific Publications, Oxford, UK.

Yaalon, D.H., 1967. Factors affecting the lithification of eolianite and interpretation of its environmental significance in the coastal plain of Israel. Journal of Sedimentary Research 37, 1189-1199.

Yaalon, D.H., Dan, J., 1967. Factors controlling soil formation and distribution in the Mediterranean coastal plain of Israel during the Quaternary. Quaternary soils, 321-338.

Zeder, M.A., 2011. The Origins of Agriculture in the Near East. Current Anthropology 52, S221-S235.

Zviely, D., Kit, E., Rosen, B., Galili, E., Klein, M., 2009. Shoreline migration and beach-nearshore sand balance over the last 200 years in Haifa Bay (SE Mediterranean). Geo-Marine Letters 29, 93-110.

Zviely, D., Sivan, D., Ecker, A., Bakler, N., Rohrlich, V., Galili, E., Boarreto, E., Klein, M., Kit, E., 2006. Holocene evolution of the Haifa Bay area, Israel, and its influence on ancient tell settlements, The Holocene, pp. 849-861.

5. Discussion and Conclusions

The amalgamation of geophysical and petro-sedimentological analysis carried out in the current study along with the existing logs (Figs. 1.1, 2.2, 3.1c, d) has enabled the establishment of a stratigraphical correlation between the terrestrial – shallow shelf environments and the identification of a total of six units across the coastal sections of the study area (Figs. 2.4, 2.5, 3.3, 3.5). The dating of the terrestrial units of the lowland has, enabled chronostratigraphical correlation with the interpreted units from the shallow shelf and the coastal cliff sequence and thus the development of a 4-D evolutionary model of the central Israeli coastal area. This chronostratigraphical reconstruction has been linked to both global and regional environmental proxies, thus highlighting the triggering and driving forces that shaped the Israel coastal evolution over the last 110 ka.

5.1. Summary of main findings

The identified coastal units deposited over the last glacial-interglacial cycle consist mainly of quartz sand in various forms: at the base of the sequence as a lithified calcareous sandstone, while the overlying unconsolidated units have undergone pedogenesis, forming loams of various types. These units have been covered since the Mid-Holocene by windblown sand (Fig. 3.5a, d; Roskin et al., 2015). Based on these unit definitions five depositional environments – terrestrial (soils), wetland (clay loam), beach (both unconsolidated and lithified sand) and aeolian in addition to an anthropogenic signature have been identified. The petro-sedimentological characteristics and geophysical attributes of the current coastal offshore-terrestrial units and the depositional environments they represent are as follows:

1. ***Terrestrial*** – These units include the orange, red and brown palaeosols, barren of fauna and pollen, consisting of loamy sand to silty clayey sand, with MS values of 50–250 ($\times 10^{-8}$ m^3 kg^{-1}) and low $CaCO_3$ content (Fig. 3.3). The MS values correlate with the varying silt-clay percent and ferro-magnetic minerals, which point to fine aeolian dust, deposited by rain into the unconsolidated and porous sand stratigraphy, driving the pedogenic processes (Gvirtzman and Wieder, 2001; Tsatskin et al., 2008, 2015). The boundary between the palaeosol units can also be identified as clear reflectors in the marine geophysical data (Figs. 2.3, 2.4). The distinctive soil-sequence boundaries are interpreted as representing variations in deposition of higher silt and clay ratios material as seen in the lowland borehole based litho-stratigraphy and petro-sedimentological analysis (Fig. 2.8). $CaCO_3$ content is derived from shell fragments that have been transported inland from the coastal zone/beach. The extent of the pedogenesis process determines the concentration of $CaCO_3$; the longer the process of pedogenesis, the lower is the concentration of $CaCO_3$, as a result of carbonate dissolution due to leaching (Dan et al., 1968; Yaalon, 1997; Porat et al., 2004; Tsatskin et al., 1999). Based on the high sand content (higher than 70 %) and their associated ages, these palaeosols are interpreted to have been formed in the relatively moderate to flat topography of the coastal plain a few hundred metres to several kilometres from the palaeo-coastline when sea level was lower, during most of the last glacial-interglacial period (100 to 8 ka; Figs. 3.7, 3.8, 3.9).
2. ***Wetland*** – These units consist of organic (about 1 %) clay to sandy clay loam sediments which are $CaCO_3$-free. Offshore wetland lens-shaped fill units were mapped through the geophysical surveys consisting of chaotic low-amplitude reflections to of subparallel sub-horizontal high amplitude reflections. The greatest accumulations of the wetland dark silty clay sediments are found in the deepest topographic lows covering incised palaeosol surfaces near the palaeo-

drainage stream intersections (Fig. 2.8). This spatial correlation would suggest that the coastal streams played a major role in contributing depositing material into these wetlands. Although in the terrestrial side the unit contains no microfauna or pollen, *Zannichellia palustris* seeds were identified. These sedimentological properties and the aquatic plant seeds support the interpretation of these sediments being deposited in a brackish marsh environment, while the lack of palaeontological and palynological remains, together with the extended episode of the unit's existence dated in the current research (21–10 ka), suggest prolonged exposure of the sediment to aerial conditions and oxidation.

3. ***Beach*** – These lithologies include beach facies of both unconsolidated sand and calcareous sandstone, consisting of poorly-sorted coarse to fine quartz sand with fractions of ~85% sand, ~10% silt, ~5% clay (Appendix 3.1, 3.2; Fig. 3.3), bivalve shell fragments, allochthonous benthic microfauna and scarce red algae remains, indicating high wave energy of surf zone to the coastline environment. The beach sand and consolidated sediments that were both found in the coastal lowland range from elevations of -2.5 to +1.2 and -8.3 to +4.8 mILSD and have been dated in the current research to 130 ± 31 ka and 6.6 ± 0.9 ka respectively (Table 3.2; Fig. 3.7).
4. ***Aeolian*** – These sand facies consist of ~85% sand, ~10% silt, ~5% clay well-sorted round quartz sand (Appendix 3.2; Fig. 3.3), with terrestrial land snail shell fragments, devoid of other fauna. These characteristics suggest sediments that were windblown inland, creating terrestrial sand sheets. The aeolian sand unit range in date from 3.6 ± 0.5 ka (Table 4.4; Fig. 4.7) to present (Roskin et al., 2015).
5. ***Anthropogenic*** – In the terrestrial parts of the study area between Caesarea and Hadera stream in the Holocene Aeolian sand unit (Fig. 4.1b) amid two aeolian sand facies (Fig. 4.7) a facies greyish in colour were identified. The facies comprise of anthropogenic macro-features and

micro-features along with relatively high concentrations of P, Fe, Ca, Ti and Pb (Figs. 4.4, 4.5, 4.6). These facies were dated (Table 4.2; Fig. 4.6) in the current research, by one ^{14}C date (662 to 774 CE) and OSL age (1165 ± 110 CE).

5.1.1. Coastal chronostratigraphy for the last 115 ka

The units that comprise the sequence underlying the Israeli lowlands have been correlated with the coastal cliff sequence (Fig. 3.5) located along most of Israel's shore from Ashkelon to the Carmel coast (Fig. 1.1b). This correlation is based on the lithological descriptions, petro-sedimentological characteristics, and a stratigraphic position comparison of the current studies new OSL ages with existing published ages (Gvirtzman et al., 1983, 1998; Engelmann et al., 2001; Frechen et al., 2001, 2002; Gvirtzman and Wieder, 2001; Neber, 2002; Porat et al., 2004; Tsatskin et al., 2009; Moshier et al., 2010; Mauz et al., 2013). The correlation suggests that the coastal lowlands are dominated by palaeosol units with little if any aeolianites, whilst the coastal ridge sections consist primarily of aeolianites interbedded by palaeosols.

The basal unit of the studied sequence dates to 131 ± 30 ka (Table 3.2). Relying on the field description, sedimentological analyses (Fig. 3.3) and micromorphology (Appendix 3.1), I propose that this calcareous sandstone unit was deposited in a beach-terrestrial environment. Based on its age and the stratigraphical position and morphology of the units it can be correlated with the upper terrestrial facies of the Herzliyya *kurkar* (i.e., 98 ± 6 ka; Mauz et al., 2013). This kurkar unit is found at elevations ranging from a few metres above ILSD on the Carmel coast to about -75 mILSD in southern Israel (Fig. 3.1b; Gvirtzman et al., 1983; Frechen et al., 2004).

Overlying the Herzliyya *kurkar* is the Orange Palaeosol, which this study has dated to 104 ± 22 ka (Fig. 3.3a). A similar facies, with the same sedimentological appearance (hue, lithology, grain size, $CaCO_3$ and accompanying irregularly-shaped calcareous cemented sand nodules), has been identified 2 km south of Borehole SDC4 and dated to 87 ± 17 ka (Roskin et al., 2015). Based on this age range, the stratigraphical position of the units (Gvirtzman et al., 1983) and morphological features this red paleosol can be correlated with the Kfar Vitkin palaeosol (Gvirtzman et al., 1998; Frechen et al., 2004), which was found at elevations ranging from about +8 mILSD to about -70 mILSD (Fig. 3.1b; Gvirtzman et al., 1998; Frechen et al., 2004; Tsatskin et al., 2009). There are differences between the two units, with the Orange Palaeosol having lower silt and clay concentrations and lower MS values than the Kfar Vitkin palaeosol (Mauz et al., 2013). These sedimentological differences are interpreted to be a result of relief differences and slope angle variations between the two areas, leading to lateral erosion of sediments in the sloping areas and re-deposition in the depression (Dan et al., 1968; Yaalon, 1997; Tsatskin et al., 2009).

The Orange Palaeosol unit is covered by the Red Palaeosol, which has been dated in this study to 71 ± 18 ka (Fig. 3.3c). Based on this age this unit correlates to the coastal ridges Givat Olga Member (Fig. 3.5). During the deposition and burial time of the Red Palaeosol's parent material, from 80 to 55 ka, sand was deposited on the coastal plain of Israel in thickness ranging from 2 to 40 m (Zilberman et al., 2007; Roskin et al., 2013), forming dunes and sand sheet complexes. Since stream energies were greater during periods of low sea levels, mainly due to higher gradients and incisions (Suter and Berryhill, 1985; Anderson et al., 1996; Blum and Tōrnqvist, 2000 and ref. therein), the streams experienced limited sand deposition in their channels, with the sand accumulating at the coastal margin. The sand removal from the stream outlets and dune build-up over the rest of the area led to the formation of the lowlands sequence (Fig. 3.1c, d). The synchronous deposition of the dune-sand sheet complex (up to 40 m) and the slow sand sheet accumulation in the coastal lowland (up to 4 m) resulted in the concurrent development of the coastal ridges Givat Olga Member (aeolianites interbedded by Nahsholim Palaeosol; Gvirtzman et al., 1983, 1998) and soil formation of the lowland Red Palaeosol (Figs. 3.5 and 3.6; Frechen et al., 2002; Mauz et al., 2013).

The Red Palaeosol is overlain by a dark reddish-brown to brown unit with sandy clayey loam to sandy loam grain texture. This Brown Palaeosol consists of high Fe and Al concentrations, which are in agreement with fluctuating MS values, and is dated to between 58 ± 8 and 36 ± 9 ka (Figs. 3.3, 3.4). The carbonate percentage, particle size, MS and chronology of the Brown Palaeosol have been comparable to the lower coastal cliff Netanya palaeosol sub-unit (Fig. 3.5; Gvirtzman and Wieder, 2001). The upper sub-units of the Netanya palaeosol are dated from 12 to 8 ka at varying elevations ranging from +10 mILSD to about +40 mILSD in an N-S section from the Sharon coast to Ashkelon in the south (Figs. 3.5, 4.1b; Gvirtzman et al., 1983; 1998; Frechen et al., 2002; Porat et al., 2004; Mauz et al., 2013). Even though the top of the lowland Netanya palaeosol was not dated in this study (Appendix 3.3) the unit's surface was dated in a similar geomorphic location south of Rishon-Lezion (Fig. 3.1b) to 8.6 ± 2.5 ka (Roskin et al., 2016).

In several boreholes adjacent to the stream channels, and in the shallow marine parts of the study area, a dark silty-clay deposit was identified overlying the Brown Palaeosol. This wetland facies, dated in the current study from 21 ± 4 to 10 ± 2 ka, has also been identified in other location along the Carmel coast (Kadosh et al., 2004; Cohen-Seffer et al., 2005; Sivan et al., 2011 among others) adjacent to stream systems but was not detected on the higher coastal ridge sequence (Fig. 3.4).

The uppermost unit identified in the lowlands consists of four sandy units deposited from 6.6 to 0.1 ka (Fig. 3.6; Roskin et al., 2015; Shtienberg et al., 2017) which correspond closely to three aeolian units deposited on the coastal ridges (6.2 to 0.1 ka): Hadera; Ta'arukha sand; and the Tel-Aviv *kurkar* (Gvirtzman et al., 1983).

5.2. The Late Quaternary coastal evolution of Israel and implicating forcing factors

The chronostratigraphy developed in this study for the shallow shelf and terrestrial parts of the central Israeli coast enables a temporal correlation to be made with both global and regional environmental proxies, and thus develop hypotheses for the drivers of the evolution of this coastline over the last 110 ka. In the following sections, the contribution of global sea-level, together with regional climate, is specifically discussed.

5.2.1. Forcing factors effecting Israel's coastal evolution

5.2.1.1. Low sea levels and their controls on sedimentation gaps

From about 110 ka to the Middle Holocene, the continental shelf was partially exposed due to lower than present sea levels (Fig. 3.6). The common parent material of the last glacial-interglacial coastal sequence of Israel and the relatively continuous ages (Figs. 3.4, 3.5) suggest that the longshore transport of sand from the Nile Delta to the coastal zone was fairly continuous during most of the period studied. However, both the lowland and coastal cliff sequences highlight a possible depositional time gap in the Netanya palaeosol from about 33 to 12 ka (Figs. 3.5, 3.6). This disruption in sand accumulation (that later led to the formation of this soil unit) is supported by various studies from across the southern (Zilberman et al., 2007; Roskin et al., 2011a), central (Gvirtzman et al., 1998; Gvirtzman and Wieder, 2001; Sivan and Porat, 2004) and northern (Zviely et al., 2006; Elyashiv, 2013) Israeli coastal plain. In fact only a single age of 19 ± 2 ka has been obtained (Frechen et al., 2001) from a coastal ridge in central Israel. Global eustatic sea level curves (Spratt and Lisiecki, 2015), regional eustatic sea level proxy records (Anzidei et al., 2011; Rohling et al., 2014), local RSL data for the Holocene (Sivan et al., 2001) and erosive unconformity from subsurface profiles (Schattner et al., 2010, 2015) suggest that this gap is associated with the LGM lowstand (33 to 15 ka).

During the lowstand, sea level ranged from -85 to -130 mILSD, and the shoreline was situated below the shelf-break (Figs. 3.6i, 3.7e). The shelf-break curvature – exceeding 1º – (Almagor et al., 2000) and its ridged surface (Schattner et al., 2010, 2015) served as a further barrier to easterly aeolian transportation of sand (Posamentier et al., 1992; Mauz et al., 2013; Shtienberg et al., 2016). A depositional gap of aeolian sediments during lower sea level phases has previously been described for other Mediterranean coastal areas, and the Eastern Atlantic, for example: Egypt (El-Asmar, 1994; El-Asmar and Wood, 2000), Tunisia (Mauz et al., 2009; Elmejdoub et al., 2011) southern Spain (Zazo et al., 2008) and the Canary Islands (von Suchodoletz, et al., 2010), occurring from 70 ka in the Mediterranean and from 30 ka in the Canary Islands to the Mid-Holocene. The longer hiatuses in sedimentation documented in the northern coasts of Egypt (shelf-break curvature 0.15 º) and northern Tunisia (0.1 º) are presumed to be the result of the shallower coastal profile, compared to Israel’s shelf bathymetry (0.5 º) (Almagor et al., 2000; Sade et al., 2006; Amante et al., 2009).

At the end of the LGM (about 20 to 19 ka), sea level rose rapidly, reaching -85 m by 15 ka (Fig. 3.6h; Lambeck and Purell, 2005). As a result of the fast transgression (Waelbroeck et al., 2002; Rohling et al., 2014; Spratt and Lisiecki 2015), accommodation space outpaced sediment supply, hindering sand deposition on the coastal plain until 12 ka.

5.2.1.2. Regional processes affecting pedogenesis

The environments of deposition and post-depositional changes on Israel's palaeo-coastal plain have inevitably been affected by climate change. Such regional processes are identified in the sediments of both the lowland coastal plain and the coastal cliffs. These aeoliane quartz sediments underwent pedogenesis processes across most of Israel's palaeo-coastal plain leading to the soil formation of Netanya palaeosol (Fig. 3.5; Gvirtzman et al., 1983; Gvirtzman and Wieder, 2001; Neber, 2002; Tsatskin et al., 2008). The MS values (80–250 $\times 10^{-8}$ m^3 kg^{-1}), which are high compared to the other units found in the Quaternary sequence, and the red-dark brown hues are the result of continuous enrichment by aeolian dust and illuviation of the clay's associated magnetic iron-rich minerals (Fig. 3.3b), e.g. smectite (Dan et al., 1968). These petro-sedimentological characteristics are temporally associated with regional climate proxies that include lower $\delta^{18}O$ values and oak types (Fig. 3.6c to f; Bar-Matthews et al., 2003; Revel et al., 2010; Langgut et al., 2011), suggesting relatively wetter climatic conditions during pedogenesis (Yaalon; 1997; Tsatskin and Ronen, 1999; Gvirtzman and Wieder, 2001). These wetter climatic conditions, coeval with Sapropel S2, influenced fluctuations in the Saharan dust supply enhancing pedogenesis across the northwest African region (Bozzano et al., 2002) and even reaching the canary Islands (von Suchodoletz et al., 2010).

5.2.2. Evolution of the Coastal Plain of Israel during the Late Quaternary

During MIS5e, sea level was 1 to 7 m higher than at present (Fig. 3.6i; Galili et al., 2007; Hearty et al., 2007; Kopp et al., 2009, 2013; Rohling et al., 2014; Dutton et al., 2015; Spratt and Lisiecki, 2015; Sivan et al., 2016). Based on the current study reconstructed topography of the Late Pleistocene calcareous sandstone surface (Fig. 3.2), together with the elevations of the

Herzliyya *kurkar* surface along Israel's coastal plain (Gvirtzman et al., 1983), I propose that over this period, inland flooding occurred, creating an irregular coastline with estuaries, bays and headlands (Fig. 3.7a). Based on a simplified reconstruction combining sea level data from Spratt and Lisiecki (2015) and modern-day bathymetry of the Israeli continental shelf (Hall, 1994), the approximate distance from present shoreline is shown in figure 3.6h from 115 ka onward. This reconstruction accounts for the low Isostasy rates calculated by various GIA models previously made for the coast of Israel for key periods in the interglacial cycle. Sivan et al. (2016) model generated GIA corrections values ranging between + 5.4 to - 1.8 m for the MIS 5.5. For the Holocene, lower rates, of ≤ 0.2 mm/y, were computed by various modelled scenarios (depending on site and earth model) (Sivan et al., 2001; Lambeck and Purcell, 2005; Stocchi and Spada, 2009). Overall, the GIA vertical uncertainty is lower than ±5 m (resulting in vertical distance differences that are lower than 0.75 km) for variable glacio-hydro-isostatic response of the earth and ocean to the growth and decay of ice sheets and thus are relatively negligible for evaluating shoreline changes during the regression and early stages of the transgression.

From about 110 to 80 ka, sea level fluctuated by magnitudes of about ± 25 m, while the shoreline was located up to 5 km westward (Fig. 3.6h). Nilotic sand, which continued to be deposited on the palaeo-shores (present day offshore) of Israel, was windblown inland, dispersing on the palaeo-coastal plain. The aeolian sand covered the basal aeolianite as a thin (about 1 to 2 m thick) sand sheet (Fig. 3.7b), in some areas leaving the surface exposed for long periods. The sedimentological characteristics of the overlying Orange palaeosol, consisting of light orange sandy loam with hard calcareous cemented irregularly-shaped sand pebbles. The pebble size and abundance decrease from bottom to the top of the unit, were identified in the Hadera–Alexander lowland (Fig. 3.1c, d) and on the Carmel coast (Frechen et al., 2004; Tsatskin et al., 2009; Roskin et al., 2015). These characteristics suggest that the basal aeolianite surface partly weathered back to its parent material. The weathered aeolianite material and newly deposited Nilotic quartz sand underwent pedogenesis to form the Kfar Vitkin Palaeosol. In the Carmel coast this unit has a red–dark red colour, high MS values and higher silt and clay contents (Fig. 3.3; Frechen et al., 2004; Tsatskin et al., 2009; Mauz et al., 2013). The ages of the unit correlate to similar dark red silty clayey palaeosols that formed on the northern coasts of Egypt and Tunisia (El-Asmar and Wood, 2000; Elmejdoubet al., 2011) correlating with the wetter climate of Sapropel 3 (Fig. 3.6).

Between 80 and 55 ka, sand accumulated across the coastal plain, covering the Kfar Vitkin Palaeosol (Fig. 3.7c). Deposition was limited close to the stream outlets, eventually resulting in sand sheets only 2 m thick. Following stabilization at about 55 ka, the sand unit close to the streams slowly underwent pedogenesis forming the Red Palaeosol (Figs. 3.5, 3.6, 3.7c). The pedogenesis process was controlled by the interaction of dust accumulations and precipitation. The source of the dust that accumulated on the coastal plain of Israel was either solely or jointly supplied by the wide exposed shelf, Sahara deserts (Enzel et al., 2008), or the north of the Sinai-Negev dune field (Ben-David, 2003; Crouvi et al., 2012). The post-depositional pedogenic process took place during wetter periods, enabling hydrolytic weathering of silicate minerals and leaching of dispersed clay minerals in the soil profile. The process ended when sand deposition exceeded the pedogenic process, resulting in the burial of the soil, and leading to a new pedogenetic cycle (Yaalon, 1967, 1997; Tsatskin et al., 1999; Gvirtzman and Wieder, 2001; Mauz et al., 2013). Due to the low to moderate silty-clay content, the light hues contain relatively low concentrations of Fe, Al, and the MS values of the Red Palaeosol. This unit is interpreted as a moderately developed palaeosol (Fig. 3.3b). I propose that the formation of the Red Palaeosol is the outcome of the relatively dry conditions which prevailed between 80 and 55 ka, in light of the relatively constant aeolian dust supply during the formation of the three lowland palaeosol units from 80 to 25 ka (Fig. 3.6c to e; Cheddadi and Rossignol-Strick, 1995; Larrasoaña et al., 2008). In other locations, distant from the stream paths, dune-sand sheet complexes up to 40 m thick were deposited, eventually cementing to the lower exposed units of the present-day shore-parallel ridges (i.e. Givat Olga member; Figs. 3.5, 3.7c; Gvirtzman et al., 1998; Engelmann et al., 2001; Mauz et al., 2013).

The regressing sea level reached about -65 mILSD by 55 ka, and from about 55 to 35 ka it fluctuated by about ± 10 m (Fig. 3.6h; Waelbroeck et al., 2002; Rohling et al., 2014). During this time of RSL stability, windblown quartz sediments covered Israel's palaeo-coastal plain (Fig. 3.7d) by an average thickness of about 3.5 m (Fig. 3.5a). Based on a correlation conducted for this study across most of Israel's coastal plain and in two shallow shelf locations (depth shallower than -40 mILSD) located offshore in southern (Ashkelon; Porat et al., 2003) and central (Hadera; Shtienberg et al., 2016) coasts of Israel, it is evident that this sand sheet underwent pedogenesis to form theNetanya Palaeosol (Gvirtzman et al., 1983; Gvirtzman and Wieder, 2001; Neber, 2002; Tsatskin et al., 2008). The sedimentological and petrophysical characteristics of Netanya Palaeosol suggest a fully developed soil (Yaalon, 1997; Gvirtzman and Wieder, 2001) along most of the palaeo-coastal plain of Israel: covering the calcareous ridges as well as the lowland deposits. Regional climate proxies indicate that the pedogenesis of the Netanya palaeosol occurred during the transition from wet (55 to 45 ka) to dry (45 to 35 ka) climate (Fig. 3.6; Cita et al., 1977; Cheddadi and Rossignol-Strick, 1995; Revel et al., 2010). These changing climate periods were accompanied by a relatively constant dust accumulation (Enzel et al., 2008), interpreted from the MS values (Fig. 3.6) of the Ocean Drilling Program ODP 160-976 (see location in Fig. 3.1b; Larrasoañaet al., 2008).

A rapid drop in sea level occurred from about 35 ka to 20 ka, when sea level fell from about - 85 mILSD to a minimum of about - 135 mILSD (Rohling et al., 2014), resulting in shoreline migration from approximately 11 km to 14 km offshore (Fig. 3.6h). The regressing coastline was accompanied by increased windiness and dry and cold conditions, which continued until approximately 16 ka (Fig. 3.6; Bar-Matthews et al., 2000; McGee et al., 2010; Revel et al., 2010; Roskin et al., 2011a, 2011b). Much like the coastal areas of northern Tunisia (Elmejdoub et al., 2011) and the Huelva coast in south-western Spain (Zazo et al., 2005), the low sea level and climate conditions left the coast and exposed shelf sediment-starved, inducing an erosional hiatus.

At the end of the LGM, sea level rapidly rose, (Fig. 3.6h; Waelbroeck et al., 2002; Lambeck and Purell, 2005; Spratt and Lisiecki 2015), hindering sand deposition on the coastal plain unit until 12 ka. A dark-grey silty clay facies, identified adjacent to the streams in the Alexander and Hadera lowlands (Figs. 3.3, 3.7e), relates to the formation of wetlands at this time. These wetlands resemble, in their location and age, to others on the coast and the shallow shelf of southern (Porat et al., 2003), central (Neev et al., 1978; Kadosh et al., 2004; Sivan et al., 2011; Shtienberg et al., 2016), and northern (Avnaim-Katav et al., 2012; Elyashiv et al., 2016) Israel. As suggested by Sivan et al. (2011), Elyashiv et al. (2016) and Shtienberg et al. (2016), such units were deposited on the coastal plain as a result of stream flooding affected by rising sea level and a wetter climate, which changed from about 15 ka, as a result of the extreme insolation values (Fig. 3.6c, d; Bar-Matthews et al., 2000; Revel et al., 2010; Langgut et al., 2011).

During the Pleistocene-Holocene transition, sea level continued with its transgressing trend (Fig. 3.6h; Lambeck and Bard, 2000), and the palaeo-shoreline was located about 3 km offshore of its current position (Fig. 3.6h). Consequently, sediment transport recommenced from the Nile Delta by the longshore currents and was carried landward by the wind. The depositing sand underwent pedogenesis forming the upper sub-units of Netanya Palaeosol identified on the coastal ridges and lowlands from 12 to 8 ka (Fig. 3.5; Gvirtzman and Wieder, 2001; Porat et al., 2004; Roskin et al., 2016).

The earliest documented deposition of the upper, unconsolidated, sand identified on the brown Palaeosol, is approximately 8 ka (Fig. 3.5; Gvirtzman and Wieder, 2001; Mauz et al., 2013), and is proposed to be the result of two contributing factors: (a) erosion of the Nile Delta as a result of the rising sea levels, thus increasing the sediment discharge to the Levantine basin (Fig. 3.6h; Stanley and Warne, 1998; Revel et al., 2010); and (b) slower sea level rise. The high sediment discharge hypothesis is supported by higher sedimentation rates of 55 cm/ka and 110 cm/ka calculated from the deep-sea Cores 9505 and MS27PT (Fig. 3.1a; Revel et al., 2010; Langgut et al., 2011), respectively, and higher fluxes of up to 180 cm/ka in the shallow marine Cores V115, V101, located 1.5 km seaward from the current shoreline in a water depth of -30 m (Fig 3.1b; Mor-Federman, 2012). In addition, the shoreline reached about 1.5 km offshore from its present position (Fig. 3.6h).

Archaeological observations from the coast confirm that sea level continued to rise during the early stages of the Holocene until about 6 to 7 ka, when transgression slowed considerably. Then, at about 6 to 4 ka, as sea level and the coastline almost reached their present elevation and location (Fig. 5.1; Sivan et al., 2001, 2004b; Anzidei et al., 2011; Toker et al., 2012), the volumes of windblown sand which accumulated along the coast increased (Roskin et al., 2015 and ref. therein). The initiation and timing of the current wind-induced beach sand build-up is dated to about 5 ka in the shallow shelf by Porat et al. (2003), Reinhardt et al. (2006), Goodman-Tchernov et al. (2009), and on the coast mainly by Roskin et al. (2015). During this period, the shoreline reached about 1.5 km offshore from its present position (Fig. 3.6h).

A 1.5 m-thick bioclastic sand facies (Figs. 3.3, 3.4), found in the current study in the lowland area of the Alexander stream, was dated to between about 6.6 and 3.3 ka (Table 3.2). Based on its location, elevation range (+1.3 to +0.3 mILSD), the relatively high percentage of the bioclasts, and the covering aeolian sand unit, I suggest that in the stream outlets the sea penetrated inland and created estuaries (Appendix 3.2; Fig. 5.1). In these areas the coastline reached approximately 1 km inland at about 4 ka as suggested by Raban and Galili. (1985), and regressed to its current position by 3 ka. These late Holocene embayments resemble, on a smaller scale, those described in Haifa Bay and the Zevulun Plain (Fig. 3.1; Zviely et al., 2006; Porat et al., 2008; Elyashiv et al., 2016). From 6 to 4 ka, a sequence of bioclastic sand 1 to 3 m thick was deposited along most of Israel’s coastal cliff. This bioclastic sand eventually calcified to aeolianite (Tel Aviv *kurkar*) (Fig. 5.1; Gvirtzman et al., 1998; Frechen et al., 2002; Porat et al., 2004), although its formation has yet to be properly examined. As the sea level and coastline position stabilized, greater volumes of sand were windblown inland (Fig. 5.1). The aeolian sand overlaid the lowland areas around the estuaries, and created sand bars which enclosed the estuarine systems leading to their initial desiccation. Overall, the Holocene sand unit reached thickness of up to about 9 m (Fig. 4.3b; Roskin et al., 2015).

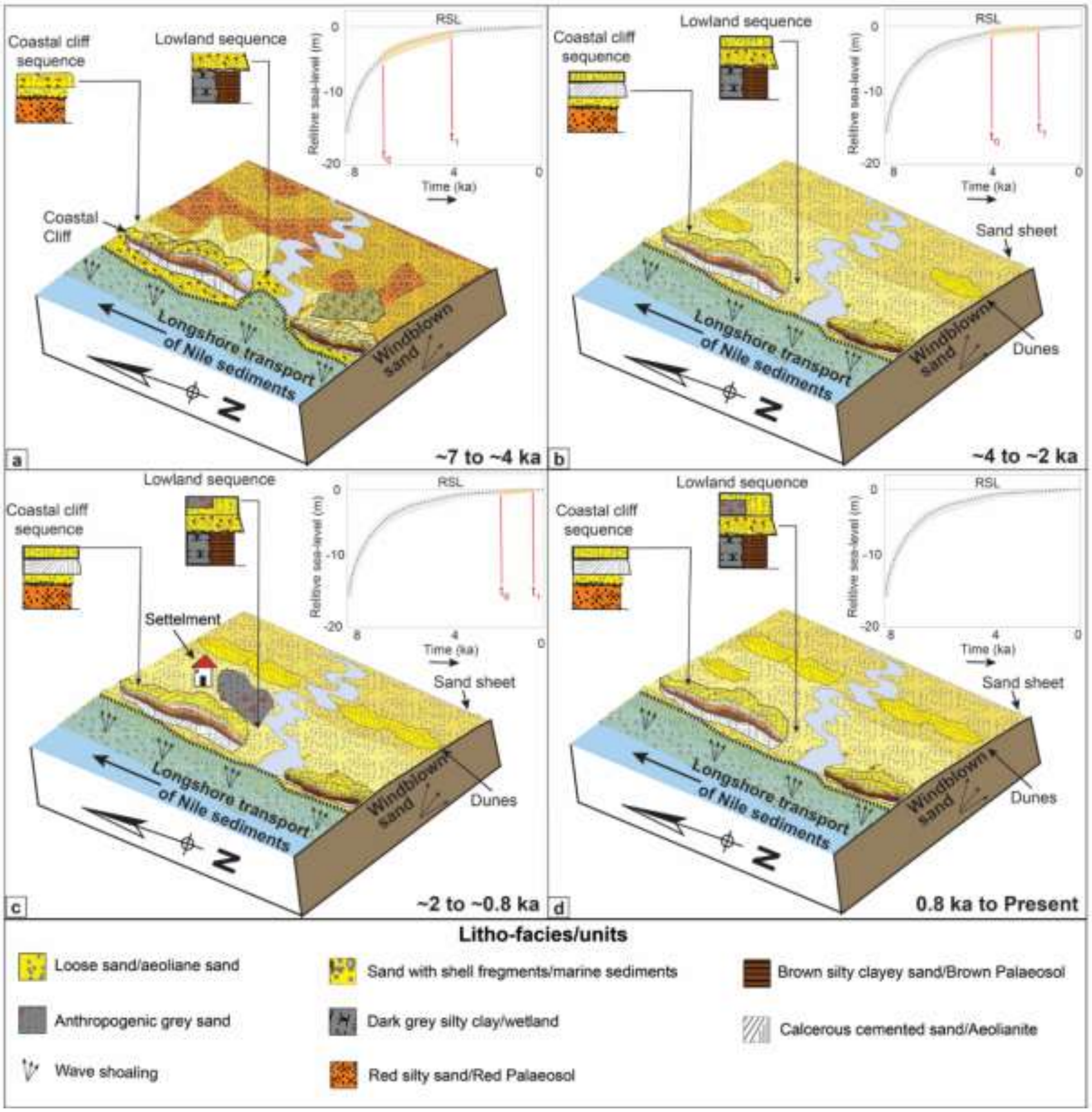

Figure 5.1: Schematic models (not to scale) of the mid-late Holocene evolution of Israel's coastal plain from Ashkelon to the Carmel coast. The evolution is portrayed through four periods: (a) about 7 to 4 ka; (b) about 4 to 2 ka; (c) about 2 to 0.8 ka; (d) and about 0.8 ka to present. Sea level curve (Sivan et al., 2001), annotated by orange polygon and evolving coastal lowland/cliff sequence is portrayed in their appropriate period.

5.2.3. Anthropogenic markers on the coastal Holocene sand

In the area of Caesarea – Hadera (Fig. 4.1c) historical human activities has also changed the coastal environment. These alterations are expressed by anthropogenic grey facies covering an area of 1.4 km^2 with an overall volume of about 4.8 km^3 (Fig. 4.3c), without evidence for widespread historical structures. This grey facies differs from the underlying aeolian facies and the overlying facies in their petro-sedimentological (Fig. 4.4), mineralogical and element compositions (Fig. 4.6) as well as their microscopic components (Fig. 4.5). Although they are sandy, the facies are grey-coloured and include macroscopic artefacts such a pottery and glass. In addition, they include the mineral carbonated hydroxylapatite that typically occurs in anthropogenic sediments from prehistoric (Shahack-Gross et al., 2004) and historic (Regev et al., 2015) sites. Ash, micro-charcoal (as well as high MS values) all support the occurrence of fire, whilst the presence of plant phytoliths and elements such as copper and lead are typical evidence of human habitation in the sedimentary record.

Based on the extent (Fig. 4.3c) and its sedimentological properties this facies is interpreted as being a pedo-sediment that is the outcome of an amended aeolian sand made suited for agricultural use (Ward and Summers, 1993; Blume and Leinweber, 2004). This postulation is supported by comparing the sedimentological properties of this unit with the underlying and overlaying units. The anthropogenic horizon consistently has: (i) higher organic content; (ii) higher P, S and Ca concentrations, (iii) existence of phytoliths, and (iv) calcitic-clay coatings surrounding the quartz sand grains. The higher organic content and the elevated elemental concentrations are interpreted as being the product of fertilization, with the fertilizer having been derived from domestic or urban trash, which could also, explains the presence of pottery, glass and rock fragments. The calcitic-clay coatings may indicate incipient pedogenesis (compare with the clay coatings around the quartz sand in the palaeosol; Fig. 4.5d, e). Moreover, fertilization added silt (Fig. 4.4; Table 4.3) to the original sand that enhanced the water adhesion properties of the sediment, which is also beneficial for agriculture. Reuse of organic rich material in the past, for agricultural fertilization, has been documented in other regions throughout the Mediterranean and the Middle East, including Crete, Greece, Egypt and Iraq and date as far back as the third millennium (Wilkinson, 1989; Bull et al., 2001).

The chronological constraint of these activities is based on new dates together with previously published ages that enable the dating of the various sand facies. The lower aeolian sand facies that covers most of the research area was radiometrically dated by Roskin et al. (2015) and Frechen et al. (2002). Based on these ages and previous studies conducted in the central-north coast of Israel (Kadosh et al., 2004; Porat et al., 2004; Cohen-Seffer et al., 2005; Mauz et al., 2013; Shtienberg et al., 2017) the initial timing of the aeolian sand incursion and stabilisation is estimated to be between 6 ka and 4.8 ka (Fig. 4.7), i.e. the Chalcolithic period to Bronze Age. The grey coloured, artefact-containing, anthropogenic sand facies (Table 4.4; Figs. 4.1c, 4.3c) is chronologically constrained between 3.3 ka and 0.85 ka (Fig. 4.7; Roskin et al., 2015), i.e., Iron Age to Crusader. Because OSL dates the last time a sediment was exposed to sunlight (Murray and Wintle, 2000; Roskin et al., 2011a, 2015) the current study better constrained the formation of the anthropogenic facies and coastal cultivation period through indirect dating using archaeological remains and historical records. Dating of the pottery remains and Fatimid quarter dirham coin excavated in the field area along with the archaeobotanic finds from Caesarea all point to the fields being operated throughout early Islamic times. This inference is supported by historical descriptions from Early Islamic period writers that praise the agricultural produce of the city (Avni, 2014; Ramsay and Holum, 2015). Other sources point out that even after the Crusader conquest of Caesarea, during the 12^{th} century, and until the battle of Hittin (1101 to 1087 CE), Caesarea was still involved in the agricultural production of wheat, olives, citrus and figs (Prawer, 1972; Ramsay and Holum, 2015). The archaeological finds and historical records together with the radiometric ages of the current study show that the agricultural system was large, and dates to the Islamic period.

The anthropogenic sand facies (Figs. 4.7, 5.1c, d) are covered by yellow aeolian sand which was deposited after 0.85 ka, i.e., the Crusader period. During the Crusader period the city of Caesarea was under constant attacks resulting in declining human presence in the area of Caesarea - Hadera (Porath, 2000). The decrease in human activity caused reestablishment of vegetation growth and sand stabilization. Based on existing ages from the adjacent coastal plain and neighbouring coastal escarpment (Fig. 4.1b; Frechen et al., 2001; Salmon, 2013; Roskin et al., 2015) it is hypothesised that the upper sand was deposited and stabilized from 0.6 ka until present (Fig. 5.1d).

5.2.4. Implications and conclusions of the study

This is the first combined high resolution geophysical and geological study to be conducted along the open coast of Israel (at less than 30 m water depth), merging marine and terrestrial data that covers a period of more than 110 ka. The terrestrial data used in the current study examines for the first time the Late Pleistocene history of the coastal lowlands of Israel through a combination of high-resolution petro-sedimentological methods, OSL ages and correlation to adjacent dated marine and coastal units. The combination of continuous marine seismic data with core data drilled on land has enabled the 4-D reconstruction of the palaeogeography and landscape evolution processes of an area that was exposed to changing environmental conditions over a period of 115 ka. Along the northern parts of the study area, in the southern hinterland of Caesarea, the impact of an urban settlement on its periphery was explored. The anthropogenic impact has been assessed by integrating the petro-sedimentological analyses and radiometric dating with historical records and archaeological finds. Such a comprehensive multi-disciplinary approach to the study of cored sediments outside ancient human settlements is the first to have been conducted in the coastal area of the southern Levant.

The coastal reconstruction, combined with earlier interpretations of the coastal cliff sequences, reveal that over the last glacial-interglacial cycle the stratigraphy of the coastal plain of Israel was dominated mainly by aeolian, and to a lesser extent, fluvial, processes. Only later, during the Holocene, was the landscape directly affected by a marine transgression. The units overlying the Pleistocene aeolianite were deposited in four environments:

1. The oldest palaeosol units were formed in a terrestrial environment over the course of thousands of years;
2. The early Holocene's wetland-silty clay units were deposited in a calm, fresh to brackish, water environment, with increasing siltation in response to rising sea levels;
3. The Nilotic sand unit started to accumulate at about 8 ka on the shallow shelf and coastal plain. In the lowland areas from about 6 ka to about 4 ka a poorly-sorted coarse to fine quartz sand consisting of bivalve fragments and allochthonous benthic microfauna was deposited in a high wave energy beach environment;
4. As the sea level stabilized, greater volumes of sand were windblown inland, depositing in an aeolian environment resulting in the progradation of the coastline.

The conclusions drawn from this holistic study are:

a. The chronological association between the lowland and coastal cliff sequences reveals dissimilarities in lithologies over time. The author proposes that these differences, which often occur over distances smaller than 1 km, are the result of local factors, such as the ancient topography and locations of stream courses, which subsequently affected the depositional/erosional rate and soil-forming processes. As a result, two aeolianite units that exist in the coastal cliff are missing in the lowland sequence, and are replaced by thicker and more developed palaeosol units.

b. The fluvial system location did not change considerably from about 80 to 5 ka. However, the streams had a profound influence on the stratigraphical composition of the sedimentary facies, due to fluvial-induced erosion that shaped the evolving topography and consequently, relief variations between the lowland and cliff-controlled aeolian, pedogenesis and alluvial processes.

c. Correlation between sea-level fluctuations over the last glacial-interglacial cycle, during periods of RSL lower than -20 mILSD, and the coastal sedimentological sequence shows no distinct influence of sea level on the deposition and formation of the coastal sequence – apart from two periods: during the LGM lowstand (33 to 15 ka), and from 15 to 12 ka. The author suggests that a gap in deposition of about 20 ka was caused by the low RSL from 33 to 15 ka, which prevented sediments from reaching the palaeo-coastal plain, while from 15 to 12 ka the rapid transgression outpaced sedimentation supply to the coast.

d. A set of indicators was characterised, allowing for differentiating between natural and anthropogenic sedimentary units. Moreover, these indicators, which include macro-features (e.g., sherds and glass fragments), micro-features (e.g., phytoliths, wood ash, micro-charcoal) and elemental concentrations of P, Fe, Ca, Ti, Cu and Pb, can be used for differentiating between anthropogenic facies of various types, enabling a better understanding of human-environment relationships.

e. The identification of agricultural fields confirms the hypothesis that a large city such as Caesarea was supported by an agricultural hinterland. The dating of the agricultural pedo-sediment burial to the Crusader period fits with historical evidence for the decline and abandonment of this originally Roman urban centre.

The initiation of this holistic study called for a collaboration with specialists who supported the research led by the author. Consequently, the author gathered a group of researchers from complementary fields, comprising of geophysics, geology, sedimentology, geomorphology, archaeology and history, who contributed from their experience to strengthen the general perceptions. These disciplines were then used by the author to enhance the interpretation of the data and thus strengthen the hypothesis developed for the spatial and temporal evolution of this coastal zone (i.e. the inner shelf, the shore and the coastal plain). It seems that this interdisciplinary approach also contributed benefits to the cooperating researchers who were exposed to different disciplines and collaborations.

The understanding gained from this integrated study could serve as an example for other similar coastal areas across the southern parts of the Mediterranean basin that consist of lowland-ridge morphologies with relatively flat to moderately steep shelf and coast, comprising aeolianites, palaeosol units and alluvial facies, supplied with siliciclastic sediments and desert dust from the Sahara. This reconstruction can also be of use for archaeological and engineering purposes. Archaeologists can use 4-D litho-stratigraphical mapping for targeting ancient sites of habitation which changed according to the (now submerged) surface lithology, distance from palaeo-water sources and rising sea levels. A connection between wetland sequences and ancient settlement having already been established in Israel's central coastal area, suggests that there is a high archaeological potential offshore. Finally, engineers can make use of such high-resolution subsurface data for future infrastructure planning intended to be built/buried in or on the shelf's shallow subsurface. These include marinas and harbours, gas pipes, electricity cables and communication networks.

5.2.5. Research drawbacks and open questions for future research

The combined methodologies and the holistic approach used in this study have enabled the author to seamlessly integrate shallow-marine and terrestrial records and fulfil the main objective of the study. However, because relatively few studies have been conducted in these areas and due to funding limitations the drawbacks of the current work are:

(1) There is an absence of relevant core datasets drilled offshore needed to strengthen the seismic interpretation and also enable the building of a direct chronology. Moreover, the combination of sedimentological data from boreholes drilled offshore near seismics sections could have enabled an improved correlation between the seismic stratigraphy constructed offshore and the known terrestrial units.

(2) Due to the technical characteristics of the geophysical method, used in the current study, the seismic survey did not acquire subsurface data in depths shallower than -4 mILSD. These gaps make it difficult to establish a correlation between the shoreline and the shallow offshore stratigraphies.

(3) Due to the relatively limited number of OSL ages measured in the study, and OSL dating uncertainties a correlation between the coastal zone morphogenesis and chronostratigraphy to global (sea level) and regional processes (climate) was somewhat limited.

(4) The terrestrial stratigraphic record of the lowlands acquired in the current study only provides point information from seven locations. Although the sediment retrieved from the cores was analysed by robust methods, an integration of the borehole data with continuous methodologies (i.e. GPR, EM) could have better presented the subsurface morphology and its spatial changes.

The current research has also raised additional research questions yet to be studied:

1. What was the source of the dust responsible for the formation of the palaeosol units? Did the contributing sources (i.e., Sahara desert, exposed shelf, North-Sinai dune field) change during the formation periods of the palaeosols (100 to 8 ka)?
2. What were the environmental characteristics (climate, sediments deposited in the coastal area) that led to the formation of the Holocene aeolianite unit (i.e., Tel Aviv *kurkar*)?
3. Was the fertilizing of sandy sediments pioneered in Caesarea, or was it a part of a wider (possibly even earlier) phenomenon?

These questions are proposed to be the focus of future work to be conducted along the coastal area of Israel.

5.3. References

Almagor, G., Gill, D., Perath, I., 2000. Marine Sand Resources Offshore Israel. Marine Georesources & Geotechnology 18, 1-42.

Amante, C., Eakins, B.W., 2009. ETOPO1 1 arc-minute global relief model: procedures, data sources and analysis. US Department of Commerce, National Oceanic and Atmospheric Administration, National Environmental Satellite, Data, and Information Service, National Geophysical Data Center, Marine Geology and Geophysics Division Colorado.

Anderson, J.B., Abdulah, K., Sarzalejo, S., Siringan, F., Thomas, M., 1996. Late Quaternary sedimentation and high-resolution sequence stratigraphy of the east Texas shelf. Geological Society, London, Special Publications 117, 95-124.

Anzidei, M., Antonioli, F., Benini, A., Lambeck, K., Sivan, D., Serpelloni, E., Stocchi, P., 2011. Sea level change and vertical land movements since the last two millennia along the coasts of southwestern Turkey and Israel. Quaternary International 232, 13-20.

Avnaim-Katav, S., Almogi-Labin, A., Sandler, A., Sivan, D., Porat, N., Matmon, A., 2012. The chronostratigraphy of a quaternary sequence at the distal part of the nile littoral cell, Haifa Bay, Israel. Journal of Quaternary Science 27, 675-686.

Avni, G., 2014. The Byzantine-Islamic transition in Palestine: an archaeological approach. Oxford University Press.

Bar-Matthews, M., Ayalon, A., Gilmour, M., Matthews, A., Hawkesworth, C.J., 2003. Sea–land oxygen isotopic relationships from planktonic foraminifera and speleothems in the Eastern Mediterranean region and their implication for paleorainfall during interglacial intervals. Geochimica et Cosmochimica Acta 67, 3181-3199.

Bar-Matthews, M., Ayalon, A., Kaufman, A., 2000. Timing and hydrological conditions of Sapropel events in the Eastern Mediterranean, as evident from speleothems, Soreq cave, Israel. Chemical Geology 169, 145-156.

Ben-David, R., 2003. Changes in desert margin environments during the climate changes of the Upper Quaternary. Unpublished Ph. D. thesis, Hebrew University of Jerusalem.

Blum, M.D., Tōrnqvist, T.E., 2000. Fluvial responses to climate and sea-level change: a review and look forward. Sedimentology 47, 2-48.

Blume, H.-P., Leinweber, P., 2004. Plaggen Soils: landscape history, properties, and classification. Journal of Plant Nutrition and Soil Science 167, 319-327.

Bozzano, G., Kuhlmann, H., Alonso, B., 2002. Storminess control over African dust imput to the Moroccan Atlantic margin (NW Africa) at the time of maxima boreal summer insolation- a record of the last 220 kyr. Palaeogeography, Palaeoclimatology, Palaeoecology 183, 155-168.

Bull, I., Phillip PB, Richard PE, 2001. An Organic Geochemical Investigation of te Practice of Manuring at a Minoan Site on Pseira Island, Crete. Geoarchaeology 16, 223-242.

Cheddadi, R., Rossignol-Strick, M., 1995. Improved preservation of organic matter and pollen in eastern Mediterranean sapropels. Paleoceanography 10, 301-309.

Cita, M.B., Vergnaud-Grazzini, C., Robert, C., Chamley, H., Ciaranfi, N., d'Onofrio, S., 1977. Paleoclimatic record of a long deep sea core from the eastern Mediterranean. Quaternary Research 8, 205-235.

Cohen-Seffer, R., Greenbaum, N., Sivan, D., Jull, T., Barmeir, E., Croitoru, S., Inbar, M., 2005. Late Pleistocene–Holocene marsh episodes along the Carmel coast, Israel. Quaternary International 140-141, 103-120.

Crouvi, O., Schepanski, K., Amit, R., Gillespie, A.R., Enzel, Y., 2012. Multiple dust sources in the Sahara Desert: The importance of sand dunes. Geophysical Research Letters 39, L13401.

Dan, J., Yaalon, D.H., Koyumdjisky, H., 1968. CATENARY SOIL RELATIONSHIPS IN ISRAEL, 1. THE NETANYA CATE NATANYA CATENA. Geoderma 2, 95-120.

Dutton, A., Carlson, A.E., Long, A.J., Milne, G.A., Clark, P.U., DeConto, R., Horton, B.P., Rahmstorf, S., Raymo, M.E., 2015. Sea-level rise due to polar ice-sheet mass loss during past warm periods. Science 349, aaa4019.

El-Asmar, H.M., 1994. Aeolianite sedimentation along the northwestern coast of Egypt: evidence for middle to late quaternary aridity. Quaternary Science Reviews 13, 699-708.

El-Asmar, H.M., Wood, P., 2000. Quaternary shoreline development- the northwestern coast of Egypt. Quaternary Science Reviews 19, 1137-1149.

Elmejdoub, N., Mauz, B., Jedoui, Y., 2011. Sea-level and climatic controls on late Pleistocene coastal aeolianites in the Cap Bon peninsula, northeastern Tunisia. Boreas 40, 198-207.

Elyashiv, H., 2013. The Late Pleistocene-Holocene sedimentary evolution of Zevulun Plain : focusing on the wetlands MA Thesis Faculty of Natural Sciences, Leon H. Charney School of Marine Sciences, The Dr. Moses Sreauss Dept. of Marine Geosciences, University of Haifa, Israel.

Elyashiv, H., Bookman, R., Zviely, D., Avnaim-Katav, S., Sandler, A., Sivan, D., 2016. The interplay between relative sea-level rise and sediment supply at the distal part of the Nile littoral cell. The Holocene 26, 248-264.

Engelmann, A., Neber, A., Frechen, M., Boenigk, W., Ronen, A., 2001. Luminescence chronology of Upper Pleistocene and Holocene aeolianites from Netanya South - Sharon Coastal Plain, Israel. Quaternary Science Reviews 20, 799-804.

Enzel, Y., Amit, R., Dayan, U., Crouvi, O., Kahana, R., Ziv, B., Sharon, D., 2008. The climatic and physiographic controls of the eastern Mediterranean over the late Pleistocene climates in the southern Levant and its neighboring deserts. Global and Planetary Change 60, 165-192.

Frechen, M., Dermann, B., Beonigk, W., Ronen, A., 2001. luminesence chronology of the aeolianites from the section at givat olga-coastal plain of israel. Quaternary Science Reviews 20, 805-809.

Frechen, M., Neber, A., Dermann, B., Alexander, T., Boenigk, W., Raban, A., 2002. Chronostratigraphy of aeolianites fromthe Sharon Coastal Plain of Israel. Quaternary International, 31-44.

Frechen, M., Neber, A., Tsatskin, A., Boenigk, W., Ronen, A., 2004. Chronology of Pleistocene sedimentary cycles in the Carmel Coastal Plain of Israel. Quaternary International 121, 41-52.

Galili, E., Zviely, D., Ronen, A., Mienis, H.K., 2007. Beach deposits of MIS 5e high sea stand as indicators for tectonic stability of the Carmel coastal plain, Israel. Quaternary Science Reviews 26, 2544-2557.

Goodman-Tchernov, B.N., Dey, H.W., Reinhardt, E.G., McCoy, F., Mart, Y., 2009. Tsunami waves generated by the Santorini eruption reached Eastern Mediterranean shores. Geology 37, 943-946.

Gvirtzman, G., Netser, M., Katsav, E., 1998. Last-Glacial to Holocene kurkar ridges, hamra soils, and dune fields in the coastal belt of central Israel. Israel Journal of Earth Sciences 47, 27-46.

Gvirtzman, G., Shachnai, E., Bakler, N., Ilani, S., 1983. Stratigraphy of the Kukar group (Quaternary) of the coastal palin of Israel. Geological Survey of Israel, Current Research, 70-82.

Gvirtzman, G., Wieder, M., 2001. Climate of the last 53,000 years in the eastern med based on soil-sequence Stratigraphy in coastla plain Israel. Quaternary Science Reviews 20, 1827-1849.

Hall, J.K., 1994. Bathymetric chart of the eastern Mediterranean Sea. Geologic Structure of the Northen Mediterranean (Cruise 5 of the Akademic Nikolaj Strakhov).

Hearty, P.J., Hollin, J.T., Neumann, A.C., O'Leary, M.J., McCulloch, M., 2007. Global sea-level fluctuations during the Last Interglaciation (MIS 5e). Quaternary Science Reviews 26, 2090-2112.

Kadosh, D., Sivan, D., Kutiel, H., Weinstein-Evron, M., 2004. A late quaternary paleoenvironmental sequence from Dor, Carmel coastal plain, Israel. Palynology 28, 143-157.

Kopp, R.E., Simons, F.J., Mitrovica, J.X., Maloof, A.C., Oppenheimer, M., 2009. Probabilistic assessment of sea level during the last interglacial stage. Nature 462, 863-867.

Kopp, R.E., Simons, F.J., Mitrovica, J.X., Maloof, A.C., Oppenheimer, M., 2013. A probabilistic assessment of sea level variations within the last interglacial stage. Geophysical Journal International 193, 711-716.

Lambeck, K., Bard, E., 2000. Sea-level change along the French Mediterranean coast for the past 30,000 years. Earth and Planetary Science Letters 175, 203-222.

Lambeck, K., Purcell, A., 2005. Sea-level change in the Mediterranean Sea since the LGM: model predictions for tectonically stable areas. Quaternary Science Reviews 24, 1969-1988.

Langgut, D., Almogi-Labin, A., Bar-Matthews, M., Weinstein-Evron, M., 2011. Vegetation and climate changes in the South Eastern Mediterranean during the Last Glacial-Interglacial cycle (86 ka): new marine pollen record. Quaternary Science Reviews 30, 3960-3972.

Larrasoaña, J.C., Roberts, A.P., Rohling, E.J., 2008. Magnetic susceptibility of eastern Mediterranean marine sediments as a proxy for Saharan dust supply? Marine Geology 254, 224-229.

Mauz, B., Elmejdoub, N., Nathan, R., Jedoui, Y., 2009. Last interglacial coastal environments in the Mediterranean–Saharan transition zone. Palaeogeography, Palaeoclimatology, Palaeoecology 279, 137-146.

Mauz, B., Hijma, M.P., Amorosi, A., Porat, N., Galili, E., Bloemendal, J., 2013. Aeolian beach ridges and their significance for climate and sea level: Concept and insight from the Levant coast (East Mediterranean). Earth-Science Reviews 121, 31-54.

McGee, D., Broecker, W.S., Winckler, G., 2010. Gustiness: The driver of glacial dustiness? Quaternary Science Reviews 29, 2340-2350.

Mor-Federman, T., 2012. Chemical Characterization and Provenance Study of the Israeli Inner Shelf's Holocene Sediments. MS.c thesis Marine Geo-Sciences. The University of Haifa (in Hebrew, English abstract), Haifa.

Moshier, S., Master, D., Leport, J., Wheatley, D., Felker, B., Lavigne, E., College, W., 2010. Reconstruction of the Ancient Landscapes and Paleoenvitonments of the geological foundations of the ancient seaport Ashkelon, Israel, GSA Annual Meeting & Exposition, Minneapolls, Minnesota USA.

Murray, A.S., Wintle, A.G., 2000. Luminescence dating of quartz using an improved single-aliquot regenative-dose protocol. Radiation Measurments 32, 57-73.

Neber, A., 2002. Sedimentological properies of Quternary deposits on the Central coastline of Israel. Unpublished Ph.D. Dissertation, Department of Archaeology,University of Haifa, Israel.

Neev, D., Schanai, E., Hall, J.K., Bakler, N., Ben-Avraham, Z., 1978. The Young (Post Loewr Pliocene) Geological History of the Caesarea. Israel Journal of Earth Sciences 28, 43-46.

Porat, N., Avital, A., Frechen, M., Almogi-Labin, A., 2003. Chronology of upper Quaternary offshore successions from the southeastern Mediterranean Sea, Israel. Quaternary Science Reviews 22, 1191-1199.

Porat, N., Sivan, D., Zviely, D., 2008. Late Holocene embayment infill and shoreline migration, Haifa Bay, Eastern Mediterranean. Israel Journal of Earth Sciences 57, 21-31.

Porat, N., Wintle, A.G., Ritte, M., 2004. Mode and timing of kurkar and hamra formation, central coastal plain, Israel. Israel Journal of Earth Sciences 53, 13-25.

Porath, Y., 2000. Caesarea–1994–1999. Hadashot Arkheologiyot: Excavations and Surveys in Israel (in Hebrew), 34-40.

Posamentier, H.W., Allen, G.P., James, D.P., Tesson, M., 1992. Forced regressions in a sequence stratigraphic framework: concepts, examples, and exploration significance (1). AAPG Bulletin 76, 1687-1709.

Prawer, J., 1972. The Latin Kingdom of Jerusalem: European Colonialism in the Middle Ages Weidenfeld, London.

Ramsay, J., Holum, K., 2015. An archaeobotanical analysis of the Islamic period occupation at Caesarea Maritima, Israel. Vegetation History and Archaeobotany 24, 655-671.

Regev, L., Cabanes, D., Homsher, R., Kleiman, A., Weiner, S., Finkelstein, I., Shahack-Gross, R., 2015. Geoarchaeological Investigation in a Domestic Iron Age Quarter, Tel Megiddo, Israel. Bulletin of the American Schools for Oriental Research (BASOR) 374, 135-157.

Reinhardt, E.G., Goodman, B.N., Boyce, J.I., Lopez, G., van Hengstum, P., Rink, W.J., Mart, Y., Raban, A., 2006. The tsunami of 13 December A.D. 115 and the destruction of Herod the Great's harbor at Caesarea Maritima, Israel. Geology 34, 1061.

Revel, M., Ducassou, E., Grousset, F.E., Bernasconi, S.M., Migeon, S., Revillon, S., Mascle, J., Murat, A., Zaragosi, S., Bosch, D., 2010. 100,000 Years of African monsoon variability recorded in sediments of the Nile margin. Quaternary Science Reviews 29, 1342-1362.

Rohling, E.J., Foster, G.L., Grant, K.M., Marino, G., Roberts, A.P., Tamisiea, M.E., Williams, F., 2014. Sea-level and deep-sea-temperature variability over the past 5.3 million years. Nature 508, 477-482.

Roskin, J., Katra, I., Blumberg, D.G., 2013. Particle-size fractionation of eolian sand along the Sinai-Negev erg of Egypt and Israel. Geological Society of America Bulletin 126, 47-65.

Roskin, J., Porat, N., Tsoar, H., Blumberg, D.G., Zander, A.M., 2011a. Age, origin and climatic controls on vegetated linear dunes in the northwestern Negev Desert (Israel). Quaternary Science Reviews 30, 1649-1674.

Roskin, J., Sivan, D., Bookman, R., Porat, N., Shtienberg, G., 2016. Beach buildup and coastal aeolian sand incursions off the Nile cell during the Holocene Poster presented in the annual IGRG Congress; the University of Haifa, 33.

Roskin, J., Sivan, D., Shtienberg, G., Roskin, E., Porat, N., Bookman, R., 2015. Natural and human controls of the Holocene evolution of the beach, aeolian sand and dunes of Caesarea (Israel). Aeolian Research 19, 65-85.

Roskin, J., Tsoar, H., Porat, N., Blumberg, D.G., 2011b. Palaeoclimate interpretations of Late Pleistocene vegetated linear dune mobilization episodes: evidence from the northwestern Negev dunefield, Israel. Quaternary Science Reviews 30, 3364-3380.

Sade, A.R., Hall, J.K., Amit, G., Golan, A., Gur-Arieh, L., Tibor, G., 2006. The Israel national bathymetric survey—A new look at the seafloor off Israel. Israel Journal of Earth Sciences 55, 185-187.

Salmon, Y., 2013. A Second Millennium Geo-archaeological and Palaeo-environmental Study of the Nami Region: An Integrated Approach to a Coastal and Maritime Study, The Department of Maritime Civilizations. The University of Haifa, The University of Haifa.

Schattner, U., Gurevich, M., Kanari, M., Lazar, M., 2015. Levant jet system—effect of post LGM seafloor currents on Nile sediment transport in the eastern Mediterranean. Sedimentary Geology 329, 28-39.

Schattner, U., Lazar, M., Tibor, G., Ben-Avraham, Z., Makovsky, Y., 2010. Filling up the shelf — A sedimentary response to the last post-glacial sea rise. Marine Geology 278, 165-176.

Shahack-Gross, R., Berna, F., Karkanas, P., Weiner, S., 2004. Bat guano and preservation of archaeological remains in cave sites. Journal of Archaeological Science 31, 1259-1272.

Shtienberg, G., Dix, J.K., Roskin, J., Waldmann, N., Bookman, R., Bialik, O.M., Porat, N., Taha, N., Sivan, D., 2017. New perspectives on coastal landscape reconstruction during the Late Quaternary: A test case from central Israel. Palaeogeography, Palaeoclimatology, Palaeoecology 468, 503-519.

Shtienberg, G., Dix, J., Waldmann, N., Makovsky, Y., Golan, A., Sivan, D., 2016. Late-Pleistocene evolution of the continental shelf of central Israel, a case study from Hadera. Geomorphology 261, 200-211.

Sivan, D., Greenbaum, N., Cohen-Seffer, R., Sisma-Ventura, G., Almogi-Labin, A., 2011. The origin and disappearance of the late Pleistocene–early Holocene short-lived coastal wetlands along the Carmel coast, Israel. Quaternary Research 76, 83-92.

Sivan, D., Lambeck, K., Toueg, R., Raban, A., Porath, Y., Shirman, B., 2004b. Ancient coastal wells of Caesarea Maritima, Israel, an indicator for relative sea level changes during the last 2000 years. Earth and Planetary Science Letters 222, 315-330.

Sivan, D., Porat, N., 2004. Evidence from luminescence for Late Pleistocene formation of calcareous aeolianite (kurkar) and paleosol (hamra) in the Carmel Coast, Israel. Palaeogeography, Palaeoclimatology, Palaeoecology 211, 95-106.

Sivan, D., Sisma-Ventura, G., Greenbaum, N., Bialik, O.M., Williams, F.H., Tamisiea, M.E., Rohling, E.J., Frumkin, A., Avnaim-Katav, S., Shtienberg, G., Stein, M., 2016. Eastern Mediterranean sea levels through the last interglacial from a coastal-marine sequence in northern Israel. Quaternary Science Reviews 145, 204-225.

Sivan, D., widowinski, S., Lambeck, K., Galili, E., Raban, A., 2001. Holocene sea level changes based on archeological sites off northen israel Palaeogeography, Palaeoclimatology, Palaeoecology 167, 101-117.

Spratt, R.M., Lisiecki, L.E., 2015. A Late Pleistocene sea level stack. Climate of the Past Discussions 11, 3699-3728.

Stanley, D.J., Warne, A.G., 1998. Nile Delta in its destruction phase. Journal of Coastal Research 14, 794-825.

Stocchi, P., Spada, G., 2009. Influence of glacial isostatic adjustment upon current sea level variations in the Mediterranean. Tectonophysics 474, 56-68.

Suter, J.R., Berryhill Jr, H.L., 1985. Late Quaternary shelf-margin deltas, northwest Gulf of Mexico. AAPG Bulletin 69, 77-91.

Toker, E., Sivan, D., Stern, E., Shirman, B., Tsimplis, M., Spada, G., 2012. Evidence for centennial scale sea level variability during the Medieval Climate Optimum (Crusader Period) in Israel, eastern Mediterranean. Earth and Planetary Science Letters 315-316, 51-61.

Tsatskin, A., Gendler, T.S., Heller, F., Dekman, I., Frey, G.L., 2009. Towards understanding paleosols in Southern Levantine eolianites: Integration of micromorphology, environmental magnetism and mineralogy. Journal of Mountain Science 6, 113-124.

Tsatskin, A., Gendler, T.S., Heller, F., Ronen, A., 2008. Near-surface paleosols in coastal sands at the outlet of Hadera stream (Israel) in the light of archeology and luminescence chronology. Journal of Plant Nutrition and Soil Science 171, 524-532.

Tsatskin, A., Ronen, A., 1999. Micromorphology of a Mousterian paleosol in aeolianites at the site Habonim, Israel. Catena 34, 365-384.

Tsatskin, A., Sandler, A., Avnaim-Katav, S., 2015. Quaternary subsurface paleosols in Haifa Bay, Israel: A new perspective on stratigraphic correlations in coastal settings. Palaeogeography, Palaeoclimatology, Palaeoecology 426, 285-296.

von Suchodoletz, H., Oberhänsli, H., Hambach, U., Zöller, L., Fuchs, M., Faust, D., 2010. Soil moisture fluctuations recorded in Saharan dust deposits on Lanzarote (Canary Islands) over the last 180ka. Quaternary Science Reviews 29, 2173-2184.

Waelbroeck, C., Labeyrie, L., Michel, E., Duplessy, J.C., McManus, J., Lambeck, K., Balbon, E., Labracherie, M., 2002. Sea-level and deep water temperature changes derived from benthic foraminifera isotopic records. Quaternary Science Reviews 21, 295-305.

Ward, S.C., Summers, R.N., 1993. Modifying sandy soils with the fine residue from bauxite refining to retain phosphorus and increase plant yield. Fertilizer Research, 151-156.

Wilkinson, T.J., 1989. Extensive Sherd Scatters and Land Use Intensity: Some Recent Results. Journal of Field Archaeology 16, 31-46.

Yaalon, D.H., 1967. Factors affecting the lithification of eolianite and interpretation of its environmental significance in the coastal plain of Israel. Journal of Sedimentary Research 37, 1189-1199.

Yaalon, D.H., 1997. Soils in the Mediterranean region- what makes them diffrent? Catena 28, 157-169.

Zazo, C., Mercier, N., Lario, J., Roquero, E., Goy, J.-L., Silva, P.G., Cabero, A., Borja, F., Dabrio, C.J., Bardají, T., Soler, V., García-Blázquez, A., Luque, L.d., 2008. Palaeoenvironmental evolution of the Barbate–Trafalgar coast (Cadiz) during the last ~140 ka: Climate, sea-level interactions and tectonics. Geomorphology 100, 212-222.

Zazo, C., Mercier, N., Silva, P.G., Dabrio, C.J., Goy, J.L., Roquero, E., Soler, V., Borja, F., Lario, J., Polo, D., de Luque, L., 2005. Landscape evolution and geodynamic controls in the Gulf of Cadiz (Huelva coast, SW Spain) during the Late Quaternary. Geomorphology 68, 269-290.

Zilberman, E., Porat, N., Roskin, J., 2007. The middle to Late-Pleistocene sand sheet sequence of Kerem Shalom, western Negev – an archive of coastal sand incursion. Geological Survey of Israel GSI/13/2007, 23p.

Zviely, D., Sivan, D., Ecker, A., Bakler, N., Rohrlich, V., Galili, E., Boarreto, E., Klein, M., Kit, E., 2006. Holocene evolution of the Haifa Bay area, Israel, and its influence on ancient tell settlements, The Holocene, pp. 849-861.

Supplementary

Existing log database:

1/50-hadera	Sandstone	677875.58	3586629	12.9	0.7	The hydrological survice of Israel - report
1/50-hadera	Clay/Sand	677875.58	3586629	0.7	-20.8	The hydrological survice of Israel - report
1/50-hadera	Sandstone	677875.58	3586629	-20.8	-25.5	The hydrological survice of Israel - report
1/51-hadera	Loam	678462.41	3589211.6	8.5	6.6	The hydrological survice of Israel - report
1/51-hadera	Clay	678462.41	3589211.6	6.6	0.5	The hydrological survice of Israel - report
1/51-hadera	Sandstone	678462.41	3589211.6	0.5	-18	The hydrological survice of Israel - report
1/vitkin	Sand	675383.93	3583777.1	20	18.5	The hydrological survice of Israel - report
1/vitkin	Loam	675383.93	3583777.1	18.5	16	The hydrological survice of Israel - report
1/vitkin	Silt/Clay	675383.93	3583777.1	16	11.5	The hydrological survice of Israel - report
11/Caesarea	Sand	679712.78	3599369.3	9.5	5.5	The hydrological survice of Israel - report
11/Caesarea	Clay/Sand	679712.78	3599369.3	5.5	-2.5	The hydrological survice of Israel - report
11/Caesarea	Sand/Silt	679712.78	3599369.3	-2.5	-9.5	The hydrological survice of Israel - report
11/Caesarea	Sandstone	679712.78	3599369.3	-9.5	-19	The hydrological survice of Israel - report
12/kfar vitkin	Sand	675765.36	3582254.7	17	2.65	The hydrological survice of Israel - report
12/kfar vitkin	Sandstone	675765.36	3582254.7	2.65	-0.35	The hydrological survice of Israel - report
137/68-natania	Clay/Sand	675623.48	3579431.3	42	29.85	The hydrological survice of Israel - report
137/68-natania	Clay	675623.48	3579431.3	29.85	15.75	The hydrological survice of Israel - report
16/vitkin	Sand	676301.31	3582455.8	18	15	The hydrological survice of Israel - report
16/vitkin	Loam	676301.31	3582455.8	15	8.5	The hydrological survice of Israel - report
16/vitkin	Clay/Sand	676301.31	3582455.8	8.5	4.5	The hydrological survice of Israel - report
16/vitkin	Silt/Clay	676301.31	3582455.8	4.5	-5	The hydrological survice of Israel - report
16/vitkin	Sand	676301.31	3582455.8	-5	-11.5	The hydrological survice of Israel - report
16/vitkin	Silt/Clay	676301.31	3582455.8	-11.5	-20.5	The hydrological survice of Israel - report
16/vitkin	Clay	676301.31	3582455.8	-20.5	-32	The hydrological survice of Israel - report
16/vitkin	Clay/Sand	676301.31	3582455.8	-32	-50	The hydrological survice of Israel - report
16/vitkin	Sandstone	676301.31	3582455.8	-50	-63	The hydrological survice of Israel - report
2/Hadasim	Sand	675898.06	3574836.2	17.57	14.57	The hydrological survice of Israel - report
2/Hadasim	Loam	675898.06	3574836.2	14.57	-16.93	The hydrological survice of Israel - report
2/Hadasim	Sand	675898.06	3574836.2	-16.93	-24.43	The hydrological survice of Israel - report
2/Hadasim	Sandstone	675898.06	3574836.2	-24.43	-49.23	The hydrological survice of Israel - report
2/michmoret	Loam	677037.82	3586997.8	31.9	25.3	The hydrological survice of Israel - report
2/michmoret	Sand	677037.82	3586997.8	25.3	24.4	The hydrological survice of Israel - report
2/michmoret	Sandstone	677037.82	3586997.8	24.4	7.7	The hydrological survice of Israel - report
2/power station/ hadera	Sand	677605.91	3593974.8	5	-1	Israel's electric corparation - report (1982)
2/power station/ hadera	Clay	677605.91	3593974.8	-1	-7	Israel's electric corparation - report (1982)
2/power station/ hadera	Clay/Sand	677605.91	3593974.8	-7	-8	Israel's electric corparation - report (1982)
2/power station/ hadera	Sandstone	677605.91	3593974.8	-8	-13.3	Israel's electric corparation - report (1982)
20/a caesarea	Sand	677904.49	3595401.2	6	5	The hydrological survice of Israel - report
20/a caesarea	Sandstone	677904.49	3595401.2	5	-14	The hydrological survice of Israel - report
25/natania	Loam	674947.65	3578737.3	23	18	The hydrological survice of Israel - report
25/natania	Clay/Sand	674947.65	3578737.3	18	9	The hydrological survice of Israel - report

25/natania	Sandstone	674947.65	3578737.3	9	8.5	The hydrological survice of Israel - report
27-natania	Clay/Sand	676493.19	3577508.9	17.2	-25.8	The hydrological survice of Israel - report
27-natania	Sandstone	676493.19	3577508.9	-25.8	-31.8	The hydrological survice of Israel - report
29/ natania	Loam	675098.06	3574829.8	35.79	33.54	The hydrological survice of Israel - report
29/ natania	Sandstone	675098.06	3574829.8	33.54	29.79	The hydrological survice of Israel - report
3/Hadera power station	Sand	677694.59	3594426.7	5.5	2	Israel's electric corparation - report (1982)
3/Hadera power station	Sand/Gravel	677694.59	3594426.7	2	-2	Israel's electric corparation - report (1982)
3/Hadera power station	Clay	677694.59	3594426.7	-2	-6	Israel's electric corparation - report (1982)
3/Hadera power station	Sandstone	677694.59	3594426.7	-6	-10.5	Israel's electric corparation - report (1982)
3156/ caesarea	Sand/Silt	678688.75	3599796.2	3	0	The hydrological survice of Israel - report
3156/ caesarea	Sandstone	678688.75	3599796.2	0	-6	The hydrological survice of Israel - report
36/natania	Sand	675136.83	3580721.5	20	15.2	The hydrological survice of Israel - report
36/natania	Clay/Sand	675136.83	3580721.5	15.2	8	The hydrological survice of Israel - report
36/natania	Sand	675136.83	3580721.5	8	4	The hydrological survice of Israel - report
36/natania	Clay/Sand	675136.83	3580721.5	4	-2	The hydrological survice of Israel - report
36/natania	Sandstone	675136.83	3580721.5	-2	-7	The hydrological survice of Israel - report
37-natania	Clay	675616.17	3576870.8	15.3	6.8	The hydrological survice of Israel - report
37-natania	Sand	675616.17	3576870.8	6.8	-0.5	The hydrological survice of Israel - report
37-natania	Clay	675616.17	3576870.8	-0.5	-4.9	The hydrological survice of Israel - report
37-natania	Sandstone	675616.17	3576870.8	-4.9	-24.2	The hydrological survice of Israel - report
38/natania	Sand/Gravel	674851.86	3572794.4	30	29	The hydrological survice of Israel - report
38/natania	Clay	674851.86	3572794.4	29	17	The hydrological survice of Israel - report
38/natania	Sandstone	674851.86	3572794.4	17	8.5	The hydrological survice of Israel - report
39/natania	Sand	675957.14	3574395.3	20.1	9.1	The hydrological survice of Israel - report
39/natania	Clay	675957.14	3574395.3	9.1	-19.9	The hydrological survice of Israel - report
39/natania	Sand	675957.14	3574395.3	-19.9	-23.9	The hydrological survice of Israel - report
39/natania	Sandstone	675957.14	3574395.3	-23.9	-29.9	The hydrological survice of Israel - report
40/Natania	Sand	674714.49	3573735.7	39.48	32.48	The hydrological survice of Israel - report
40/Natania	Clay	674714.49	3573735.7	32.48	23.98	The hydrological survice of Israel - report
40/Natania	Sandstone	674714.49	3573735.7	23.98	17.98	The hydrological survice of Israel - report
41/a Natania	Sandstone	673096.83	3570007.8	30.32	14.32	The hydrological survice of Israel - report
41/natania	Sand	675808.18	3572884	19	14	The hydrological survice of Israel - report
41/natania	Silt/Clay	675808.18	3572884	14	11.48	The hydrological survice of Israel - report
41/natania	Sand/Gravel	675808.18	3572884	11.48	5.54	The hydrological survice of Israel - report
41/natania	Silt/Clay	675808.18	3572884	5.54	-11	The hydrological survice of Israel - report
41/natania	Sandstone	675808.18	3572884	-11	-17	The hydrological survice of Israel - report
41/natania	Sandstone	675808.18	3572884	-17	-31	The hydrological survice of Israel - report
41/v Yakom	Silt/Clay	674768.17	3570442.3	5.225	4.225	The hydrological survice of Israel - report
41/v Yakom	Clay	674768.17	3570442.3	4.225	-0.275	The hydrological survice of Israel - report
41/v Yakom	Sand/Silt	674768.17	3570442.3	-0.275	-19.77	The hydrological survice of Israel - report
41/v Yakom	Sandstone	674768.17	3570442.3	-19.775	-21.77	The hydrological survice of Israel - report
41T/B Yakom A	Loam	672726.78	3569520.2	20.2	14.2	The hydrological survice of Israel - report
41T/B Yakom A	Sandstone	672726.78	3569520.2	14.2	3.7	The hydrological survice of Israel - report
42/0 Flick	Sand	672772.26	3572661.6	3.52	-0.48	The hydrological survice of Israel - report
42/0 Flick	Sandstone	672772.26	3572661.6	-0.48	-52.48	The hydrological survice of Israel - report
42/1 Odim	Loam	674777.35	3571942.7	14.94	12.94	The hydrological survice of Israel - report
42/1 Odim	Sandstone	674777.35	3571942.7	12.94	4.74	The hydrological survice of Israel - report

42/2 Beit yehoshoa	Loam	675993.07	3571187.5	26.14	19.14	The hydrological survice of Israel - report
42/2 Beit yehoshoa	Sandstone	675993.07	3571187.5	19.14	-17.36	The hydrological survice of Israel - report
42/a Flick	Sandstone	673037.25	3572907.1	3.47	1.47	The hydrological survice of Israel - report
42/a2 Beit yehoshoa	Clay/Sand	676001.88	3571196.7	26.17	13.17	The hydrological survice of Israel - report
42/a2 Beit yehoshoa	Loam	676001.88	3571196.7	13.17	4.17	The hydrological survice of Israel - report
42/natania	Sand/Gravel	674346.52	3572514.9	31.55	31.55	The hydrological survice of Israel - report
42/natania	Sand	674346.52	3572514.9	31.55	29.98	The hydrological survice of Israel - report
42/natania	Sand/Gravel	674346.52	3572514.9	29.98	28.49	The hydrological survice of Israel - report
42/natania	Sand	674346.52	3572514.9	28.49	27.55	The hydrological survice of Israel - report
42/natania	Loam	674346.52	3572514.9	27.55	23.55	The hydrological survice of Israel - report
42/natania	Sandstone	674346.52	3572514.9	23.55	21.34	The hydrological survice of Israel - report
42/natania	Sandstone	674346.52	3572514.9	21.34	14.29	The hydrological survice of Israel - report
43/2 Kfar neter	Loam	676207.88	3571442	22.04	12.04	The hydrological survice of Israel - report
43/2 Kfar neter	Sand	676207.88	3571442	12.04	6.04	The hydrological survice of Israel - report
43/2 Kfar neter	Loam	676207.88	3571442	6.04	3.04	The hydrological survice of Israel - report
43/2 Kfar neter	Sandstone	676207.88	3571442	3.04	-18.96	The hydrological survice of Israel - report
43/v Odim	Sand	674975.1	3573026.9	32.21	26.71	The hydrological survice of Israel - report
43/v Odim	Sandstone	674975.1	3573026.9	26.71	20.21	The hydrological survice of Israel - report
43-natania	Loam	675353.11	3576045.2	16	14.5	The hydrological survice of Israel - report
43-natania	Sandstone	675353.11	3576045.2	14.5	8	The hydrological survice of Israel - report
44/a-natania	Sandstone	673897.39	3575825.2	42	17.7	The hydrological survice of Israel - report
44/b-natania	Clay	674368.1	3576281	46	43	The hydrological survice of Israel - report
44/b-natania	Sandstone	674368.1	3576281	43	31	The hydrological survice of Israel - report
44/v natania	Loam	675371.82	3575135.4	21.37	13.87	The hydrological survice of Israel - report
44/v natania	Sandstone	675371.82	3575135.4	13.87	11.17	The hydrological survice of Israel - report
45/0-natania	Sandstone	673999.22	3578167.7	20	-9	The hydrological survice of Israel - report
45/2-natania	Clay/Sand	677631.72	3583078.3	30	17	The hydrological survice of Israel - report
45/2-natania	Sand	677631.72	3583078.3	17	-4	The hydrological survice of Israel - report
45/2-natania	Sandstone	677631.72	3583078.3	-4	-20	The hydrological survice of Israel - report
45/a3-natania	Sand	674079.4	3578159.3	21.8	17.3	The hydrological survice of Israel - report
45/a3-natania	Sandstone	674079.4	3578159.3	17.3	-34.2	The hydrological survice of Israel - report
45/a-natania	Clay/Sand	674039.41	3578158.5	20	16.5	The hydrological survice of Israel - report
45/a-natania	Sandstone	674039.41	3578158.5	16.5	-6	The hydrological survice of Israel - report
45/b-natania	Sand	674079.4	3578159.3	30.6	26.6	The hydrological survice of Israel - report
45/b-natania	Sandstone	674079.4	3578159.3	26.6	21.6	The hydrological survice of Israel - report
45/v-natania	Clay/Sand	675845.21	3577405.6	14.9	4.9	The hydrological survice of Israel - report
45/v-natania	Sandstone	675845.21	3577405.6	4.9	-0.1	The hydrological survice of Israel - report
46/1-natania	Clay/Sand	675558.94	3578679.9	31.1	18.1	The hydrological survice of Israel - report
46/1-natania	Sandstone	675558.94	3578679.9	18.1	12.1	The hydrological survice of Israel - report
46/2-natania	Clay	676774.22	3579405	9.3	5.3	The hydrological survice of Israel - report
46/2-natania	Loam	676774.22	3579405	5.3	2.3	The hydrological survice of Israel - report
46/2-natania	Clay	676774.22	3579405	2.3	-0.7	The hydrological survice of Israel - report
46/2-natania	Sandstone	676774.22	3579405	-0.7	-9.7	The hydrological survice of Israel - report
46/a-natania	Clay/Sand	674660.66	3580531.7	16.9	11.3	The hydrological survice of Israel - report
46/a-natania	Sandstone	674660.66	3580531.7	11.3	-26.2	The hydrological survice of Israel - report
46/b1-natania	Silt/Clay	675114.34	3579870.9	19	10	The hydrological survice of Israel - report
46/b1-natania	Sandstone	675114.34	3579870.9	10	1	The hydrological survice of Israel - report
47/1-givaat shapira	Sandstone	676565.14	3581301.1	37.7	1.7	The hydrological survice of Israel - report
47/tb-bitan aharon	Sand	675561.71	3582430.6	12	-5	The hydrological survice of Israel - report
47/tb-bitan aharon	Sandstone	675561.71	3582430.6	-5	-12	The hydrological survice of Israel - report
48/0a-vitkin	Sandstone	675442.21	3584637.5	5	-15	The hydrological survice of Israel - report
48/0-vitkin	Sandstone	675354.56	3584716.7	4	-15.7	The hydrological survice of Israel - report

48/1-vitkin	Sandstone	676962.6	3583369.6	6.2	5.2	The hydrological survice of Israel - report
48/1-vitkin	Clay	676962.6	3583369.6	5.2	-0.8	The hydrological survice of Israel - report
48/1-vitkin	Sandstone	676962.6	3583369.6	-0.8	-9.2	The hydrological survice of Israel - report
48/b-beit yanai	Sand	676341.32	3584397	22.9	18.4	The hydrological survice of Israel - report
48/b-beit yanai	Clay/Sand	676341.32	3584397	18.4	11.9	The hydrological survice of Israel - report
48/b-beit yanai	Sandstone	676341.32	3584397	11.9	1.3	The hydrological survice of Israel - report
49a/michmoret	Clay/Sand	676351.63	3585837.4	6	-4	The hydrological survice of Israel - report
49a/michmoret	Sandstone	676351.63	3585837.4	-4	-7	The hydrological survice of Israel - report
5/hophit	Sand	675626.98	3584553.3	7.5	4	The hydrological survice of Israel - report
5/hophit	Loam	675626.98	3584553.3	4	0	The hydrological survice of Israel - report
5/hophit	Sand	675626.98	3584553.3	0	-9.5	The hydrological survice of Israel - report
5/v caesarea	Sand	677905.73	3595341.2	6	4	The hydrological survice of Israel - report
5/v caesarea	Clay	677905.73	3595341.2	4	2	The hydrological survice of Israel - report
5/v caesarea	Clay/Sand	677905.73	3595341.2	2	-1	The hydrological survice of Israel - report
5/v caesarea	Sandstone	677905.73	3595341.2	-1	-12.9	The hydrological survice of Israel - report
51a/hadera	Sandstone	676697.45	3590405.4	9	6.5	The hydrological survice of Israel - report
52/a givat olga	Loam	676793.27	3591577.6	6	0.5	The hydrological survice of Israel - report
52/a givat olga	Sandstone	676793.27	3591577.6	0.5	-8.9	The hydrological survice of Israel - report
52v/Caesarea	Loam	677883.74	3591080	22	15	The hydrological survice of Israel - report
52v/Caesarea	Sandstone	677883.74	3591080	15	2	The hydrological survice of Israel - report
53a/Hadera	Sandstone	677298.65	3593258.3	6	-8.9	The hydrological survice of Israel - report
54/0 Caesarea	Sand/Gravel	677450.74	3595481.8	4.8	-19.8	The hydrological survice of Israel - report
54/0 Caesarea	Clay	677450.74	3595481.8	-19.8	-21.7	The hydrological survice of Israel - report
54/0 Caesarea	Sandstone	677450.74	3595481.8	-21.7	-69	The hydrological survice of Israel - report
54/01 caesarea	Sand	677672.06	3595516.4	7	2.5	The hydrological survice of Israel - report
54/01 caesarea	Sandstone	677672.06	3595516.4	2.5	0	The hydrological survice of Israel - report
54/06 caesarea	Sand	677479.73	3595482.4	5	-10	The hydrological survice of Israel - report
54/06 caesarea	Sandstone	677479.73	3595482.4	-10	-19.5	The hydrological survice of Israel - report
54/a1 caesarea	Sand	677875.74	3595340.6	6.6	3.1	The hydrological survice of Israel - report
54/a1 caesarea	Loam	677875.74	3595340.6	3.1	1.1	The hydrological survice of Israel - report
54/a1 caesarea	Sandstone	677875.74	3595340.6	1.1	-13.7	The hydrological survice of Israel - report
54/s caesarea	Sand	677426.83	3595477.3	2	-1	The hydrological survice of Israel - report
54/s caesarea	Sand/Gravel	677426.83	3595477.3	-1	-5	The hydrological survice of Israel - report
54/s caesarea	Clay/Sand	677426.83	3595477.3	-5	-5.8	The hydrological survice of Israel - report
54/s caesarea	Sandstone	677426.83	3595477.3	-5.8	-16.5	The hydrological survice of Israel - report
55/0/1 Caesarea	Loam	677910.03	3597551.7	11	5	The hydrological survice of Israel - report
55/0/1 Caesarea	Sandstone	677910.03	3597551.7	5	-22	The hydrological survice of Israel - report
55/1 caesarea	Sand	679761.17	3597029.9	20	17.5	The hydrological survice of Israel - report
55/1 caesarea	Clay/Sand	679761.17	3597029.9	17.5	14.5	The hydrological survice of Israel - report
55/1 caesarea	Sandstone	679761.17	3597029.9	14.5	13.3	The hydrological survice of Israel - report
55/a Caesarea	Sandstone	677812.54	3597429.7	10.1	-23.6	The hydrological survice of Israel - report
55/s caesarea	Clay/Sand	677687.46	3596707	10	4	The hydrological survice of Israel - report
55/s caesarea	Sand/Gravel	677687.46	3596707	4	-20	The hydrological survice of Israel - report
55/s caesarea	Clay	677687.46	3596707	-20	-26	The hydrological survice of Israel - report
55/s caesarea	Sand/Gravel	677687.46	3596707	-26	-33	The hydrological survice of Israel - report
55/s caesarea	Clay	677687.46	3596707	-33	-41	The hydrological survice of Israel - report
55/s caesarea	Sandstone	677687.46	3596707	-41	-80	The hydrological survice of Israel - report
56/a caesarea	Sand	678571.6	3599415.7	6.2	2.2	The hydrological survice of Israel - report
56/a caesarea	Clay/Sand	678571.6	3599415.7	2.2	-6.8	The hydrological survice of Israel - report
56/a caesarea	Sandstone	678571.6	3599415.7	-6.8	-18.8	The hydrological survice of Israel - report
56A/Kisaria	Sand	678517.62	3599414.6	5	1	The hydrological survice of Israel - report
56A/Kisaria	Clay/Sand	678517.62	3599414.6	1	-2	The hydrological survice of Israel - report
6/Caesarea	Sand	677848.61	3595153	6	0.3	The hydrological survice of Israel - report
6/Caesarea	Clay/Sand	677848.61	3595153	0.3	-3.5	The hydrological survice of Israel - report

6/Caesarea	Sandstone	677848.61	3595153	-3.5	-12	The hydrological survice of Israel - report
6/hophit	Sand	675622.16	3584544.2	8	5.5	The hydrological survice of Israel - report
6/hophit	Loam	675622.16	3584544.2	5.5	-1.5	The hydrological survice of Israel - report
6/hophit	Sand	675622.16	3584544.2	-1.5	-3	The hydrological survice of Israel - report
7/143-natania	Sand	673765.13	3573843.2	28	23	The hydrological survice of Israel - report
7/143-natania	Sandstone	673765.13	3573843.2	23	12	The hydrological survice of Israel - report
7/Caesarea	Sand	677844.55	3594816.9	6	-0.3	The hydrological survice of Israel - report
7/Caesarea	Clay	677844.55	3594816.9	-0.3	-5	The hydrological survice of Israel - report
7/Caesarea	Sandstone	677844.55	3594816.9	-5	-12.5	The hydrological survice of Israel - report
7/hophit	Sand	675297.81	3584558.5	7	-4	The hydrological survice of Israel - report
9/nativ Beit yehoshoa	Sand	675614.94	3571579.8	21.2	20.2	The hydrological survice of Israel - report
9/nativ Beit yehoshoa	Loam	675614.94	3571579.8	20.2	4.2	The hydrological survice of Israel - report
9/nativ Beit yehoshoa	Sand	675614.94	3571579.8	4.2	1.7	The hydrological survice of Israel - report
9/nativ Beit yehoshoa	Silt/Clay	675614.94	3571579.8	1.7	-2.8	The hydrological survice of Israel - report
9/nativ Beit yehoshoa	Sandstone	675614.94	3571579.8	-2.8	-19.8	The hydrological survice of Israel - report
9/nativ Beit yehoshoa	Sandstone	675614.94	3571579.8	-19.8	-28.6	The hydrological survice of Israel - report
A/ Odim	Sandstone	673905.59	3571534.7	16.67	5.17	The hydrological survice of Israel - report
A/51-hadera	Sandstone	676697.41	3590407.4	9	6.5	The hydrological survice of Israel - report
A/55 caesarea	Sandstone	677812.54	3597429.7	10.1	4.6	The hydrological survice of Israel - report
A/57 zarka	Sand	679050.51	3601406	6	5.7	The hydrological survice of Israel - report
A/57 zarka	Clay	679050.51	3601406	5.7	-1.6	The hydrological survice of Israel - report
A/57 zarka	Sand/Silt	679050.51	3601406	-1.6	-2.6	The hydrological survice of Israel - report
A/57 zarka	Sandstone	679050.51	3601406	-2.6	-12.3	The hydrological survice of Israel - report
A/avihail	Loam	676476.91	3580729.1	23.9	17.4	The hydrological survice of Israel - report
A/avihail	Sand with shells	676476.91	3580729.1	17.4	-16.2	The hydrological survice of Israel - report
A/avihail	Sandstone	676476.91	3580729.1	-16.2	-19.1	The hydrological survice of Israel - report
A/michmoret	Sand	676471.8	3586800.1	17	16.2	The hydrological survice of Israel - report
A/michmoret	Loam	676471.8	3586800.1	16.2	14	The hydrological survice of Israel - report
A/michmoret	Sand	676471.8	3586800.1	14	-1	The hydrological survice of Israel - report
A/michmoret	Loam	676471.8	3586800.1	-1	-5.5	The hydrological survice of Israel - report
A/michmoret	Sandstone	676471.8	3586800.1	-5.5	-11	The hydrological survice of Israel - report
A/sdot-yam	Sand	677816.39	3596759.6	8	7.4	The hydrological survice of Israel - report
A/sdot-yam	Silt	677816.39	3596759.6	7.4	5.8	The hydrological survice of Israel - report
A/sdot-yam	Loam	677816.39	3596759.6	5.8	4.5	The hydrological survice of Israel - report
A/sdot-yam	Silty sand	677816.39	3596759.6	4.5	0	The hydrological survice of Israel - report
A/sdot-yam	Loam	677816.39	3596759.6	0	-5	The hydrological survice of Israel - report
A/sdot-yam	Sandstone	677816.39	3596759.6	-5	-6.7	The hydrological survice of Israel - report
A1/alexander	Clay/Sand	677940.62	3584930	4.1	-7.9	The hydrological survice of Israel - report
A1/alexander	Clay	677940.62	3584930	-7.9	-10.4	The hydrological survice of Israel - report
A49/alexander	Clay/Sand	676351.63	3585837.4	6.4	-3.6	The hydrological survice of Israel - report
A49/alexander	Sandstone	676351.63	3585837.4	-3.6	-27.6	The hydrological survice of Israel - report
A50/michmoret	Clay/Sand	675970.36	3587689.9	8.2	2.7	The hydrological survice of Israel - report
A50/michmoret	Sandstone	675970.36	3587689.9	2.7	-16.1	The hydrological survice of Israel - report
Acker1	Sand	677932.63	3593071.4	17	15	A. Ecker, 1999. Atlas-Selected Geological cross-sections and subsurface maps in the coastal aquifer of israel . GSI/18/
Acker1	Sandstone	677932.63	3593071.4	15	1	A. Ecker, 1999. Atlas-Selected Geological cross-sections and subsurface maps in the coastal aquifer of israel . GSI/18/
Acker2	Sand	676687.93	3591835.4	4	1	A. Ecker, 1999. Atlas-Selected Geological cross-sections and subsurface maps in the coastal aquifer of israel . GSI/18/

Acker2	Loam	676687.93	3591835.4	1	-9	A. Ecker, 1999. Atlas-Selected Geological cross-sections and subsurface maps in the coastal aquifer of israel . GSI/18/
Acker2	Sandstone	676687.93	3591835.4	-9	-21	A. Ecker, 1999. Atlas-Selected Geological cross-sections and subsurface maps in the coastal aquifer of israel . GSI/18/
Acker3	Sandstone	677540.43	3590752.8	24	14	A. Ecker, 1999. Atlas-Selected Geological cross-sections and subsurface maps in the coastal aquifer of israel . GSI/18/
Acker4	Loam	676677.83	3584083.9	12	0	A. Ecker, 1999. Atlas-Selected Geological cross-sections and subsurface maps in the coastal aquifer of israel . GSI/18/
Acker4	Clay	676677.83	3584083.9	0	-5	A. Ecker, 1999. Atlas-Selected Geological cross-sections and subsurface maps in the coastal aquifer of israel . GSI/18/
Acker4	Sandstone	676677.83	3584083.9	-5	-10	A. Ecker, 1999. Atlas-Selected Geological cross-sections and subsurface maps in the coastal aquifer of israel . GSI/18/
Acker5	Loam	676826.44	3584249.9	17	0	A. Ecker, 1999. Atlas-Selected Geological cross-sections and subsurface maps in the coastal aquifer of israel . GSI/18/
Acker5	Sand	676826.44	3584249.9	0	-3	A. Ecker, 1999. Atlas-Selected Geological cross-sections and subsurface maps in the coastal aquifer of israel . GSI/18/
Acker5	Loam	676826.44	3584249.9	-3	-8	A. Ecker, 1999. Atlas-Selected Geological cross-sections and subsurface maps in the coastal aquifer of israel . GSI/18/
Acker5	Clay	676826.44	3584249.9	-8	-11	A. Ecker, 1999. Atlas-Selected Geological cross-sections and subsurface maps in the coastal aquifer of israel . GSI/18/
Acker5	Sand	676826.44	3584249.9	-11	-17	A. Ecker, 1999. Atlas-Selected Geological cross-sections and subsurface maps in the coastal aquifer of israel . GSI/18/
Acker5	Sandstone	676826.44	3584249.9	-17	-24	A. Ecker, 1999. Atlas-Selected Geological cross-sections and subsurface maps in the coastal aquifer of israel . GSI/18/
Acker6	Loam	676242.67	3589615.8	2	1	A. Ecker, 1999. Atlas-Selected Geological cross-sections and subsurface maps in the coastal aquifer of israel . GSI/18/
Acker6	Sand	676242.67	3589615.8	1	-1	A. Ecker, 1999. Atlas-Selected Geological cross-sections and subsurface maps in the coastal aquifer of israel . GSI/18/
Acker6	Sandstone	676242.67	3589615.8	-1	-45	A. Ecker, 1999. Atlas-Selected Geological cross-sections and subsurface maps in the coastal aquifer of israel . GSI/18/
Acker7	Loam	677361.01	3590239	23	16	A. Ecker, 1999. Atlas-Selected Geological cross-sections and subsurface maps in the coastal aquifer of israel . GSI/18/
Acker7	Sand	677361.01	3590239	16	1	A. Ecker, 1999. Atlas-Selected Geological cross-sections and subsurface maps in the coastal aquifer of israel . GSI/18/
Acker7	Sandstone	677361.01	3590239	1	-5	A. Ecker, 1999. Atlas-Selected Geological cross-sections and subsurface maps in the coastal aquifer of israel . GSI/18/
Acker8	Siltstone	673352.33	3579954.7	-13	-18.8	A. Ecker, 1999. Atlas-Selected Geological cross-sections and subsurface maps in the coastal aquifer of israel . GSI/18/
A-Hagoel/givat shapira	Loam	676656.17	3582223.1	12.9	8.4	The hydrological survice of Israel - report

A-Hagoel/givat shapira	Sandstone	676656.17	3582223.1	8.4	4.7	The hydrological survice of Israel - report
Av/51-hadera	Clay	677904.59	3590070.2	8.7	2.7	The hydrological survice of Israel - report
Av/51-hadera	Sandstone	677904.59	3590070.2	2.7	-3.3	The hydrological survice of Israel - report
B/ Odim	Sand	674002.96	3571176.7	17.37	16.87	The hydrological survice of Israel - report
B/ Odim	Sandstone	674002.96	3571176.7	16.87	4.17	The hydrological survice of Israel - report
B/51-hadera	Sand	676969.04	3590331	13.4	11.4	The hydrological survice of Israel - report
B/51-hadera	Sandstone	676969.04	3590331	11.4	10.6	The hydrological survice of Israel - report
B/51-hadera	Clay/Sand	676969.04	3590331	10.6	7.8	The hydrological survice of Israel - report
B/51-hadera	Sand	676969.04	3590331	7.8	2.4	The hydrological survice of Israel - report
B/51-hadera	Sandstone	676969.04	3590331	2.4	-21.6	The hydrological survice of Israel - report
B/52 givatolga	Clay/Sand	677054.83	3592473.1	6	-3	The hydrological survice of Israel - report
B/52 givatolga	Sandstone	677054.83	3592473.1	-3	-14	The hydrological survice of Israel - report
B/53 givatolga	Sandstone	677441.51	3593121.2	4.8	-11.7	The hydrological survice of Israel - report
B/avihail	Loam	676915.97	3580778.2	7.9	-5.1	The hydrological survice of Israel - report
B/avihail	Clay/Sand	676915.97	3580778.2	-5.1	-10.1	The hydrological survice of Israel - report
B/avihail	Sandstone	676915.97	3580778.2	-10.1	-15.5	The hydrological survice of Israel - report
B/bitan	Loam	675817.73	3582625.9	20.7	18.2	The hydrological survice of Israel - report
B/bitan	Sand	675817.73	3582625.9	18.2	8.7	The hydrological survice of Israel - report
B/bitan	Sandstone	675817.73	3582625.9	8.7	-5.6	The hydrological survice of Israel - report
B-Hagoel/givat shapira	Loam	676709.15	3582564.2	8.3	3.8	The hydrological survice of Israel - report
B-Hagoel/givat shapira	Sand	676709.15	3582564.2	3.8	0.1	The hydrological survice of Israel - report
B-Hagoel/givat shapira	Sandstone	676709.15	3582564.2	0.1	-0.2	The hydrological survice of Israel - report
Caesarea	Sand	679887.56	3598172.7	16	13	The hydrological survice of Israel - report
Caesarea	Clay/Sand	679887.56	3598172.7	13	8.8	The hydrological survice of Israel - report
Caesarea	Clay	679887.56	3598172.7	8.8	-4	The hydrological survice of Israel - report
Caesarea	Clay/Sand	679887.56	3598172.7	-4	-7	The hydrological survice of Israel - report
Caesarea	Sand	679887.56	3598172.7	-7	-11	The hydrological survice of Israel - report
Caesarea	Sandstone	679887.56	3598172.7	-11	-13	The hydrological survice of Israel - report
Caesarea harbor entarence1	Sand	677375.83	3598088.8	-5.4	-8.4	Nir, Y., 1977. Jet drilling in the sea off the Hadera Electric power station site. GSI/MG/9/
Caesarea harbor entarence1	Sand with shells	677375.83	3598088.8	-8.4	-9.9	Nir, Y., 1977. Jet drilling in the sea off the Hadera Electric power station site. GSI/MG/9/
Caesarea harbor entarence1	Clay	677375.83	3598088.8	-9.9	-12.3	Nir, Y., 1977. Jet drilling in the sea off the Hadera Electric power station site. GSI/MG/9/
Caesarea harbor entarence2	Sand	677351.23	3598069.3	-6.4	-8.9	Nir, Y., 1977. Jet drilling in the sea off the Hadera Electric power station site. GSI/MG/9/
Caesarea harbor entarence2	Sand with shells	677351.23	3598069.3	-8.9	-10.4	Nir, Y., 1977. Jet drilling in the sea off the Hadera Electric power station site. GSI/MG/9/
Caesarea harbor entarence3	Sand	677335.63	3598049.9	-7.1	-9.1	Nir, Y., 1977. Jet drilling in the sea off the Hadera Electric power station site. GSI/MG/9/
Caesarea harbor entarence3	Sandstone	677335.63	3598049.9	-9.1	-10.6	Nir, Y., 1977. Jet drilling in the sea off the Hadera Electric power station site. GSI/MG/9/
Caesarea harbor entarence4	Sand	677390.18	3597927	-7.4	-10.8	Nir, Y., 1977. Jet drilling in the sea off the Hadera Electric power station site. GSI/MG/9/

Caesarea harbor entarence5	Sand	677391.91	3597940.1	-6	-6.5	Nir, Y., 1977. Jet drilling in the sea off the Hadera Electric power station site. GSI/MG/9/
Caesarea harbor entarence5	Sand with shells	677391.91	3597940.1	-6.5	-10	Nir, Y., 1977. Jet drilling in the sea off the Hadera Electric power station site. GSI/MG/9/
Caesarea harbor entarence6	Sand	677391.45	3597962.1	-7	-7.9	Nir, Y., 1977. Jet drilling in the sea off the Hadera Electric power station site. GSI/MG/9/
Caesarea harbor entarence6	Sandstone	677391.45	3597962.1	-7.9	-10.3	Nir, Y., 1977. Jet drilling in the sea off the Hadera Electric power station site. GSI/MG/9/
Caesarea harbor entarence7	Sand	677335.65	3597758.9	-7.2	-8.4	Nir, Y., 1977. Jet drilling in the sea off the Hadera Electric power station site. GSI/MG/9/
Caesarea harbor entarence7	Sand with shells	677335.65	3597758.9	-8.4	-9.4	Nir, Y., 1977. Jet drilling in the sea off the Hadera Electric power station site. GSI/MG/9/
Caesarea harbor entarence7	Sand	677335.65	3597758.9	-9.4	-10.6	Nir, Y., 1977. Jet drilling in the sea off the Hadera Electric power station site. GSI/MG/9/
Caesarea intermid harbor 1	Sand with shells	677486.57	3597764	-4.2	-5.1	Nir, Y., 1977. Jet drilling in the sea off the Hadera Electric power station site. GSI/MG/9/
Caesarea intermid harbor 1	Sandstone	677486.57	3597764	-5.1	-5.7	Nir, Y., 1977. Jet drilling in the sea off the Hadera Electric power station site. GSI/MG/9/
Caesarea intermid harbor2	Sandstone	677603.08	3597740.4	-2.4	-4.8	Nir, Y., 1977. Jet drilling in the sea off the Hadera Electric power station site. GSI/MG/9/
Caesarea/beach seaction	Sand	677246.84	3594797.5	1	0.7	The hydrological survice of Israel - report
Caesarea/beach seaction	Sandstone	677246.84	3594797.5	0.7	-9	The hydrological survice of Israel - report
Caesarea25	Sand with shells	677343.97	3597840.1	18.5	13.5	The hydrological survice of Israel - report
Caesarea25	Sand	677343.97	3597840.1	13.5	11.75	The hydrological survice of Israel - report
Caesarea25	Sandstone	677343.97	3597840.1	11.75	11.5	The hydrological survice of Israel - report
CH/1156 caesarea	Sand/Silt	678694.79	3599794.4	4.3	1.3	The hydrological survice of Israel - report
CH/1156 caesarea	Sandstone	678694.79	3599794.4	1.3	-4.7	The hydrological survice of Israel - report
CH/2156 caesarea	Sand/Silt	678691.79	3599794.3	4.3	1.3	The hydrological survice of Israel - report
CH/2156 caesarea	Sandstone	678691.79	3599794.3	1.3	-4.7	The hydrological survice of Israel - report
CH/3156 caesarea	Sand	678688.75	3599796.2	4.3	1.3	The hydrological survice of Israel - report
CH/3156 caesarea	Sandstone	678688.75	3599796.2	1.3	-4.7	The hydrological survice of Israel - report
CH/4156 caesarea	Sand/Silt	678686.73	3599797.2	4.3	1.3	The hydrological survice of Israel - report
CH/4156 caesarea	Sandstone	678686.73	3599797.2	1.3	-4.7	The hydrological survice of Israel - report
CH/5156 caesarea	Sand/Silt	678696.81	3599793.4	4.3	1.3	The hydrological survice of Israel - report
CH/5156 caesarea	Sandstone	678696.81	3599793.4	1.3	-4.7	The hydrological survice of Israel - report
Crauze-natania	Clay	676165.52	3579822.6	19.2	15.2	The hydrological survice of Israel - report
Crauze-natania	Sandstone	676165.52	3579822.6	15.2	8.5	The hydrological survice of Israel - report
D/1 sdot-yam	Sand	678790.1	3598040	15	10.2	The hydrological survice of Israel - report
D/1 sdot-yam	Sandstone	678790.1	3598040	10.2	7	The hydrological survice of Israel - report
D/beit yanai	Loam	675884.83	3583737.5	10	6	The hydrological survice of Israel - report
D/beit yanai	Sandstone	675884.83	3583737.5	6	-11	The hydrological survice of Israel - report
D/sdot-yam	Paleosol	678800.1	3598040.2	15	13.5	The hydrological survice of Israel - report
D/sdot-yam	Sand	678800.1	3598040.2	13.5	6.5	The hydrological survice of Israel - report

D/sdot-yam	Sandstone	678800.1	3598040.2	6.5	3	The hydrological survice of Israel - report
G/avihail	Sand	676098.65	3580641.3	46	36	The hydrological survice of Israel - report
G/avihail	Sandstone	676098.65	3580641.3	36	0	The hydrological survice of Israel - report
Gas-station Hashahar N/1	Sand	674907.48	3575293.9	35	25	The hydrological survice of Israel - report
Gas-station Hashahar N/1	Loam	674907.48	3575293.9	25	23	The hydrological survice of Israel - report
Gas-station Hashahar N/1	Sand	674907.48	3575293.9	23	9	The hydrological survice of Israel - report
Gas-station Hashahar N/1	Clay	674907.48	3575293.9	9	5	The hydrological survice of Israel - report
Gas-station Hashahar N/1	Sand	674907.48	3575293.9	5	3	The hydrological survice of Israel - report
Gas-station Hashahar N/1	Loam	674907.48	3575293.9	3	-5	The hydrological survice of Israel - report
Gas-station Hashahar N/1	Sand	674907.48	3575293.9	-5	-8	The hydrological survice of Israel - report
Givat olga	Sandstone	677441.51	3593121.2	5	-11.5	The hydrological survice of Israel - report
Givat olga/hadera	Sand	677396.46	3590459.8	20	19.5	The hydrological survice of Israel - report
Givat olga/hadera	Loam	677396.46	3590459.8	19.5	10	The hydrological survice of Israel - report
Givat olga/hadera	Sandstone	677396.46	3590459.8	10	3	The hydrological survice of Israel - report
H/51-hadera	Sandstone	677341.63	3590208.6	22.1	19.3	The hydrological survice of Israel - report
H/vitkin	Sand	677896.4	3584649.1	6.1	4.3	The hydrological survice of Israel - report
H/vitkin	Loam	677896.4	3584649.1	4.3	-1.4	The hydrological survice of Israel - report
H/vitkin	Silt	677896.4	3584649.1	-1.4	-10.4	The hydrological survice of Israel - report
H/vitkin	Loam	677896.4	3584649.1	-10.4	-19.4	The hydrological survice of Israel - report
H/vitkin	Silt	677896.4	3584649.1	-19.4	-22.9	The hydrological survice of Israel - report
H/vitkin	Silt/Clay	677896.4	3584649.1	-22.9	-28.4	The hydrological survice of Israel - report
H/vitkin	Sandstone	677896.4	3584649.1	-28.4	-40.5	The hydrological survice of Israel - report
H3149/alexander	Clay/Sand	676390.56	3585259.1	7.2	6.2	The hydrological survice of Israel - report
H3149/alexander	Sandstone	676390.56	3585259.1	6.2	-43.8	The hydrological survice of Israel - report
Hadasim-mahadrim1	Sand	675908.06	3574836.4	17.57	14.57	The hydrological survice of Israel - report
Hadasim-mahadrim1	Loam	675908.06	3574836.4	14.57	-16.93	The hydrological survice of Israel - report
Hadasim-mahadrim1	Sand	675908.06	3574836.4	-16.93	-24.43	The hydrological survice of Israel - report
Hadasim-mahadrim1	Sandstone	675908.06	3574836.4	-24.43	-49.23	The hydrological survice of Israel - report
Hadera power plant	Sand	677522.9	3594023.1	8	4.5	Nir, Y., 1977. Jet drilling in the sea off the Hadera Electric power station site. GSI/MG/9/
Hadera power plant	Clay	677522.9	3594023.1	4.5	3	Nir, Y., 1977. Jet drilling in the sea off the Hadera Electric power station site. GSI/MG/9/
Hadera power plant	Sand	677522.9	3594023.1	3	-3	Nir, Y., 1977. Jet drilling in the sea off the Hadera Electric power station site. GSI/MG/9/
Hadera power plant	Clay	677522.9	3594023.1	-3	-16	Nir, Y., 1977. Jet drilling in the sea off the Hadera Electric power station site. GSI/MG/9/
Hadera power plant/1	Sand	676900.09	3593427.1	-2.1	-4.1	Nir, Y., 1977. Jet drilling in the sea off the Hadera Electric power station site. GSI/MG/9/
Hadera power plant/1	Clay/Sand	676900.09	3593427.1	-4.1	-7.2	Nir, Y., 1977. Jet drilling in the sea off the Hadera Electric power station site. GSI/MG/9/
power plant/1	Sandstone	676900.09	3593427.1	-7.2	-7.6	Nir, Y., 1977. Jet drilling in the sea off the Hadera Electric power station site. GSI/MG/9/

Hadera power plant/10	Sand	675387.18	3593506.9	-20	-24	Nir, Y., 1977. Jet drilling in the sea off the Hadera Electric power station site. GSI/MG/9/
Hadera power plant/10	Sand with shells	675387.18	3593506.9	-24	-25.5	Nir, Y., 1977. Jet drilling in the sea off the Hadera Electric power station site. GSI/MG/9/
Hadera power plant/10	Clay	675387.18	3593506.9	-25.5	-26	Nir, Y., 1977. Jet drilling in the sea off the Hadera Electric power station site. GSI/MG/9/
Hadera power plant/11	Sand	675270.23	3593745.5	-22	-26	Nir, Y., 1977. Jet drilling in the sea off the Hadera Electric power station site. GSI/MG/9/
Hadera power plant/11	Sand with shells	675270.23	3593745.5	-26	-27	Nir, Y., 1977. Jet drilling in the sea off the Hadera Electric power station site. GSI/MG/9/
Hadera power plant/11	Sand	675270.23	3593745.5	-27	-28	Nir, Y., 1977. Jet drilling in the sea off the Hadera Electric power station site. GSI/MG/9/
Hadera power plant/11	Clay	675270.23	3593745.5	-28	-28.3	Nir, Y., 1977. Jet drilling in the sea off the Hadera Electric power station site. GSI/MG/9/
Hadera power plant/12	Sand with shells	676133.23	3595398.6	-15.2	-21.5	Nir, Y., 1977. Jet drilling in the sea off the Hadera Electric power station site. GSI/MG/9/
Hadera power plant/13	Sand	675896.21	3595203.7	-17.4	-17.9	Nir, Y., 1977. Jet drilling in the sea off the Hadera Electric power station site. GSI/MG/9/
Hadera power plant/13	Sand with shells	675896.21	3595203.7	-17.9	-22.6	Nir, Y., 1977. Jet drilling in the sea off the Hadera Electric power station site. GSI/MG/9/
Hadera power plant/13	Clay	675896.21	3595203.7	-22.6	-23.6	Nir, Y., 1977. Jet drilling in the sea off the Hadera Electric power station site. GSI/MG/9/
Hadera power plant/13	Sandstone	675896.21	3595203.7	-23.6	-24.4	Nir, Y., 1977. Jet drilling in the sea off the Hadera Electric power station site. GSI/MG/9/
Hadera power plant/14	Sand	675740.53	3595235.4	-19.7	-20.2	Nir, Y., 1977. Jet drilling in the sea off the Hadera Electric power station site. GSI/MG/9/
Hadera power plant/14	Sand with shells	675740.53	3595235.4	-20.2	-21.9	Nir, Y., 1977. Jet drilling in the sea off the Hadera Electric power station site. GSI/MG/9/
Hadera power plant/14	Clay	675740.53	3595235.4	-21.9	-24.2	Nir, Y., 1977. Jet drilling in the sea off the Hadera Electric power station site. GSI/MG/9/
Hadera power plant/14	Sandstone	675740.53	3595235.4	-24.2	-24.4	Nir, Y., 1977. Jet drilling in the sea off the Hadera Electric power station site. GSI/MG/9/
Hadera power plant/15	Sand	675538.28	3595294.3	-22.3	-23.3	Nir, Y., 1977. Jet drilling in the sea off the Hadera Electric power station site. GSI/MG/9/
Hadera power plant/15	Sand with shells	675538.28	3595294.3	-23.3	-26.8	Nir, Y., 1977. Jet drilling in the sea off the Hadera Electric power station site. GSI/MG/9/

Hadera power plant/15	Clay	675538.28	3595294.3	-26.8	-28.3	Nir, Y., 1977. Jet drilling in the sea off the Hadera Electric power station site. GSI/MG/9/
Hadera power plant/16	Sand	676240.86	3593771.5	-10	-10.3	Nir, Y., 1977. Jet drilling in the sea off the Hadera Electric power station site. GSI/MG/9/
Hadera power plant/16	Sand with shells	676240.86	3593771.5	-10.3	-12.1	Nir, Y., 1977. Jet drilling in the sea off the Hadera Electric power station site. GSI/MG/9/
Hadera power plant/16	Clay	676240.86	3593771.5	-12.1	-16	Nir, Y., 1977. Jet drilling in the sea off the Hadera Electric power station site. GSI/MG/9/
Hadera power plant/17	Sand	676098.89	3593720.6	-11.8	-12.1	Nir, Y., 1977. Jet drilling in the sea off the Hadera Electric power station site. GSI/MG/9/
Hadera power plant/17	Sand with shells	676098.89	3593720.6	-12.1	-13.3	Nir, Y., 1977. Jet drilling in the sea off the Hadera Electric power station site. GSI/MG/9/
Hadera power plant/17	Clay	676098.89	3593720.6	-13.3	-16.8	Nir, Y., 1977. Jet drilling in the sea off the Hadera Electric power station site. GSI/MG/9/
Hadera power plant/18	Sand	675917.28	3593796.9	-14.2	-14.7	Nir, Y., 1977. Jet drilling in the sea off the Hadera Electric power station site. GSI/MG/9/
Hadera power plant/18	Sand with shells	675917.28	3593796.9	-14.7	-16.7	Nir, Y., 1977. Jet drilling in the sea off the Hadera Electric power station site. GSI/MG/9/
Hadera power plant/18	Clay	675917.28	3593796.9	-16.7	-19.4	Nir, Y., 1977. Jet drilling in the sea off the Hadera Electric power station site. GSI/MG/9/
Hadera power plant/19	Sand	675734.52	3593832.1	-16.5	-18.7	Nir, Y., 1977. Jet drilling in the sea off the Hadera Electric power station site. GSI/MG/9/
Hadera power plant/19	Clay	675734.52	3593832.1	-18.7	-20.5	Nir, Y., 1977. Jet drilling in the sea off the Hadera Electric power station site. GSI/MG/9/
Hadera power plant/2	Sand	676826.7	3593445.6	-3.9	-5.9	Israel's electric corparation - report (1982)
Hadera power plant/2	Sand with shells	676826.7	3593445.6	-5.9	-6.7	Israel's electric corparation - report (1982)
Hadera power plant/2	Sandstone	676826.7	3593445.6	-6.7	-6.9	Israel's electric corparation - report (1982)
Hadera power plant/20	Sand	675648.49	3593881.3	-17.8	-19.3	Israel's electric corparation - report (1982)
Hadera power plant/20	Clay	675648.49	3593881.3	-19.3	-22.8	Israel's electric corparation - report (1982)
Hadera power plant/20	Sandstone	675648.49	3593881.3	-22.8	-24.3	Israel's electric corparation - report (1982)
Hadera power plant/21	Sand	675486.27	3593939	-19.7	-21.2	Israel's electric corparation - report (1982)
Hadera power plant/21	Sand with shells	675486.27	3593939	-21.2	-21.7	Israel's electric corparation - report (1982)
Hadera power plant/21	Sandstone	675486.27	3593939	-21.7	-24.5	Israel's electric corparation - report (1982)

Hadera power plant/22	Sand	676095.91	3594203.6	-12.6	-18.3	Israel's electric corparation - report (1982)
Hadera power plant/22	Clay/Sand	676095.91	3594203.6	-18.3	-21.1	Israel's electric corparation - report (1982)
Hadera power plant/22	Sandstone	676095.91	3594203.6	-21.3	-27.7	Israel's electric corparation - report (1982)
Hadera power plant/23	Sand/Gravel	676019.5	3593739	-13.5	-19	Israel's electric corparation - report (1982)
Hadera power plant/23	Sand	676019.5	3593739	-19	-19.5	Israel's electric corparation - report (1982)
Hadera power plant/23	Sand/Silt	676019.5	3593739	-19.5	-20.5	Israel's electric corparation - report (1982)
Hadera power plant/23	Clay/Sand	676019.5	3593739	-20.5	-21.5	Israel's electric corparation - report (1982)
Hadera power plant/23	Sandstone	676019.5	3593739	-21.5	-43.5	Israel's electric corparation - report (1982)
Hadera power plant/24	Sand	675576.25	3589340.1	-21	-26	Israel's electric corparation - report (1982)
Hadera power plant/24	Silt/Clay	675576.25	3589340.1	-26	-31	Israel's electric corparation - report (1982)
Hadera power plant/24	Clay/Sand	675576.25	3589340.1	-31	-32	Israel's electric corparation - report (1982)
Hadera power plant/24	Sandstone	675576.25	3589340.1	-32	-47.7	Israel's electric corparation - report (1982)
Hadera power plant/25	Sand/Gravel	675653.63	3595229.7	-21	-25.5	Israel's electric corparation - report (1982)
Hadera power plant/25	Silt/Clay	675653.63	3595229.7	-25.5	-30	Israel's electric corparation - report (1982)
Hadera power plant/25	Clay/Sand	675653.63	3595229.7	-30	-30.5	Israel's electric corparation - report (1982)
Hadera power plant/25	Sand/Silt	675653.63	3595229.7	-30.5	-33	Israel's electric corparation - report (1982)
Hadera power plant/25	Sandstone	675653.63	3595229.7	-33	-35	Israel's electric corparation - report (1982)
Hadera power plant/26	Sand	675401.82	3593863.2	-21.3	-25.3	Israel's electric corparation - report (1982)
Hadera power plant/26	Silt/Clay	675401.82	3593863.2	-25.3	-29.8	Israel's electric corparation - report (1982)
Hadera power plant/26	Sand/Silt	675401.82	3593863.2	-29.8	-33.8	Israel's electric corparation - report (1982)
Hadera power plant/26	Sandstone	675401.82	3593863.2	-33.8	-35.8	Israel's electric corparation - report (1982)
Hadera power plant/27	Sand	675566.49	3593590.6	-20	-26	Israel's electric corparation - report (1982)
Hadera power plant/27	Clay	675566.49	3593590.6	-26	-30	Israel's electric corparation - report (1982)
Hadera power plant/27	Clay/Sand	675566.49	3593590.6	-30	-31	Israel's electric corparation - report (1982)
Hadera power plant/27	Sand/Silt	675566.49	3593590.6	-31	-33	Israel's electric corparation - report (1982)
Hadera power plant/27	Sandstone	675566.49	3593590.6	-33	-34	Israel's electric corparation - report (1982)
Hadera power plant/28	Sand	675415.14	3593654.5	-20.8	-25.8	Israel's electric corparation - report (1982)
Hadera power plant/28	Clay	675415.14	3593654.5	-25.8	-31.3	Israel's electric corparation - report (1982)
Hadera power plant/28	Sand/Silt	675415.14	3593654.5	-31.3	-33.3	Israel's electric corparation - report (1982)

Hadera power plant/28	Sandstone	675415.14	3593654.5	-33.3	-51	Israel's electric corparation - report (1982)
Hadera power plant/29	Sand	675158.31	3594128.2	-26.5	-31.5	Israel's electric corparation - report (1982)
Hadera power plant/29	Sand/Silt	675158.31	3594128.2	-31.5	-35	Israel's electric corparation - report (1982)
Hadera power plant/29	Sandstone	675158.31	3594128.2	-35	-58.5	Israel's electric corparation - report (1982)
Hadera power plant/3	Sand	676595.82	3593437.8	-5.4	-7.4	Israel's electric corparation - report (1982)
Hadera power plant/3	Clay	676595.82	3593437.8	-7.4	-9.4	Israel's electric corparation - report (1982)
Hadera power plant/3	Sand	676595.82	3593437.8	-9.4	-11.4	Israel's electric corparation - report (1982)
Hadera power plant/30	Sand	675006.29	3594128.1	-26.2	-30.7	Israel's electric corparation - report (1982)
Hadera power plant/30	Clay	675006.29	3594128.1	-30.7	-32.2	Israel's electric corparation - report (1982)
Hadera power plant/30	Sand/Silt	675006.29	3594128.1	-32.2	-34.7	Israel's electric corparation - report (1982)
Hadera power plant/30	Sandstone	675006.29	3594128.1	-34.7	-55.5	Israel's electric corparation - report (1982)
Hadera power plant/31	Sand	674961.59	3593774.1	-26.3	-30.9	Israel's electric corparation - report (1982)
Hadera power plant/31	Clay/Sand	674961.59	3593774.1	-30.9	-35	Israel's electric corparation - report (1982)
Hadera power plant/31	Sand	674961.59	3593774.1	-35	-36	Israel's electric corparation - report (1982)
Hadera power plant/31	Sandstone	674961.59	3593774.1	-36	-57.8	Israel's electric corparation - report (1982)
Hadera power plant/32	Sand	674919.78	3593619.2	-26.4	-30.9	Israel's electric corparation - report (1982)
Hadera power plant/32	Clay/Sand	674919.78	3593619.2	-30.9	-33.6	Israel's electric corparation - report (1982)
Hadera power plant/32	Sandstone	674919.78	3593619.2	-33.6	-60.4	Israel's electric corparation - report (1982)
Hadera power plant/33	Sand	674969.7	3593333.2	-26	-30.2	Israel's electric corparation - report (1982)
Hadera power plant/33	Clay/Sand	674969.7	3593333.2	-30.2	-33.5	Israel's electric corparation - report (1982)
Hadera power plant/33	Sandstone	674969.7	3593333.2	-33.5	-49	Israel's electric corparation - report (1982)
Hadera power plant/34	Sand	674959.42	3593976.1	-26.7	-30.6	Israel's electric corparation - report (1982)
Hadera power plant/34	Silt/Clay	674959.42	3593976.1	-30.6	-32.5	Israel's electric corparation - report (1982)
Hadera power plant/34	Clay/Sand	674959.42	3593976.1	-32.5	-34.7	Israel's electric corparation - report (1982)
Hadera power plant/34	Sandstone	674959.42	3593976.1	-34.7	-57.2	Israel's electric corparation - report (1982)
Hadera power plant/35	Sand	674949.8	3593134.8	-24.4	-29	Israel's electric corparation - report (1982)
Hadera power plant/35	Clay/Sand	674949.8	3593134.8	-29	-32.3	Israel's electric corparation - report (1982)
Hadera power plant/35	Sandstone	674949.8	3593134.8	-32.3	-68	Israel's electric corparation - report (1982)
Hadera power plant/36	Sand	675298.81	3594105.1	-23.2	-27.7	Israel's electric corparation - report (1982)

Hadera power plant/36	Clay/Sand	675298.81	3594105.1	-27.7	-29.2	Israel's electric corparation - report (1982)
Hadera power plant/36	Sand/Silt	675298.81	3594105.1	-29.2	-31.1	Israel's electric corparation - report (1982)
Hadera power plant/36	Sandstone	675298.81	3594105.1	-31.1	-64.3	Israel's electric corparation - report (1982)
Hadera power plant/37	Sand	675269.95	3594146.5	-21.6	-25.1	Israel's electric corparation - report (1982)
Hadera power plant/37	Silt/Clay	675269.95	3594146.5	-25.1	-30	Israel's electric corparation - report (1982)
Hadera power plant/37	Clay/Sand	675269.95	3594146.5	-30	-31.4	Israel's electric corparation - report (1982)
Hadera power plant/37	Clay/Sand	675269.95	3594146.5	-31.4	-32.9	Israel's electric corparation - report (1982)
Hadera power plant/37	Sandstone	675269.95	3594146.5	-32.9	-60.9	Israel's electric corparation - report (1982)
Hadera power plant/38	Sand	675577.14	3594139.9	-19	-24	Israel's electric corparation - report (1982)
Hadera power plant/38	Clay/Sand	675577.14	3594139.9	-24	-29.8	Israel's electric corparation - report (1982)
Hadera power plant/38	Sandstone	675577.14	3594139.9	-29.8	-59.8	Israel's electric corparation - report (1982)
Hadera power plant/39	Sand	675712.98	3594148.7	-17.5	-23	Israel's electric corparation - report (1982)
Hadera power plant/39	Sandstone	675712.98	3594148.7	-23	-58.5	Israel's electric corparation - report (1982)
Hadera power plant/4	Sand	676400.67	3593491.8	-7.8	-9.8	Israel's electric corparation - report (1982)
Hadera power plant/4	Clay	676400.67	3593491.8	-9.8	-13	Israel's electric corparation - report (1982)
Hadera power plant/4	Sandstone	676400.67	3593491.8	-13	-13.2	Israel's electric corparation - report (1982)
Hadera power plant/40	Sand	675887.35	3594132.3	-15.5	-20	Israel's electric corparation - report (1982)
Hadera power plant/40	Clay/Sand	675887.35	3594132.3	-20	-25	Israel's electric corparation - report (1982)
Hadera power plant/40	Sandstone	675887.35	3594132.3	-25	-56.25	Israel's electric corparation - report (1982)
Hadera power plant/41	Sand	676055.18	3594141.8	-13.5	-19.5	Israel's electric corparation - report (1982)
Hadera power plant/41	Clay/Sand	676055.18	3594141.8	-19.5	-22	Israel's electric corparation - report (1982)
Hadera power plant/41	Sandstone	676055.18	3594141.8	-22	-55	Israel's electric corparation - report (1982)
Hadera power plant/42	Sand	676171.68	3594167.2	-12	-17	Israel's electric corparation - report (1982)
Hadera power plant/42	Clay/Sand	676171.68	3594167.2	-17	-20.2	Israel's electric corparation - report (1982)
Hadera power plant/42	Sand	676171.68	3594167.2	-20.2	-22.2	Israel's electric corparation - report (1982)
Hadera power plant/42	Sandstone	676171.68	3594167.2	-22.2	-52	Israel's electric corparation - report (1982)
Hadera power plant/43	Sand	676319.38	3594134.2	-9.5	-14	Israel's electric corparation - report (1982)
Hadera power plant/43	Clay/Sand	676319.38	3594134.2	-14	-14.5	Israel's electric corparation - report (1982)
Hadera power plant/43	Sand	676319.38	3594134.2	-14.5	-15	Israel's electric corparation - report (1982)

Hadera power plant/43	Sandstone	676319.38	3594134.2	-15	-55.6	Israel's electric corparation - report (1982)
Hadera power plant/44	Sand	676421.19	3594144.3	-8.5	-24.3	Israel's electric corparation - report (1982)
Hadera power plant/44	Clay/Sand	676421.19	3594144.3	-24.3	-25.3	Israel's electric corparation - report (1982)
Hadera power plant/44	Sandstone	676421.19	3594144.3	-25.3	-50.5	Israel's electric corparation - report (1982)
Hadera power plant/45	Sandstone	676581.15	3594147.6	-8.5	-53.7	Israel's electric corparation - report (1982)
Hadera power plant/46	Sand	677226.08	3594157	-1.7	-6	Israel's electric corparation - report (1982)
Hadera power plant/46	Sand/Silt	677226.08	3594157	-6	-6.5	Israel's electric corparation - report (1982)
Hadera power plant/46	Sandstone	677226.08	3594157	-6.5	-27	Israel's electric corparation - report (1982)
Hadera power plant/47	Sand	675022.7	3593914.4	-25.7	-30.3	Israel's electric corparation - report (1982)
Hadera power plant/47	Clay/Sand	675022.7	3593914.4	-30.3	-34	Israel's electric corparation - report (1982)
Hadera power plant/47	Sand/Silt	675022.7	3593914.4	-34	-35	Israel's electric corparation - report (1982)
Hadera power plant/47	Sandstone	675022.7	3593914.4	-35	-67	Israel's electric corparation - report (1982)
Hadera power plant/48	Sand	675081.96	3593660.6	-25.5	-29	Israel's electric corparation - report (1982)
Hadera power plant/48	Sand/Silt	675081.96	3593660.6	-29	-33.2	Israel's electric corparation - report (1982)
Hadera power plant/48	Clay/Sand	675081.96	3593660.6	-33.2	-35	Israel's electric corparation - report (1982)
Hadera power plant/48	Sandstone	675081.96	3593660.6	-35	-66.3	Israel's electric corparation - report (1982)
Hadera power plant/5	Sand	676197.08	3593518.6	-10	-12	Israel's electric corparation - report (1982)
Hadera power plant/5	Sand/Gravel	676197.08	3593518.6	-12	-14	Israel's electric corparation - report (1982)
Hadera power plant/5	Clay	676197.08	3593518.6	-14	-15.2	Israel's electric corparation - report (1982)
Hadera power plant/6	Sand	676029.09	3593468.1	-11.7	-12.7	Israel's electric corparation - report (1982)
Hadera power plant/6	Sand with shells	676029.09	3593468.1	-12.7	-14.7	Israel's electric corparation - report (1982)
Hadera power plant/6	Sand	676029.09	3593468.1	-14.7	-15.8	Israel's electric corparation - report (1982)
Hadera power plant/6	Clay	676029.09	3593468.1	-15.8	-17.2	Israel's electric corparation - report (1982)
Hadera power plant/7	Sand	675909.2	3593510.6	-13.5	-15	Israel's electric corparation - report (1982)
Hadera power plant/7	Sand with shells	675909.2	3593510.6	-15	-17.6	Israel's electric corparation - report (1982)
Hadera power plant/7	Clay	675909.2	3593510.6	-17.6	-19.2	Israel's electric corparation - report (1982)
Hadera power plant/8	Sand	675709.42	3593546.5	-16	-17	Israel's electric corparation - report (1982)
Hadera power plant/8	Sand with shells	675709.42	3593546.5	-17	-21.7	Israel's electric corparation - report (1982)
Hadera power plant/8	Clay	675709.42	3593546.5	-21.7	-22	Israel's electric corparation - report (1982)

Hadera power plant/9	Sand	675575.89	3593667.8	-18	-24.8	Israel's electric corparation - report (1982)
Hadera power plant/9	Clay	675575.89	3593667.8	-24.8	-25.8	Israel's electric corparation - report (1982)
Hadera power plant-2	Sand	677603.91	3593974.7	5	-1	Israel's electric corparation - report (1982)
Hadera power plant-2	Clay	677603.91	3593974.7	-1	-7	Israel's electric corparation - report (1982)
Hadera power plant-2	Clay/Sand	677603.91	3593974.7	-7	-8	Israel's electric corparation - report (1982)
Hadera power plant-2	Sandstone	677603.91	3593974.7	-8	-13	Israel's electric corparation - report (1982)
Hadera/A1	Sand	677272	3594375	6	-0.2	The hydrological survice of Israel - report
Hadera/A1	Sand/Gravel	677272	3594375	-0.2	-1.5	The hydrological survice of Israel - report
Hadera/A1	Clay/Sand	677272	3594375	-1.5	-3.5	The hydrological survice of Israel - report
Hadera/A1	Clay	677272	3594375	-3.5	-4.5	The hydrological survice of Israel - report
Hadera/A10	Sand	677001	3594456	-5.5	-6.8	The hydrological survice of Israel - report
Hadera/A10	Sand/Gravel	677001	3594456	-6.8	-8	The hydrological survice of Israel - report
Hadera/A10	Clay/Sand	677001	3594456	-8	-9	The hydrological survice of Israel - report
Hadera/A10	Sandstone	677001	3594456	-9	-9.5	The hydrological survice of Israel - report
Hadera/A2	Sand	677241	3594381	5	-0.5	The hydrological survice of Israel - report
Hadera/A2	Clay	677241	3594381	-0.5	-1	The hydrological survice of Israel - report
Hadera/A2	Sand/Gravel	677241	3594381	-1	-2	The hydrological survice of Israel - report
Hadera/A2	Sand	677241	3594381	-2	-4	The hydrological survice of Israel - report
Hadera/A2	Clay	677241	3594381	-4	-5	The hydrological survice of Israel - report
Hadera/A3	Sand	677217	3594392	4	-1	The hydrological survice of Israel - report
Hadera/A3	Sandstone	677217	3594392	-1	-1.5	The hydrological survice of Israel - report
Hadera/A4	Sand	677186.5	3594403.5	2	-4.5	The hydrological survice of Israel - report
Hadera/A4	Clay/Sand	677186.5	3594403.5	-4.5	-5.5	The hydrological survice of Israel - report
Hadera/A4	Sand/Gravel	677186.5	3594403.5	-5.5	-6.5	The hydrological survice of Israel - report
Hadera/A4	Clay	677186.5	3594403.5	-6.5	-8.5	The hydrological survice of Israel - report
Hadera/A4	Sandstone	677186.5	3594403.5	-8.5	-9.5	The hydrological survice of Israel - report
Hadera/A5	Sand	677118	3594416	-1.5	-4.5	The hydrological survice of Israel - report
Hadera/A5	Sand/Gravel	677118	3594416	-4.5	-5	The hydrological survice of Israel - report
Hadera/A5	Clay/Sand	677118	3594416	-5	-6.5	The hydrological survice of Israel - report
Hadera/A5	Clay	677118	3594416	-6.5	-7	The hydrological survice of Israel - report
Hadera/A6	Sand	677095	3594420	-2	-4	The hydrological survice of Israel - report
Hadera/A6	Sand/Gravel	677095	3594420	-4	-4.5	The hydrological survice of Israel - report
Hadera/A6	Clay/Sand	677095	3594420	-4.5	-6	The hydrological survice of Israel - report
Hadera/A6	Clay	677095	3594420	-6	-7	The hydrological survice of Israel - report
Hadera/A7	Sand	677088	3594423	-3	-4.3	The hydrological survice of Israel - report
Hadera/A7	Sand/Gravel	677088	3594423	-4.3	-5.3	The hydrological survice of Israel - report
Hadera/A7	Clay/Sand	677088	3594423	-5.3	-7.8	The hydrological survice of Israel - report
Hadera/A7	Clay	677088	3594423	-7.8	-8.3	The hydrological survice of Israel - report
Hadera/A7	Sandstone	677088	3594423	-8.3	-8.6	The hydrological survice of Israel - report
Hadera/A8	Sand	677055	3594440	-4	-5.5	The hydrological survice of Israel - report
Hadera/A8	Sand/Gravel	677055	3594440	-5.5	-6.5	The hydrological survice of Israel - report
Hadera/A8	Clay/Sand	677055	3594440	-6.5	-8.5	The hydrological survice of Israel - report
Hadera/A8	Sandstone	677055	3594440	-8.5	-9	The hydrological survice of Israel - report
Hadera/A9	Sand	677027	3594452	-5	-6.5	The hydrological survice of Israel - report
Hadera/A9	Sand/Gravel	677027	3594452	-6.5	-7.5	The hydrological survice of Israel - report
Hadera/A9	Clay/Sand	677027	3594452	-7.5	-8.5	The hydrological survice of Israel - report
Hadera/A9	Sandstone	677027	3594452	-8.5	-9	The hydrological survice of Israel - report
Hadera/B1	Sand	677224	3594377	2.5	-4	The hydrological survice of Israel - report
Hadera/B1	Sand/Gravel	677224	3594377	-4	-4.5	The hydrological survice of Israel - report

Hadera/B1	Clay/Sand	677224	3594377	-4.5	-6	The hydrological survice of Israel - report
Hadera/B1	Clay	677224	3594377	-6	-7	The hydrological survice of Israel - report
Hadera/B2	Sand	677194	3594386.5	1.5	-3.2	The hydrological survice of Israel - report
Hadera/B2	Clay/Sand	677194	3594386.5	-3.2	-5.2	The hydrological survice of Israel - report
Hadera/B2	Sand/Gravel	677194	3594386.5	-5.2	-6.5	The hydrological survice of Israel - report
Hadera/B2	Sandstone	677194	3594386.5	-6.5	-7.5	The hydrological survice of Israel - report
Hadera/B3	Sand	677138	3594399.8	-1.8	-5	The hydrological survice of Israel - report
Hadera/B3	Sand/Gravel	677138	3594399.8	-5	-6	The hydrological survice of Israel - report
Hadera/B3	Clay/Sand	677138	3594399.8	-6	-7	The hydrological survice of Israel - report
Hadera/B3	Clay	677138	3594399.8	-7	-7.8	The hydrological survice of Israel - report
Hadera/B4	Sand	677106	3594407	-2	-4	The hydrological survice of Israel - report
Hadera/B4	Sand/Gravel	677106	3594407	-4	-5	The hydrological survice of Israel - report
Hadera/B4	Clay/Sand	677106	3594407	-5	-7	The hydrological survice of Israel - report
Hadera/B4	Clay	677106	3594407	-7	-8.4	The hydrological survice of Israel - report
Hadera/B5	Sand	677078.5	3594411	-2.9	-4.7	The hydrological survice of Israel - report
Hadera/B5	Sand/Gravel	677078.5	3594411	-4.7	-5.7	The hydrological survice of Israel - report
Hadera/B5	Clay/Sand	677078.5	3594411	-5.7	-7.9	The hydrological survice of Israel - report
Hadera/B5	Clay	677078.5	3594411	-7.9	-8.9	The hydrological survice of Israel - report
Hadera/B6	Sand	677043	3594423	-3.9	-5.4	The hydrological survice of Israel - report
Hadera/B6	Sand/Gravel	677043	3594423	-5.4	-6.7	The hydrological survice of Israel - report
Hadera/B6	Clay/Sand	677043	3594423	-6.7	-8.2	The hydrological survice of Israel - report
Hadera/B6	Sandstone	677043	3594423	-8.2	-10.3	The hydrological survice of Israel - report
Hadera/B7	Sand	677015	3594436	-4.5	-6	The hydrological survice of Israel - report
Hadera/B7	Sand/Gravel	677015	3594436	-6	-7.5	The hydrological survice of Israel - report
Hadera/B7	Clay/Sand	677015	3594436	-7.5	-8.5	The hydrological survice of Israel - report
Hadera/B7	Clay	677015	3594436	-8.5	-9	The hydrological survice of Israel - report
Hadera/B8	Sand	676986.5	3594440.8	-5	-6.5	The hydrological survice of Israel - report
Hadera/B8	Sand/Gravel	676986.5	3594440.8	-6.5	-7.5	The hydrological survice of Israel - report
Hadera/B8	Clay/Sand	676986.5	3594440.8	-7.5	-8.5	The hydrological survice of Israel - report
Hadera/B8	Sandstone	676986.5	3594440.8	-8.5	-10	The hydrological survice of Israel - report
Havazelet hasharon	Sand	674877.54	3581656.3	21	14	The hydrological survice of Israel - report
Havazelet hasharon	Sandstone	674877.54	3581656.3	14	-23	The hydrological survice of Israel - report
Hotel galli-hanaz	Sand	674457.92	3580177.5	19	17.5	The hydrological survice of Israel - report
Hotel galli-hanaz	Sandstone	674457.92	3580177.5	17.5	14	The hydrological survice of Israel - report
Intermidiate mole Caesarea2	Sandstone	677635.56	3597717.1	-2.9	-4.3	The hydrological survice of Israel - report
Iria/natania	Paleosol	674276.31	3576853.2	44.5	43.4	The hydrological survice of Israel - report
Iria/natania	Sandstone	674276.31	3576853.2	43.4	37.4	The hydrological survice of Israel - report
K1/railtrack	Sand	678036.08	3590193	9	6.4	Israel's Railways-report
K1/railtrack	Sand	678036.08	3590193	6.4	3	Israel's Railways-report
k2/railtrack	Sand/Silt	677854.31	3589841.2	10	8	Israel's Railways-report
k2/railtrack	Sand	677854.31	3589841.2	8	6.5	Israel's Railways-report
k2/railtrack	Sand/Silt	677854.31	3589841.2	6.5	5	Israel's Railways-report
k34/Caesarea	Loam	678769.55	3597099.4	15	9	Israel's Railways-report
k34/Caesarea	Sandstone	678769.55	3597099.4	9	0	Israel's Railways-report
K4/railtrack	Sand/Silt	677704.46	3589056.9	5	1	Israel's Railways-report
K5/railtrack	Sand/Silt	677618.01	3588448	7	1	Israel's Railways-report
K6/railtrack	Sand	677616.45	3588038.9	19	15	Israel's Railways-report
Kisaria/1	Sand	680325.05	3598781.9	15	1.5	The hydrological survice of Israel - report
Kisaria/2	Sand	680325.05	3598781.9	15	13.5	The hydrological survice of Israel - report
Kisaria/2	Clay/Sand	680325.05	3598781.9	13.5	-3	The hydrological survice of Israel - report
Kisaria/2	Sandstone	680325.05	3598781.9	-3	-14	The hydrological survice of Israel - report
Michmoret	Loam	677043.72	3587002.9	32.2	25.6	The hydrological survice of Israel - report
Michmoret	Sand	677043.72	3587002.9	25.6	24.7	The hydrological survice of Israel - report
Michmoret	Sandstone	677043.72	3587002.9	24.7	8	The hydrological survice of Israel - report

Miramar/michmoret	Loam	675880.81	3587328	4.6	-5.4	The hydrological survice of Israel - report
Miramar/michmoret	Sand	675880.81	3587328	-5.4	-15.4	The hydrological survice of Israel - report
Miramar/michmoret	Sandstone	675880.81	3587328	-15.4	-36.4	The hydrological survice of Israel - report
Nastisin/Hadera	Loam	677098.63	3588413.3	10.6	8.6	The hydrological survice of Israel - report
Nastisin/Hadera	Sandstone	677098.63	3588413.3	8.6	-10.4	The hydrological survice of Israel - report
Natanya 18	Sand with shells	673357.33	3580859	13	11.65	The hydrological survice of Israel - report
Natanya 18	Sand/Gravel	673357.33	3580859	11.65	11.15	The hydrological survice of Israel - report
Natanya 18	Sandstone	673357.33	3580859	11.15	7.5	The hydrological survice of Israel - report
Natanya 19	Sand/Gravel	672123.51	3580859.5	28.5	27.15	The hydrological survice of Israel - report
Natanya 19	Silt/Clay	672123.51	3580859.5	27.15	25	The hydrological survice of Israel - report
Natanya 20	Sand	673511.87	3582163.3	16.5	12.65	The hydrological survice of Israel - report
Natanya 20	Silt/Clay	673511.87	3582163.3	12.65	11.5	The hydrological survice of Israel - report
Natanya 21	Paleosol	673696.01	3582178.3	13	9.5	The hydrological survice of Israel - report
Natanya 21	Loam	673696.01	3582178.3	9.5	7.65	The hydrological survice of Israel - report
Natanya 21	Sandstone	673696.01	3582178.3	7.65	5	The hydrological survice of Israel - report
Natanya 22	Sandstone	673135.69	3582785.2	18	16.5	The hydrological survice of Israel - report
Nativ/ Beit yehoshoa	Loam	675654.25	3570640.5	22.14	0.14	The hydrological survice of Israel - report
Nativ/ Beit yehoshoa	Sandstone	675654.25	3570640.5	0.14	-2.86	The hydrological survice of Israel - report
Natnia-Cityhall 41	Clay	675258.32	3572872.7	21	21	The hydrological survice of Israel - report
Natnia-Cityhall 41	Sand	675258.32	3572872.7	21	14.59	The hydrological survice of Israel - report
Natnia-Cityhall 41	Clay	675258.32	3572872.7	14.59	8.08	The hydrological survice of Israel - report
Natnia-Cityhall 41	Loam	675258.32	3572872.7	8.08	8	The hydrological survice of Israel - report
Natnia-Cityhall 41	Clay	675258.32	3572872.7	8	3.74	The hydrological survice of Israel - report
Natnia-Cityhall 41	Clay	675258.32	3572872.7	3.74	2.65	The hydrological survice of Israel - report
Natnia-Cityhall 41	Clay	675258.32	3572872.7	2.65	-3	The hydrological survice of Israel - report
Natnia-Cityhall 41	Loam	675258.32	3572872.7	-3	-12.01	The hydrological survice of Israel - report
Natnia-Cityhall 41	Sand/Gravel	675258.32	3572872.7	-12.01	-16.35	The hydrological survice of Israel - report
Natnia-Cityhall 41	Sandstone	675258.32	3572872.7	-16.35	-22.87	The hydrological survice of Israel - report
Natnia-Cityhall 41	Sandstone	675258.32	3572872.7	-22.87	-27	The hydrological survice of Israel - report
NH/1 caesarea	Clay/Sand	677019	3592125.3	7.5	2.5	The hydrological survice of Israel - report
NH/1 caesarea	Sandstone	677019	3592125.3	2.5	-42.5	The hydrological survice of Israel - report
NH/10 caesarea	Clay/Sand	677513.4	3596563.3	6	4.5	The hydrological survice of Israel - report
NH/10 caesarea	Sandstone	677513.4	3596563.3	4.5	0.5	The hydrological survice of Israel - report
NH/11a caesarea	Sand	678146.44	3596276.4	5.1	4.1	The hydrological survice of Israel - report
NH/11a caesarea	Sand/Gravel	678146.44	3596276.4	4.1	1.1	The hydrological survice of Israel - report
NH/11a caesarea	Sandstone	678146.44	3596276.4	1.1	-1.9	The hydrological survice of Israel - report
NH/12 caesarea	Sand	678649.73	3596218.8	14	13	The hydrological survice of Israel - report
NH/12 caesarea	Clay	678649.73	3596218.8	13	10	The hydrological survice of Israel - report
NH/12 caesarea	Sandstone	678649.73	3596218.8	10	-2.8	The hydrological survice of Israel - report
NH/14 caesarea	Sand	677739.15	3595657.8	6.5	-4	The hydrological survice of Israel - report
NH/14 caesarea	Loam	677739.15	3595657.8	-4	-7.5	The hydrological survice of Israel - report
NH/14 caesarea	Loam	677739.15	3595657.8	-7.5	-33.5	The hydrological survice of Israel - report
NH/15 caesarea	Sand	677703.17	3595947.1	5	3.5	The hydrological survice of Israel - report
NH/15 caesarea	Sand/Gravel	677703.17	3595947.1	3.5	0.5	The hydrological survice of Israel - report
NH/15 caesarea	Sandstone	677703.17	3595947.1	0.5	-5	The hydrological survice of Israel - report
NH/16 Caesarea	Loam	678381.44	3599421.8	4	2	The hydrological survice of Israel - report
NH/16 Caesarea	Sandstone	678381.44	3599421.8	2	-20	The hydrological survice of Israel - report
NH/2 Caesarea	Sand	677229.62	3592726.8	7	0	The hydrological survice of Israel - report
NH/2 Caesarea	Sandstone	677229.62	3592726.8	0	-7	The hydrological survice of Israel - report
NH/21 caesarea	Sand	678002.67	3594135	8	6	The hydrological survice of Israel - report

NH/21 caesarea	Sandstone	678002.67	3594135	6	2.7	The hydrological survice of Israel - report
NH/22 Caesarea	Sand	678653.03	3594026.4	20	17.5	The hydrological survice of Israel - report
NH/22 Caesarea	Sandstone	678653.03	3594026.4	17.5	-15	The hydrological survice of Israel - report
NH/24 caesarea	Sand	678157.11	3595276.4	6	4	The hydrological survice of Israel - report
NH/24 caesarea	Clay	678157.11	3595276.4	4	-6.7	The hydrological survice of Israel - report
NH/24 caesarea	Sandstone	678157.11	3595276.4	-6.7	-8	The hydrological survice of Israel - report
NH/25 Caesarea	Sand	678649.48	3595166.6	29	22	The hydrological survice of Israel - report
NH/25 Caesarea	Loam	678649.48	3595166.6	22	20	The hydrological survice of Israel - report
NH/25 Caesarea	Sandstone	678649.48	3595166.6	20	5	The hydrological survice of Israel - report
NH/26 Caesarea	Sandstone	678095.81	3594855.1	7	3	The hydrological survice of Israel - report
NH/27 caesarea	Sand with shells	677535.22	3595991.7	4.8	-5.2	The hydrological survice of Israel - report
NH/27 caesarea	Loam	677535.22	3595991.7	-5.2	-8.2	The hydrological survice of Israel - report
NH/27 caesarea	Sandstone	677535.22	3595991.7	-8.2	-25.2	The hydrological survice of Israel - report
NH/3 Caesarea	Sand	677197.52	3593796.3	5	2.5	The hydrological survice of Israel - report
NH/3 Caesarea	Siltstone	677197.52	3593796.3	2.5	-7.5	The hydrological survice of Israel - report
NH/4 Caesarea	Clay	677258	3594257.6	6	-4	The hydrological survice of Israel - report
NH/4 Caesarea	Sandstone	677258	3594257.6	-4	-11	The hydrological survice of Israel - report
NH/4a caesarea	Clay/Sand	677264.96	3594259.8	3.2	-2.3	The hydrological survice of Israel - report
NH/4a caesarea	Sandstone	677264.96	3594259.8	-2.3	-11.7	The hydrological survice of Israel - report
NH/5 caesarea	Sand	677874.5	3595400.6	4.5	1.5	The hydrological survice of Israel - report
NH/5 caesarea	Sandstone	677874.5	3595400.6	1.5	-19.1	The hydrological survice of Israel - report
NH/5413 caesarea	Sand	678099.07	3595665.3	5.6	-4.4	The hydrological survice of Israel - report
NH/5413 caesarea	Sandstone	678099.07	3595665.3	-4.4	-6.4	The hydrological survice of Israel - report
NH/548 caesarea	Sand	677893.43	3595791.1	4.6	-0.4	The hydrological survice of Israel - report
NH/548 caesarea	Sandstone	677893.43	3595791.1	-0.4	-35.4	The hydrological survice of Israel - report
NH/548-1 caesarea	Sand	678089.07	3595665.1	5.7	0.7	The hydrological survice of Israel - report
NH/548-1 caesarea	Sandstone	678089.07	3595665.1	0.7	-3.3	The hydrological survice of Israel - report
NH/6 caesarea	Sandstone	677392	3594936.5	4.9	-4.1	The hydrological survice of Israel - report
NH/9 caesarea	Sandstone	677559.49	3596559.3	6.5	-0.5	The hydrological survice of Israel - report
NH/9a caesarea	Sand	677573.73	3596160.5	6	0.5	The hydrological survice of Israel - report
NH/9a caesarea	Sandstone	677573.73	3596160.5	0.5	-1	The hydrological survice of Israel - report
NH/a19 caesarea	Sand	677969.92	3595332.5	5	3	The hydrological survice of Israel - report
NH/a19 caesarea	Sandstone	677969.92	3595332.5	3	1	The hydrological survice of Israel - report
NH/a8 caesarea	Sand/Gravel	677905.87	3595818.3	5.3	-2.2	The hydrological survice of Israel - report
NH/a8 caesarea	Sandstone	677905.87	3595818.3	-2.2	-33.7	The hydrological survice of Israel - report
NH/sh2 caesarea	Clay/Sand	677918.87	3596253.7	4.8	2.3	The hydrological survice of Israel - report
NH/sh2 caesarea	Sand	677918.87	3596253.7	2.3	-0.2	The hydrological survice of Israel - report
NH/sh2 caesarea	Sand/Gravel	677918.87	3596253.7	-0.2	-4.2	The hydrological survice of Israel - report
NH/sh2 caesarea	Clay	677918.87	3596253.7	-4.2	-8.7	The hydrological survice of Israel - report
NH/sh2 caesarea	Sandstone	677918.87	3596253.7	-8.7	-9.4	The hydrological survice of Israel - report
NH/sh3 caesarea	Sand	677910.2	3595947.4	6	4.8	The hydrological survice of Israel - report
NH/sh3 caesarea	Clay/Sand	677910.2	3595947.4	4.8	3	The hydrological survice of Israel - report
NH/sh3 caesarea	Sandstone	677910.2	3595947.4	3	2.3	The hydrological survice of Israel - report
NH/sh4 caesarea	Clay/Sand	677902.82	3595675.2	3.6	2.2	The hydrological survice of Israel - report
NH/sh4 caesarea	Sand	677902.82	3595675.2	2.2	-2.9	The hydrological survice of Israel - report
NH/sh4 caesarea	Sandstone	677902.82	3595675.2	-2.9	-10.9	The hydrological survice of Israel - report
NH5/ Caesarea	Sand	677341.16	3594589.4	5	0	The hydrological survice of Israel - report
NH5/ Caesarea	Sandstone	677341.16	3594589.4	0	-12	The hydrological survice of Israel - report
NH6/Caesarea	Sand	677394.12	3594930.6	6	5.5	The hydrological survice of Israel - report
NH6/Caesarea	Sandstone	677394.12	3594930.6	5.5	-9.5	The hydrological survice of Israel - report
Northern mole caesarea1	Sand	677295.35	3597821.1	-6.4	-8.1	Nir, Y., 1977. Jet drilling in the sea off the Hadera Electric power station site. GSI/MG/9/

Northern mole caesarea1	Sandstone	677295.35	3597821.1	-8.1	-10.4	Nir, Y., 1977. Jet drilling in the sea off the Hadera Electric power station site. GSI/MG/9/
Northern mole caesarea2	Sand	677317.37	3597820.5	-6.4	-7.6	Nir, Y., 1977. Jet drilling in the sea off the Hadera Electric power station site. GSI/MG/9/
Northern mole caesarea2	Sand with shells	677317.37	3597820.5	-7.6	-8.6	Nir, Y., 1977. Jet drilling in the sea off the Hadera Electric power station site. GSI/MG/9/
Northern mole caesarea2	Sand	677317.37	3597820.5	-8.6	-10.8	Nir, Y., 1977. Jet drilling in the sea off the Hadera Electric power station site. GSI/MG/9/
Northern mole caesarea2	Sandstone	677317.37	3597820.5	-10.8	-11	Nir, Y., 1977. Jet drilling in the sea off the Hadera Electric power station site. GSI/MG/9/
NRD/1	Clay	680814.55	3602869.8	3.5	-2.5	The hydrological survice of Israel - report
P. bur/caesarea	Sand	678684.06	3599298	8	4	The hydrological survice of Israel - report
P. bur/caesarea	Sandstone	678684.06	3599298	4	1.5	The hydrological survice of Israel - report
P. gur/caesarea	Sand	678848.67	3600236.6	12	9	The hydrological survice of Israel - report
P. gur/caesarea	Clay/Sand	678848.67	3600236.6	9	6.5	The hydrological survice of Israel - report
P. gur/caesarea	Sandstone	678848.67	3600236.6	6.5	3	The hydrological survice of Israel - report
P. kryzman/caesarea	Sand	679346.73	3600141.9	24	23	The hydrological survice of Israel - report
P. kryzman/caesarea	Loam	679346.73	3600141.9	23	22	The hydrological survice of Israel - report
P. kryzman/caesarea	Sandstone	679346.73	3600141.9	22	6.5	The hydrological survice of Israel - report
P. Yakum h	Silt/Clay	673923.51	3569834.8	11	3	The hydrological survice of Israel - report
P. Yakum h	Sand	673923.51	3569834.8	3	-6	The hydrological survice of Israel - report
P. Yakum h	Sandstone	673923.51	3569834.8	-6	-15	The hydrological survice of Israel - report
P.ozi/1 caesarea	Sand	678703.02	3599348.4	9	5	The hydrological survice of Israel - report
P.ozi/1 caesarea	Sandstone	678703.02	3599348.4	5	-2	The hydrological survice of Israel - report
Pakidim/bitan aharon	Sand	676301.31	3582455.8	18	2.5	The hydrological survice of Israel - report
Pakidim/bitan aharon	Loam	676301.31	3582455.8	2.5	-5	The hydrological survice of Israel - report
Pakidim/bitan aharon	Sand	676301.31	3582455.8	-5	-11.5	The hydrological survice of Israel - report
Pakidim/bitan aharon	Paleosol	676301.31	3582455.8	-11.5	-20.5	The hydrological survice of Israel - report
Pakidim/bitan aharon	Sandstone	676301.31	3582455.8	-20.5	-32	The hydrological survice of Israel - report
Pardes lita/vitkin	Sandstone	675761.05	3583434.8	9	1.2	The hydrological survice of Israel - report
Railtrack1	Sand	675856.56	3576270.6	15	14.2	Israel's Railways-report
Railtrack1	Clay/Sand	675856.56	3576270.6	14.2	12	Israel's Railways-report
Railtrack2	Clay/Sand	675859.67	3576799.8	14.8	13.9	Israel's Railways-report
Railtrack2	Sand	675859.67	3576799.8	13.9	13.2	Israel's Railways-report
Railtrack2	Clay/Sand	675859.67	3576799.8	13.2	12.6	Israel's Railways-report
Railtrack3	Sand	675892.68	3577091.5	21	20	Israel's Railways-report
Railtrack3	Clay/Sand	675892.68	3577091.5	20	18	Israel's Railways-report
Railtrack4	Sand	675996.96	3577807.8	18	16.2	Israel's Railways-report
Railtrack4	Clay/Sand	675996.96	3577807.8	16.2	16	Israel's Railways-report
Railtrack4	Clay	675996.96	3577807.8	16	15.6	Israel's Railways-report
Railtrack4	Sandstone	675996.96	3577807.8	15.6	15	Israel's Railways-report
Railtrack5	Clay/Sand	676092.92	3578150.8	23	20	Israel's Railways-report
Railtrack6	Sand	678658.87	3590692.9	10	7.5	Israel's Railways-report
Railtrack6	Sandstone	678658.87	3590692.9	7.5	7	Israel's Railways-report
Rosko/havazelet hashron	Sand	674663.77	3581691.9	25	18	The hydrological survice of Israel - report
Rosko/havazelet hashron	Sandstone	674663.77	3581691.9	18	8.5	The hydrological survice of Israel - report
Sdot-yam	Clay	678285.53	3597289.4	8	5.25	The hydrological survice of Israel - report
Sdot-yam	Sand	678285.53	3597289.4	5.25	2.75	The hydrological survice of Israel - report
Sdot-yam	Sandstone	678285.53	3597289.4	2.75	1.5	The hydrological survice of Israel - report

SecACaesarea SH3	Sand	679915.66	3598023.3	15	9	The hydrological survice of Israel - report
SecACaesarea SH3	Clay/Sand	679915.66	3598023.3	9	1	The hydrological survice of Israel - report
SecACaesarea SH3	Clay	679915.66	3598023.3	1	-10	The hydrological survice of Israel - report
SecACaesarea SH3	Clay/Sand	679915.66	3598023.3	-10	-13	The hydrological survice of Israel - report
SecACaesarea SH3	Sandstone	679915.66	3598023.3	-13	-55	The hydrological survice of Israel - report
SecB56A/Caesarea	Sand	678553.06	3599345.3	6	0	The hydrological survice of Israel - report
SecB56A/Caesarea	Clay/Sand	678553.06	3599345.3	0	-6	The hydrological survice of Israel - report
SecB56A/Caesarea	Sandstone	678553.06	3599345.3	-6	-12	The hydrological survice of Israel - report
SecBCaesarea N.H.16	Sand	678403.85	3598822.2	6	0	The hydrological survice of Israel - report
SecBCaesarea N.H.16	Sandstone	678403.85	3598822.2	0	-6	The hydrological survice of Israel - report
SecBCaesarea SH3	Sand	678568.57	3598595.5	15	9	The hydrological survice of Israel - report
SecBCaesarea SH3	Sandstone	678568.57	3598595.5	9	-5	The hydrological survice of Israel - report
Sharone north 16	Loam	676402.04	3569877.7	32.27	27.27	The hydrological survice of Israel - report
Sharone north 16	Sandstone	676402.04	3569877.7	27.27	0.27	The hydrological survice of Israel - report
Southern Mole Caesarea1	Sand/Gravel	677302.99	3597790.2	-6.7	-7.1	The hydrological survice of Israel - report
Southern Mole Caesarea1	Sand	677302.99	3597790.2	-7.1	-12	The hydrological survice of Israel - report
Southern Mole Caesarea1	Sandstone	677302.99	3597790.2	-12	-12.2	The hydrological survice of Israel - report
T/1 caesarea	Sand	679319.08	3599061.1	13	11.5	The hydrological survice of Israel - report
T/1 caesarea	Clay	679319.08	3599061.1	11.5	5	The hydrological survice of Israel - report
T/1 caesarea	Sandstone	679319.08	3599061.1	5	3	The hydrological survice of Israel - report
T/1143 Natania	Sandstone	673765.13	3573843.2	36.78	-40.22	The hydrological survice of Israel - report
T/1153 hadera	Clay/Sand	678149.3	3593282.9	20.2	17.2	The hydrological survice of Israel - report
T/1153 hadera	Sandstone	678149.3	3593282.9	17.2	14.2	The hydrological survice of Israel - report
T/1154-caesarea	Sand	678036.19	3595416.9	4.9	0.9	The hydrological survice of Israel - report
T/1154-caesarea	Clay/Sand	678036.19	3595416.9	0.9	-5.1	The hydrological survice of Israel - report
T/1154-caesarea	Silt/Clay	678036.19	3595416.9	-5.1	-8.1	The hydrological survice of Israel - report
T/1154-caesarea	Sandstone	678036.19	3595416.9	-8.1	-11.1	The hydrological survice of Israel - report
T/1156 caesarea	Sand/Silt	678694.42	3599812.4	4	1	The hydrological survice of Israel - report
T/1156 caesarea	Sandstone	678694.42	3599812.4	1	-5	The hydrological survice of Israel - report
T/2 caesarea	Sand	679454.56	3599764.1	14	11	The hydrological survice of Israel - report
T/2 caesarea	Silt	679454.56	3599764.1	11	10.5	The hydrological survice of Israel - report
T/2 caesarea	Sandstone	679454.56	3599764.1	10.5	8	The hydrological survice of Israel - report
T/2153 hadera	Clay/Sand	678149.36	3593279.9	20.2	17.2	The hydrological survice of Israel - report
T/2153 hadera	Sandstone	678149.36	3593279.9	17.2	14.2	The hydrological survice of Israel - report
T/2154 caesarea	Sand	678036.13	3595419.9	4.9	0.9	The hydrological survice of Israel - report
T/2154 caesarea	Clay/Sand	678036.13	3595419.9	0.9	-5.1	The hydrological survice of Israel - report
T/2154 caesarea	Silt/Clay	678036.13	3595419.9	-5.1	-8.1	The hydrological survice of Israel - report
T/2154 caesarea	Sandstone	678036.13	3595419.9	-8.1	-11.1	The hydrological survice of Israel - report
T/2156 caesarea	Sand/Silt	678691.75	3599796.3	3	0	The hydrological survice of Israel - report
T/2156 caesarea	Sandstone	678691.75	3599796.3	0	-6	The hydrological survice of Israel - report
T/4156 caesarea	Sand/Silt	678686.73	3599797.2	3	0	The hydrological survice of Israel - report
T/4156 caesarea	Sand/Silt	678686.73	3599797.2	0	-6	The hydrological survice of Israel - report
T/5156 caesarea	Sand/Silt	678696.81	3599793.4	3	0	The hydrological survice of Israel - report
T/5156 caesarea	Sandstone	678696.81	3599793.4	0	-6	The hydrological survice of Israel - report
T1/michmoret	Sand	675467.48	3586419.3	3.9	0.9	The hydrological survice of Israel - report
T1/michmoret	Sandstone	675467.48	3586419.3	0.9	-26.1	The hydrological survice of Israel - report
T1149/alexander	Clay/Sand	676394.47	3585263.2	7.2	6.2	The hydrological survice of Israel - report
T1149/alexander	Sandstone	676394.47	3585263.2	6.2	-43.8	The hydrological survice of Israel - report
T2/ taninim	Sand	678989.9	3601434.8	5.5	2.5	The hydrological survice of Israel - report
T2/ taninim	Clay	678989.9	3601434.8	2.5	-0.5	The hydrological survice of Israel - report
T2/ taninim	Sand/Silt	678989.9	3601434.8	-0.5	-3.5	The hydrological survice of Israel - report
T2/ taninim	Sandstone	678989.9	3601434.8	-3.5	-15.5	The hydrological survice of Israel - report
T2/michmoret	Sandstone	675530.53	3586223.6	3	-2	The hydrological survice of Israel - report

T2/vitkin	Clay/Sand	675807.11	3582655.7	20	17.3	The hydrological survice of Israel - report
T2/vitkin	Sand	675807.11	3582655.7	17.3	-0.7	The hydrological survice of Israel - report
T2/vitkin	Sandstone	675807.11	3582655.7	-0.7	-2.3	The hydrological survice of Israel - report
T2149/alexander	Clay/Sand	676392.52	3585261.2	7.2	6.2	The hydrological survice of Israel - report
T2149/alexander	Sandstone	676392.52	3585261.2	6.2	-43.8	The hydrological survice of Israel - report
T3/ taninim	Clay	680128.19	3601528.3	6	-7	The hydrological survice of Israel - report
T3/ taninim	Sandstone	680128.19	3601528.3	-7	-9	The hydrological survice of Israel - report
T4149/alexander	Clay/Sand	676390.5	3585262.1	7.2	6.2	The hydrological survice of Israel - report
T4149/alexander	Sandstone	676390.5	3585262.1	6.2	-18.8	The hydrological survice of Israel - report
Taninim C	Sand	678854.37	3601691.6	-0.04	-0.74	The hydrological survice of Israel - report
Taninim C	Clay	678854.37	3601691.6	-0.74	-1.19	The hydrological survice of Israel - report
Taninim C	Clayey Sand	678854.37	3601691.6	-1.19	-5.46	The hydrological survice of Israel - report
Taninim C	Loam	678854.37	3601691.6	-5.46	-7.89	The hydrological survice of Israel - report
Taninim C	Sandstone	678854.37	3601691.6	-7.89	-9.04	The hydrological survice of Israel - report
Taninim river	Clay	680541.96	3600866.8	6.5	5.3	The hydrological survice of Israel - report
Taninim river	Sandstone	680541.96	3600866.8	5.3	3.2	The hydrological survice of Israel - report
Taninim/4T	Sand	679000.92	3602835.3	4.3	-0.7	The hydrological survice of Israel - report
Taninim/4T	Clay/Sand	679000.92	3602835.3	-0.7	-2.7	The hydrological survice of Israel - report
Taninim/4T	Sandstone	679000.92	3602835.3	-2.7	-15.7	The hydrological survice of Israel - report
Taninim/5T	Clay	680833.86	3603193.3	4.3	-0.37	The hydrological survice of Israel - report
Taninim/5T	Sandstone	680833.86	3603193.3	-0.37	-4.2	The hydrological survice of Israel - report
Taninim/Amok	Clay	680541.96	3600866.8	5.6	-6.4	The hydrological survice of Israel - report
Taninim/Amok	Sandstone	680541.96	3600866.8	-6.4	-27.4	The hydrological survice of Israel - report
Taninim/T2	Sand	679989.67	3601455.5	5.6	2.6	The hydrological survice of Israel - report
Taninim/T2	Clay	679989.67	3601455.5	2.6	-0.4	The hydrological survice of Israel - report
Taninim/T3	Clay	679828.88	3601492.2	5.9	-7.1	The hydrological survice of Israel - report
Tb/50-givat olga	Sandstone	677095.01	3588104.2	22.1	16.1	The hydrological survice of Israel - report
TF1/Hadera	Sand	677514.81	3593736.8	4.5	-0.3	The hydrological survice of Israel - report
TF1/Hadera	Clay	677514.81	3593736.8	-0.3	-1.8	The hydrological survice of Israel - report
TF1/Hadera	Sand	677514.81	3593736.8	-1.8	-4.5	The hydrological survice of Israel - report
TF1/Hadera	Sandstone	677514.81	3593736.8	-4.5	-7.5	The hydrological survice of Israel - report
Top Kanoman-natania	Loam	675982.36	3574627.9	25	-7	The hydrological survice of Israel - report
Top Kanoman-natania	Clay/Sand	675982.36	3574627.9	-7	-25	The hydrological survice of Israel - report
Top Kanoman-natania	Sandstone	675982.36	3574627.9	-25	-75	The hydrological survice of Israel - report
V/Vitkin	Sand	676421.51	3584388.6	28.4	26.4	The hydrological survice of Israel - report
V/Vitkin	Loam	676421.51	3584388.6	26.4	21.4	The hydrological survice of Israel - report
V/Vitkin	Sandstone	676421.51	3584388.6	21.4	14.9	The hydrological survice of Israel - report
v101-marine	Sand	671386.85	3583604.7	-36.5	-36.7	Artifical Island Project-report 2003
v101-marine	Silt/Clay	671386.85	3583604.7	-36.7	-43.4	Artifical Island Project-report 2003
v101-marine	Sand	671386.85	3583604.7	-43.4	-44.4	Artifical Island Project-report 2003
v102-marine	Silt/Clay	670780.68	3580501.8	-35.2	-43.1	Artifical Island Project-report 2003
v103-marine	Silt/Clay	670084.28	3580807.5	-38	-40.5	Artifical Island Project-report 2003
v103-marine	Sandstone	670084.28	3580807.5	-40.5	-42.4	Artifical Island Project-report 2003
v104-marina	Silt/Clay	667877.66	3579171.8	-46.6	-54.5	Artifical Island Project-report 2003
v1-marine	Silt	671392.94	3594794.5	-47	-53.5	Artifical Island Project-report 2003
v2-marine	Clay	672774.73	3591474.6	-38.5	-41.4	Artifical Island Project-report 2003
v2-marine	Sand	672774.73	3591474.6	-41.4	-43.5	Artifical Island Project-report 2003
v4-marine	Silt/Clay	669586	3590033.5	-46.9	-54.8	Artifical Island Project-report 2003
v65-marine	Silt/Clay	666510.2	3586514.6	-54.1	-62	Artifical Island Project-report 2003
v6-marine	Silt/Clay	671254.62	3585652.3	-39.7	-47.6	Artifical Island Project-report 2003
v7-marine	Silt/Clay	668893.18	3585075.6	-45.7	-53.6	Artifical Island Project-report 2003
Vinget-Natania	Sandstone	673102.03	3570728.1	15	-45	The hydrological survice of Israel - report
Yakom B	Loam	673470.5	3570805.7	13.6	12.1	The hydrological survice of Israel - report
Yakom B	Sandstone	673470.5	3570805.7	12.1	-0.2	The hydrological survice of Israel - report

Yakom H	Silt/Clay	673930.57	3569344.9	7.22	5.22	The hydrological survice of Israel - report
Yakom H	Sandstone	673930.57	3569344.9	5.22	0.72	The hydrological survice of Israel - report
Hps16	Sand	675479.85	3594346.6	-21	-26	Israel's electric corparation - report (1982)
Hps16	Clay	675479.85	3594346.6	-26	-30	Israel's electric corparation - report (1982)
Hps16	Sand/Clay	675479.85	3594346.6	-30	-32	Israel's electric corparation - report (1982)
Hps16	Sandstone	675479.85	3594346.6	-32	-40	Israel's electric corparation - report (1982)
Hps22	Sand	676095.91	3594203.6	-12	-18	Israel's electric corparation - report (1982)
Hps22	Sand/Clay	676095.91	3594203.6	-18	-21	Israel's electric corparation - report (1982)
Hps22	Sandstone	676095.91	3594203.6	-21	-27	Israel's electric corparation - report (1982)
Hps39	Sand with shells	675399	3594200	-22	-25	Israel's electric corparation - report (1982)
Hps39	Clay	675399	3594200	-25	-30	Israel's electric corparation - report (1982)
Hps39	Sand/Clay	675399	3594200	-30	-31	Israel's electric corparation - report (1982)
Hps39	Sand/Silt	675399	3594200	-31	-33	Israel's electric corparation - report (1982)
Hps39	Sandstone	675399	3594200	-33	-40	Israel's electric corparation - report (1982)
Hps48	Sand	676796.92	3594160.8	-4.5	-11	Israel's electric corparation - report (1982)
Hps48	Sandstone	676796.92	3594160.8	-11	-20	Israel's electric corparation - report (1982)
Hps50	Sand	677049.87	3594159.6	-1.7	-6	Israel's electric corparation - report (1982)
Hps50	Sand/Clay	677049.87	3594159.6	-6	-7	Israel's electric corparation - report (1982)
Hps50	Sandstone	677049.87	3594159.6	-7	-20	The hydrological survice of Israel - report
NH3_C	Sand	677197.52	3593796.3	5	2.5	The hydrological survice of Israel - report
NH3_C	Sandstone	677197.52	3593796.3	2.5	-7.5	The hydrological survice of Israel - report
Caesarea26	Shell/sand	675650.94	3598237	-28.5	-31.85	The hydrological survice of Israel - report
Caesarea26	Sand/Clay	675650.94	3598237	-31.82	-32.85	The hydrological survice of Israel - report
Caesarea26	Clay	675650.94	3598237	-32.85	-35	The hydrological survice of Israel - report
Caesarea25	Shell/sand	676409.21	3598087	-18.5	-23.5	The hydrological survice of Israel - report
Caesarea25	Sand	676409.21	3598087	-23.5	-25.25	The hydrological survice of Israel - report
Caesarea25	Kurkar	676409.21	3598087	-25.25	-25.5	The hydrological survice of Israel - report
Caesarea NH24.A	Sand	678063.65	3595435.4	7.5	4.1	The hydrological survice of Israel - report
Caesarea NH24.A	Loam	678063.65	3595435.4	4.1	2.7	The hydrological survice of Israel - report
Caesarea NH24.A	sandy/Clay	678063.65	3595435.4	2.7	2.7	The hydrological survice of Israel - report
Caesarea NH24.B	Sand	678128.74	3595460.8	6.5	5.9	The hydrological survice of Israel - report
Caesarea NH24.B	sandy/Clay	678128.74	3595460.8	5.9	4.4	The hydrological survice of Israel - report
Caesarea NH24.B	sand	678128.74	3595460.8	4.4	4.05	The hydrological survice of Israel - report
Caesarea NH24.B	Loam	678128.74	3595460.8	4.05	3.2	The hydrological survice of Israel - report
Caesarea NH24.B	sandy/Clay	678128.74	3595460.8	3.2	3	The hydrological survice of Israel - report
Caesarea NH24.B	Clay	678128.74	3595460.8	3	3	The hydrological survice of Israel - report

4207

שחזור התפתחות אזור החוף של מרכז ישראל לאורך הרביעון המאוחר

גלעד שטיינברג

תקציר

אזור-החוף, הכולל בתחומו אזורים יבשתיים וימיים נושא בקרבו רצפים סדימנטריים שעלולים לספק מידע מפורט אודות שינויים בתהליכים שהתרחשו בסביבות אלה. לאורך הרביעון שינויים יחסיים במפלס הים השפיעו בצורה משמעותית על דפוסי הסרה ודפוזיציה, כמו גם על הפצתם של סדימנטים בלתי מגובשים לאורך סביבת החוף. בנוסף, תהליכים טבעיים בסקלות אזוריות (אקלים) עד מקומיות (טופוגרפיה, השפעות נחליות) ומאז עלייתם הדומיננטיות של האדם השפעות אינרטרופוגניות, מהוים גורם המעצב את מורפולוגיית אזור החוף כמו גם את מבנה החתך הסטרטיגרפי. המחקר הנוכחי חוקר את ההשפעות של מפלס הים היחסי, שינויי אקלים כמו גם תהליכים מקומיים על התפתחתות המורפולוגיה החופית לאורך הרביעון המאוחר על ידי שיחזור המשלב מודל בעל ארבעה מימדים וקורולציה לאותם תהליכים.

אזור מחקר ממוקם במרכז החוף של ישראל ומשתרע מנחל אלכסנדר ועד לנחל תנינים, מעומק מים של 30 מטרים ועד למרחק של 1.5 קמ׳ ממקום קו החוף הנוכחי. אזור זה נבחר בשל המאפיינים המורפולוגים היחידות הסדימנטריות המצויים בו והמצאותם של ממצאים אנטרופוגניים בתחומה של העיר הקדומה קיסריה שיושבה בין מהתקופה פרסית ועד לתקופה הצלבנית. שיטות המחקר ככלו מתודולוגיות מתחומים שונים ואיחוד של מידע קיים הכלל מפות ידוג קרקע, סריגי גבהים של מישור החוף, מפות עומקים של המדף הרדוד, שלוש מאות קידוחים ליתולוגים, דוחות חפירה, רישומים היסטורים, כמו גם סקרים אקוסוטים של פרופילי תת הקרקע מהמדף הרדוד. בנוסף נערכו סקרים אקוסטים וימי קידוחים באזור החוף. אלה כללו פרופילים באורך כולל של 110 קמ׳ ושבעה גלעינים רציפים שנקדחו במרזבות בין רכסי האאוליאנית בקרבת הנחלים באזורים הנמוכים. הגלעינים נחקרו באמצעות אנליזות פטרו-סדימנטריות, תארוכים רדיומטרים ופטרוגרפיה.

בהתבסס על אנליזת הסטרטיגרפיה הסיסמית ותצורתן המרחבית שש יחידות סיסמיות ושבע משטחים אופיינו ופוענחו עבור המדף הרדוד. היחידות הסיסמיות נקשרו ליחידות הליתולוגיות ממידע הקידוחים הקיים והתוצאות מהאנליזות הפטרו-סדימנטולוגיות של הגלעינים היבשתיים. הקורולציה בין המידע מהסביבות השונות אפשר ליצור את הכרונוסטרטיגרפיה של אזור המחקר. המודל החדש אפשר להבחין שחול קוורצי שהגיע מדלתת הנילוס לחופי ישראל והוסע על ידי הרוח אל תוך היבשה התגבש ליצירת אבן חול אאולית או שעבר תהליך של פדוגנזה ליצירת שלום יחידות פלאוסולים בגוונים כותם-חום לפני 110 - 8 אלף שנים. יחידה חרסיתית טינית כהה וביצתית הושקעה בין הרכסים בסביבת נחלי החוף על גבי יחידת הפלאוסול העליונה משיא תקופת הקרח האחרונה ועד לתחילת ההולקן. היחידות האלה כוסו על ידי חולות קוורציים חופיים ואאולים לפני 6.6 – 0.1 אלף שנים.

המודל שנוצר במחקר זה אפשר לבחון את השפעת תהליכים גלובליים-מקומיים על אזור החוף כמו גם את הזיהוי של שינויים דיאכרוניים ואי רציפויות בליתולוגיה בין החתך של האזורים הנמוכים לאלה של המצוק החופי שנחקרו בעבר. הנחלים התגלו ככוח דומיננתי שאחראי על עיצוב החתך הסטרטיגרפי בשל השפעותיו הארוזיביות. כתוצאה מכך הבדלי הגבהים בין האזורים הנמוכים למצוק החופי השפיעו על תהליכי הפדוגנזה כמו גם על תהליכי נחליים בתקופה של לפני 80 – 5 אלף שנים. האקלים, שבעיקר השפיע כתוצאה משינויי המשקעים וכמויות השקעת האבק, עיצב את תהליכי הפדוגנזה; בעוד שמפלסי הים הנמוכים, במהלך שיא תקופת הקרח האחרונה, הפריעו להשקעת סדימנטים נילותים לאורך המדף הרדוד וגם להשקעה אאולית וכתוצאה מכך הגבילו את ההצטרבות של הסדימנטים באזור החוף הקדום.

בסביבת העיר הקדומה קיסריה ארבעה פציאסים מרכיבים את יחידת החול העליונה של החתך. מתוך ארבעת אלה הפציאס העליון והתחתון זוהו כסדימנטים טבעיים חופיים ונילותים בעוד שתי הפציאסים המצויים בינהם, הכוללים חולות אפורים עשירים בשיירי קרמיה שברי זכוכית ולבני בניה , סווגו כחולות אנטרופוגניים. הפציאסים האנטרופגניים תוארכו לתקופה האיסלמית ופוענחו כליתולוגיה של ערימת זבל ובעוד השני כסדימנט חקלאי שעבר מודיפיקציה המעלה את פוריותה כתוצאה מפעולות של דישון. בהתבסס על המורפולוגיה של פני השטח בו נמצא הסדימנט החקלאי בצירוף עם פני האקויפר הגבוהים ואיזכורים היסטוריים אזור החוף הממוקם דרומית לקיסריה נחשד ששימש בעבר כשטח חקלאיות של העיר קסריה.

מודל השחיזור של הפליאוגיאוגרפיה של המחקר הנוכחי מיצג הבנת תהליכי התפתחות אזור חוף לאורך תקופת הקרח-בין קרחונית האחרונה תוך הצגת השפעותיהם של תהליכים מקומיים-גלובליים ולכן יכול לשמש דוגמה עבור אזורי חוף סיליסיקלסטים בקווי רוחב נמוכים בעלי שיפוע מדף מתון. כמו כן, השחיזור בעל ארבעת המימדים בעל פוטנציאל לזיהוי אזורי התיישבות קדומים ביחס לשינוי הסובב. הגישה ההוליסטית של המחקר שנערך מחוץ לגבולות העיר קיסריה הקדומה יכולה להיות רלוונטית לאתרים ארכיאולוגים נוספים ברחבי אגן הים התיכון. ברם, בעל פוטנציאל לצבירת ידע נוסף אודות אוכלוסיות קדומות, הקשר שלהן והשפעותיהם על הסביבה.

שחזור התפתחות אזור החוף של מרכז ישראל לאורך הרביעון המאוחר

גלעד שטיינברג

חיבור לשם קבלת התואר "דוקטורט לפילוסופיה"

אוניברסיטת חיפה
הפקולטה למדעי הרוח
החוג לציוויליזציות ימיות

פברואר 2017

שחזור התפתחות אזור החוף של מרכז ישראל
לאורך הרביעון המאוחר

מאת: גלעד שטיינברג
בהנחיית: ד"ר דורית סיון
ד"ר ג'סטין דיקס

חיבור לשם קבלת התואר "דוקטורט לפילוסופיה"

אוניברסיטת חיפה
הפקולטה למדעי הרוח
החוג לציוויליזציות ימיות

פברואר 2017